Development of SuperCam Calibration Target and scientific capabilities of combined and standoff instruments: Raman and LIBS

PhD Thesis
by

José A. Manrique-Martínez

Universidad de Valladolid

Universidad de Valladolid

DEVELOPMENT OF SUPERCAM CALIBRATION TARGET AND SCIENTIFIC CAPABILITIES OF COMBINED AND STANDOFF INSTRUMENTS: RAMAN AND LIBS

TESIS DOCTORAL PRESENTADA POR

D. José A. Manrique Martínez

PARA LA OBTENCIÓN DEL TÍTULO DE DOCTOR EN CIENCIAS FÍSICAS

DIRIGIDA POR:

Fernando Rull Pérez

Guillermo Eduardo López Reyes

TESIS FINANCIADA POR:

ESP2013-48427-C3-2-R

ESP2017-87690-C3-1-R

AKNOWLEDGEMENTS

I would like to start this section of acknowledgements by thanking the external revisors and the members of the board that have helped me improving and evaluating this work. To all of them I have nothing but the deepest scientific respect. This respect is to be extended to the tutors of the thesis, F. Rull and G. López Reyes, and the moral tutor J. Medina, who gave me the opportunity to work in what I like and get a PhD in the process.

Nothing happens in science now by individual work, and because of that I would like to thank my colleagues from the research group, present and past, that have influenced and taught me a lot: Jesús, Antonio, Rafa, Álvaro and last but not least, Marco, thanks for your elf-sight for science and papers, it helped me a lot in this thesis. Special thanks to Aurelio, for several aisle lectures on how a Raman measurement **has to be done**, and the hours of his time getting the best of my samples. To my colleague/tutor, and partner in crime in everything related to space, Guillermo, there is no expression of gratitude that makes justice to your help. I am looking forward to keeping working with you. To Pablo, thanks for your help and everything I've learned from you… and many beers in several continents, I hope to keep working the impossible with you in the future.

Thanks to Thomas and Andres for your hard work that turned into great science, best wishes for your future. Thanks to INTA and Jose, Andoni, Alice… you were of great help with the SCCT, it might had been impossible to do it without your help. Also, SCCT couldn't be a reality without the help of AVS, and the best engineer I have ever seen, Charlton.

Finalmente, en español, en una clave más personal, debo dar gracias a las mujeres de mi vida: Caro, mamá y Vir. A mi madre y hermana que me demostraron con su cariño que el infinito no es una abstracción matemática. Gracias por cuidar de todo cuando no estuve donde debí. A mi mujer Carolina, solo puedo darle las gracias por su apoyo, por su paciencia, y perdón por las muchas horas que he estado lejos de casa. Espero darte el futuro que te mereces a mi lado. Te amo.

Dejo una última nota para mi alfa y mis omegas. Gracias a mi padre por ayudarme a convertir, tras demasiados años (lo admito), unos juegos y la curiosidad de un niño en una tesis doctoral. Me diste las bases para llegar más lejos de lo que nunca imaginé. A mis hijos, Isabela, que has sido una distracción maravillosa estos últimos tres años, y mi primer pensamiento cada día, y al que está por venir y distraerme, espero ser para vosotros al menos una fracción de lo que mi padre fue para mí.

Si a alguien me dejé... fue sin querer, si me lo ha de recordar espero me sepa perdonar

Prologue

The present manuscript describes the works that I have done as part of the participation of the University of Valladolid in Mars2020 mission, as part of the instrument SuperCam. This is an atypical thesis work, as there are two well differentiated aspects in it: One part more related to the development of hardware for space use, always within the context of the science to be done with that hardware; and another part related to the scientific support to instrumentation as SuperCam, or other developments done by the Research group which I belong to.

Is this activity of this research group that I have tried to remark in this work, to put in value the potential of a group that, despite its small size, is involved (as Nov 2019) in three missions for Mars exploration and future developments of instrumentation. This group composed by researchers from different backgrounds, covering from chemistry to software engineering, and of course physics, has participated in very different areas of research and technology development. That characteristic is reflected in this thesis and the wide variety of works that I have done in the last five years.

It has been my work, and still is, to be the Project Manager of the SuperCam Calibration Target. This task has been done to a wider extent of pure project management, reason why it was assigned to a profile like mine, far from engineering management, although with some experience on it. With help from other partners for some tasks, the responsibility of the technical aspects of the project has fallen on the backs of two researcher of this group, my tutor Guillermo Lopez, and myself. This work has been done in parallel to more scientific related activities, as the Science Lead of the Calibration target is my other tutor, Prof. Fernando Rull, and we do participate in both ends of the project.

The position covered, being in the engineering side one day, and in the science side the other, has been a joy for me and I value the experience acquired in this process.

Said this, I have separated the content of the thesis in three big sections, a first section as introduction, in which, despite of theory background that evaluating experts know deeply, I tried to summarize the different developments that have positioned our research group as pioneer of standoff Raman spectroscopy. During the state of the art I also remark the interest of a new branch in spectroscopy, which is the data fusion. Not only we are into standoff instrumentation, but this instrumentation, as SuperCam, can use several techniques. The line of work in which the science outcome of an experiment, taking into account all the techniques, is better than the sum of the individual analyses

is also a great part of the present work, and will be a blooming research area in the future.

In a second section I have focused on the works related to the development of the Super Cam Calibration Target. First giving a context for the mission and then going directly to the works involved in the development. The path from the concept idea to the final hardware integrated in the rover is described, with a deeper oversight of the tests done that demonstrate that this hardware will do its job and survive to the trip to Mars. All of this has been done being in the middle between the pure mechanical engineering works and the science needs from the science team, what gave me an interesting perspective of the project.

The third section summarizes several experiments that cover the possible science that can be done with standoff systems, or combined analyses using Raman and LIBS. With a small look to the development of a sample that could be a good reference material for intensity calibration, and after years of being present in our laboratory procedures was finally published and considered to be part of the calibration target of SuperCam.

I hope that this text reflects the quality and impact of the work done here, and also the great efforts that participate in projects at this level have implied for me and my tutors.

TABLE OF CONTENTS

EXECUTIVE SUMMARY

- **Chapter 1: Introduction and context**
  - 1.1 Establishes the objectives of the thesis, the remarks on the objectives and context of the work done to achieve those objectives.
  - 1.2 Provides the theoretical background to help as quick reference to the concepts used, given the multidisciplinary nature of this work.
  - 1.3 State of the art, with a look to the different related developments in the community, also addressing the work performed as part of this thesis, as well as by our research group.
- **Chapter 2: SuperCam and the SuperCam Calibration target**
  - 2.1 is focused on the description of Mars2020 mission, its objectives and how SuperCam and the science works of this thesis fit in this mission.
  - 2.2 presents SuperCam instrument, a unique analytical suite, being a completely new development not only in space exploration, but also in earth applications. This unique system is described so the calibration needs can be better understood. The two main subsystems of SuperCam described here are responsibility of Los Alamos National Laboratory and IRAP, so the section is purely descriptive, involving no work from me or any member of our group, besides the science support.
  - 2.3 covers the works done with great contribution from our side, and under our coordination, that have served to develop the SuperCam Calibration Target (SCCT). The different designs, reasons, requirements and steps prior to manufacturing are presented. The manufactured models are described with special insight into the qualification campaign. This is the most interesting test campaign of space hardware as it serves to

demonstrate that the technology will be able to perform the tasks for what it was designed in the required environments.

- **Chapter 3: Combined and standoff Raman-LIBS spectroscopy: some experiments.** This section covers the different experiments performed as part of this thesis that is intended to support the SuperCam mission objectives, using the technology or techniques of the SuperCam instrument.
    - 3.2 A new interesting application of a material is presented. Works done in our research group are summarized to present an interesting candidate for Raman Standard Reference Material that would allow to calibrate in intensity a wide range instrument, survive to pulsed laser and environmental conditions of Planetary Exploration.
    - 3.3 Presents examples on how a Standoff system detects biomarkers, and the difficulties behind this detection using standoff instruments. In vivo detection of interesting biomarkers is achieved.
    - 3.4 Presents a work done on how standoff Raman could assess the geological context of an area. This work has direct implications in the selection a site for sample caching, and gives an example of the operational advantages of these developments in space exploration.
    - 3.5 presents works done in the chemometric calculations done using Raman and LIBS: from standard univariate analyses in binary mixtures, multivariate analyses on binary and ternary mixtures, and also data fusion with LIBS. Each individual analysis sets the different capabilities of each technique separately, and the great potential of fused analysis. This work has set a path for immediate future works.

- **Chapter 4: Conclusions.** This section summarizes the results of this thesis, and relates them to the objectives of the thesis, as well as how this works will be continued in the following years, as a complement to the participation in the ExoMars and Mars 2020 operations.

1 Introduction and context

1.1 Introducción

> *"… si alguien tiene pleno conocimiento de que la "entropía de un sistema aislado aumenta constantemente", no sólo buscará una estufa para calentarse —resultado muy magro para veinte años de estudio— sino que podrá resolver una enorme cantidad de problemas, desde el funcionamiento de un motor hasta la evolución del Universo.*
>
> *Ernesto Sábato, El uno y el Universo.*

El presente texto refleja los trabajos realizados en desarrollo de sistemas remotos basados en espectroscopía Raman, y como estos trabajos nos han llevado a participar en un instrumento como SuperCam, y a tener la responsabilidad de desarrollar uno de sus componentes.

El desarrollo de la muestra de calibración, desde el concepto hasta su fabricación y entrega, ha sido el trabajo más exigente en tiempo y dedicación de la presente tesis. Representa además un objetivo cumplido de alta relevancia, al significar el inicio de la contribución española en SuperCam, y la entrega de material desarrollado desde Valladolid y que formará parte del Rover Mars2020.

He querido abordar también el tipo de trabajos que pueden realizarse mediante instrumentación de este tipo. Abarcando instrumentación remota, e instrumentación combinada, abordaremos una serie de experimentos que sirven de ciencia de soporte y ejemplo de las capacidades que SuperCam puede tener una vez esté operativo en la superficie de Marte

1.1.1 Objetivos de la tesis

En la presente tesis se han querido fijar los siguientes objetivos:

1- Sentar las bases detrás del diseño de sistemas Raman-LIBS remotos y desarrollar un sistema de laboratorio que sirva de soporte científico para SuperCam.
2- Desarrollo de un sistema de calibración para un instrumento multianalítico como SuperCam. Demostrar que el diseño cumple con las especificaciones, tanto científicas como técnicas. Fabricar un modelo de vuelo que se aceptado por JPL/NASA. Esto constituye la parte española de responsabilidad en el instrumento y que sirve de entrada a la participación en operaciones.
3- Demostrar que en el contexto de los objetivos de la misión Mars2020 los desarrollos como SuperCam son una ayuda de alto interés en la consecución de los objetivos de misión.
4- Proporcionar resultados y desarrollos de algoritmos de análisis que puedan ser empleados con datos obtenidos por SuperCam.

Objetivo 1: En primer lugar se ha querido realizar un desarrollo teórico orientado a instrumentos combinados Raman-LIBS, y a instrumentación Raman remota. Esta clase de desarrollos ganarán protagonismo en el futuro, y se han querido condensar en un texto las lecciones de relevancia obtenidas en nuestros desarrollos.

Al mismo tiempo, el grupo de investigación ERICA ha dedicado mucho tiempo y esfuerzo al desarrollo y uso de sistemas Raman remotos. Este trabajo en el que este grupo que ha sido pionero, al ser uno de los primeros grupos en el mundo desarrollando estos conceptos, no se ha visto reflejado adecuadamente en publicaciones, obteniendo poca visibilidad. En la introducción del presente trabajo se ha pretendido hacer una recopilación de los desarrollos realizados por este grupo de investigación, así como los trabajos realizados con estos desarrollos.

Estos desarrollos han afianzado la posición de liderazgo de este grupo en la aplicación de técnicas espectroscópicas a la exploración planetaria. Fruto de este liderazgo, a octubre de 2019, el grupo y la Universidad de Valladolid forman parte de tres misiones de exploración del sistema solar, cumpliendo diferentes roles. Desde la participación de liderazgo en el instrumento RLS de Exomars, del que los tutores de esta tesis son IP y responsable científico de operación, la responsabilidad como equipo de ciencia en la misión MMX, contando con F. Rull como Co-I y G. López como colaborador, o el trabajo más directamente relacionado con la presente tesis: el liderazgo técnico y científico en uno de los subsistemas del instrumento SuperCam.

Objetivo 2: Por la cantidad de trabajo y esfuerzos que implicaba, así como por su relevancia institucional y científica, el objetivo fundamental de esta tesis ha sido precisamente lo relacionado con el último instrumento mencionado. Siendo el objetivo prioritario proporcionar soporte científico al instrumento SuperCam, y sobre todo proveer un componente que permita su correcta calibración en Marte, la SuperCam Calibration Target (SCCT). Este instrumento, que es parte de la carga útil de la misión Mars2020, consiste en un instrumento remoto que utiliza múltiples técnicas analíticas, incluyendo Raman y LIBS, razón por la que la experiencia y conocimientos de este grupo de investigación son de alta relevancia.

Objetivos 3 y 4: Una de las características del grupo de investigación ERICA es la de ser un grupo multidisciplinar en el que no solamente se cuenta con la parte de desarrollo instrumental, sino también con trabajo orientado al retorno científico de la instrumentación que se desarrolla. En esta línea de trabajo, en la presente tesis se muestran algunos resultados de los trabajos científicos realizados en la línea del estudio *in situ* de Marte, en concreto la ciencia de soporte a SuperCam y en general a los desarrollos remotos Raman-LIBS. Así pues se presentarán algunos ejemplos de investigaciones relacionadas con la detección de biomarcadores mediante esta técnica,

aunque las previsiones de una detección directa en la superficie de Marte sean bajas. Se continúa también con los trabajos orientados a una mejor identificación y caracterización mineralógica que permite, por ejemplo, identificar y cuantificar mediante espectroscopía Raman procesos de alteración geológica directamente relacionados con la aparición de vida. O la caracterización geoquímica usando datos Raman y técnicas de análisis novedosas, o una combinación de varias técnicas con Raman para potenciar el retorno analítico y que permita una comprensión más pormenorizada de la composición de áreas de interés astrobiológico, tanto para Marte como para futuras misiones que puedan visitar otros cuerpos planetarios del Sistema Solar.

1.1.2 Raman remoto

La espectroscopía Raman ha demostrado ya ser una técnica de referencia en ciencias planetarias. Por diversos motivos, pero principalmente por su polivalencia, siendo capaz de detectar múltiples compuestos con la misma técnica, o por su versatilidad, al no necesitar una preparación previa especial de la muestra, esta técnica se ha ido ganando adeptos en la comunidad de astrobiólogía y cosmogeoquímica.

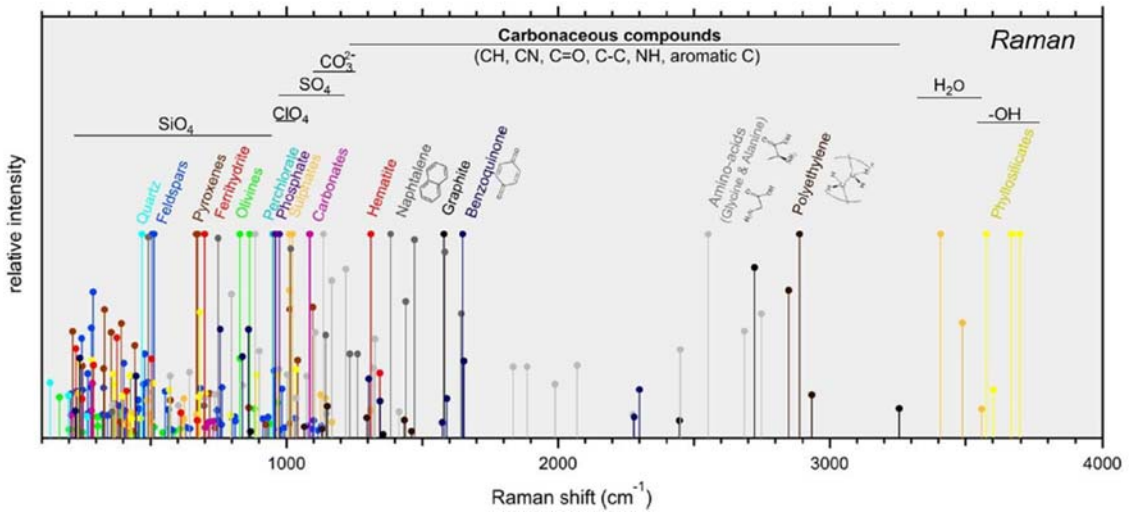

FIGURE 1-1 DIFFERENT COMPOUNDS THAT CAN BE DETECTED BY RAMAN SPECTROSCOPY

Una de sus ventajas particulares es estar basada en una interacción meramente óptica con la muestra a analizar. Al no requerir contacto ni interacción con la muestra de ningún otro tipo, permite, simplificando mucho, poder analizar cualquier muestra con la única condición de que está en el campo visual del instrumento.

Se desarrollará en ulteriores secciones, pero el Raman remoto es una realidad, toda vez que se sea capaz de lidiar con una cantidad de fotones extremadamente baja.

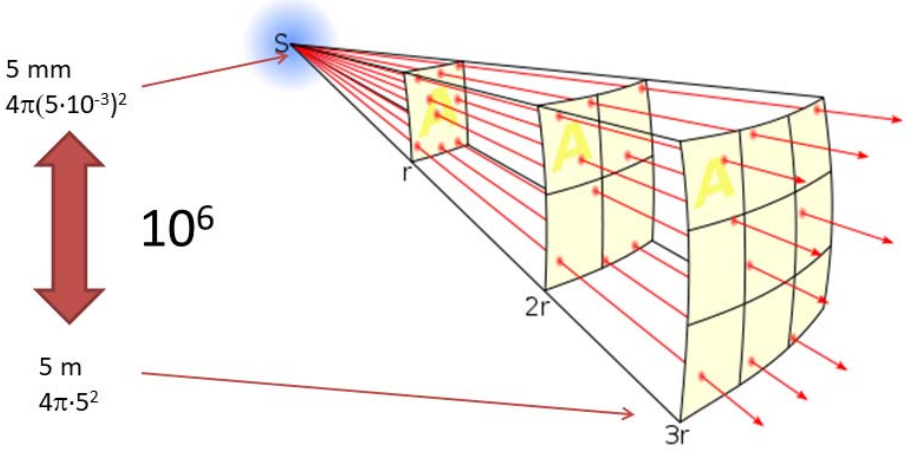

FIGURE 1-2 FLUJO LUMÍNICO EN FUNCIÓN DE LA DISTANCIA

Y es que el efecto Raman, que es un efecto bastante débil de por sí, da muy pocos fotones cuando alejamos de la muestra, requiriendo lógicamente o una mejora en los medios de detección, o la generación de más fotones fruto de la dispersión Raman.

Como ser verá después, ambas aproximaciones se toman a la hora de desarrollar instrumentos remotos. Por un lado el uso de láseres pulsados permite concentrar en lapsos muy cortos de tiempo una gran cantidad de energía y producir una gran cantidad de *fotones Raman* provenientes de la muestra. Por otro lado, la aparición de los intensificadores en el mundo de los detectores ha hecho que técnicamente no sea infrecuente encontrar en el mercado cámaras CCD capaces de llegar al límite del *single photon*, es decir, llegar a detectar un único fotón proveniente de la muestra.

Dejando aparte el reto técnico y la mejor manera de salvarlo, es conveniente preguntarse por las posibles aplicaciones de este tipo de desarrollos.

La instrumentación Raman remota ha sido un parte de desarrollos instrumentales llevados a cabo por diversos grupos de investigación y aplicada a diferentes campo y problemas. Principalmente es útil cuando el contacto con la muestra es complicado o no es una opción. Ejemplos de este caso puede ser el análisis de materiales muy calientes como coladas de lava, o materiales radiactivos, como los compuestos de uranio que se forman en los elementos de combustible de centrales nucleares. Incluso se plantea desde algunas industrias como una técnica de utilidad para analizar explosivos permitiendo una distancia de seguridad al operador. Pero es que también puede ser aplicado para acceder a zonas más amplias con una simplicidad de operaciones.

Un instrumento Raman remoto establecido en un punto podría realizar mapeos alrededor y proveer un mapa de una zona muy amplia, por ejemplo un entorno de terreno de 10 metros de radio. De querer adquirir esa información con elementos de contacto requeriría desplazamientos de equipo y personal, mientras que este tipo de

desarrollos solo requerirían el movimiento de algunos elementos ópticos. Esta capacidad es de gran interés en sus aplicaciones para exploración planetaria. Así, un hipotético instrumento capaz de Raman Remoto podría reconocer todo el entorno de un aterrizador sin necesidad de desplazamiento. O en el caso de tener capacidad de desplazamiento podría proveer información de utilidad en operaciones más complejas como son las de movimiento.

Por todos estos motivos la espectroscopía Raman remota ha ido ganando interés en la comunidad científica. Pero es que no solo acaba su interés en lo referente a las capacidades propias de la espectroscopía Raman, si no también en sus posibles sinergias con otras técnicas.

Este es el caso de la espectroscopía LIBS. Esta técnica espectroscópica utiliza un pulso de luz concentrado en una pequeña área de la muestra para inducir un plasma, y analizar después la luz proveniente de este plasma para identificar la composición elemental de la misma. Desde el punto de vista instrumental solo algunas pequeñas diferencias la separan de la espectroscopía Raman a distancia, lo que hace que con una mínima complicación añadida, el desarrollo de instrumentos combinados sea factible. Algo de alto interés si se tiene en cuenta que ambas técnicas dan información muy diferente, y complementaria, de la muestra.

1.1.3 SuperCam

SuperCam es un ejemplo de estos instrumentos combinados comentados previamente. El instrumento se describirá en la sección 2 del presente trabajo, pero a modo resumen basta con comentar que es un instrumento derivado de otro que lleva desde 2012 operando y obteniendo datos de la superficie de Marte: ChemCam. Éste es un instrumento LIBS a distancia, en el que se aprovecha la alta cantidad de luz proveniente de la ablación laser de la muestra para hacer un análisis de las líneas de emisión del plasma generado. Gracias a este instrumento se han detectado fases minerales en Marte conteniendo calcio y azufre, muy seguramente yeso o alguna forma deshidratada del mismo, formando venas entre otros materiales. Esta clase de evidencias son testimonio de una posible actividad hidrotermal pasada y por tanto son de alto interés astrobiológico.

ChemCam forma parte del Mars Science Laboratory, el rover Curiosity, y esta misión ha servido de predecesora para otra misión con una alta carga de herencia, la misión Mars2020. El éxito alcanzado por el instrumento ChemCam animó a su equipo de desarrollo a realizar un instrumento que, basándose en parte de los desarrollos realizados para ChemCam, pudiese incorporar una mayor capacidad analítica, y siempre con la capacidad de hacer estos análisis a distancia. Es así como nace SuperCam, que a la técnica LIBS y la obtención de imágenes de alto aumento en blanco y negro, ambas

en ChemCam, ahora suma nos solo las imágenes color, sino además la capacidad de obtener espectros Raman, fluorescencia, espectros de reflectancia VISIR o sonidos de la superficie de Marte.

Este instrumento que fue seleccionado por NASA en 2014 para formar parte de la misión gemela de MSL que se lanzaría en 2020, ha contado desde su fase de concepto con la participación de España y más concretamente de la Universidad de Valladolid.

1.1.4 Contexto de exploración planetaria

En el momento de la redacción de esta tesis hay cuatro misiones preparándose para su lanzamiento en 2020, y otras dos misiones, planeadas para el futuro inmediato, sin contar con las misiones implicadas en el retorno de muestras.

Las cuatro misiones planeadas para su lanzamiento en 2020 pertenecen a cuatro agencias espaciales diferentes. Exomars de ESA y ROSCOSMOS, Mars2020 de NASA y HX-1 de la agencia espacial China, CNSA, planean poner un rover en la superficie de Marte, mientras que esta última misión y HOPE de la agencia espacial de Emiratos Árabes, planean poner orbitadores en la órbita del planeta rojo. Atrás quedan los años en que la exploración del sistema solar era una batalla entre dos agencias, el año 2020 significará un hito al mandar tres misiones a la superficie de Marte y dos orbitadores, con la implicación de cinco agencias espaciales diferentes. Estas misiones se sumarán a misiones pasadas tanto de ESA, NASA y ROSCOSMOS, una misión de la agencia espacial India. En el futuro una nueva misión de la agencia japonesa JAXA tratará de retornar muestras desde Phobos, satélite de Marte. Un momento como el actual nunca antes se había dado en la exploración del Sistema Solar.

La exploración robótica de Marte comienza en la década de los sesenta, y en aquellos años la carrera espacial estaba copada por NASA y la Unión Soviética. Estos últimos no contaban entonces con una agencia espacial propiamente dicha que centralizase sus esfuerzos, en lugar de ello su programa de exploración estaba descentralizado, y fue así hasta el desmembramiento de la URSS.

Fue la URSS quien comenzó con los esfuerzos por explorar Marte mediante sondas, y lo hizo con su poco exitoso programa Mars entre los años 1960 y 1973. De este programa y sus cinco intentos de poner un aterrizador en Marte solo uno, el Mars 3, alcanzó el grado de éxito parcial al poderse posar de manera controlada en Marte y realizar un envío parcial de una imagen de su superficie. Los orbitadores en cambio tuvieron algo más de suerte y consiguieron insertar la Mars2 y Mars 3 en la órbita marciana. Éxito que se repetiría con sus misiones Mars 6 y Mars 7, que además de un fallido aterrizador llevaban un orbitador para realizar un sobrevuelo por Marte.

Dos fallidas misiones más a los satélites de Marte, Phobos 1 y Phobos 2, a finales de los 80, una misión que explotó en el lanzamiento, Mars96, y una misión que no pudo abandonar la órbita terrestre baja, Phobos-Grunt, completaron los esfuerzos rusos por la exploración de Marte, y fueron sus últimas misiones a Marte hasta la posterior implicación de ROSCOSMOS en Exomars.

NASA en cambio tuvo más suerte y completaron un exitoso programa de exploración en las décadas de los 60 y los 70. El programa Mariner realizó sobrevuelos de Marte con la Mariner 4 (1965) y consiguió la primera inserción de un orbitador en la órbita de Marte con el Mariner 9. Gracias al programa Mariner se pudo comprender al fin que los cambios en el albedo de Marte se debían a tormentas de polvo globales.

Pero el gran éxito de NASA en la década de los 70 fue el programa Viking. Viking 1 y 2 fueron las primeras misiones capaces de operar un laboratorio analítico automatizado en la superficie de Marte. Este laboratorio contaba con diferentes instrumentos para realizar la primera caracterización del entorno marciano:

- Sensores climáticos
- Cámara a color
- Sismómetro
- Sistema de fluorescencia de rayos X
- Cromatógrafo de gases
- Experimento biológico.

Este último experimento es de gran importancia dada la falta de datos sobre Marte y su superficie en aquella época. Antes de conocer las duras condiciones a las que orgánicos os microorganismo deberían enfrentarse en la superficie de Marte (Klein, 1978).

Solo uno de los tres experimentos dio un positivo, el Labeled Release (Ballou, 1978). Este resultado se ha atribuido a la posible presencia de orgánicos en el regolito marciano que pudieron pasar desapercibidos para el cromatógrafo, debido a la acción de los percloratos que los degradarían durante el calentamiento previo a la medida. Estos compuestos son unos poderos oxidantes de los que futuras misiones detectaron cantidades importantes en Marte.

Los resultados de las Viking fueron de gran relevancia y mantuvieron el interés sobre Marte, aunque no se mandaría otra misión con un aterrizador hasta finales de los años 90 con Pathfinder.

Entre medias, numerosos orbitadores fueron lanzados a Marte, consiguiendo datos morfológicos del planeta, así como datos espectroscópicos de infrarrojo.

Focalizando la atención en los aterrizadores y las técnicas que desplegaron, Pathfinder incluyó un pequeño rover, Sojourner, con capacidad de hacer diversos experimentos. Entre la base Pathfinder y Sojourner se desplegaron cámaras de imagen, sensores climatológicos, experimentos de adherencia de materiales, magnetómetros, anemómetro y un instrumento APXS.

APXS, acrónimo de Alpha Proton X-ray Spectrometer, analiza la composición de la muestra mediante el bombardeo con radiación, proveniente de una fuente radiactiva, y analizando después las partículas alfa dispersadas, así como los Rayos X producidos por esta radiación en la muestra. Es una técnica activa que permitió hacer mediciones de la composición elemental de diversas muestras alrededor de Pathfinder.

Después de Pathfinder dos misiones muy exitosas de NASA llevaron diversos experimentos en dos rover independientes, los MER, que esta vez sin depender de una base en la superficie de Marte pudieron explorar grandes extensiones de este planeta. Spirit y Opportunity fueron lanzados en 2003 y desplegaron en la superficie de Marte la siguiente instrumentación:

- Cámaras panorámicas, Pancam, y cámaras de navegación, Navcam.
- Espectrómetro de infrarrojos, Mini-TES
- Espectrómetro Mossbauer
- Instrumento APXS
- Microscopio
- Experimento magnético para el polvo
- Herramienta de abrasión

La carga útil en estas dos misiones iba muy orientada a la caracterización geoquímica de la superficie de Marte. Ningún instrumento a bordo estaba preparado para el análisis de orgánicos, al igual que pasaba con Pathfinder y Sojourner. Además, dentro de los análisis de carácter geoquímico, las técnicas activas elegidas estaban limitadas. APXS queda limitada a la detección de elementos más pesados, y Mossbauer es una técnica muy orientada a minerales de hierro.

Es con la llegada del Mars Science Laboratory cuando la exploración de Marte da un salto en complejidad técnica y analítica, haciendo que esta misión sea comparable, por su ambición, a las primeras misiones Viking.

El rover Curiosity marca una gran diferencia con sus predecesores, fundamentalmente por el salto técnico, al ser un rover alimentado por baterías de radioisótopos (las anteriores se vieron limitadas por los paneles solares), el tamaño y complejidad de los instrumentos puedo aumentar.

En este rover, de nuevo, las técnicas de análisis fueron más enfocadas a la caracterización del planeta más que a la detección directa de biomarcadores. Curiosity incorporó en su carga útil las siguientes técnicas de análisis:

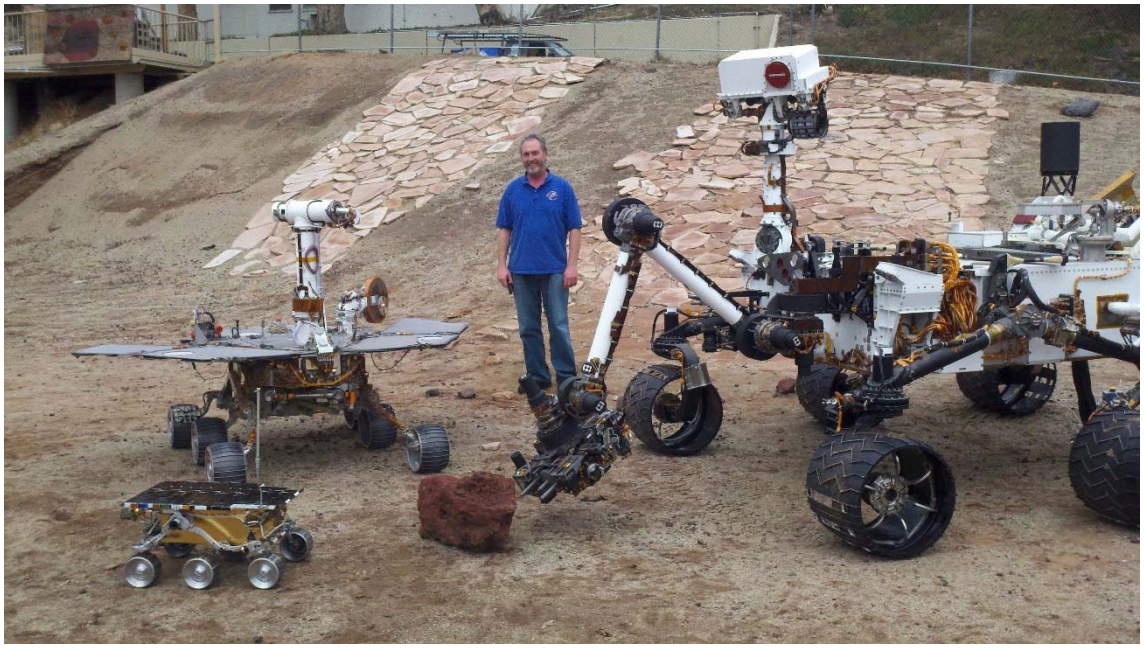

FIGURE 1-3 LOS TRES TIPOS DE ROVERS DESPLEGADOS EN MARTE HASTA LA FECHA.

- APXS. De nuevo como en previas misiones
- Difracción de rayos x sobre polvo, y fluorescencia de rayos X. Ambas en el instrumento Chemin.
- Espectroscopía de masas y cromatografía de gases, dentro del instrumento SAM.
- Mediciones de radiación con RAD.
- Reflexión de neutrones en DAN, para medir la presencia de hielo o agua en la superficie.
- Estación meteorológica, REMS, que constituyó la primera contribución española a la exploración robótica de la superficie de Marte.
- Cámaras de imagen. Desde las cámaras de navegación a la compleja cámara del mástil, MastCam, capaz de obtener imágenes multiespectrales.
- Microcámara, MAHLI. Para obtener imágenes de alto aumento de las zonas analizadas o erosionadas con el taladro de a bordo.
- ChemCam. Un instrumento LIBS remoto que es el predecesor de SuperCam.

En esta carga útil solamente SAM podría tener capacidades de detectar orgánicos, el resto de instrumentos estaban más focalizados hacia la caracterización geoquímica de Marte en incluso la preparación de misiones humanas, mediante la caracterización del clima y la radiación en la superficie de Marte.

A estos rovers hay que añadir el aterrizador Phoenix e Insight. La primera desplegó diferentes instrumentos que incluyeron un espectrómetro de masas, TEGA. Insight por otro lado ha sido diseñada con más interés en la dinámica interna del planeta.

Con este contexto previo, queda claro que los únicos instrumentos con capacidad real de descubrir orgánicos que fueron enviados a la superficie de marte fueron los pertenecientes espectrómetros de masas y cromatógrafos, pero la instrumentación de este tipo es compleja y requiere una gran cantidad de masa y consumo eléctrico que no hacen de estas técnicas unas candidatas fáciles para cualquier misión robótica.

Además, dejando de lado lo referente a biomarcadores, las herramientas disponibles para hacer una buena caracterización de la mineralogía marciana han sido también limitadas. La mayor parte de las técnicas empleadas podían dar medidas sobre la composición elemental de las muestras, pero no sobre su composición molecular o su estructura. Solo se cuentan algunas excepciones como Chemin o los Mossbauer, pero estas técnicas requerían mucho tiempo, y el volumen de muestras que se pueden analizar por estos instrumentos es limitado.

La necesidad de obtener una caracterización de la mineralogía marciana no solo basada en la composición elemental, sino también en la estructura y la composición molecular es evidente si se quieren entender algunos procesos. Esta necesidad es incluso mayor si se quieren estudiar estados diferentes de hidratación de algunos minerales. En la sección 3 veremos como un instrumento LIBS nos devuelve prácticamente las mismas medidas para una muestra de olivino o serpentina, mientras que su estructura es diferente, indicando en el caso de la serpentina que se han producido cambios en una muestra de olivino por su interacción con agua.

Estas necesidades pueden verse cubiertas por Raman, que no necesita preparación de la muestra, y que vale tanto para proporcionar información mineralógica de una muestra, como para detectar orgánicos si los hubiera.

Además, si una cosa demostró ChemCam en Curiosity, es el potencial de contar con una técnica capaz de proporcionar medidas activas de muestras a distancia, de manera que esa información pueda ser empleada para decidir a dónde ir con el rover, y dónde utilizar instrumentos de ciencia de contacto.

Raman es, una vez más, una técnica llamada a complementar al LIBS en esta área. Siendo también una técnica compatible con desarrollos de instrumentación remota, y que complementa la información obtenida mediante el LIBS.

Estos argumentos han hecho que la técnica Raman, de maneras diferentes, se haya desarrollado e implementado en futuras misiones a Marte. Exomars, en la que el instrumento RLS obtendrá espectros Raman de muestras del subsuelo marciano. O Mars

2020, que contará con un espectrómetro Raman UV para la detección de orgánicos en contacto, o SuperCam, que como se ha explicado previamente suma Raman al LIBS en sus análisis a distancia.

1.2 Teoría

En esta sección se tratarán de introducir los fundamentos básicos sobre los diferentes efectos e instrumentación relacionados con los objetivos de la tesis.

1.2.1 Efecto Raman

Chandrasekhara Venkata Raman, científico indio, descubrió el efecto homónimo en febrero del año 1928, descubrimiento que le hizo merecedor del premio Nobel de física en el año 1930. La historia sobre el descubrimiento, con un C.V. Raman viajando en barco y preguntándose el por qué del azul del mar mediterráneo es ya parte de la historia de la ciencia (Raman, 1928).

La realidad física detrás del efecto Raman supuso un cambio en la manera de entender la interacción radiación materia en esa época. Raman vino a demostrar que, contrario a la tesis imperante, la luz podría ser dispersada por mecanismos inelásticos, eliminando la dispersión Rayleigh como único efecto dispersivo de la luz en la materia. Esta capacidad de la materia de interactuar con la radiación electromagnética, robando o sumando energía a la misma y reemitiendo ondas electromagnéticas de diferente longitud de onda ya había sido identifica por Compton en la interacción entre rayos X y algunos sólidos, pero fue Raman quién descubrió el efecto en radiación visible.

En sí, el efecto Raman puede ser descrito a partir de un modelo basado en un oscilador armónico simple, en el que dos masas están unidas entre sí por un resorte de constante elástica K, lo cual es una abstracción de una molécula en la que dos átomos se encuentran unidos por un enlace (Krawczyk, s.f.).

La vibración de este sistema puede ser descrita, en términos de física clásica, mediante la ley de Hook y ley de Newton. Considerando el desplazamiento de cada uno de los átomos respecto de la posición de equilibrio, x_1 y x_2, y las masas de cada átomo como m_1 y m_2. Esta aproximación clásica al efecto Raman puede ser encontrada en diferentes manuales y materiales didácticos, y no se reproducirá aquí. Pero a modo resumen, permite pasar de la descripción de la vibración del sistema:

$$L = L_0 Cos(2\pi\vartheta t)$$

Donde L es la enlongación del enlace. A una ecuación que nos describe el momento dipolar de la molécula cuando se le somete a un campo eléctrico oscilante.

$$-P = \xi_0 E_0 Cos(2\pi\vartheta_0 t) + L_0 Cos(2\pi\vartheta t) E_0 Cos(2\pi\vartheta_0 t)(\frac{\partial\xi}{\partial t})_{L=0}$$

En esta ecuación lo que se observa es que en la molécula se producen dos efectos diferentes, cada cual con su momento dipolar asociado, uno que varía con la misma frecuencia de la radiación incidente, correspondiente con el efeto Rayleigh, y aparece otro componente que puede ser desarrollado de la siguiente manera:

$$L_0 E_0 \left(\frac{\partial \xi}{\partial t}\right)_{L=0} (Cos(2\pi(\vartheta_0 - \vartheta)t) + Cos(2\pi(\vartheta_0 + \vartheta)t))$$

Con lo que se inducen otros dos momentos dipolares en los que la frecuencia ya no coincide con la frecuencia de la radiación incidente, apareciendo uno con una frecuencia igual a la incidente más la frecuencia natural de vibración de la molécula, y otro con una frecuencia igual a la incidente menos la frecuencia natural. Es decir, dos momentos dipolares que pueden dar origen a la emisión de dos ondas electromagnéticas de frecuencia superior y frecuencia inferior a la de la radiación incidente.

Estas dos ondas emitidas se corresponden con las dos manifestaciones posibles del efecto Raman, y en términos de una dispersión elástica, corresponden con una interacción de stokes, cuando la onda incidente ha cedido energía al sistema, o antistokes, cuando la radiación incidente aumenta su energía a costa de la energía del sistema. Como se ha visto, la longitud de onda de ambas emisiones sería simétrica respecto de la longitud de onda incidente.

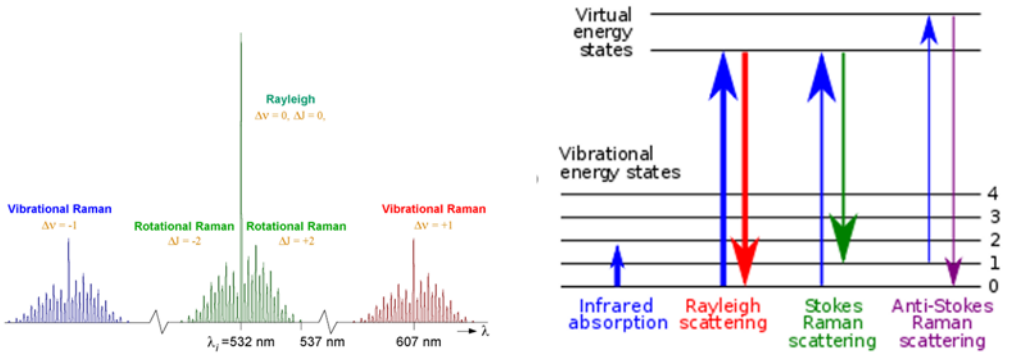

FIGURE 1-4 (A) RAMAN STOKES Y ANTISTOKES, COMO EFECTOS SIMÉTRICOS RESPECTO DE LA LONGITUD DE ONDA INCIDENTE Y (B) DIAGRAMA DE NIVELES DEL EFECTO

Más allá del efecto físico, lo realmente interesante, y lo que constituye la principal aplicación del efecto Raman, es la dependencia de este efecto con la naturaleza de la materia, en este caso con las masas de los átomos de la molécula y su enlace. Con lo que si se incide en una muestra con una radiación coherente, esto es monocromática, el resultado será que todos aquellos fotones de longitud de onda diferente a la de la fuente de irradiación portarán información de la naturaleza molecular de la muestra iluminada.

Este es el principio de la técnica Laser Raman Spectroscopy, LRS, en la que se emplea un laser como fuente de excitación y se analizan las dispersiones Raman sufridas por la radiación incidente.

En términos de la física estadística el proceso Stokes es mucho más probable que el proceso antistokes, motivo por el que la parte antistokes es rara vez utilidad enlos análisis mediante LRS. En cuanto a la componente Stokes del efecto Raman, es más probable que la antistokes, pero es mucho más improbable que la dispersión Rayleigh, que domina la interacción radiación materia. El efecto Raman es por tanto un efecto muy débil.

Se ha querido mantener esta clásica explicación por la relevancia del descubrimiento del efecto Raman y la física detrás del mismo. De esta manera se da un origen claro de la dispersión que hoy usamos como herramienta analítica, y que ya fue anticipado por Raman (Raman, 1929).

1.2.1.1 La intensidad de la dispersión Raman

En cuanto a la intensidad esperable de luz proveniente de la dispersión Raman, ésta está directamente relacionada con una magnitud llamada sección eficaz Raman. Esta sección eficaz puede ser entendida en términos probabilísticos como el tamaño de la diana alrededor de una molécula en la que, de acertar, un fotón será dispersado mediante dispersión Raman (McCreery, 2000). No es una magnitud general, y depende de cada compuesto a estudio, aunque ciertas generalidades pueden ser comentadas.

En primer lugar hay que tener en cuenta que no todas las vibraciones posibles de una molécula, sus modos normales, van a producir dispersión Raman, y solo aquellos que cumplan con las reglas de selección producirán dispersión Raman (Mills, 1964). Una cuestión interesante al respecto de estas reglas de selección es que son en cierta manera complementarias de aquellas relacionadas con la absorción que se produce en la espectroscopía Infrarroja, de manera que se puede decir que, en términos generales, los modos visibles por Raman no lo serán por IR y al revés. Hecho que puede ser de interés a la hora de fusionar datos de ambas fuentes.

Una vez se produce una dispersión Raman, como hemos dicho, ésta se producirá con mayor o menor probabilidad en función de su sección eficaz. Esta sección eficaz, y por tanto la intensidad de luz esperable correspondiente a este modo, depende de varios factores en cada molécula, pero también depende, en general, de la frecuencia de la longitud de onda de excitación, concretamente (McCreery, 2000):

$$I_R \propto I_0(\vartheta_0 - \vartheta_r)^4$$

De donde podemos establecer dos conclusiones. Una más lógica, y es que cuanto mayor sea la intensidad de la radiación incidente la Intensidad de una determinada banda Raman crecerá linealmente con ésta. La segunda conclusión tiene que ver con la dependencia de la intensidad de esta banda Raman con la cuarta potencia de la frecuencia de excitación, hecho que reviste cierta lógica si tenemos en cuenta que a mayor frecuencia de la onda de excitación, mayor energía para mover la molécula.

La consecuencia de esta dependencia es que los límites de detección que podremos alcanzar con un instrumento Raman serán, descartando ortos efectos, más bajos cuanto más alta sea la frecuencia del laser empleado, o más baja su longitud de onda.

Finalmente, en términos generales, por cada fotón Raman que obtengamos de una muestra habremos obtenido entre 10^6 y 10^9 fotones de Rayleigh. Sirva esto para hacernos una idea de la diferencia en órdenes de magnitud de ambas dispersiones.

1.2.1.2 Incidencia de la longitud de onda empleada en la excitación

Como se ha comentado ya en la sección previa, en términos generales, la sección eficaz de una dispersión Raman para cierto modo de una molécula es directamente proporcional a la cuarta potencia de la frecuencia de la radiación que produce el efecto. Y como ya se ha establecido, esto debería proporcionar límites de detección más bajos para instrumentos usando láseres de longitud de onda corta.

Pero hay otros efectos a tener en cuenta a la hora de determinar si se usa una u otra longitud de onda para un instrumento Raman. De la ecuación que nos permite calcular el desplazamiento Raman:

$$Despl.Raman[cm^{-1}] = 10^7(\frac{1}{\lambda_0[nm]} - \frac{1}{\lambda_r[nm]})$$

Podemos obtener otro resultado de interés, y es que si tenemos en cuenta un rango típico de medida de 4000 cm^{-1}, a medida que usamos una fuente de excitación con longitudes de onda más cortas, estos 4000 cm^{-1} se reparten cada vez entre menos nanómetros. De nuevo un resultado lógico si tenemos en cuenta que cuanto menor sea la longitud de onda, pequeñas variaciones en esta llevan asociado un mayor cambio en la energía.

Por este motivo, de cara al desarrollo de un instrumento LRS, cuanto menor sea la longitud de onda del laser elegido, mayor tendrá que ser la resolución espectral del instrumento para mantener la misma resolución en cuanto a desplazamiento Raman.

Además, si tenemos en cuenta la anchura espectral del laser de excitación, esto es cómo de monocromático es el laser, es lógico pensar que la anchura mínima alcanzable por una banda Raman (en nanómetros) será la del laser. Con lo que de nuevo, si pasamos

de longitud de onda a desplazamiento Raman, nos lleva a otra conclusión sobre la resolución alcanzable: cuanto menor sea la longitud de onda del laser, más estrecho (monocromático) tendrá que ser éste para mantener la resolución en términos de desplazamiento Raman.

A efectos de esta tesis, es importante remarcar la gran diferencia entre las anchuras espectrales de los láseres continuos típicos, y la de los láseres pulsados (los no semillados).

Estos dos resultados, en combinación con el introducido en la sección anterior hacen que no exista una respuesta válida en cuanto a qué laser es mejor para usarlo en espectroscopía Raman. Dejando la selección de la longitud de onda del mismo en función de la aplicación concreta, y en general, se reducirá a un compromiso entre límites de detección y resolución.

1.2.1.3 La fluorescencia

En la figura 1.4 (B), en el diagrama de niveles, habría sido más correcto incluir otros niveles relativos a las transiciones electrónicas. Estas transiciones electrónicas también pueden ser excitadas por el laser con que se ilumina la muestra, con lo que surge otro efecto a tener en cuenta en la interacción de nuestra radiación incidente con la muestra.

La fluorescencia se produce cuando niveles vibracionales reales de la muestra son excitados. Estos niveles de energía, a diferencia de lo que ocurre con los niveles energéticos asociados con el efecto Raman, son niveles energéticos reales, y por tanto tienen asociado un tiempo de permanencia del sistema en ese estado antes de su decaimiento al estado fundamental, y la emisión de un fotón. En contraposición, el efecto Raman se produce de manera instantánea ya que los niveles energéticos asociados son virtuales, y por tanto no conllevan tiempo de permanencia.

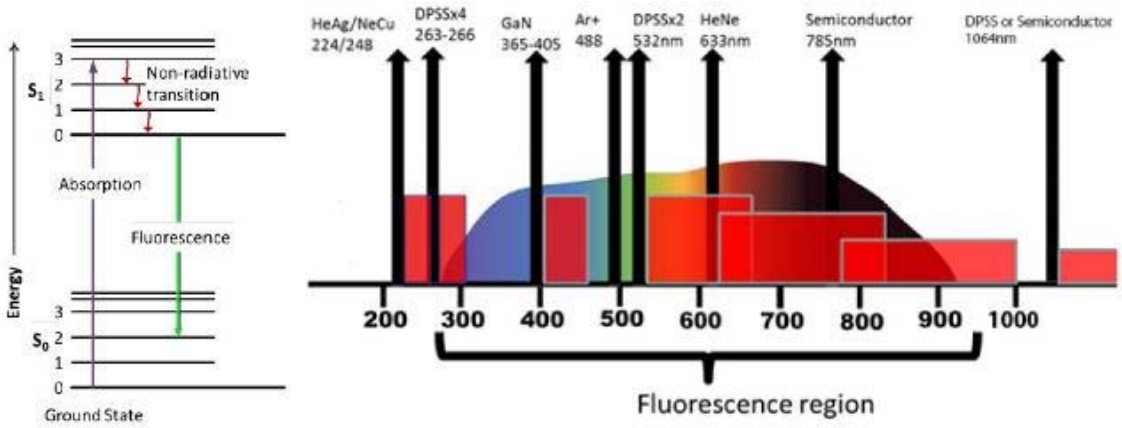

FIGURE 1-5 DISTRIBUCIÓN ESPECTRAL DE LA FLUORESCENCIA Y LOS DIFERENTES RANGOS DE MEDIDA DEPENDIENDO DEL LASER USADO PARA ESPECTROSCOPÍA RAMAN (AZO MATERIALS).

En cuanto a la naturaleza espectral de esa fluorescencia, es un fenómeno que ocurre fundamentalmente en el visible, y aunque para algunos compuestos tiene una naturaleza más o menos discreta (Venkateswaran, 1935), en general este efecto tiene una distribución continua a lo largo de la zona de luz visible del espectro electromagnético.

La fluorescencia es un problema serio a la hora de caracterizar algunas muestras mediante espectroscopía Raman, al ser un efecto que compite con el Raman y puede ser más intenso que éste, tapándolo.

Si en el apartado anterior 1.2.1.2 hablábamos de no tener un candidato claro para la mejor fuente de excitación en un instrumento Raman, ahora la decisión se complica algo más. La fluorescencia se sitúa justo entre medias de los dos extremos que antes se evaluaban, entre medias de los instrumentos infrarrojos, con gran resolución pero peor límite de detección, y los UV con mejor límite de detección pero peor resolución.

Un instrumento Raman UV puede no verse afectado por la fluorescencia al estar el rango de medida fuera de la zona de emisión de este último efecto, mientras que en un instrumento infrarrojo la energía de la radiación incidente no es suficiente para excitar los niveles vibracionales que originan la fluorescencia. No obstante, entre medias, y aunque la fluorescencia pueda jugar en contra de láseres en el rango visible, sus particularidades en el dominio temporal hacen que ciertos desarrollos tecnológicos nos permitan eliminarla.

Al principio de este apartado hablábamos de la inmediatez del efecto Raman contra cierto retraso en la emisión de fluorescencia desde que llega la onda incidente a la muestra. Este tiempo de permanencia de nuevo depende del tipo de fluorescencia, y puede variar entre unos pocos nanosegundos y los microsegundos. Esta diferencia introduce una nueva variante de la espectroscopía Raman que es de interés para la presente tesis: la Espectroscopía Raman Resuelta en Tiempo, o TRRS, por sus siglas en inglés.

En la TRRS se puede utilizar un pulso laser de unos pocos nanosegundos, y un detector con capacidad de gating, luego se explicará, para tomar pulsos muy cortos de luz, de manera que podemos ajustar la adquisición de luz en nuestro detector al momento en que se produce la emisión Raman pero aún no ha empezado la fluorescencia.

1.2.1.4 Descripción de un instrumento Raman por bloques.

Como e ha discutido previamente, para desarrollar un instrumento Raman lo primero es contar con una fuente de luz coherente, es decir, un laser. Láseres hay muchos, pudiendo ser pulsados, continuos, de gas, de estado sólido… cada láser tiene sus particularidades, y cada laser nos permitirá hacer espectroscopía Raman de una manera

diferente. Este laser ha de ser focalizado o dirigido hacia la muestra por algún sistema óptico asociado.

Después de haber excitado la muestra con este laser, y haber generado la dispersión Raman, es necesario discriminar la luz proveniente de la dispersión Rayleigh, carente de información estructural, de la proveniente de dispersión Raman. Para ello es necesario colectar la luz proveniente de la muestra mediante algún sistema óptico de colección, y después separar mediante filtros interferométricos (notch o Edge) la dispersión Rayleigh de la Raman.

En muchos de los sistemas Raman modernos las ópticas de focalización del laser y de colección de la luz de la muestra y filtrado, están integradas en un único sistema llamado cabezal Raman.

Finalmente la luz, debidamente recolectada y filtrada, debe pasar por un monocromador para separar espacialmente la luz en función de su longitud de onda, y ser detectada por algún elemento fotosensible.

Todos y cada uno de los elementos arriba descritos son elementos generales, y cada uno de esos elementos puede ser escalado y adaptado a diferentes aplicaciones y desarrollos. Esto hace de los instrumentos Raman instrumentos modulares, con una gran adaptabilidad a las necesidades dl proyecto. En la sección 1.2.3 veremos como esta modularidad se aprovecha para adecuarse a las características concretas de un instrumentoremoto.

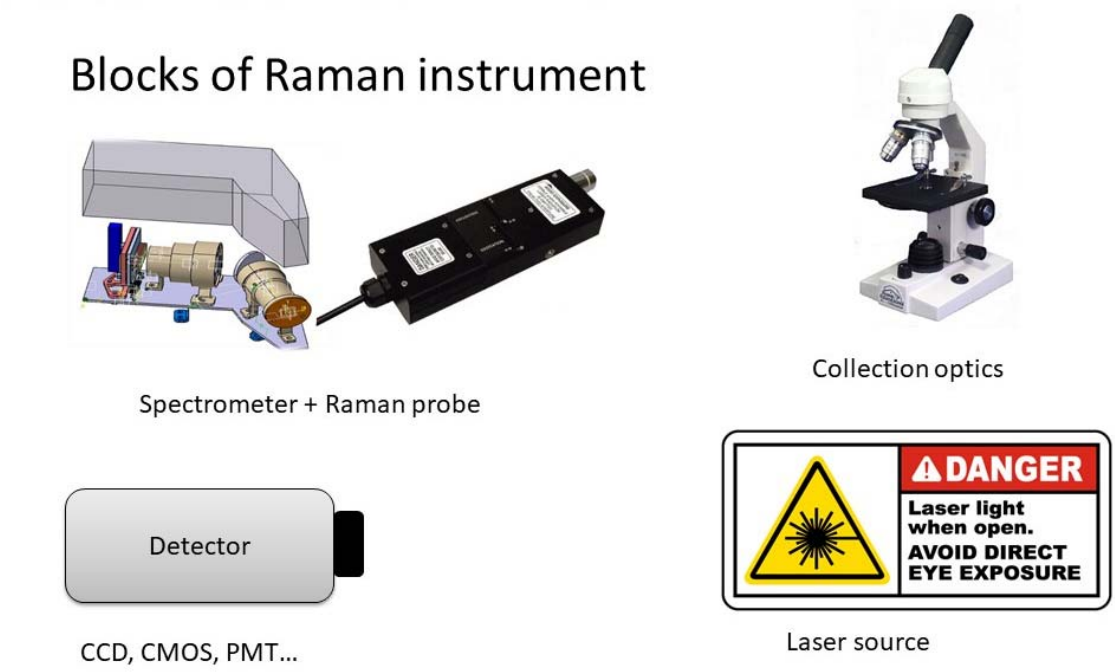

FIGURE 1-6 BLOCKS OF A TYPICAL RAMAN INSTRUMENT

1.2.2 Espectroscopía LIBS

Existen varias técnicas que pueden ser empleadas para proporcionar la composición elemental de una muestra, como la fluorescencia de Rayos X o la espectroscopía de masas, LIBS merece ser puesta en un lugar especial entre estas técnicas.

LIBS, acrónimo de Laser Induced Breakdown Spectroscopy, es una técnica analítica que, virtualmente, tiene capacidad de detectar cualquier elemento de la tabla periódica, en cualquier estado de agregación, y hacerlo además con una preparación nula de la muestra y con una relativa simplicidad instrumental.

El estudio de los espectros de emisión de plasmas es de gran interés en la comunidad científica, y son numerosos los estudios que se hacen sobre plasmas inducidos de muy diversas maneras. LIBS es un caso particular de estos estudios, inicialmente propuesto en la década de los años 60 (Schurig, 2006), y con un desarrollo paralelo, por motivos evidentes, al desarrollo del láser.

En esta técnica se focaliza un pulso laser en un área muy reducido de la muestra. Dada la naturaleza electromagnética de la luz ésta tiene asociado un campo eléctrico, al concentrarse en un pequeño spot el haz del laser la intensidad de este campo puede ser comparable al campo electrostático por el que los electrones están unidos a los átomos. Como consecuencia en la muestra se produce la ablación de una pequeña cantidad de la misma, y por tanto se induce un plasma en el que se tiene líneas de emisión de los componentes elementales de la muestra.

1.2.2.1 Eventos durante una medida LIBS

Repasaremos los diferentes eventos que ocurren durante una medida LIBS, empezando por la ablación laser. Partiendo de la ablación, en esta fase una pequeña parte de la muestra es arrancada del resto y los volátiles comienzan a evaporarse e ionizarse. Esta fase se caracteriza por un carácter térmico: el laser es absorbido por la muestra y esto induce cambios de fase, al llegar al estado de gas el material se puede ionizar por la presencia del campo eléctrico de la luz, generándose un plasma. Cabe destacar en esta fase que el tiempo requerido para la generación del plasma está por debajo del orden los nanosegundos, motivo por el que en láseres con duraciones de pulso en ese orden el resto de la energía una vez generado el plasma se emplea en calentar este vapor generado y por tanto el plasma, a la vez que se aumenta el grado de ionización.

Se genera en este momento también una onda de choque y el plasma, generado en la superficie de la muestra comienza a expandirse. Debido a esta expansión, a medida que la burbuja de plasma ocupa más volumen su temperatura empieza a caer desde los 20.00 K a los que pudo encontrarse en el momento de la inducción. En esta fase de expansión tiene un efecto claro la presión del medio en que se produce el plasma. En

vacío la expansión es rápida como lo es el enfriamiento, mientras que a presión atmosférica la expansión es más lenta.

En todo este proceso, dentro del plasma, hay partículas cargadas que están moviéndose y chocando unas con otras, on una distribución uniforme de energía. Debido a la leyes de la electrodinámica clásica, una carga que se acelera o decelera emitirá radiación electromagnética. Este efecto se llama radiación de bremsstrahlung, que viene de la palabra alemana que significa "frenado". Todas estas emisiones ocasionadas por las aceleraciones sufridas por las diferentes cargas emiten un fondo continuo que, como pasaba en el caso del Raman con la fluorescencia, compite con la emisiones atómicas que nos interesa captar para la identificación. Este fondo no aporta información sobre la muestra y carece de interés, por tanto.

Es a medida que el plasma se expande y enfría que estos choques entre partículas cargadas bajan en número e intensidad, reduciendo el fondo de bremsstrahlung, y permitiendo a las líneas de emisión de los átomos de la muestra aparecer.

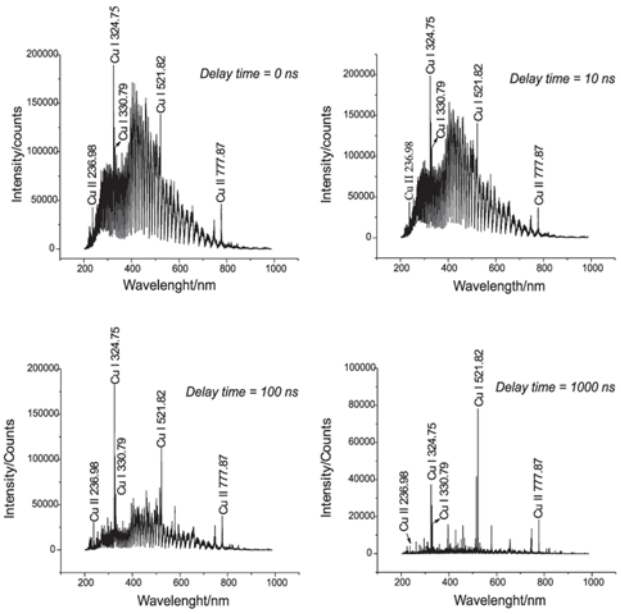

FIGURE 1-7 LIBS SPECTRUM WITH DIFFERENT DELAYS

Se puede conseguir obtener un espectro con un fondo reducido si la captación del espectro la hacemos un tiempo después de la generación del plasma. Depende de la muestra, pero en general, para sólidos en atmósfera terrestre nosotros usamos retrasos en el rango de los microsegundos.

LIBS es por tanto una técnica de un marcado carácter temporal, es decir, requiere la capacidad de obtener los datos en un lapso de tiempo concreto. Aunque algunos instrumentos en el mercado pueden funcionar sin necesidad de este sincronismo, esto

si puede tener un efecto adverso en la detección de elementos con emisiones débiles que no puedan verse sobre el fondo continuo.

Es interesante además introducir este carácter de resolución temporal por otro factor a mayores, y es que a medida que el plasma se enfría ocurren cosas diferentes. En primer lugar las líneas que recibimos son aquellas procedentes de la ionización, y posterior recaptura electrónica, de los átomos de nuestra muestra, esta emisión de luz suele ocurrir durante unos pocos microsegundos después de la generación del plasma. Entre el microsegundo y alguna decena de microsegundos tenemos emisiones provenientes de las relajaciones de los estados excitados en los átomos de la muestra. Finalmente, y siendo las más longevas, se emiten las líneas moleculares.

Estas últimas son generalmente menos intensas y más dificultosas de captar. Motivo por el que LIBS suele ser usado exclusivamente como técnica de análisis elemental, aunque tiene la capacidad de identificar moléculas. Un campo interesante de esta capacidad es la detección y caracterización de hidrocarburos.

1.2.2.2 Esquema de un instrumento LIBS

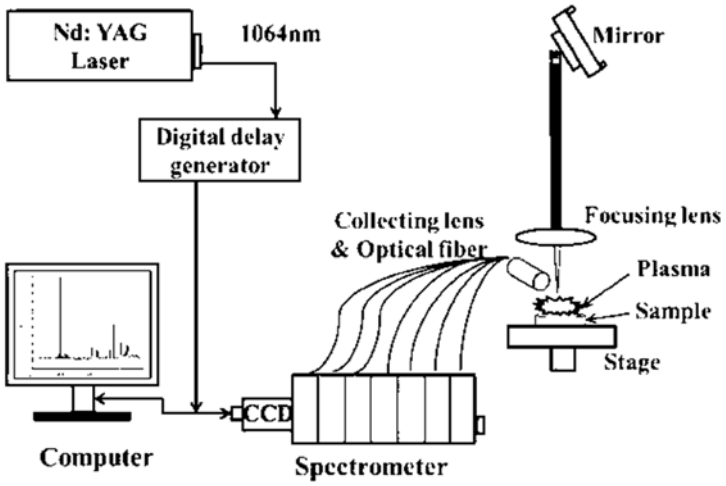

FIGURE 1-8 SCHEMATIC DIAGRAM OF LIBS SYSTEM (XIAONA, 2014).

Tal como vimos en la introducción teórica de la técnica LIBS, el proceso de obtención de un espectro LIBS es, generalmente, resuelto en el tiempo. Esta característica particular introduce ciertas necesidades instrumentales de gestión de retardos y sincronismo.

En general un instrumento LIBS cuenta con los siguientes elementos:

- Láser: es la fuente de energía utilizada para inducir el plasma en la muestra. El tipo de láser más frecuente es el Nd:YAG usando su frecuencia fundamental de 1064 nm. Una característica interesante de estos láseres es su facilidad para obtener otros armónicos mediante cristales no lineales. Para LIBS no suele ser interesante este desarrollo porque para esta técnica lo más

interesante es contar con una buena cantidad de energía. Generalmente en los láseres Nd:YAG en el mercado, la energía por pulso una vez se dobla la frecuencia para obtener 532 nm es la mitad de la que el láser proporciona en su frecuencia fundamental. Otro motivo a mayores para usar el 1064 es que está fuera del rango de medida típico, que para un espectro LIBS está entre 200 y 850 nm. Aunque no debería ser un problema debido a que el pulso del laser tiene una duración típica de nanosegundos, y la adquisición del espectro se hace unos cuantos microsegundos después, pueden aparecer interferencias. En mi experiencia con nuestro sistema usando 532 nm, en muestras translúcidas (hielos) las diferentes reflexiones internas en la muestra hacen que todavía en el momento de adquisición del espectro aparezcan fotones del láser. Eso si, existen ventajas en usar láseres de frecuencias más altas, ya que el límite de difracción que marca el tamaño mínimo de spot de análisis es inversamente proporcional a la frecuencia del láser, existiendo desarrollos micro-LIBS que emplean láseres UV (Singh, 2018).

- Espectrómetro o espectrómetros: dado el gran rango a cubrir, y la resolución típica en el orden de los 0.5 nm, puede emplearse un espectrómetro de gran rango como los de tipo Echelle, o utilizar diversas ventanas de adquisición en diferentes espectrómetros.
- Detector: el detector suele ser intensificado dado que estos sistemas tienen la capacidad de hacer gating, adquisiciones ultracortas de tiempo. Existen no obstante instrumentos que, a coste de desempeño, pueden prescindir de esta tecnología. En cualquier caso debe admitir el comandado externo para sincronización con el láser.
- Generador de retardos: este sistema es el encargado de recibir la señal del láser y después introducir el retardo deseado entre ésta y la señal de disparo al detector.
- Ópticas: las ópticas suelen incluir una lente o sistema convergente para focalizar el láser, y ópticas de colección para mandar la luz del plasma al o los espectrómetros. El primer elemento debe soportar las altas energías, y deben evitarse dobletes de lentes pegadas ya que el pegamento tiende a degradar con el laser. Para el segundo elemento si debe tenerse en cuenta el rango de medida, es difícil encontrar sistemas que permitan una buena transmitancia desde el UV hasta el IR.

1.2.3 El paso a instrumentos remotos

Una vez que ya hemos introducido los conceptos básicos de cada una de las dos técnicas que cuentan con el protagonismo en esta tesis, en esta sección nos centraremos en el uso concreto de las mismas en instrumentos remotos.

Ha sido ya descrito como el problema de la distancia afecta al flujo lumínico de señal que recogemos de una muestra, variando con la ley del cuadrado de la distancia. En ambos casos nos encontramos con fuentes luminosas que son hasta cierto punto isótropas, es decir, no tienen una dirección predominante para la emisión de luz. En el caso del LIBS toda la pluma del plasma emite en todas las direcciones. En el caso del Raman, esta dispersión puede ocurrir en casi todas las direcciones, aunque si reviste cierta predominancia en la dirección de incidencia. Así pues, a modo de estudio cualitativo, podemos evaluar el área de una semiesfera a diferentes distancias para ver su influencia en la irradiancia que la atraviesa.

Considerando la irradiancia recibida a la distancia de 1 cm como parámetro y ésta igual a 1 w/m2, por ejemplo, una fuente luminosa con una emisión isótropa a través de esta semiesfera proporcionará las siguientes irradiancias en función de la distancia :

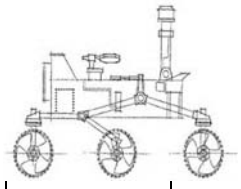

Dist. (m)	0,01	0,1	0,5	1	2	5	7
Irr. (w/m2)	1	0,01	0,0004	0,0001	0,000025	0,000004	2,04082E-06

TABLE 1-1 IRRADIANCIA EN FUNCIÓN DE LA DISTANCIA

De la tabla anterior se puede observar como para una distancia que ronde los diez metros estamos recibiendo la millonésima parte de irradiancia que la que obtendríamos con un instrumento de contacto. Esto tiene efectos particularmente importantes en el caso de la dispersión Raman, ya que como ya se ha discutido, la cantidad de fotones disponibles es mucho menor que en el caso del LIBS.

Si consideramos un láser típico de 15 mJ por pulso, y consideramos 532 nm como láser de excitación, cada fotón de 532 tendrá 3,7 $x10^{-16}$ mJ de energía. Esto nos da un total aproximado de $4x10^{16}$ fotones. Este es el número total de fotones para la excitación.

Ahora si consideramos una eficiencia en la dispersión Raman de un fotón por cada 10^6 o 10^9 fotones de excitación, esto nos permite calcular que la muestra devuelve entre 10^{10} y 10^7 fotones de Raman, en el peor escenario, a 7 metros, estamos recibiendo unos tres fotones por centímetro cuadrado y disparo. Además hay otros efectos adversos, y es que no sólo llegan fotones Raman provenientes de la muestra, lo que acrecienta el problema de detección.

Este modelo nos permite ver que a mayor superficie de colección más número de fotones para detectar, y en el caso de ópticas circulares clásicas, esto introduce una dependencia con el cuadrado del radio. Así una óptica de 10 cm de diámetro estará captando más de 200 fotones por disparo, mientras que una de 20 captará más de 900.

El problema del cuadrado de la distancia puede nos ser tal si siempre y cuando el equipo opere dentro de los límites de distancias hiperfocales, entendiendo la distancia hiperfocal de un sistema óptico como la distancia mínima de enfoque con la cuál conseguimos una mayor profundidad de campo, obteniendo un enfoque que se extiende desde la mitad de esta distancia, hasta el infinito. La expresión matemática que nos permite calcular esta distancia es:

$$H = \frac{f^2}{Nc}$$

Donde f es la focal del Sistema óptico empleado, N su apertura numérica, y c el llamado círculo de confusión. Este último concepto es el círculo mínimo que se puede distinguir en el plano focal del sistema, y está relacionado con la profundidad de foco del mismo. De esta expresión Podemos sacar dos conclusiones claras, la primera es que esta distancia dentro de la cual el cuadrado de la distancia no aplica será mayor cuanto mayor sea la focal del sistema, y cuando menor sea su apertura (relación entre su focal y diámetro), es decir, focales muy largas con sistemas muy luminosos (Hirschfeld, 1974).

El paso a hacer Raman a distancias del orden de los metros requiere, además de adaptar la óptica de colección, aumentar la potencia de la fuente de excitación. En este ejemplo, si esos 15 mJ se reparten en un pulso de 10 ns, la potencia está en el orden de los megawatios.

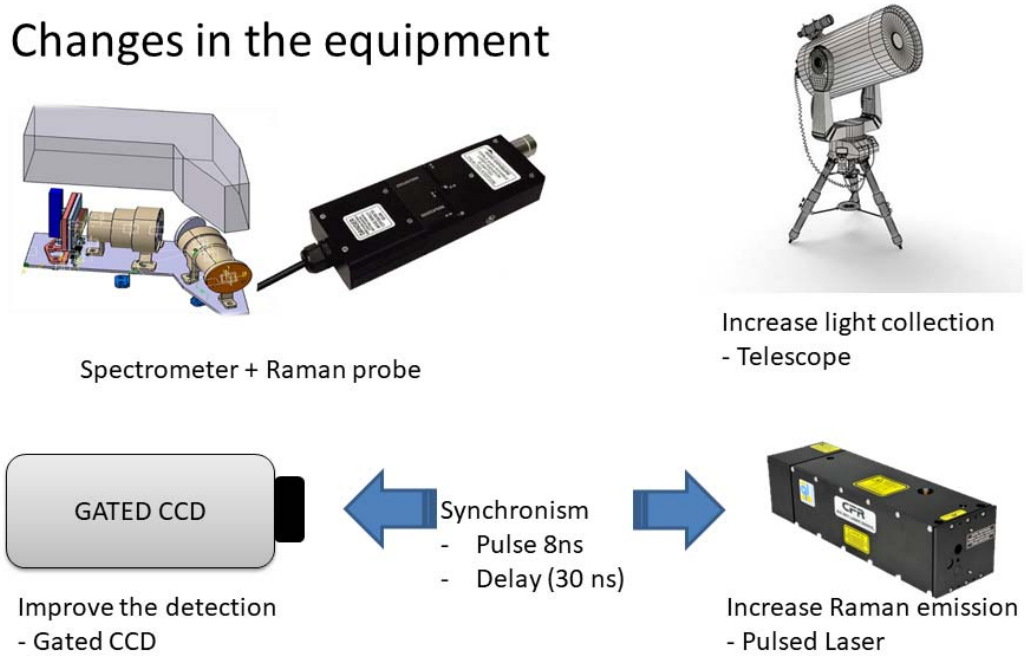

FIGURE 1-9 CHANGES IN HARDWARE FOR STANDOFF RAMAN

Esta intensidad luminosa, o flujo de fotones que llegan de la muestra lo hacen también acompañados de fotones provenientes de la iluminación difusa, considerando que no se

operará este instrumento en condiciones de oscuridad, y que no hará apuntando al Sol. Esta radiación es continua, no tiene naturaleza pulsada como el láser del ejemplo, y aunque se verá minimizada si se adapta bien el enfoque del área de colección al del área de excitación (Hirschfeld, 1974), existe esta contribución. Así pues, cuanto más nos ciñamos al pulso del láser, más ventaja le damos a los fotones Raman frente a la radiación de otra índole. Esto por tanto introduce la necesidad de cerrar al máximo la adquisición al pulso del láser, y en condiciones ideales, una medida resuelta en tiempo que permita contrarrestar la distancia, los retardos internos de los instrumentos, y sincronizar al máximo la adquisición con la llegada del pulso láser de vuelta al instrumento. El planteamiento ideal es entonces el de contar con un detector intensificado con función de gating, y capacidad de sincronizarse con el láser. Condiciones por otro lado que, como se introdujo en la sección de teoría, son típicas para un instrumento LIBS. De hecho, este requerimiento es el que permite hacer un tipo diferente de análisis Raman, que es el Raman Resulto en Tiempo.

Así pues, a modo resumen, el necesitar contrarrestar los efectos de la distancia nos implica contar con un láser pulsado, un detector intensificado con capacidad de sincronismo con el láser, y ópticas de colección más grandes.

Una opción más simple, pero no carente de limitaciones, es la de contar con un detector normal que permita la adquisición en tiempos muy cortos. Cuanto más corto sea el tiempo, sin llegar a ceñirse al pulso del láser, más se limita la contribución de la luz ambiental. Si además apoyamos esto con un láser con una alta tasa de repetición (10 KHz), podemos conseguir que en una adquisición de un milisegundo se concentren 10 eventos laser. De manera que se puede adquirir espectros Raman sin necesidad de sincronismo o intensificador. Un ejemplo realizado con un montaje mucho más sencillo, a 30 Hz con 60 mJ por pulso, puede verse en la sección 0.

Hasta el momento no se ha tenido en cuenta el LIBS ya que de momento solo estábamos evaluando la intensidad lumínica a captar. En el caso del LIBS, el plasma es mucho más luminoso que el efecto Raman (varios órdenes de magnitud) y por tanto lo que funciona para Raman, funcionará también para LIBS (incluso puede que demasiado).

Una cuestión diferente es el cómo necesitamos llevar la energía de nuestra fuente, bien el láser para la ablación, bien el láser para la excitación Raman, hasta la muestra. En el caso del Raman y dada la intensidad del láser lo mejor es mantener el haz del láser colimado y en valores de irradiancia altos. Un láser colimado nos permitirá llevar irradiancias elevadas a grandes distancias con un mínimo incremento en el tamaño de spot.

Este no es el caso del LIBS, en este caso es necesario concentrar lo máximo posible la energía del láser en un spot muy reducido. Para instrumentos remotos es necesario

entonces contar con que la óptica debe incluir algún modo de focalizar el láser para ablación a la distancia de trabajo. Generalmente esto se puede lograr introduciendo el láser por la óptica de colección, lo que permite que si está enfocado para la colección lo esté para la ablación. Es importante remarcar en este caso, que conviene evitar cualquier convergencia en la óptica que se use para focalizar el láser, y que en general el tamaño del haz y la irradiancia deben ser tenidos en cuenta de cara a no dañar las superficies ópticas.

Es importante, de cara a desarrollos de instrumentos combinados, tener en cuenta más particularidades no necesariamente asociadas con el hecho de que sea una instrumentación remota.

1.2.3.1 Instrumentación necesaria

En primer lugar, como ya se ha comentado, los rangos de medida, en términos de la longitudes de onda, para ambas técnicas no son comparables.

Un Raman que utilice 532 nm como excitación tendrá que analizar luz en un rango entre 532 nm y 675 nm, mientras que para LIBS hay que cubrir desde el UV, 200 nm, hasta el IR, 850 nm.

En general el comportamiento óptico de lentes, espejos, filtros, etc. es muy variable en rangos tan amplios, lo que hace que un filtro notch, por ejemplo, que nos valdría para separar la dispersión Rayleigh de la Raman, pueda darnos un 90 % de transmitancia para longitudes de onda mayores y menores a la cuña en 532 nm, hasta alcanzar los 300 nm y decaer en transmitancia. De cara a diseños conjuntos este es un problema cuya solución más obvia es separar la captación y medida en ventanas espectrales y hacer la separación lo antes posible. Aunque esto no siempre es posible.

Hemos establecido ya la necesidad de una cámara intensificada. Es necesario hacer algunos apuntes al respecto de estas cámaras.

1.3 Estado del arte

La instrumentación Raman y LIBS remota es de alto interés en la comunidad, un interés que ha crecido en los últimos años, como puede verse en los gráficos siguientes:

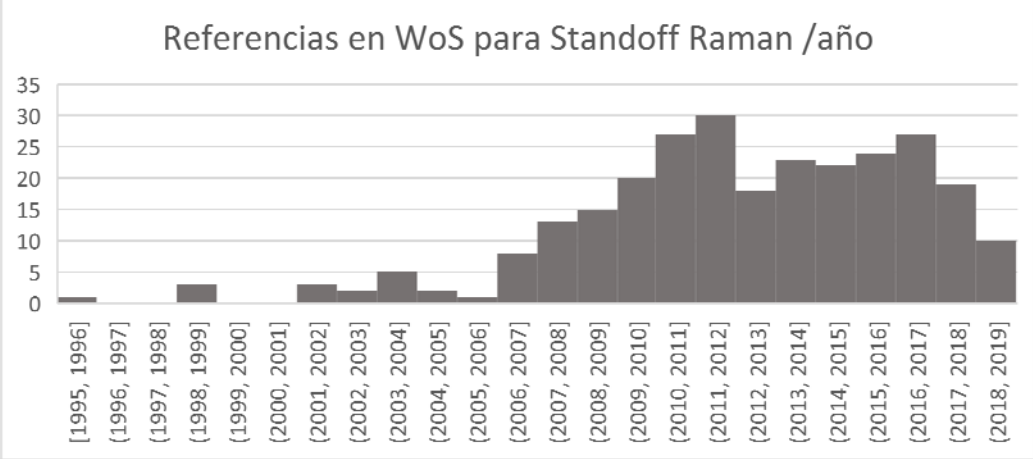

FIGURE 1-10 ENTRADAS DISPONIBLES EN WEB OF SCIENCE PARA STANDOFF RAMAN

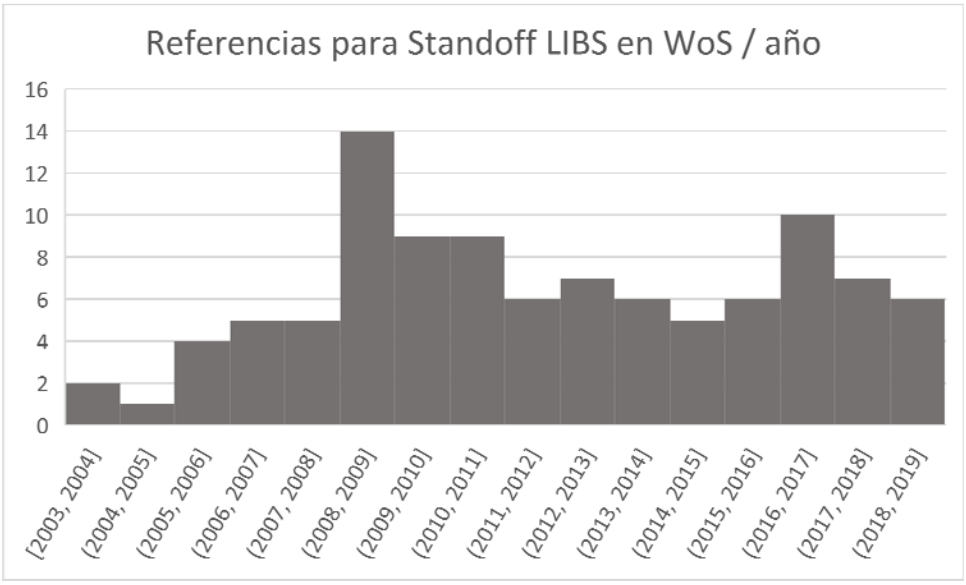

FIGURE 1-11 ENTRADAS DISPONIBLES EN WEB OF SCIENCE PARA STANDOFF LIBS

Aunque también queda claro que el interés por el Raman remoto viene de lejos, con un renovado interés a partir del año 2006, en plena efervescencia de Exomars y la posibilidad de llevar un instrumento combinado para análisis remotos (Rull, 2017). El mismo año 2006 se observa un crecimiento en el interés por el LIBS remoto, lo que coincide con la publicación de la selección de ChemCam como instrumento para la misión MSL.

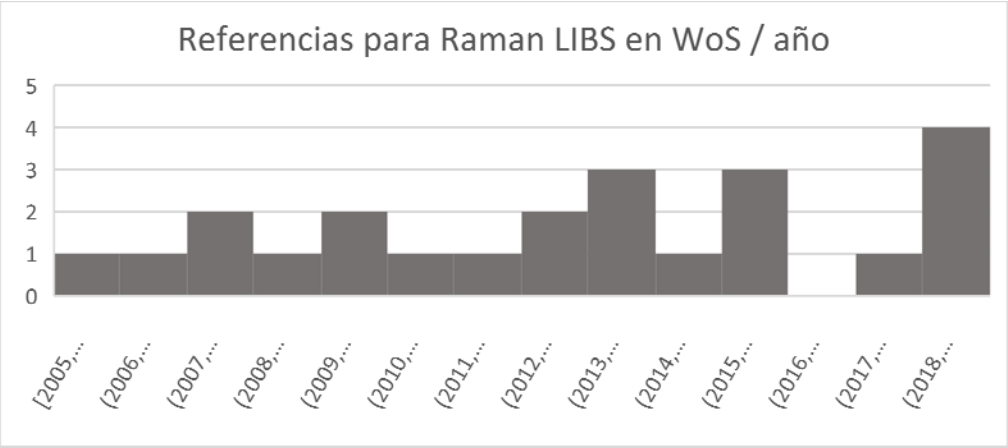

FIGURE 1-12 ENTRADAS DISPONIBLES EN WEB OF SCIENCE PARA RAMAN LIBS

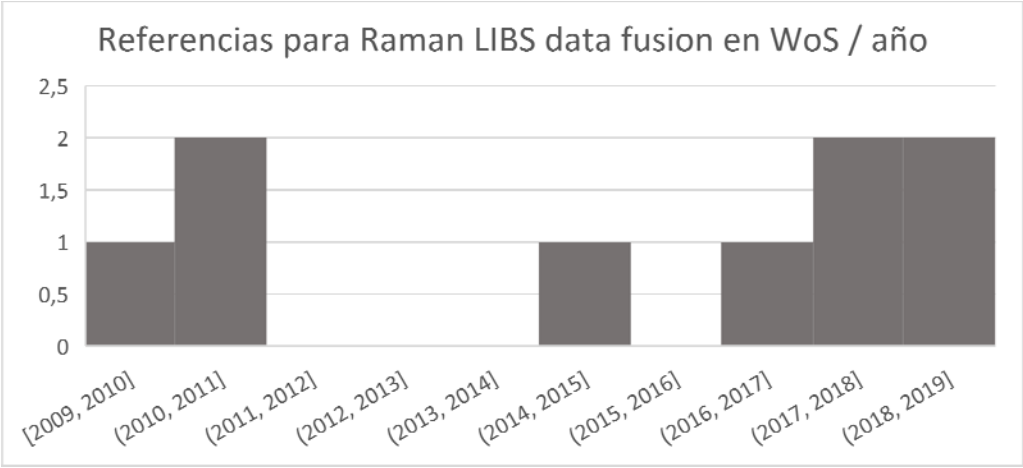

FIGURE 1-13 ENTRADAS DISPONIBLES EN WEB OF SCIENCE PARA FUSIÓN DE DATOS RAMAN LIBS

Interesante en cambio es la tendencia de las entradas correspondientes a la combinación de Raman y LIBS. No habiendo una gran incidencia para este tipo de combinación. Cabe destacar que en la Figure 1-12 se incluyen entradas en las que ambas técnicas fueron utilizadas como parte una rutina de caracterización, como en (Gazquez, 2014). De éstas, un subgrupo está relacionado con la fusión de datos de ambas técnicas (Figure 1-13).

De este rápido análisis puede sacarse una conclusión clara, que las aplicaciones espectroscópicas a distancia ya han ganado interés, y que es una realidad ya no necesariamente en la fase de I+D. A tenor de los resultados, estas técnicas combinadas se han empleado de manera profusa por separado, pero su aplicación conjunta es algo relativamente novedoso, siendo la primera entrada que devuelve WoS para su uso común de 2005, mientras que no es hasta 2009 que aparecen publicaciones relacionadas con la fusión de datos. Es la fusión de datos un campo que está poco explotado y por tanto una contribución innovadora de esta tesis, con unos primeros trabajos en esta línea en el año 2014, (Sobron, 2014). Hay que destacar la presencia de

el grupo de Javier Laserna, copando cuatro de las diez entradas devueltas para fusión de datos.

1.3.1 Desarrollos previos a los de Erica

En la Sección 1.2.3 se ha empleado una referencia en la que se desarrolla la dependencia de la ley del cuadrado de la distancia con las características ópticas de un sistema óptico para Raman remoto (Hirschfeld, 1974). Esta referencia data de 1974, por lo que podemos deducir que este tipo de desarrollos no son algo que ha aparecido en los últimos años. Lo atractivo de poder tener análisis de muestras a distancia mediante el uso de técnicas espectroscópicas activas ha hecho de los instrumentos Raman y LIBS remotos algo en lo que la comunidad científica llevaba tiempo pensando.

En verdad, el concepto de Raman remoto se ha visto ligado también a los estudios atmosféricos por medio de LIDAR (Gregersen). Esta técnica implica el envío de un haz colimado de laser pulsado a diferentes capas de la atmósfera para estudiar la señal devuelta por éstas. Entre la información que se puede extraer con esta técnica se observa la aparición de Raman relacionado con los gases atmosféricos, ya que el volumen cubierto con el haz es muy amplio, y la columna de gas muy larga. En estos tipos de instrumentos, citados también en (Hirschfeld, 1974), la excitación del láser no es focalizada, ya que la mejor manera de transportar energía en el haz a grandes distancias es colimándolo, pero al encontrarse estas capas atmosféricas a distancias hiperfocales además la regla del cuadrado de la distancia tiene un impacto severo en la intensidad de señal devuelta.

Aparte del interés combinado entre LIDAR y Raman, numerosos trabajos han sido publicados en los últimos veinte años con desarrollos diferentes. Incluyendo sistemas remotos basados en láser ultravioleta (Wu, 2000), estos sistemas tratan de mejorar los límites de detección mediante el uso de longitudes de onda cortas para ala excitación que, como ya se introdujo, llevan asociada una mayor sección eficaz del efecto Raman. El ultravioleta lleva aparejadas ciertas complicaciones, no obstante. Como son la baja resolución inherente a su diseño y la absorción por parte de la óptica.

Previo a este trabajo, se han desarrollado sistemas que utilizando un láser pulsado y un filtro acusto-óptico son capaces de dar una imagen hiperespectral, (Skinner, 1996). Estos sistemas pueden parecer interesantes, aunque revisten cierta problemática también. El primer problema es que los filtros acusto-ópticos tienen un ancho en el paso espectral generalmente muy elevado, lo que hace que pensar en sistemas Raman usando estos filtros se vea abocado al uso de láseres IR, donde un ancho de varios nanómetros tiene un menor impacto en cm^{-1}. Si se quiere utilizar alguno de estos filtros que aportan una menor ventana, entonces trabajan a una polarización muy concreta, con lo que un

efecto típicamente despolarizado en la mayoría de los casos, como el Raman, se perdería antes de entrar al filtro sintonizable.

El grupo de profesor Sharma, de la Universidad de Hawái, destaca en los últimos años como grupo de referencia en uso remoto de técnicas espectroscópicas, consolidándose como pioneros en este campo. Este grupo ha desarrollado números conceptos de instrumentos y alcanzado distancias cada vez mayores mediante el empleo de ópticas de telescopio más grandes, 8 pulgadas, láseres de 100 mJ, con distancias hiperfocales por encima de los 500 metros (Misra, 2012).

Es en definitiva un campo ya explotado, con conceptos desarrollados desde los años 70. En este campo el grupo de investigación ERICA, con mi participación incluso antes de ser doctorando, ha sido pionero también.

En el caso del LIBS, la complicación no es en sí la detección de señales luminosas bajas tanto como alcanzar la irradiancia necesaria para general el plasma. Desarrollos de LIBS remoto aparecen publicados a finales de los años 80 (Cremers, 1987), con un desarrollo notable de la técnica como instrumentación de laboratorio y de campo durante los años noventa e inicios de los 2000, incluso con aplicaciones a muestras de interés para la exploración Marciana (Thompson, 2006).

1.3.2 Desarrollos ERICA

El primer Desarrollo de ERICA se realizó para su testeo en las campañas AMASE, realizadas en las islas de Svalvard, como análogo marciano. Este primer desarrollo solo utilizaba espectroscopía Raman, y como fuente de excitación empleaba un laser pulsado Nd:YAG doblado, de 532 nm, con un pulso de 8 ns y 25 mJ por pulso. El láser en este desarrollo era colimado e introducido en el eje óptico del sistema mediante una configuración de espejos, por delante de la óptica de colección. Esta óptica de colección consistía en un telescopio Newton de 114 mm de apertura y 1000 mm de focal.

Este primer desarrollo contaba en el plano focal del telescopio con dos caminos ópticos posibles para poder realizar imagen u obtener espectro. En este diseño se empleaba un cabezal Raman, acoplado mediante lente en el plano focal, para dirigir la señal captada al espectrómetro. El espectrómetro empleaba una red de doble track y fue revisado en su configuración a partir de un espectrómetro HoloSpec de Kaiser Optical Systems.

Este instrumento, en esta configuración, contando con un disco de confusión de 200 micras en el plano focal del telescopio, cuenta con una distancia hiperfocal de 400 metros, y efectivamente pudo ofrecer espectros del hielo de los glaciares a distancias superiores a los cien metros (Rull, 2011).

Un sistema posterior cambió el sistema de colección, en este caso utilizando un telescopio de tipo Maksutov de 125 mm de apertura, y f 15. La configuración Maksutov permitió contener en un tubo óptico de menor tamaño al desarrollo previo una focal dos veces superior. El aumento en la focal y el diámetro, a pesar de una f más alta que en el anterior diseño, ofrecían todavía una distancia hiperfocal superior a los 400 metros, distancias que siguen estando muy por encima de los límites de detección del instrumento.

En ambos, para la detección, se empleó una cámara CCD intensificada ANDOR que ya incluía la electrónica de sincronización con el láser. Estos desarrollos remotos son pioneros en su diseño a ser instrumentos de campo. Permitieron además establece, en colaboración con desarrollos paralelos por Sharma (Sharma, 2003), que si bien el acople mediante fibras ópticas entre la colección y el espectrómetro era más robusto y operativo, existe una pérdida sustancial de luz en el acople a fibra.

Un desarrollo posterior de nuestro grupo de investigación se hace en colaboración con la, ahora desaparecida, Ixion. Este desarrollo prescinde del uso de un detector intensificado, y pasa a utilizar objetivos de cámara fotográfica como elementos ópticos de colección. Un sistema más compacto, que entre en pesos típicos de espacio, es muy atractivo. La electrónica asociada a los intensificadores es también un riesgo, y se evalúa entonces si se puede desarrollar un sistema que, si bien lo realice espectros a 100 metros, pueda contener la complejidad técnica y obtener espectros a distancias en el entorno de los 10 metros.

Se desarrolla un sistema con capacidad para usar dos lentes diferentes:

- Objetivo 300 mm f:4: que ofrece una distancia hiperfocal de 110 metros
- Objetivo 70 mm f:2: que ofrece una distancia hiperfocal de 12 metros

Dependiendo del tipo de distancias de trabajo se puede intercambiar las lentes. Mientras que la lente de menor focal ofrece una distancia hiperfocal mayor, a rangos de distancia cortos ofrece una óptica muy luminosa, capaz de captar señales más débiles. En esta configuración, no obstante, el tamaño de área de análisis es superior, al ser menor la focal, y supera el centímetro a distancias de 1,6 metros.

La lente de 300 mm de focal permite un rango de trabajo mucho más amplio antes de verse afectada por la pérdida por cuadrado de la distancia, permitiendo además una capacidad de focalizar en un diámetro menor la imagen de la fibra de captación. En este sistema el spot de análisis a la distancia antes fijada es de 5 mm.

Ante la variabilidad de los tamaños de spot, y la reducción en las distancias focales empleadas con respecto a los desarrollos previos, se estima necesario introducir mejoras en la parte del láser. Se introduce un láser más potente, con pulsos de energía

de 60 mJ, y se monta un expansor variable del haz. En este sistema el láser no se introduce en el eje óptico, siendo un sistema exclusivamente de laboratorio, en que el operador desplaza en sistema de colección para adecuarse a la posición del láser a las diferentes distancias.

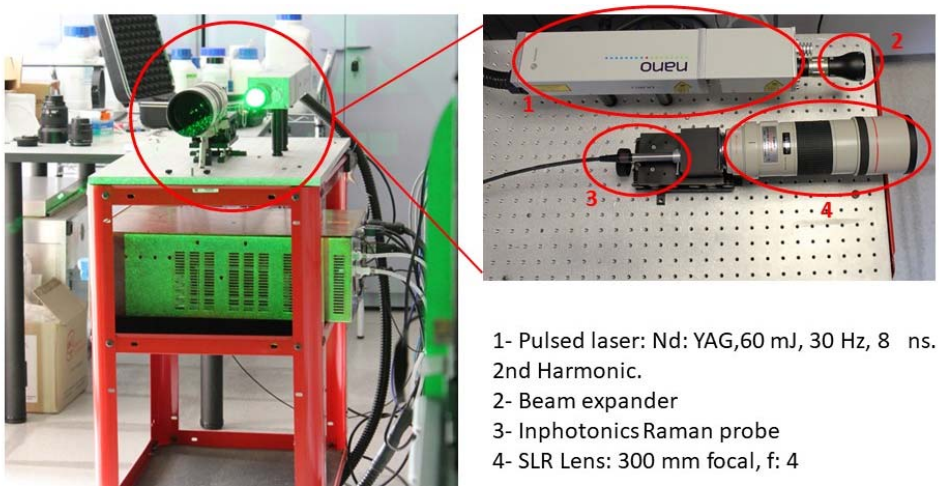

FIGURE 1-14 SISTEMA REMOTO CON LENTE DE 300 MM

El poder contar con una mayor energía del láser y un expansor de haz permite adecuar el tamaño del láser sobre la muestra al tamaño del área de colección, manteniendo unos valores de irradiancia razonablemente altos.

En este sistema un cambio adicional ocurre en el detector, pasando de un sistema intensificado a una CCD Andor Newton, no EMCCD como la mayoría de esa serie, pero si una CCD con capacidad de realizar lecturas a una elevada tasa de refresco y tiempos de adquisición muy cortos, siendo capaz de alcanzar los 1600 Hz de captación.

Este sistema permite operar el láser, que ahora alcanza los 30 Hz frente a los 10 Hz de los primeros desarrollos, a su máxima tasa de repetición, ajustando el tiempo de adquisición al máximo para captar un pulso del láser y poca luz de fondo. A diferencia de lo que ocurre en los desarrollos que emplean un intensificador, la CCD empleada en este desarrollo no tiene capacidad de hacer gating ni de bajar al límite de los nanosegundos, por lo que este desarrollo no tiene la capacidad de hacer estudios resueltos en tiempo. No permite por tanto discriminar entre fluorescencia y Raman, y no permite adaptarse a los diferentes tiempos de vuelo del láser en función de la distancia. En lugar de esta sincronización, se adapta el tiempo de exposición, aunque con el mínimo, y comandando el disparo de la CCD mediante la señan de entrada del láser, se cubren las distancias dentro de esos 10 metros de referencia sin adaptación.

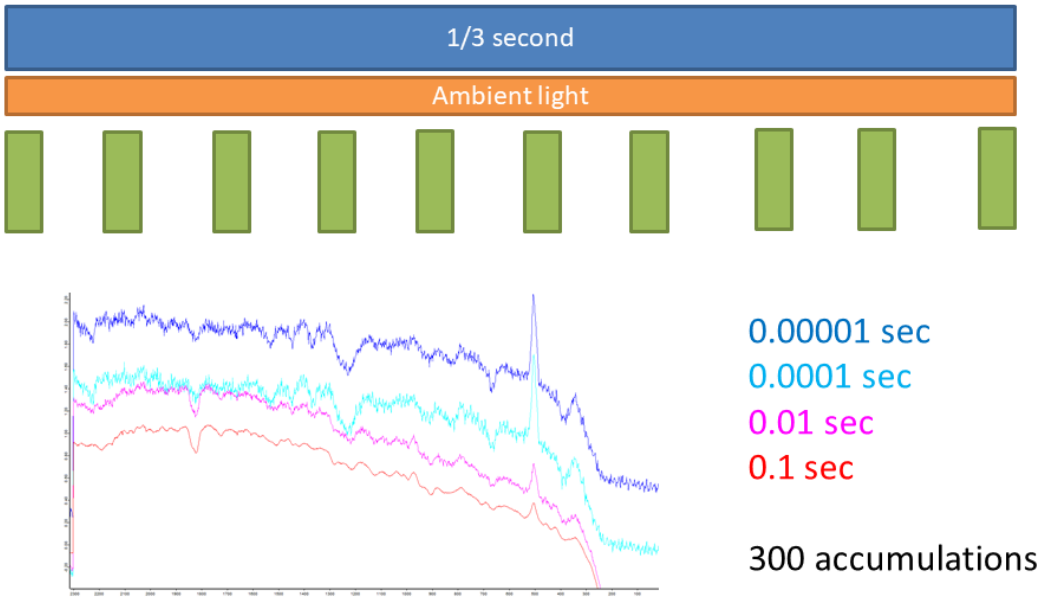

FIGURE 1-15 PRINCIPIO DE OPERACIÓN DEL INSTRUMENTO REMOTO NO SINCRONIZADO

En la figura 1-15 se muestra el principio de operación de este instrumento, y una comparativa de diferentes espectros en que se cómo, a medida que se reduce el tiempo de adquisición, se disminuye el fondo.

Con este instrumento he podido realizar diversas pruebas y ensayos, incluyendo la prueba de detección de biomarcadores en 3.3. Permite este sistema obtener un buen compromiso entre simplicidad, distancia operativa y resolución para equipos remotos.

Finalmente, con la entrada de nuestro grupo de investigación en el grupo de ciencia de SuperCam, y con la responsabilidad técnica asociada del desarrollo de su muestra de calibración, de la que soy responsable técnico, bajo la dirección del responsable científico, F. Rull, se hace necesario actualizar el sistema remoto.

El nuevo sistema ha llegado con retraso por diferentes problemas financieros del grupo, así como por la carga de trabajo que ha implicado el desarrollo del SCCT. Pero actualmente el grupo ya cuenta con un sistema combinado Raman-LIBS, con capacidad de hacer análisis en rango similares a los de SuperCam, aunque actualmente se encuentra fijado a la distancia de la muestra de calibración del Mast Unit.

En este nuevo desarrollo se vuelve a un detector intensificado, pero esta vez se acopla una segunda óptica con un acople directo a fibra para hacer LIBS. El mismo láser antes descrito se emplea en esta ocasión para hacer Raman, adaptando el tamaño de stpot al de colección, o para hacer LIBS, reduciendo el spot a tamaños por debajo del milímetro.

Para el análisis de luz procedente del plasma se usa un espectrómetro Echelle, de Andor, con un rango de lectura entre 200 y 850 nm, y una resolución mejor de 0,1 nm. El acople se hace mediante una lente de 50 mm a f:1,8. El detector es otra cámara Andor intensificada.

Este sistema ha servido para hacer numerosas pruebas que han constatado un problema que también SuperCam tuvo que abordar, y que estuvo presente en anteriores diseños de nuestro grupo: la inclusión del intensificador acarrea una gran pérdida de resolución. Esto es debido a la aparición de bordes difusos en el fósforo del intensificador que hacen que la imagen de la rendija del espectrómetro pueda aumentar su anchura en el plano focal.

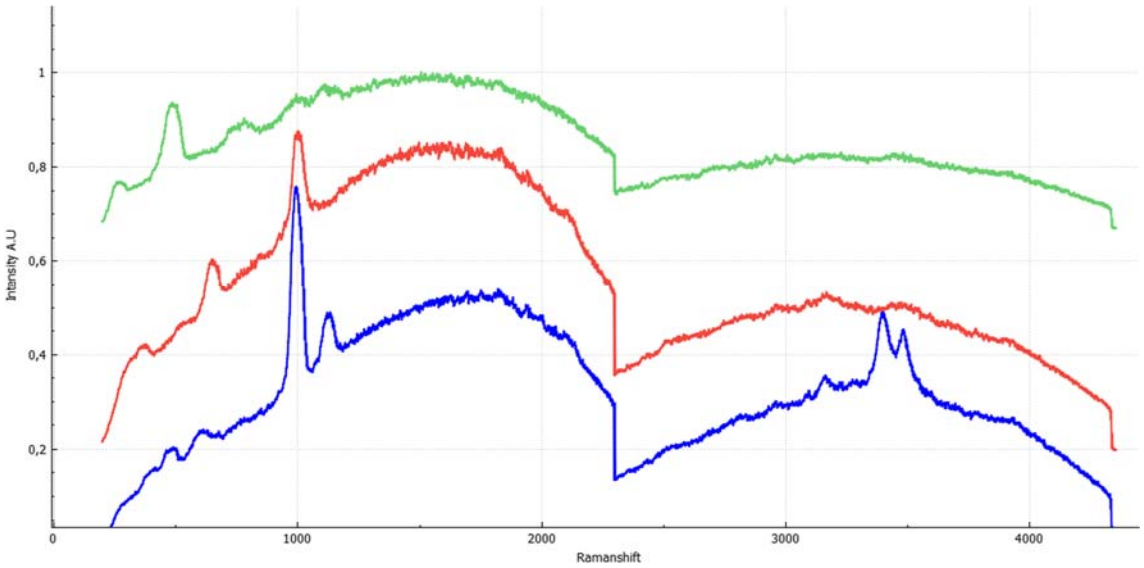

FIGURE 1-16 ESPECTROS OBTENIDOS CON EL SISTEMA REMOTO RESUELTO EN TIEMPO DE: YESO (AZUL), DIOPSIDO (ROJO) Y ORTOCLASA (VERDE).

En concreto, con nuestro sistema, con una fibra de 200 micras actuando como rendija obtenemos resoluciones, en Raman, superiores a los 25 cm^{-1}, 40 cm^{-1} en la banda principal del yeso mostrado en Fig. 1-16. Esta resolución es inaceptable para aplicaciones en mineralogía, de hecho, casi no se distinguen la banda principal del yeso y el diópsido. La sustitución de una fibra de 200 micras por una de 50 micras acarrea una pérdida de luz de un 75 %, aunque soluciona en parte el problema de la resolución. Para ello contamos con una mejora que no he podido implementar en la preparación de esta tesis: una fibra multi núcleo con siete núcleos de 50 micras que en un lado tienen configuración circular, aumentando el área de captación de luz en el lado de la lente, y configuración lineal en el otro, simulando una rendija de 50 micras. No se han realizado pruebas, pero esta configuración, similar a la empleada por SuperCam, puede mejorar la resolución del sistema y dejarlo en valores del entorno de 10 cm^{-1}. El material no ha

estado disponible para publicar resultados en este tesis, pero es una mejora del sistema a realizar de manera inmediata.

1.3.3 Desarrollos remotos en exploración planetaria.

Finalmente, y focalizándome en los desarrollos de sistemas remotos para exploración planetaria, hago un repaso a los sistemas propuestos hasta la fecha y los que volarán en un futuro inmediato.

Si hay una misión que ha significado un punto de inflexión para la espectroscopía Raman aplicada a ciencias planetarias, esa es Exomars. En momentos previos de definición de la misión Exomars contaba con un sistema combinado Raman-LIBS que además era remoto, como se relata en (Rull, 2017). Llegando incluso a desarrollarse un espectrómetro para abarcar todo el rango, diseño a cargo de la empresa TNO. Cambios en la misión al final decantaron la balanza del lado de un instrumento Raman de contacto, pero constituye la primera vez que un sistema combinado Raman-LIBS estaba considerado para una misión de exploración planetaria.

LIBS entraría después al anunciarse la inclusión de ChemCam (Wiens, 2012), contando con la colaboración de IRAP, que ya participaban en Exomars en RLS, y que habían jugado un papel importante en lo tocante a LIBS remoto. Chemcam es el primer instrumento LIBS remoto que se emplea en exploración planetaria, y lleva dando espectros de la superficie marciana desde el año 2012 hasta la actualidad.

Años después, con la decisión de NASA de lanzar una segunda misión con una gran carga de herencia (Mars2020) se llega a SuperCam, (Wiens, 2017), que ahora si constituye el primer instrumento combinado Raman-LIBS y remoto para ambas técnicas, que se incluye en una carga útil de exploración planetaria.

Durante el año 2020 se lanzará además otra misión China, HX-1, que constituye el primer intento de su agencia espacial de aterrizar carga útil en Marte. Dentro del rover que forma parte de la misión se ha incluido un instrumento LIBS muy similar a ChemCam, pero del que no he podido encontrar bibliografía relevante.

Para el futuro no existen, al menos de momento, misiones planteadas que puedan incluir desarrollos remotos. MMX incorporará un Raman de contacto en su rover MASCOT, y para un hipotético Europa Lander se ha propueto también un instrumento Raman, pero dado el concepto de misión sería de contacto, y parecido a Sherloc o RLS (JPL, 2016).

2 SuperCam and the SuperCam Calibration Target

2.1 MARS2020 mission

Mars2020 mission is flagship mission from NASA with a high heritage from the previous, and highly successful, mission Mars Science Laboratory. The mission is included in a long term plan that has as goal the human exploration of Mars.

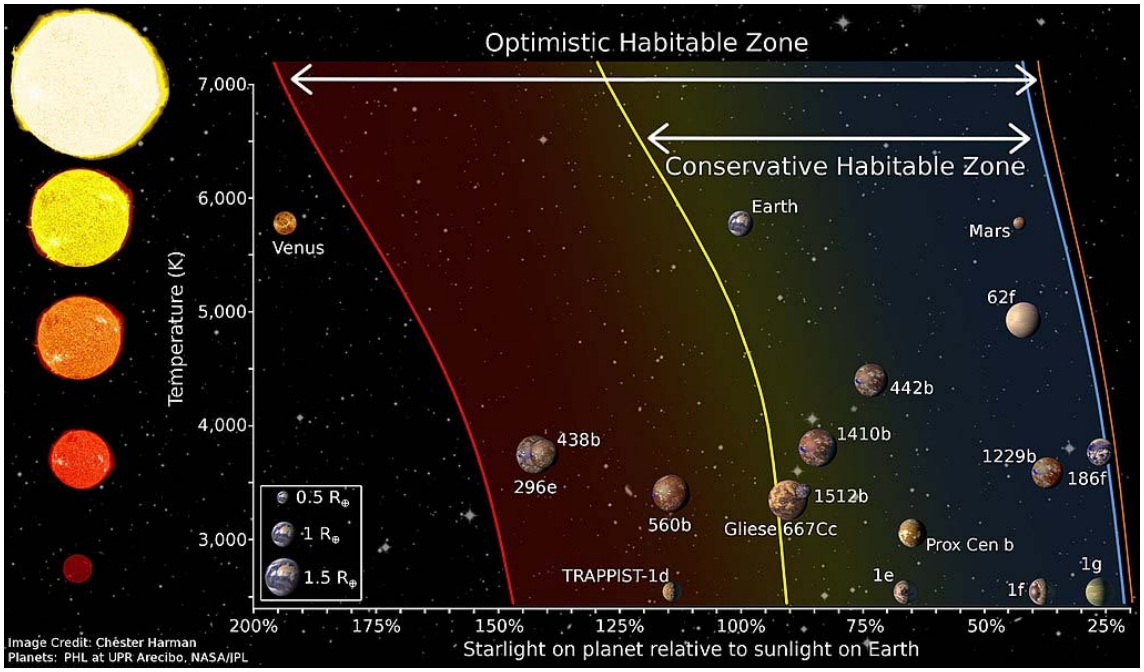

FIGURE 2-1 PLANETS KNOWN IN HABITABLE ZONE

Since Viking missions, the position of Mars within what can be called a conservative habitable zone of our solar System has made the red planet of great interest for astrobiology. Later missions have contributed to know more about its habitability increasing its astrobiological interest. Now we know that water flowed in Mars in a distant past, that there was an active geology, a thicker atmosphere, and conditions that could lead to the emergence of life. Mars 2020 will focus on the past and present habitability of Mars, participating in the Mars Sample Return Program (Foust, 2019) and also help in the development of tools and knowledge capital for human exploration.

The payload was selected according to these objectives and includes several analytical techniques, with a remarkable presence of a new technique in planetary exploration as Raman spectroscopy, present in two of the instruments. Again, the high heritage of the mission is evident in part of the selected payload, with some space to new concepts.

2.1.1 Definition and background

In 2011 the Mars Science Laboratory was launched, for that mission with a estimated cost of 2600 millions of Dollars several key components and technology were developed.

For first time a mobile platform was powered with a RTG (Radioisotopes Thermal Generator) allowing higher mass and power consumption of science payload than in previous missions. Since its deployment on the surface of Mars in 2012 to present days, MSL (Mars Science Laboratory) has contributed to a better knowledge of Mars exceeding its initial mission time of 23 months representing a great success from the scientific point of view and the engineering development of the mission.

This success and some of the technological developments used in MSL were found to be useful in the definition of a new flagship mission to Mars, Mars2020. This mission would take advantage of the developments made for the MSL rover, the arm and the mobility system among others, and its EDL (Entry and Descent Module, the skycrane), to develop a new rover with an improved payload that could play a role in the next two challenges to be faced by NASA: the samples return (allowing a greater scientific outcome using earth based laboratories) and the human exploration of Mars. In a effort to contain the costs associated to the development in some areas, part of the spare components from MSL have been used in the assembly of Mars2020.

From MSL scientific outcome it was evident that at least some regions of Mars could have been habitable in the past. Although there is some lack of definition on the time frame of this habitability, and if life finally could appear or not. To fill this gap in the knowledge of Mars the best possible option is to leave behind the constrains derived from the instrumentation that could be sent to Mars, and take selected samples from Mars to Earth where could be analyzed with ground based equipment.

With this in mid, the science payload could be then defined not to directly find biomarkers, but with the objective of analyzing the geological context looking for the best outcrops where biomarkers could be preserved (JPL, 2013). The payload was then announced in July 2014, also reflecting MSL heritage in the final selection of some instruments, leaving space for the new requirements on payload. If this scientific payload is compared to the scientific payload on MSL it is evident how resources have been redistributed from instrumentation to cover one of the main objectives of the mission, the collection of samples for their later return to Earth.

2.1.2 Objectives and context in future missions

FIGURE 2-2 MARS 2020 LOGO

NASA's seeking for signs of life on Mars is evident in the definition of the objectives of the Mars2020 mission. As commented before, and once identified the need of taking samples back to Earth, need also identified in the Planetary Decadal survey for the decade of 2013-2022 as a great priority, this search of biomarkers can be addressed in a different way. This way implies to give some efforts to the identification of the best context in which life could have existed on Mars, and the evidences of this past life could have been preserved from the harsh environment of Mars, but not necessarily trying to detect these signatures *in situ*. In the objectives defined for the mission there is also a spot to human exploration, as some technology developments could be tested in this mission, as well as getting a deeper, and more human exploration oriented, scientific knowledge of the planet. Can water be found in low latitudes? What can be extracted from the underground on Mars? Do we know enough about the Martian climate? All of these have been considered and summarized in four main objectives for the mission that are as follows:

- **Objective A:** Explore an astrobiologically relevant ancient environment on Mars, its geological processes and history, including the assessment of past habitability. It was already discussed, there are evidences of past water flowing on mars, and we have enough data to say that in the past some regions of Mars could host life, but unfortunately, more data is needed on the geological history of these regions. It is necessary then to have a good understanding of the geological processes that happened in a determined area, and also to have a good idea of its history and time scale.

This better understanding of the geology of the area needs to be done at different scales, and this a lesson learned from different mission. There is always a changing picture of Mars when analyzing the orbiter data and comparing them to the data collected *in situ* by landers and rovers. The full picture could only be obtained with multiscale observations, placing in the context of morphology and other data from orbiters, the more detailed findings and measurements from the rover.

The aim of this effort to better understand the geological past of a region of interest of Mars surface is to get a better assessment of past habitability.

Habitability requires the confluence of four different factors: the presence of raw materials that could be turned into organic chemistry (so called CHONPS), an energy source to power all the chemical transformations that life means, the presence of liquid water to be used but possible life forms, and favorable conditions for the emergence, evolution and persistence of life. In this last requirement we can include the presence of liquid water for sustained period of time, this is not a seasonal appearance, the salinity of that water, pH, temperature, energy of the water (was it still, or was it a raw stream) …

FIGURE 2-3 CONDITIONS OF A HABITABLE ENVIRONMENT (JPL)

Once the habitability has been assessed, there is another geological factor to study which is the potential preservation of this habitability. In this case, the geology of the area may have recorded several environments during Mars geological history, so a good geological study of different layers and units is of capital importance to understand if the region was habitable during a time enough to allow lifeforms.

To accomplish this objective, it has been found by NASA that the following measurements need to be done (JPL, 2013):

- Context imaging
- Context mineralogy
- Fine-scale imaging
- Fine-scale mineralogy
- Fine-scale chemistry

The payload selected should be able to address these kinds of measurements required to understand better the geology and habitability of Mars.

- **Objective B:** Asses the biosignature potential preservation within the selected geological environment and search for potential biosignatures. The current conditions of Mars are not the best place to preserve complex organic compounds that are usually related to life. UV radiation and other oxidants can have degraded the organics into smaller simpler compounds and therefore, it is particularly important to look for these biomarkers in places where they could have survived while protected from the environment.

Not only is important for these compounds to be preserved, but also the conditions in which they appeared, which could be crossed with the geological history of the zone and provide a better understanding of the moment and conditions in which life emerged.

So, first, it is needed to define what compounds are directly understood as a consequence of past lifeforms. The scientific report distinguish between two main

groups of these biomarkers, Definitive BioSignatures, understood as those organic compounds too complex to be explained without the presence of life like ADN, and Potential BioSignatures, that are those that might have a biological origin but not necessary mean the presence of life for their existence, as could be some amino acids that appear in Miller-kind experiments. These final kind of biosignatures can also be a result of the weathering and degradation of the DBS. This a difficult task that has no perfect agreement among the scientific community.

Apart from the definition of biosignatures, measurements are required to asses their preservation from the martian environment, along with the possible detection of PBS, and given the low amount expected, those measurements are inherently needed at grain scale, so microscopic techniques and micro imaging are required for the objective B, along with the capabilities to understand the geochemical context of the possible detection, and being able of the detection of PBS or DBS in these measurements.

In this context, the following chart describes the capabilities of several techniques and their requirements in terms of processing of the sample:

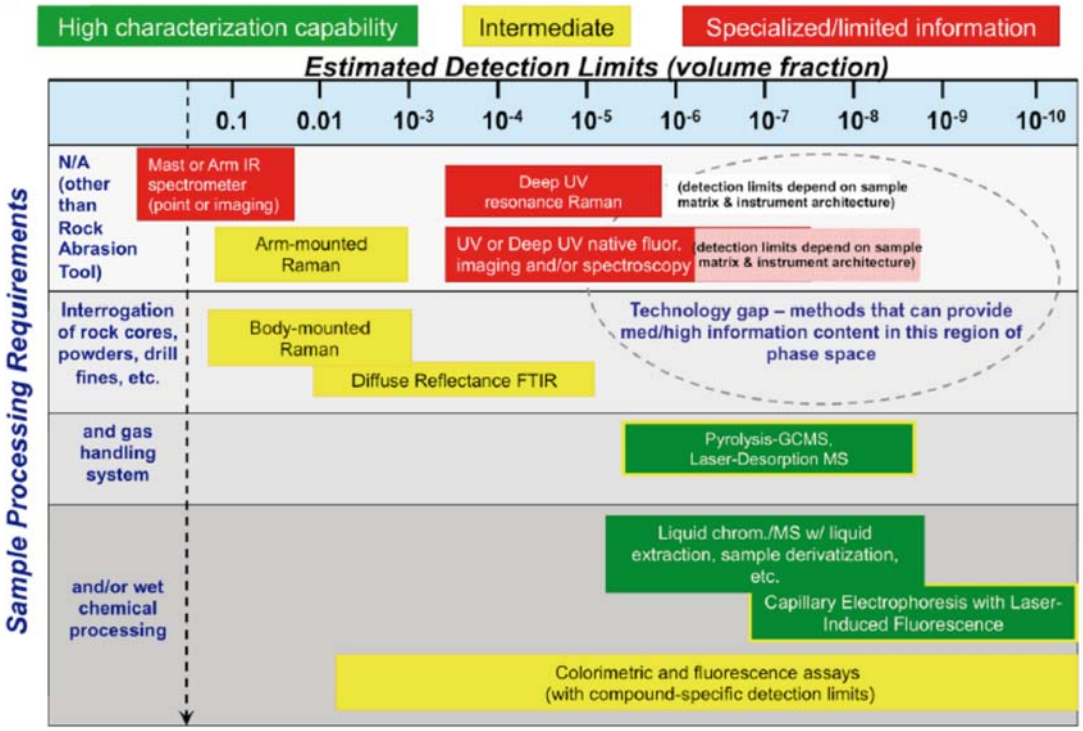

FIGURE 2-4 INSTRUMENTATION FOR MEASURING ORGANICS (JPL)

In the chart, just techniques for the measuring of organics are evaluated, in the context of the Mars2020 mission, which is intended to be a “field agent” for sample collection more than an analytical laboratory itself. Because of this, those techniques that require more complex processing could be discarded. On the other hand, if we are looking for techniques that require no, or almost not, processing, the table shows several examples of vibration spectroscopy techniques with several mentions to Raman spectroscopy based instruments.

This approach of understanding the Mars2020 rover as a field agent is also supported by the following table from the reference (JPL, 2013), in which the in-situ analysis of Possible Biomarkers is compared against the Earth based laboratories.

TABLE 2-1 BIOSIGNATURE ANALYSIS IN SITU VS EARTH BASED (JPL)

Measurement Factor	*In Situ* PBS Analysis	Earth Lab PBS Analysis
Spatial Resolution/ Target Mass or Volume	Wide FOV "bulk" analyses averaging many mineral grains and surfaces. Focused beam analyses down to ~10 mm.	Bulk analyses or individual mineral grains; Focused beam analyses down to < 10 nm.
Sample Preparation	Minimized due to complexity. Abrading, powdering, possible to combine simple reagents.	Abritrarily complex solid (thin section), gas, or liquid extractions and separations.
Limit of Detection	Typically in the ppmw-ppbw range for bulk analysis. Can go lower with extra sample prep.	Can achieve <pptw (10^{-12}) for targeted compounds in small bulk samples or extracts.
Selectivity	Many techniques are broad-band by design, with some ambiguity accepted. Others target selected species with higher sensitivity.	Multiple techniques available to pick arbitrary species out of matrix with a targeted molecular probes or high mass resolution.
Structural Analysis	Possible but limited in scope and possible LOD of compounds.	Molecule structure can be unambiguously identified.
Replicate Analysis	Limited by mission scope, resources, and analytical power.	Arbitrarily high capability; samples can also be archived.
Responsive Analysis	Highly capable as long as follow-up is within mission scope, instrument capability, and rover range. Otherwise, limited.	Extremely capable as long as follow-up analysis is possible with returned samples (limited only by variety collected).

It is clear then that the Mars2020 rover should focus more in the selection of good samples and candidates to preserve biosignatures or primary detection of those, than a complete detection based on complex analytical techniques, and the payload was selected according to this principle.

- **Objective C:** Sample return and support to the future mission to return scientifically selected samples to Earth. Since the first definition fo the objectives of the mission until the present days several changes and advances have been made towards a sample return mission. At the moment, the greatest advance is that ESA will join forces with NASA to accomplish this mission with expected launch 2026, with a joint confirmation from both agencies expected for beginning of 2020.

This joint mission implies a total of three launches of three different spacecrafts from which Mars2020 is the first one. After Mars2020 finds and select what samples are the best candidates to be collected for their return to Earth, another mission will be launched including a fetching rover from ESA, that will gather the sample tubes collected by Mars2020 and put them in a surface platform from NASA. This platform will include a launcher that will get the samples to Mars orbit where another mission, from ESA, will catch them and do the trip back to Earth. Schematic design of the mission is shown in the next figure from ESA.

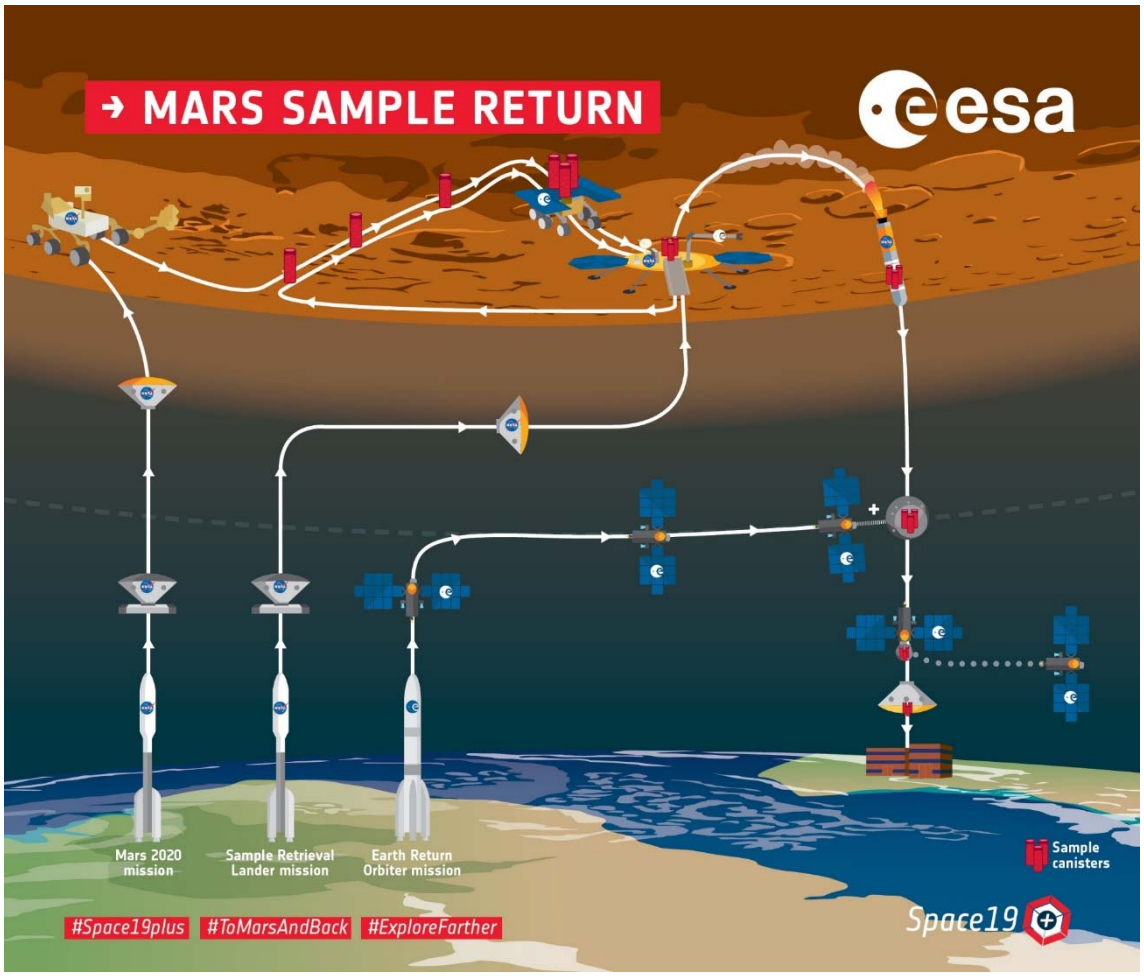

FIGURE 2-5 MARS SAMPLE RETURN JOINT MISSION. (ESA)

As it was stated in previous objective, the general agreement among the scientific community is that a definitive detection and characterization of possible biosignatures in Mars could only happen with equipment and techniques used on Earth. Also, in parallel with this increasing interest in the astrobiology community, the technical developments are now making possible to face this challenge.

Said this, the objective for Mars2020 mission is to be able to take several caches from selected samples, store them in a safe container that is later compatible with the return mission. In this line, the factors to take into account in the decision of what to take back to Earth are basically the following three:

- The cache has enough scientific value to be taken to Earth. In this evaluation the scientific payload of the Rover is the only tool available.
- The cache is compliant with the Planetary Protection requirements. This means that the caching was done with clean hardware that ensures that possible micro organism or spores that could be sent to Mars are not contaminating the samples and taken back. This could mean a false detection of biosignatures when the samples are analyzed on Earth. Also, the caching of the sample needs to be safe for

Earth, avoiding the leak of foreign contaminants once on Earth, and the opposite way, not allowing Earth contaminants to get into the container until in an adequate facility.

- The cache is feasible to be stored and is compatible with the technical constrains and requirements.

- **Objective D:** contribute to the human exploration of Mars. Again, since the initial concept and definition of objectives of the Mars2020 mission, bold advances have been done towards the landing of humans on Mars. The announcement of Artemis program, that means the return of human missions to the Moon, remarked that going back to the Moon is a necessary step before going to Mars, and this human exploration of Mars is part of the objectives of Artemis. Mars 2020 is also a contributor to this final goal, as can be seen in the following diagram of technologies and previous developments needed to put humans on Mars in the decade of 2030s.

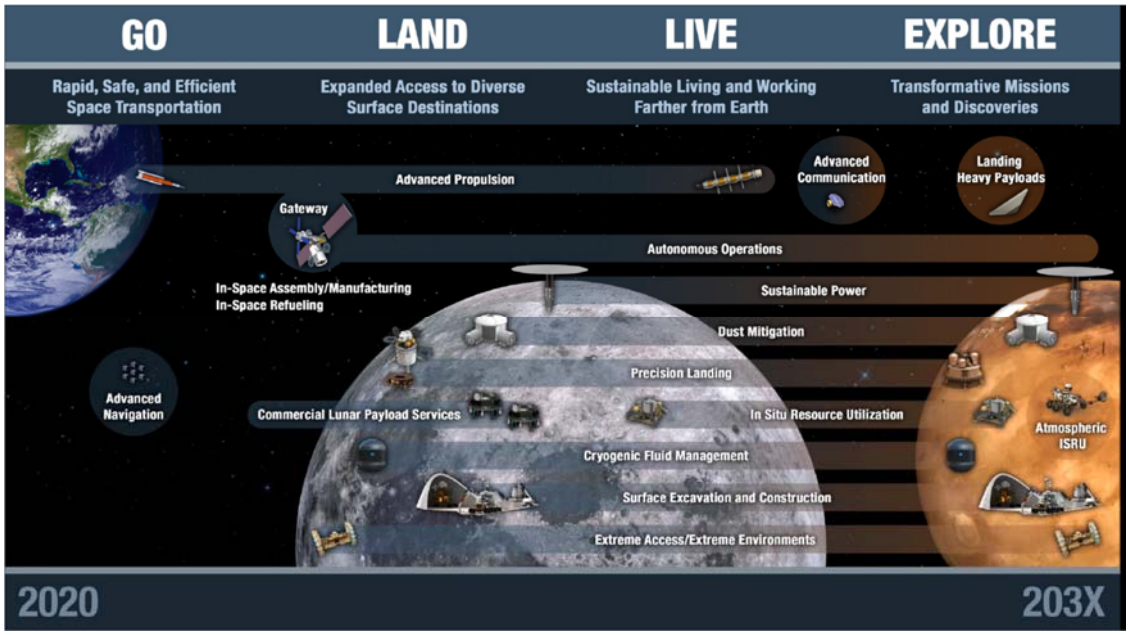

FIGURE 2-6 TECHNICAL DEVELOPMENTS NEEDED FOR HUMAN EXPLORATION OF MARS (MEPAG)

Mars2020 needs to contribute to the human exploration of Mars providing useful information from Mars and the environment and possible threats that future astronauts will face. Also, given the characteristics of this kind of missions, the self sustainability of the base on Mars will be necessary, and that means identify key materials and compounds that can be used by humans, for example water.

It is necessary for this exploration to have a deep knowledge of martian climate and weather, sand storms could represent a major risk for human settlements on Mars and their characterization and prediction is crucial. Another risk, omnipresent on Mars, is the dust. It is necessary to improve what we know of the dust and its interaction with flight hardware to evaluate the possible threats derived from it. Another important factor is, could this dust represent a threat to the astronauts itself? Is it toxic?

Characterization of the dust is then a major priority. In this same evaluation risks, are there any organics or biocontaminats that could also represent a threat? This needs to be addressed.

Water is an important asset for human exploration and it represents an example of the importance of having a deep understanding of the geochemical nature of Mars, sources of water, hydrated minerals, is there water trapped in the permafrost? How much?

Finally, as a preparation for the human exploration, Mars2020 could be used a testing platform for technologies to be used in this human missions. For example the development of systems to extract O_2 from the atmospheric CO_2 or to extract water from the subsurface. Another example could be the self navigating and landing technologies, a better characterization of what is happening to the EDL.

All of these examples could addressed directly by the rover or coud be addressed using the return samples, however, it is clear that Mars2020 will play a key role in the human exploration of Mars.

2.1.3 Mission details

Mars2020 mission has its launch window schedule between July 17th and Augus 5th 2020, with an estimated date of landing of Feb 17th 2021. Its prime mission time, this is the nominal time of the mission, is of one Mars Year (687 Earth days), although it is expected that it will last longer, as its twin mission did.

The selected landing site is Jezero Crater. This landing site was selected in early 2019 after several workshops, and was selected among the other two finalist sites, NE Syrtis and Columbia Hills. Both, Jezero and NE Syrtis are close and both are in the Syrtis Major quadrangle.

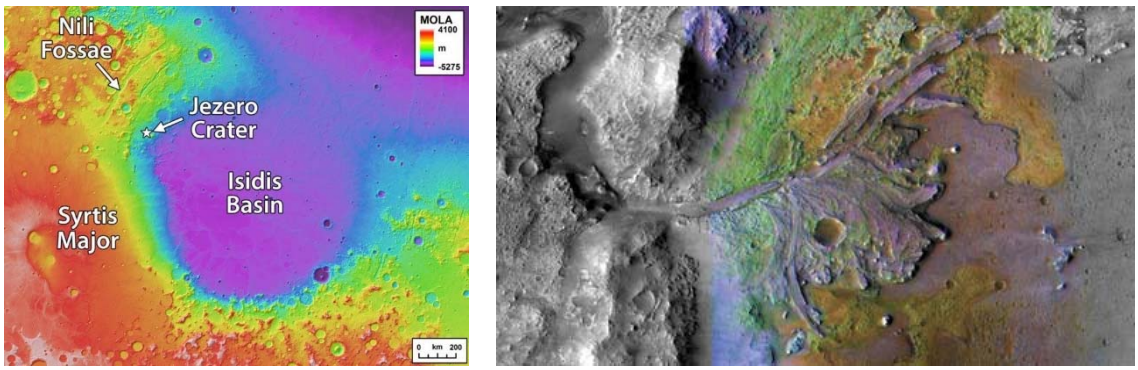

FIGURE 2-7 JEZERO LAKE POSITION, AND ITS INTAKE FAN.

This landing site was selected because at lest in two moments of its geological past could had water, in fact it looks like it was a lake once, and this water lasted for a long time in Jezero. Low energy water, as in a lake, and preserving that water for a long time, are

arguments that make Jezero a unique place to look for past life on Mars. Also its proximity to NE Syrtis make feasible to do a 2 in 1 extended mission, and exit the lake towards Nili Fossae.

The Mars 2020 Rover is a high heritage rover, with several components shared with curiosity, although some systems have been updated. Both mission will use the same system for the entry and descent, the famous skycrane, and both mission will use similar chasis and motion systems, also with the same power source (Radioisotopes Thermal Generator).

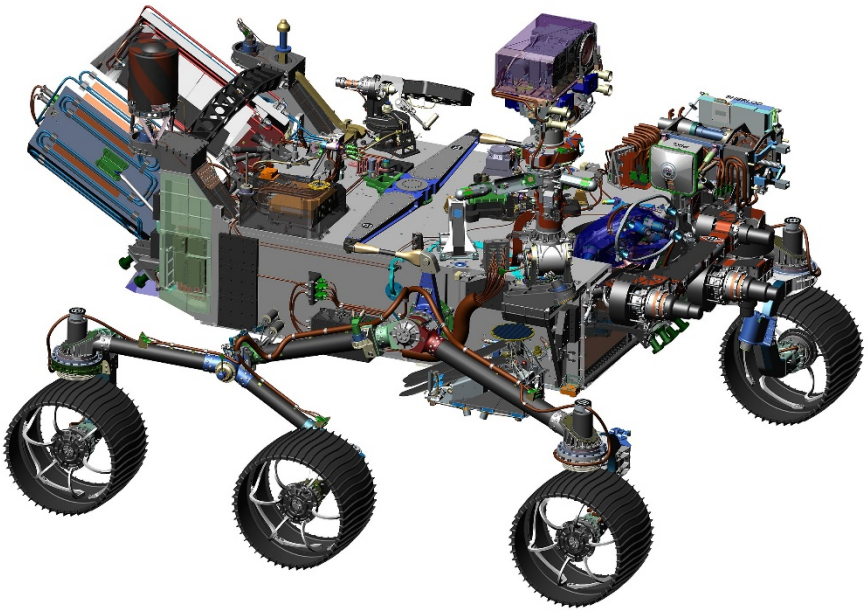

FIGURE 2-8 MARS 2020 ROVER 3D MODEL

The arm has changed, as it now has more payload attached to it, and the drill of the Sample Caching System has also grown.

The SCS is of great importance as it is the capital element to fulfil requirement C, and also because is the first step of an ambitious, multi mission plan to return samples to earth. On Mars, the drill will be able to perform similar functions to RAT, abrading the surface of a target to get details from underneath its oxidation crust, or extract cores from a selected target. Different bids will be available in the belly pan, where the storage of the samples is also carried out. The system will have the capability to extract and store 42 samples into a sealed and sterilized tube..

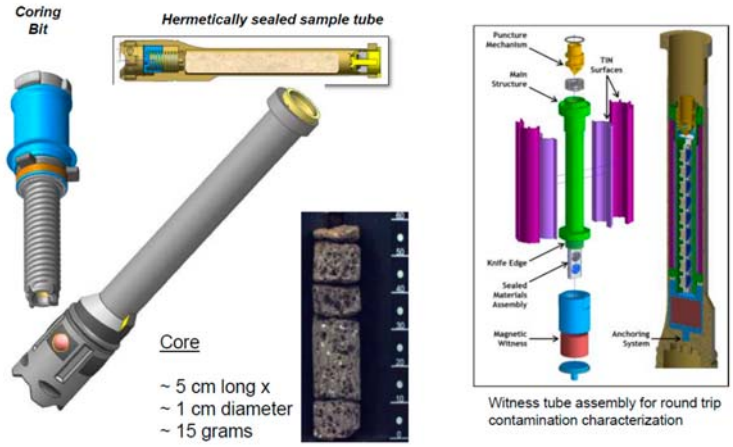

FIGURE 2-9 SAMPLES AND WHITENESS TUBES OF THE SCS (JPL)

Along with the samples witness tubes will be stored to monitor the possible contamination that has been accumulated, and have this into account in the measurements to be done on earth.

A final interesting feature that will travel with Mars 2020 Rover is another technological demonstrator: the heliscout. Martian atmosphere is over 100 times lighter than Earth's atmosphere, and that makes a real challenge to any flying hardware. JPL is taking this opportunity to fly a lightweight, solar powered, double rotor helicopter that will fly around the Mars2020 Rover and will operate during the first days of the mission. The technologies and lessons learned can be used in the future for a new breed of exploring drones.

2.1.4 Payload

After the setting of the objectives of the mission NASA could define the best payload to serve those objectives. In its preliminary report (JPL, 2013), before the final selection, it was discussed the kind of measurements that might be needed depending on each objective:

TABLE 2-2 OBJECTIVES OF THE MISSION VS MEASUREMENTS NEEDED (JPL)

Objective A *Geology*	Objective B *Biosignatures*	Objective C *Caching*	Objective D *HEO/Tech*
THRESHOLD Instruments addressing all 6 threshold measurements			OPTIONS
Measurements/Capabilities	**Measurements/Capabilities**	**Measures/Capabilities**	
•Context Imaging •Fine-Scale Imaging •Context Mineralogy •Fine-Scale Elem Chem •Fine-scale Mineralogy	•Context Imaging •Fine-Scale Imaging •Context Mineralogy •Fine-Scale Elem Chem •Fine-scale Mineralogy •Reduced/Organic C detection	•Context Imaging •Fine-Scale Imaging •Context Mineralogy •Fine-Scale Elem Chem •Fine-scale Mineralogy	• ISRU Demo • EDL Data • EDL Precision & Site Access • Surface Weather Monitoring • Biohazards to Astronauts
BASELINE OPTIONS Enhanced-capability instrument(s) in THRESHOLD category OR add one of the following:			
•Subsurface Sensing •Organic C detection	•2nd method of Organic C Detection	•Organic C Detection	
ENHANCED OPTIONS Enhanced-capability instrument(s) in THRESHOLD category **AND** an additional BASELINE or ENHANCED instrument			
	•Molecular Analysis		

The first three objectives share the same kind of measurements, while the last one, the one related to human exploration, may need specific developments to be addressed.

Apart from this objective-oriented definition of the payload, the operation of the rover can be also taken into account for the definition of the payload. Given the complexity of any operation including the displacement of the rover, previous data helping in the decision making on where to go with the rover is always welcomed. In the case of MSL, the availability of a complete imaging suite from navcams, along with Mastacm (incorporating some spectroscopical features) and ChemCam providing high magnification images and elemental composition data around the rover, helped in the decision making on where to move the rover and proceed with contact techniques.

Another factor to remark before describing the complete payload to be sent to Mars is the high heritage of the mission. This heritage takes profit of the experience, developments and lessons learned from MSL to reduce risks in the development and manufacturing of the new rover. Said this, the science payload of Mars 2020 mission is composed by the following instruments:

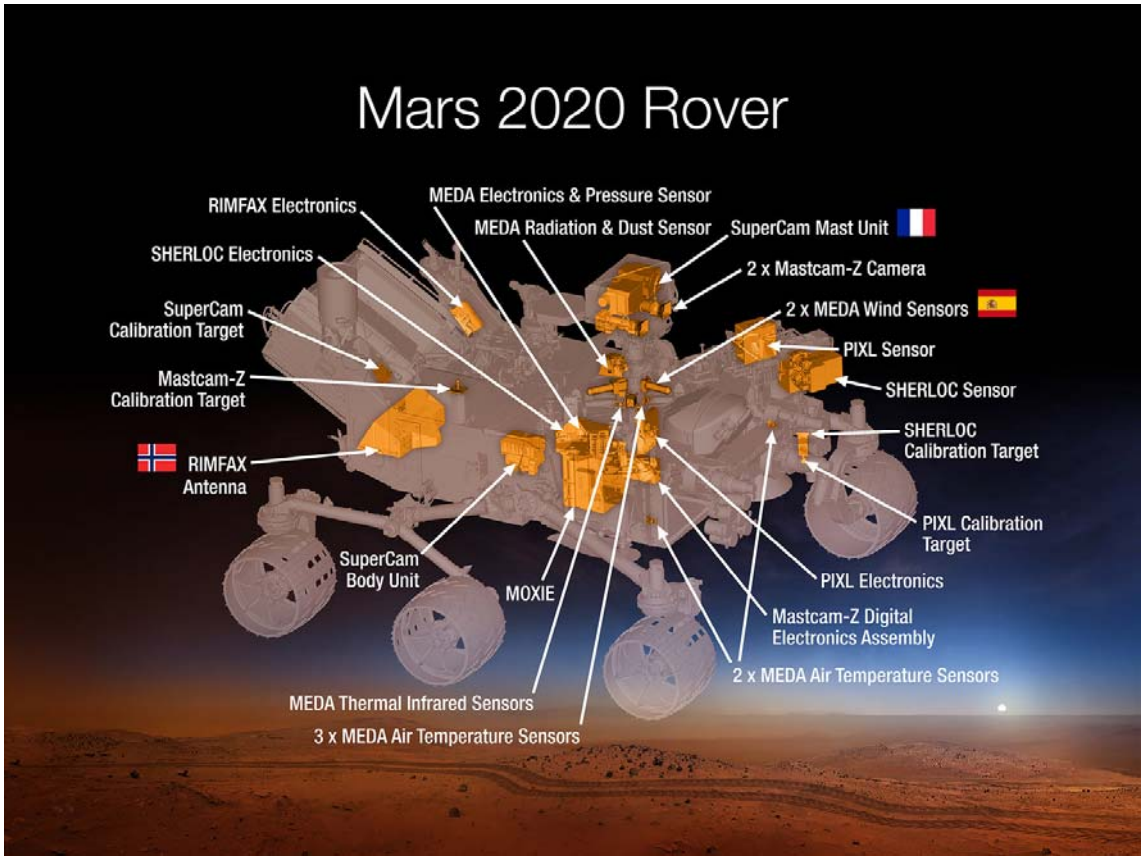

FIGURE 2-10 SCIENCE PAYLOAD OF THE MARS 2020 ROVER (JPL)

2.1.4.1 MastcamZ:

MastcamZ is a direct successor of Mastcam, and as in the latest, the general description of this instrument could be a stereoscopic camera system capable of taking color images and short videos, or providing some spectroscopic data of the objects thanks to a filter wheel. The main difference in MastcamZ is the incorporation of zoom capabilities and a better image quality.

The principal investigator is Jim Bell, from Arizona State University, and the technical and science team of MastCamZ includes researchers from JPL and Niels Bohr Institute among other institutions (Bell, 2016).

MastcamZ will be mounted on the rover mast, right under the Mast Unit of SuperCam (to be described further on). It consist on two cameras mounted at 2 meter height and separated by 24 cm, that will provide 3D stereoscopic images of the surface of Mars. The total weight of the system y 4 kilograms and regarding the technical capabilities, the cameras will provide color images with a resolution of 1600 by 1200 maximum. The final resolution can be changed by taking ROIs. Regarding the color, the quality would be similar to a consumer camera based on a bayer filter matrix. Thanks to the zooming capabilities of MastcamZ, now the achievable resolution can vary from 150 microns per pixel to 500 microns mm per pixel at 2 meter distance, or between 0.74 and 2.7 cm per pixel at 100 meters.

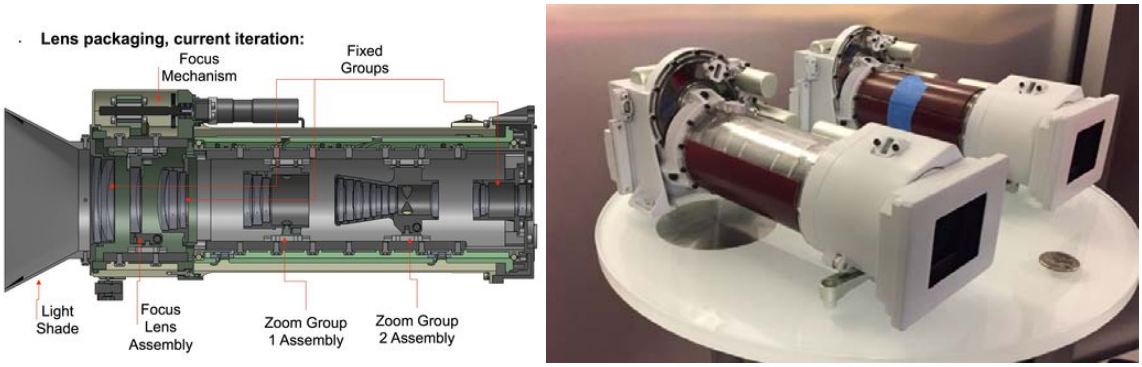

FIGURE 2-11 MASTCAMZ OPTICAL DESIGN AND MODEL

The cameras of MastCamZ will cover a spectral range from 400 to 1000 nm, and this range can be swept by means of 11 narrowband filters.

This instrument will be able to characterize the martian landscape morphology, given a context for other measurements. Will be used to asses the topography, stratigraphy and in general to obtain a good picture of the past geologic processes that happened in the analysis area. At the same time it will provide information about the texture and more concise characteristics of outcrops. It will also observe the sky, characterizing the opacity of the atmosphere, observe clouds or dust storms that will help in the study of martian

weather. Finally, MastcamZ will give support to operations providing information that will help with rover navigation, and providing information from what has been called “remote science” suite.

Given the characteristics of the instrument, its imaging capabilities can mean an asset for the objectives A, B and C, identifying the best context for biomarkers and geological processes, as well as objective D helping with a better understanding of the climate dynamics of Mars.

2.1.4.2 MEDA:

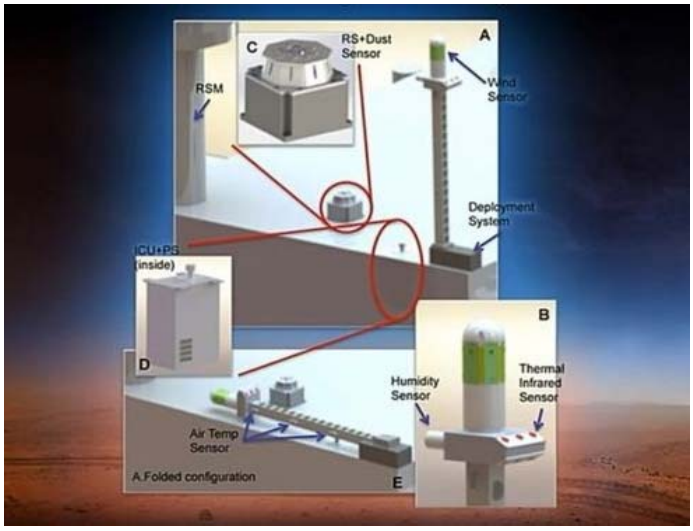

FIGURE 2-12 MEDA SENSORS (JPL)

Continuing with the heritage instruments, MEDA, standing for Mars Environmental Dynamics Analyzer represents the evolution of the weather station on board MSL, REMS. MEDA is also the main contribution of Spain to Mars 2020 mission, the PI is J.A. Manfredi from the Astrobiology Center, CAB. MEDA incorporates several sensors on the mast and the rover deck allowing to investigate (Manfredi, 2013): characteristics of the dust and the transparency of the atmosphere, dynamics of dust lifting and deposition, dust storms; general weather dynamics in Mars, with measurements of pressure, temperature, humidity or wind direction and speed; Correlate local atmospheric dynamics with large scale weather; the cycle of water in present Mars; study of the irradiance on Mars depending of the seasons; possible weathering conditions of the samples candidate for a caching, cooperate in the better understanding of the measurements and operations of other instruments as Moxie.

MEDA will provide useful information not only for the operations and objective C, also for objective D. As it was explained before, the dust is of great interest when studying Mars in preparation of human exploration. In absence of water, that is a factor that modulates the weather on Earth, the dust in suspension in the atmosphere on Mars, for

example, changes the irradiance received by the surface, meaning that the dynamics of the dust might have a great impact in the local and global climate of Mars. Also, the dust, its grain size and abundance among other characteristics, are of great interest when designing functional devices or structures to host a human mission on mars.

2.1.4.3 MOXIE:

Moxie represents a direct approach to the objective D, as it consists on a concept model of a technology that is directly intended to be used in the human exploration of Mars.

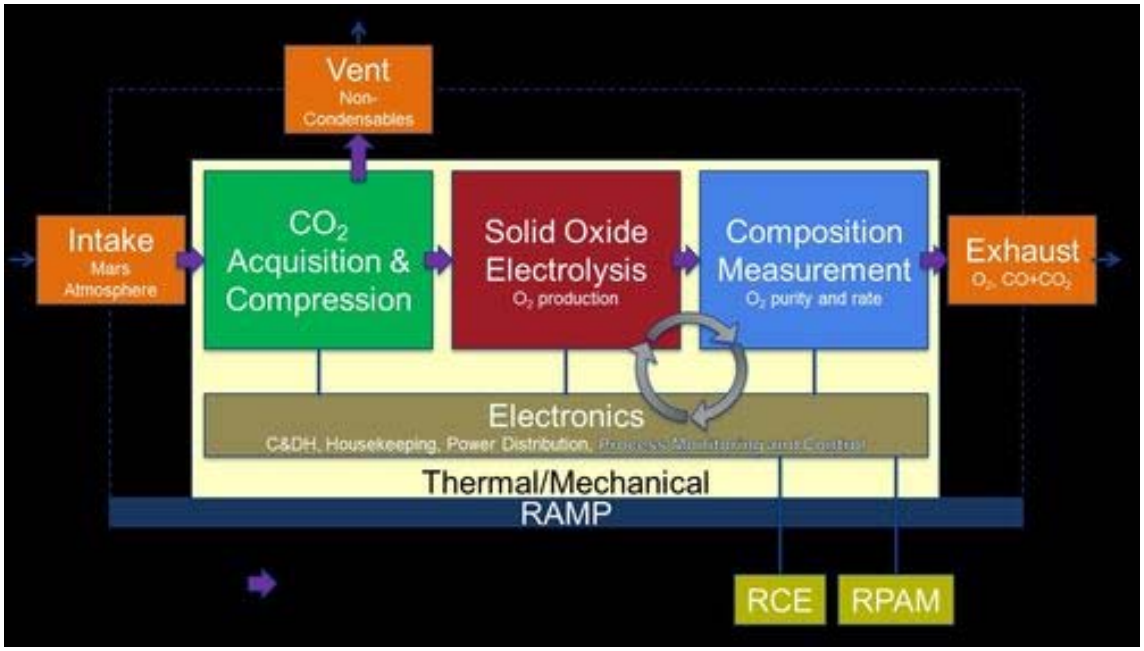

FIGURE 2-13 MOXIE WORKING SCHEMATICS

Moxie is a technological demonstrator for a system that could be used on Mars to obtain O_2 (Hecht, 2015) from martian atmosphere. This oxygen will be needed not only for the habitat of the astronauts, that will have to spend a long time on Mars, but also as propellant for the return mission. In this line, the minimum estimation is that at least 30 tons of oxygen would be needed for the launch from Mars, and this means that the transportation of that resource from Earth makes no sense at all. The best way to solve this is the In Situ Resource Utilization (ISRU), and produce the needed oxygen on Mars.

Moxie will be able to collect CO_2 from the atmosphere, compress it and heat it up to 800 ºC, adapting to the variable conditions on Mars, and obtain the oxygen by electrolysis to check later the purity of the products. At Moxie scale, a minimum of 10 grams of oxygen per hour will be produced, and this is supposed to be a 1% scale of the intended hardware to be used at the human exploration stage.

During the operation of the large scale system, it will need to work continuously for a long time to produce the needed amount of oxygen. This continuous operation implies

a need of adaptability to a very extrem environment with abrupt changes in temperature, atmospheric conditions, dust quantity, etc. For that reason this technology demonstrator needs to be tested at Mars before sending a full scale technology.

2.1.4.4 PIXL:

PIXL stands for Planetary Instrument for X-ray Lithochemistry, and it is one of the instruments mounted on the arm of the rover, making part of the called "proximity science" instrumentation of the mission. Its measurements are directly related to the geochemistry characterization of Mars, and therefore with the objectives A, B and C, providing fine scale imaging and elemental composition in image context. But also could play its role in the objective D identifying interesting materials that could be processed on Mars in the framework of ISRU, as Moxie. For example titanium oxides can be used for manufacturing of mechanical parts if a processing is developed.

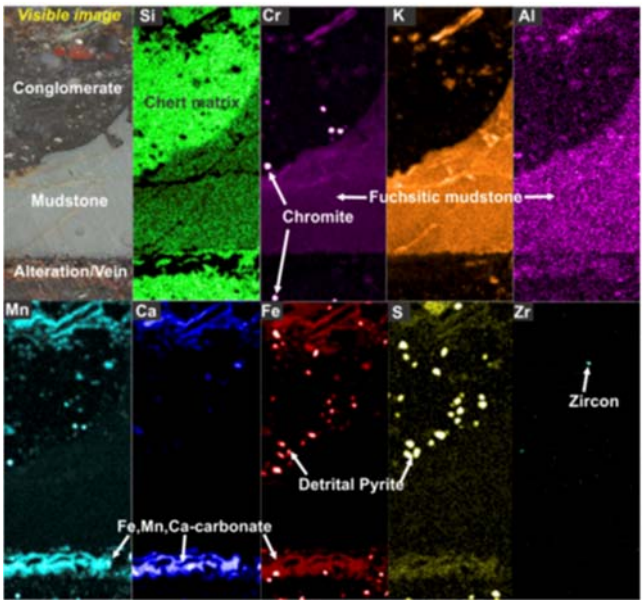

FIGURE 2-14 EXAMPLE OF A XRF IMAGE OBTAINED WITH PIXL

PIXL is an imaging XRF instrument with a submillimeter resolution, in fact, the X ray beam will have a 120 microns diameter. This beam will scan the surface of the samples allowing also flexibility in the measurement, being able to provide a full map, a point or a line. As happens with the technique, lighter elements are difficult to be detected, but elements from Na can be detected (Allwood, 2015).

2.1.4.5 SHERLOC:

Sherloc is, appart from the drill, the other tool to be placed in the arm, and along with PIXL completes the proximity science suite on board Mars 2020. SHERLOC standing for

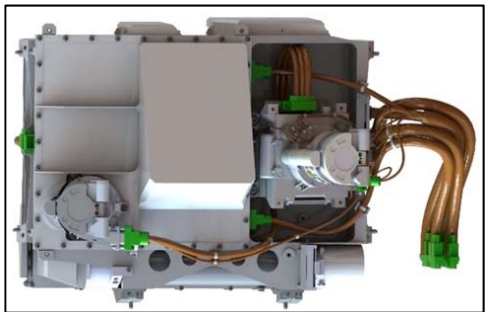

FIGURE 2-15 SHERLOC INSTRUMENT

Scanning Habitable Environments with Raman & Luminescence for Organics & Chemicals will be able to obtain Raman spectra in a 50 microns spot, and use its scan capability to obtain a Raman image of the sample in a area of 7x7 mm. the excitation source of this Raman instrument is a UV (248.6 nm) laser, and the whole system has been designed to minimize the detection limit of organics (Beegle, 2015). As it was covered in the introductory section, the Raman cross section gets bigger when the excitation source shifts to shorter wavelengths, and to be more concise, this relation is inversely proportional to the fourth power of its wavelength.

Another advantage of the UV excitation source, as discussed previously, is the fact that when obtaining a Raman spectrum, the spectral range to be measured covers from 250 to 270 nm, and that regions is far from the fluorescence emissions. Furthermore, the high energy of the excitation source enables resonances more easily that can improve the signal strength. However, the use of UV also implies difficulties to obtain a good resolution and could be problematic for mineralogy, and for that reason this feature could be more related to the objective B, and C. anyway, to the date, no results from this instrument could examined by the author nor were published, so the final resolution of this instrument could not be fairly evaluated. On the other hand, SHERLOC will also be available to study the fluorescence induced by the laser, giving extra analytical information.

Another feature from this instrument is its capability to obtain context images with a great magnification thanks to the add on called WATSON, standing for Wide Angle Topographic Sensor for Operations and eNgineering, that is a direct successor of MSL's MAHLI. With this add on, this instrument will have a imaging system mounted on the arm with a spatial resolution of 30 microns, covering an area of 2.3 x 1.5 cm. This imaging capability will have, as MAHLI did, several applications in the study of textures of samples, and also in the inspections to be done in the rover, helping with the engineering during operations.

2.1.4.6 RIMFAX:

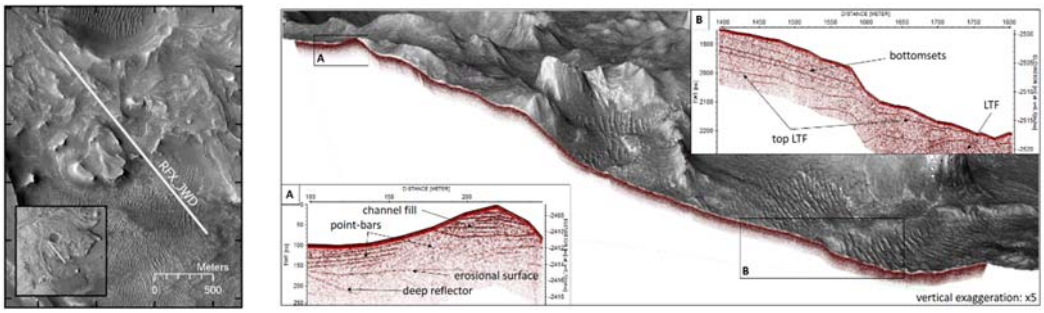

FIGURE 2-16 SIMULATION OF A CUTOFF MEASUREMENT OF RIMFAX IN JEZERO

The Radar Imager for Mars' SubsurFAce eXperiment its an interesting instrument for large scale geology, for objective A, and also for objective D. It also has a similar instrument on board another mission, ExoMars in this case, called WISDOM. This instrument will be able to use Ground Penetration Radar to map the vertical under the rover down to 10 meters depth (Eide, 2019). In combination with the displacement of the rover it will be able to provide cutoffs of the landing site at 10 cm of horizontal resolution, giving information of the layers under the rover and some idea of the kind of materials. It is specially interesting in the pursue of underground water reservoirs. More specifically, RIMFAX will be able to provide the following information: the depth of the regolith layer, identify the different layers and relate them to visible outcrops, characterize the stratigraphy of the area (key to understand past environment on Mars). In the figure 2.15, a simulation of a typical measurement of RIMFAX during the displacement of the rover is shown. Different layers of deposits on Jezero will be measured by RIMFAX.

2.1.4.7 SUPERCAM:

The final instrument to be described in the present work is SuperCam, the instrument that counts with the collaboration of the University of Valladolid and had coped most of the time of the author due to his technical responsibilities and management role, reason for it has been covered in its own section.

Anyhow, as a general description of the instrument, it is part of the remote science suite of the Rover, and will be able to use several spectroscopic technique at distances of some meters around the rover. Its unique combination of spectroscopic information of the elemental composition of a target, and also its structure, gives the power of having a pre-analysis on some targets that will be similar (with limitations from its stand-off operation) to the combined measurements of PIXL and SHERLOC.

2.2 SuperCam instrument

> *"I think if you do something and it turns out pretty good, then you should go do something else wonderful, not dwell on it for too long. Just figure out what's next.".*
>
> *Steve Jobs*

The quote above, from Steve Jobs, could not only describe his restless pursue to conquer the market of consumer electronics, but the current environment of space sciences. Go further, do more, do it better.

The SuperCam instrument is the Mars 2020 successor of ChemCam instrument on MSL-Curiosity. ChemCam uses LIBS spectroscopy, already described in the introduction chapter, to get elemental composition of targets around the rover, and also provides high magnification images of the targets. This instrument meant a breakthrough in the way operations and science were done in robotic exploration. For the first time an active spectroscopic technique could be used to characterize targets in the range of some meters. These standoff measurements mean a great advantage not only helping in the selection of the places to go with the rover, but also in the quantity of data that can be done, since from the operational point of view, a grat area around the rover can be assessed without moving the rover, increasing the data available covering more samples.

Now in SuperCam, in addition to LIBS, other spectroscopic techniques have been included such as: Time Resolved Raman Spectroscopy, Time Resolved Luminiscence, Visible-Infra Red reflectance spectroscopy, microimaging and sound recording. This complete suite of analytical techniques has increased the complexity of SCAM when compared to ChemCam.

2.2.1 Background

Talking about the background of SupeCam necessarily should start with its predecessor, and almost twin instrument, ChemCam. This instrument is a joint venture between Los Alamos National Laboratory in the US, and L'Institut de Recherche en Astrophysique et Planétologie in France. The last institution is also involved in ExoMars, and was there when the concept of RLS instrument was also a combined instrument called ExLIBRIS. Both institutions have great experience in the use of LIBS applied to Planetary Sciences and worked together in the development of a Stand-off LIBS instrument to be included in MSL, and are working together again for SuperCam. So when talking about the background and the situation behind SuperCam it should be remarked that the instrument has some heritage from another instrument, and more important, has a core team that have been working together since MSL with a greatly successful instrument.

ChemCam then has been providing remote elemental composition of the targets on Mars since 2012 thanks to its stand off LIBS capabilities, and also, thanks to the RMI, high magnification context images of the target. ChemCam was the first instrument ever to use this technique in a planetary exploration mission, a technique that is *virtually able* to detect any element and meant a different approach to the previous spectroscopic techniques deployed on Mars.

Previous to ChemCam and SuperCam, the mineralogy done on Mars was done using techniques such as Sojourner's APXS, standing for Alpha-proton X-ray Spectrometer, that used a radioactive source to irradiate the sample with alpha particles and measured the backscattered particles and X-Ray generated, or the Mössbauer spectrometers that were part of MER rovers. Those two techniques required contact with the sample and long times for data acquisition, lager than 10 hours in both cases, also in the case of Mössbauer instrument there were limits of the technique, very oriented to iron bearing minerals. A different approach was given by Mini-TES, providing thermal infrared spectroscopic data from the surface, but again this technique has its limitations, or the mass spectrometer on board Phoenix. So looking at the previous techniques it is clear that stand-off LIBS meant a change in the way things were done in operations. ChemCam is a simpler instrument form the operational point of view (not the technical), gives a complete information of the samples, in a short time and without contact, and also at a smaller scale than the mentioned techniques. This means more samples analyzed per sol and more science data to understand Mars and help operations. This kind of developments started in the late 80's and have became more and more popular as the technical advances allowed more compact lasers and detectors, making their way to Mars with ChemCam, and will be followed by SuperCam and another stand-off libs instrument from China, also to be launched in 2020.

ChemCam used a Q switched NdYAG laser (1064 nm), focalized using a telescope (both located in the mast) to reach the limit of plasma induction, and used the same focalizing optics to collect the light from the plasma. The emission from the plasma was then analyzed in the three spectrometers in the body of Curiosity (Wiens, 2012) (Maurice, 2012).

The Mast Unit in ChemCam was developed by CNES and IRAP, and included the telescope, the laser and the RMI. Starting with the RMI, it used a monochrome sensor, that means that the images are in black and white. The other companion of the RMI in the Mast Unit The laser in ChemCam provides 24 mJ during 8 ns pulses, with the capability of operating up to 10 Hz. With this power, it was able to reach the GW/cm^2 required to induce the plasma. Both use the Schmidt-Cassegrain telescope of 110 mm as optical element.

The Body Unit receives the light collected by the Mast Unit through an optical fiber for its analysis. In this Unit, the whole optical range is separated into three optical windows: the UV covering from 240 to 342 nm, the Violet covering from 380 to 470 nm, and the VNIR covering from 474 to 900 nm. The light is separated according to its wavelength in an optical demultiplexer and then introduced in each spectrometer. The spectrometers are Czerny-Turner, and use CCD detectors, not intensified and not gated.

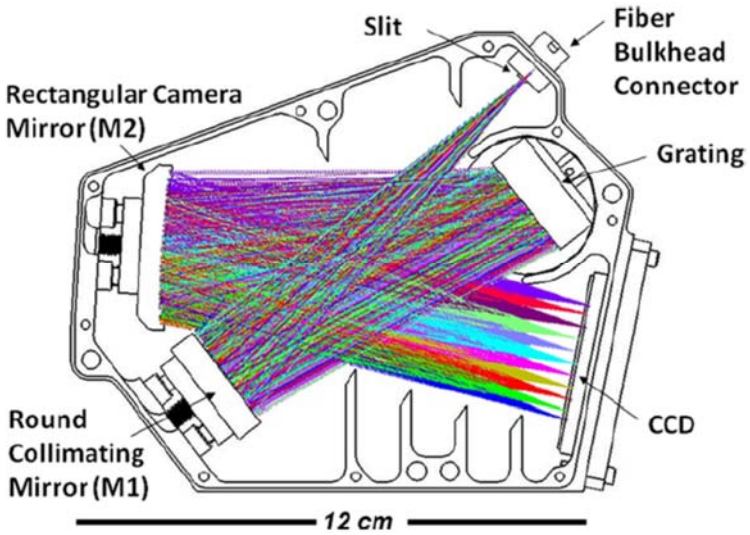

FIGURE 2-17 OPTICAL DESIGN OF THE SPECTROMETERS IN CHEMCAM (R. WIENS 2012)

ChemCam has provided valuable information from Mars with grat findings. Discovery of Manganese rich phases, or Boron, or the detection of gypsum veins are just some examples. It is thanks to this success, demonstrated robustness and exceptional aid during operations that made a successor of ChemCam of great interest for Mars2020 mission.

2.2.2 SuperCam

FIGURE 2-18 SUPERCAM LOGO

While in the development of ChemCam its PI wanted to *"keep it as simple as possible"*, in SuperCam the path was set to a more complete instrument. How to make better what already is a very successful instrument?

SuperCam parts from a similar structural design to ChemCham and incorporates more analytical capabilities in addition to LIBS:

- Time Resolved Raman: the infrared pulsed laser that is used for LIBS can be introduced in a different path through a Harmonic Generator to obtain a 532 nm pulsed laser. This is used to induce Raman scattering in the sample and then

analyze the spectrum with some time resolving capabilities. This time resolving is a must when trying to separate luminescence from Raman.

- Time Resolved Luminescence: in this case the same setting used for Raman is used, but the time window for the acquisition of data changes to allow the induced luminescence to be analyzed in the spectrometers.
- VISIR: The same spectrometer used to get data from the visible spectral window can be used to measure the reflectance spectrum of the samples. In SuperCam it has also been included an IR spectrometer to measure the same reflectance spectrum in the IR range.
- Micro Imaging: As a difference and evolution from ChemCam, SuperCam uses a color sensor, providing color images of the selected samples.
- Sound recording: During the plasma events of a LIBS measurement the sound produced by the shock wave of the plasma can be recorded and analyzed. This recording can provide some information of the texture of the sample.

All of this new measurements are also done at distances of several meters, providing more information from the analyzed samples. No only more information, but complementary, as each technique show a different feature from the samples.

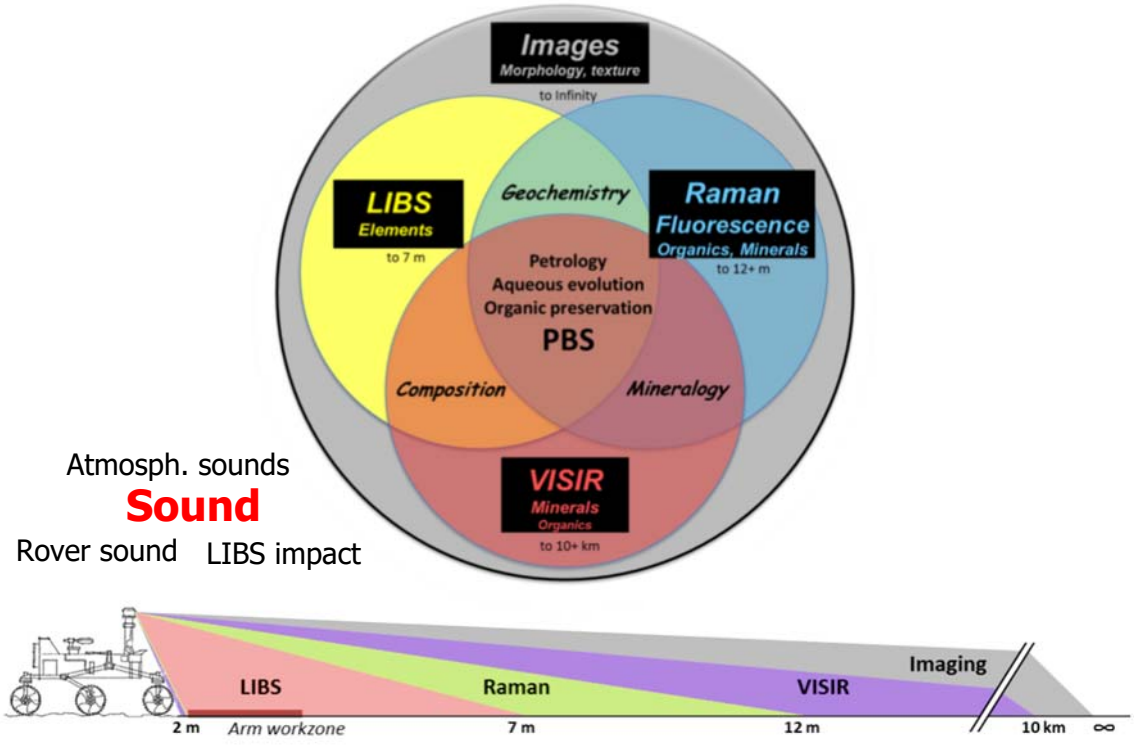

FIGURE 2-19 SUPERCAM CAPABILITIES AND MEASURING DISTANCES (LANL-IRAP)

LIBS will provide information of the elemental composition of the sample, Raman can identify molecules and structure (and vibrational bands not visible by VISIR), VISIR mineral groups (and vibrational bands not visible by Raman), imaging the morphology and fluorescence can identify minor elements in the sample, while sound can provide

information of how well agglomerated a material is. All together are capable of great synergy when characterizing the surface of Mars.

Related to the objectives of the mission, SuperCam will be able to provide remote sensing to help with operations, but at the same time will be able to provide analysis at fine scale, including a complete geochemical characterization of the sample in addition to its morphology and context, all of these directly related to objective A and B. Also in the case of objective B, the vibrational techniques as Raman and VISIR spectroscopy will be able to directly detect organics, fulfilling to some extent the objective B. Of course, thanks to the combination of all these techniques at distance it will help to select the best areas where proximity science can be used and together select the best samples for caching, covering also objective C.

2.2.2.1 Science requirements for SuperCam

At the moment of writing this work the details of Supercam instrument have not been published in deep. It is planned to have several detailed papers in a special issue of Space Science Reviews covering complete information of the instrument. Until that, just a few aspects can be disclosed in the present work, including the requirements that set the capabilities that the scientific community ask to SuperCam:

- The instrument shall be able to measure elemental composition by LIBS on the surface of Mars, for selected elements, from 2 to 7 m.
- The instrument shall be able to measure depth profile of elemental composition on the surface of Mars from 2 to 5 m.
- SuperCam shall be able to record audio signals from 100 Hz to 10 kHz on the surface of Mars, with a sensitivity large enough to monitor a LIBS impact source at 4 m.
- The instrument shall be able to acquire Raman and luminescence data at target ranges of 2 and 7 m, with a goal of 12 m.
- The instrument shall be able to detect with VISIR mineralogical composition on the surface of Mars from 2 m to 10 km.
- The instrument shall be able to acquire color images at target ranges of 2 m to 10 km.
- The instrument shall be able to detect on the surface of Mars mineralogical composition and organics from 2 to 7m, with a goal of 12 m.
- The instrument shall be able to determine the atmospheric concentrations of some molecular species.
- The instrument should be able to perform onboard calibration of its different detectors and techniques.

These requirements can be, and in fact have been, expanded into more concise technical requirements of lower level. The instrument needs to be built around these requirements to provide the scientific team the tools required to fulfill the mission requirements.

2.2.2.2 Overview

Now we know what SuperCam is capable of doing and the expected science to be done with it we can give a look to the instrument itself.

As in ChemCam, SuperCam has been separated into three different subsystems, each of one responsibility of a different institution. To the team that developed ChemCam, LANL and IRAP, responsible for the Body Unit (SCBU) and the Mast Unit (SCMU), it has ben added the University of Valladolid, responsible for the Calibration Target, SCCT (Wiens, 2017).

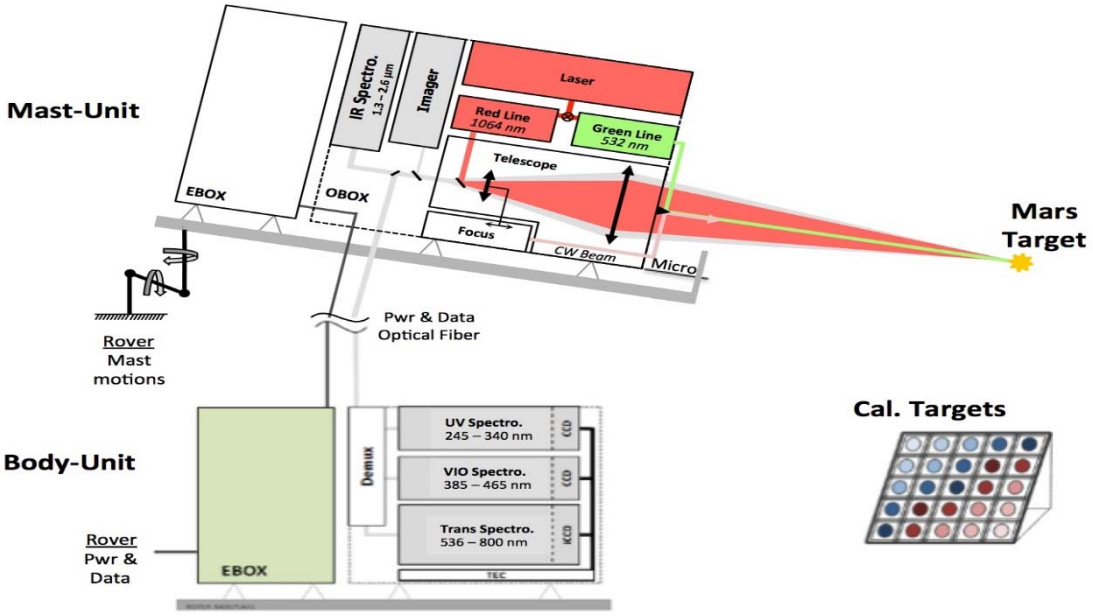

FIGURE 2-20 SUPERCAM CAPABILITIES AND MEASURING DISTANCES (LANL-IRAP)

Regarding the placement of each subsystem in the Rover, it has been maintained a great heritage from ChemCam. The positions of each component remain the same. The SCMU is placed at the top of the mast, the SCBU is placed inside the body of Mars 2020 rover, connected to the SCMU by optical fiber and other power connectors. Finally, the calibration targets are placed in the same position of ChemCam's.

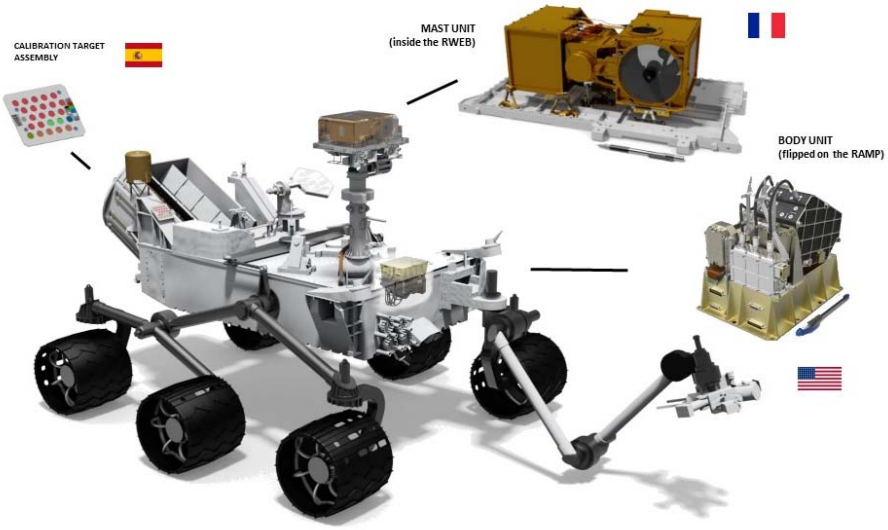

FIGURE 2-21 SUPERCAM ELEMENTS IN THE ROVER (LANL-IRAP)

This position allows a better correlation between the calibration measurements on ChemCam when compared to SuperCam's. In the detailed description it will be shown what is new, and what has been upgraded since ChemCam.

AS FOR THE ORGANIZATION AND THE TEAM BEHIND THE INSTRUMENT, THE MAIN DIFFERENCE WITH CHEMCAM IS THE INCLUSION OF SPANISH PARTICIPATION IN THE DEVELOPMENT OF THE HARDWARE. IN THIS CASE, THE UNIVERSITY OF VALLADOLID HAS THE LEADING ROLE IN THE VERIFICATION OF CALIBRATION, AS WELL AS THE RESPONSIBILITY FOR THE DESIGN, DEVELOPMENT AND MANUFACTURING OF THE SCCT. THE FOLLOWING FIGURE SHOWS THE TOP LEVEL ORGANIZATION CHART:

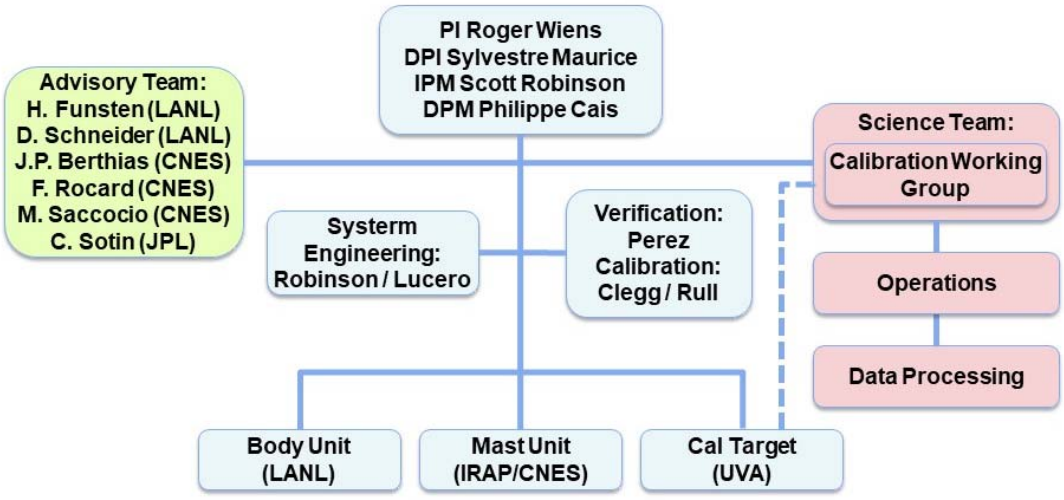

FIGURE 2-22 SUPERCAM TOP LEVEL ORGANIZATION CHART (LANL)

2.2.2.3 SCAM technical overview

Getting into the details of the different elements of SCAM, the first evident difference with ChemCam is everything related to the new vibrational spectroscopy techniques.

SCMU:

In the case of the Mast Unit, the inclusion of Raman spectroscopy made necessary the inclusion of a higher frequency laser source than the one used for LIBS. In this case, this source was obtained by frequency doubling the ground emission of the Nd:YAG laser that is used for plasma generation for LIBS. This option uses the same laser source for both techniques reducing the extra weight of including different sources. Using some crystals (KTP for example) it is possible to add up two photons from a 1064 IR laser to get the energy necessary to produce a 532 nm photon. An optical switch can change the optical path of the laser and select between the two wavelengths (Perez, 2017).

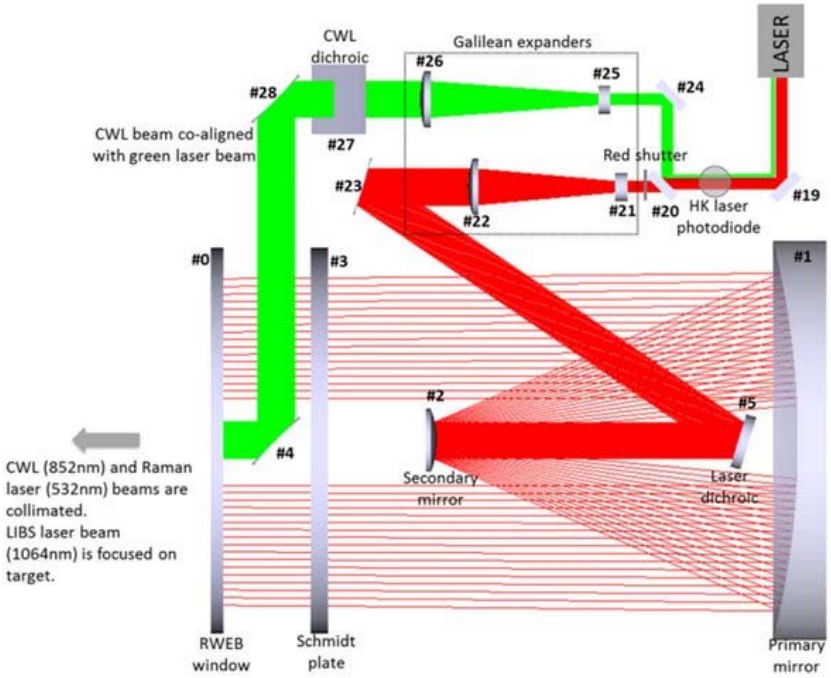

FIGURE 2.26 OPTICAL PATHS OF LASERS (R. PEREZ, CNES)

Now for the red line, the 1064 laser beam is expanded using a galilean telescope and introduced in the optical path of the Schmidt-Cassegrain telescope in a manner that

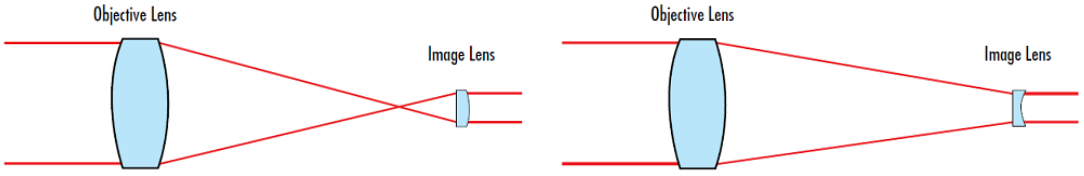

FIGURE 2.25 AND 2.26 DIFFERENCES BETWEEN A KEPLERIAN BEAM EXPANDER AND A GALILEAN (EDMUND OPTICS)

ensures that when the telescope is focusing on a point, the laser is also focused on that point. The use of this galilean expander is usual when dealing with high power lasers that could induce damages in the optics if the beam is too concentrated. The objective is to be able to focalize the laser into spots of a similar size to ChemCam, this is between 350 and 550 microns depending on the distance and material.

In the case of the green line, the 1064 nm is introduced in the second harmonic generator where the beam is turned into 532 nm and filtered to eliminate the remaining 1064 nm laser. Typically in commercial lasers this conversion is approximately a 50% efficient in terms of energy, that means that the energy per pulse of green laser is the half of the energy of the ground infrared wavelength, in the case of SuperCam, the ground energy is 14 mJ per pulse (4ns) for 1064 nm and 11 mJ per pulse for the 532 nm (Wiens, 2017). The beam in this case will remain collimated although is expanded to limit damages in the optics. As difference with the red line, it is not introduced in the optical path of the telescope but introduced in the optical axis of the system by means of a mirror situated in the center of the Schmidt plate.

The light collected from the LIBS event, the Raman analysis, or simple for imaging can go then through three different paths. In the first one and more obvious, the collected light is filtered through a notch filer and focalized in the optical fiber that will take it to the spectrometers. The notch filter is necessary to avoid the entrance of laser in the fiber that could induce parasite emissions. The other option for this light is to be used to obtain an image in the RMI, now providing color images, HDR capabilities and covering the visible spectrum.

A third option is to introduce the collected light into the IR spectrometer.

FIGURE 2.26 SUPERCAM IR SPECTROMETER (J.M. REESS, LESIA)

The IR spectrometer in SuperCam uses an Acousto Optical Tunable Filter to focus the light in a light detecting element and measure intensity during the spectral sweep of the filter (Reess, 2019). The AOTF uses crystals that act as bandpass filters but can change the spectral position of this band depending on the frequency on an acoustic wave that is introduced in the crystal. Varying this frequency it is possible to seep the spectral range and collect intensity measurements in any step. This same kind of filters are used for hyperspectral imaging in other instruments.

Finally, a microphone is implemented to record the sound made by the LIBS spark in the material. The characteristics of the soundwave collected can give information of the texture and physical characteristics of the material that has been shot. Also this microphone will be able to record sounds of the rover and wind, helping with the weather studies and the engineering during operations.

SCBU:

The SuperCam Body Unit is the subsystem of SuperCam where the spectrometers are placed. Here the lught coming from the different measures is analyzed.

The light collected by the SCMU and carried to the SCBU through the optical fiber needs to be separated into three different spectral windows. As happened in ChemCam, due to the broad area of the electromagnetic spectrum that needs to be analyzed in LIBS measurements, the incoming signal is split into three different windows according to its wavelength, and then each of those windows analyzed in a dedicated spectrometer.

This separation in the three spectral windows is done by means of an optical demultiplexer. In this element the light exiting the fiber is collimated, and then passes through three lowpass optical filters. The light is then refocused in a dedicated fiber and carried to each specific spectrometer.

In the SCBU three spectrometers are used for the measurement, quite similar to que ones used in ChemCam, with one big exception, the Visible spectrometer.

The two shorter wavelength spectrometers keep the same optical design used in ChemCam with great results. The visible spectrometer, on the other hand, needed a different approach given the constrains associated with Raman spectroscopy, basically demanding a higher sensitivity.

The following table shows the main characteristics of each of these spectrometers:

TABLE 2-3 MAIN CHARACTERISTICS OF THE SPECTROMETERS IN THE SCBU AND THE IR (R. WIENS, 2017)

Table IV: SuperCam spectral characteristics				
Spectrometer	Ultraviolet	Violet	Visible	Infrared
Type	Czerny-Turner	Czerny-Turner	Transmission	AOTF
Location	Body	Body	Body	Mast
Function	LIBS	LIBS, VISIR	Raman, LIBS, VISIR	VISIR
Detector	CCD	CCD	ICCD	Photodiode
Range (nm)	240–340	385–475	535–855 (150–7000 cm^{-1})	1300–2600
No. channels	2048	2048	6000	256
Resolution, FWHM	0.20 nm	0.20 nm	0.3–0.4 (10 cm^{-1})	30 cm^{-1}
Field of view	0.7 mrad	0.7 mrad	0.7 mrad	1.15 mrad
Exp. duration	≥3 ms	≥3 ms	≥100 ns	40 s scan

The visible spectrometer is the one covering all the Raman range. Typically when using 532 nm excitation source and a Raman instrument cover a range of 4000 cm^{-1} maximum, that is from 532 to 675 nm, but in the case of SuperCam several interesting LIBS lines occur in the IR range, reason why the range of this spectrometer is extended. The great distinct characteristic of this spectrometer, besides its optical design, range and resolution, it's the detection part, that needs to provide the time resolving power to the instrument.

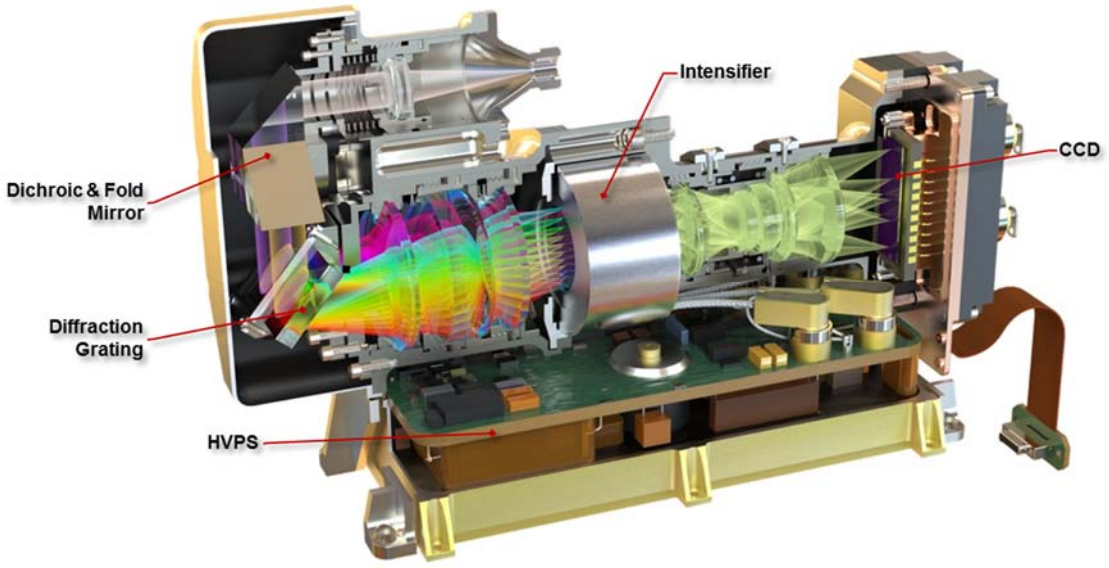

FIGURE 2.27 SUPERCAM VISIBLE SPECTROMETER (LANL)

Time resolving in SCAM happens thanks to a time-gated intensifier included between the monochromator and the CCD. The main reason for having an intensified detector is not only the time resolving capabilities, also the fact that Raman effect is a weak signal

and that faint light is really hard to collect when using stand off Raman. Tis also introduces an extra requirement on the hardware that is adaptability, since the signal strength coming from Raman and LIBS are several orders of magnitude different. This adaptability is introduced by changing the gain in the intensifier from its maximum value for Raman to its minimum for LIBS and VISIR (Perez, 2017). The introduction of this intensifier, however, comes with a price in terms of resolution.

The intensifiers usually mean a reduction of the resolution due to some ghosting effects that happen in the phosphor screen. As a result, a straight line becomes blurry and spectral resolution is lost. This effect was dramatic in the development of the Time Resolved Raman system at UVA, with FWHM bandwidths in the order of 30 cm^{-1}. This needs to be taken into account when dimensioning the monocromator, and it is a difficult effect to measure with anticipation. In the case of SCAM this was solved by spreading the spectral range into three tracks in the spectrometer, decision taken with the aid of tests on a development unit, EDU. This change also allowed to increase the slit width from 20 to 30 microns, introducing more light into the spectrometer while improving then resolution (the pixel resolution is better than 2.5 cm^{-1}) (Wiens, 2017).

The resulting spectrometer suite, the three spectrometers in the SCBU and the AOTF IR mounted on the mast cover more than 1900 nm of range, giving service to four different spectroscopic techniques. This could be a good definition at first sight of the complexity of SuperCam.

SCCT:

In words of ChemCam's and SuperCam's PI, Roger Wiens, the only thing from ChemCam that he would have changed is the Calibration Target. The caliobration target in an instrument like ChemCam, or SuperCam, serves not only for a wavelength calibration of the spectrometers, but also for the chemometric calculations. LIBS measurements are affected by matrix effects, environmental conditions and other factors that make advisable to have a good set of samples to do calibration curves of some elements *in situ*. SuperCam is planned to provide estimations of concentration of some key elements with an accuracy better than the 10%, and a part of the responsibility to achieve that performance falls on the calibration target.

The SuperCam calibration target is the subsystem under Spanish responsibility. The PI of this element is Prof. Fernando Rull, from the University of Valladolid, and for its development and manufacturing this institution counted on the collaboration of several other institutions from five countries. In Spain a complete team including four universities, INTA and a technological partner (AVS) was arranged.

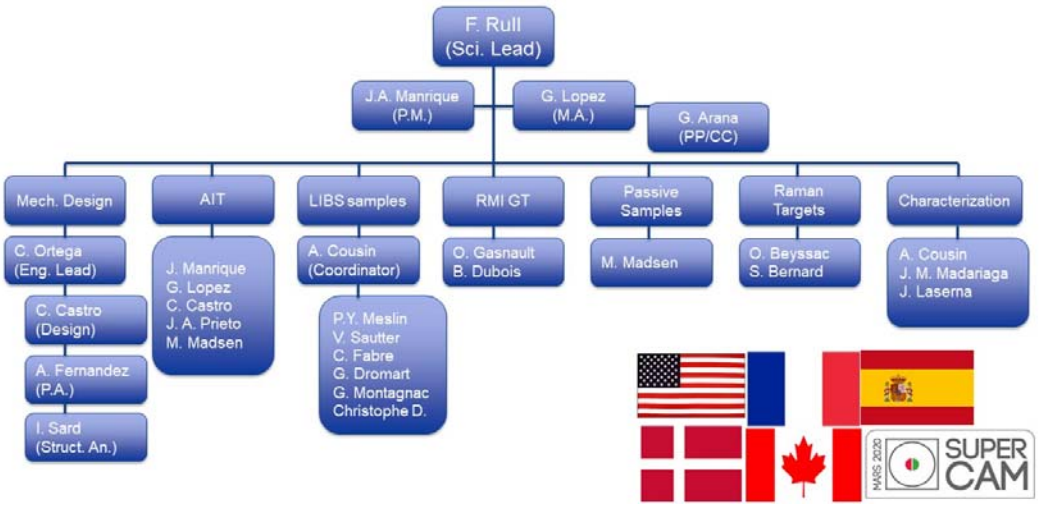

FIGURE 2.28 SCCT DEVELOPMENT TEAM CHART

Added Value Solutions, AVS, provided the technical support in the structural design and manufacturing of the different parts of the SCCT holder. Several research groups in France helped with the manufacturing of the samples, under coordination of IRAP and the reflectance samples were provided by Niehls Bhor Institute. In Spain, the science group including the University of Valladolid (UVA), University of Basque Country (EHU), Complutense University of Madrid (UCM) and the University of Malaga (UMA), took charge of the characterization and scientific assessment of the samples, along with the general participation in the science of the instrument. INTA gave its support during AIT activities. UVA took charge of the technical coordination, with the Mission Assurance and Project Management under its responsibility (this last one being author's responsibility).

The technical details of the SCCT are introduced in the following section 2.3.

Final remarks and status:

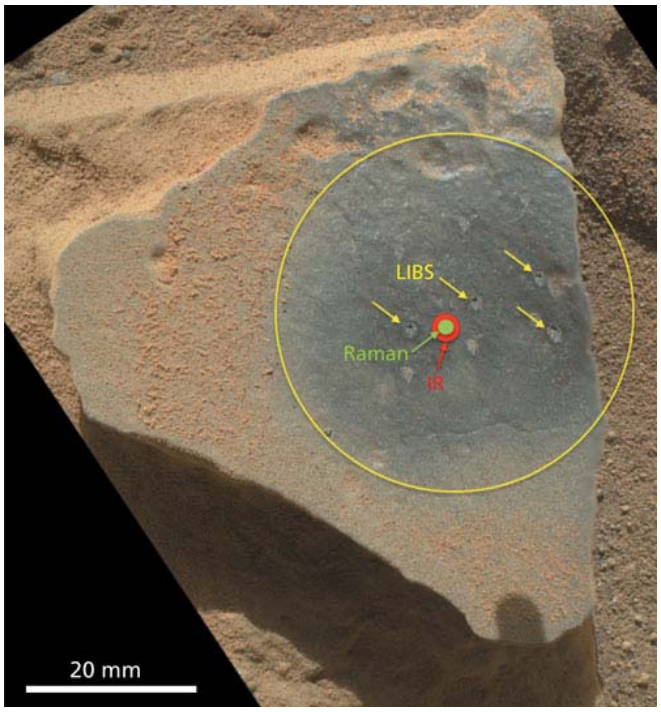

FIGURE 2.29 FOOTPRINTS OF DIFFERENT SPECTRAL TECHNIQUES (R.WIENS 2017).

SuperCam instrument presents a unique opportunity to understand better the geological processes and past of Mars. Not only will be able to use different analytical techniques, each of one shows a different feature of the samples, it will be able to do all these measurements coaligned. The different techniques may have a different measuring scale, Raman analysis spot will not be as small as LIBS, but they will be done on the same sample, on the same spot, opening a new line of possibilities when using data from different techniques to be combined in chemometric calculations. Again, in this capability an important role is played by the calibration target, since it will make available the same set of samples to be measured by all the techniques, giving a cross calibration between measurements. In figure 2.27 the different sizes for each technique can be seen for a sample at 2.5 meters (Wiens, 2017). The yellow circle shows the area that will be clean of dust after its removal with the first laser shots. Please observe that the size of the LIBS spot will remain constant with distance, to some extent, because it is focalized at each distance by the telescope of the SCMU. The Raman spot will get bigger with distance as it is not focalized, it is collimated, and the VISIR depends on the field of view, that of course gets a wider area when distance increases.

While writing the present work, the flight model of SuperCam was already delivered to JPL and integrated in the rover. Due to schedule constrains only limited functional testing could be done with both flight models of the SCMU and SCBU and results are not for public disclosure at the moment. However, a special issue of Space Science Reviews will include three papers from SuperCam with more detailed results and descriptions.

2.3 SuperCam Calibration Target

Science cannot progress without reliable and accurate measurement of what it is you are trying to study. The key is measurement, simple as that.

Robert D. Hare

Robert D. Hare dedicated his life to psychiatry, a field of knowledge far from physics, but his realization about the importance of measurement, capital in physics, led him to the development of the Psychopathy Checklist, PCL, a way to measure and have a better diagnostic of possible psychopaths. In his quote, he states the importance in science of a reliable and accurate measurement, something that is in the core of sciences like physiscs or chemistry. In first place it is absolutely necessary the tool that will provide the measurement, it is impossible to think about measuring mass without a scale, or length without a ruler. In second place, and as important as the first, is the calibration of the measuring tool, so the results can be given with certainty.

In the case of SuperCam, a complete and multianalytical tool like this instrument would be incomplete without a proper calibration, accurate chemometric calculations depend on a good calibration, the Raman spectra cannot be properly provided without knowledge of the excitation source, the VISIR are impossible without a good characterization of the ilumation spectrum and black current... If that calibration was important for ChemCam, the inclusion of more techniques has made it crucial in SuperCam to have good calibration target. This important component of the instrument has received great support and careful planning and design from the science team, remarking its capital importance in the performance of SCAM instrument in Mars.

2.3.1 Description

SuperCam instrument, which was deeply described in the previous section (3.2), will be able to use six different analytical techniques to characterize samples in the surface of Mars, and will do that without contact, up to distances of several meters, expanding the science range of the Mars2020 rover and providing more information during operations.

The six different techniques to be used by SuperCam are:

- Laser Induced Breakdown Spectroscopy (LIBS): providing elemental composition of the target and based on emission lines from a plasma induced on the sample by concentrating the light from a pulsed light source in a spot of a few microns.

- Time resolved Raman: providing structural information of the sample, it is a vibrational spectroscopy technique based on the inelastic interaction of light and matter. When the

excitation source is a pulsed laser and the detector is gated, and synchronized with the laser, it is possible to separate different moments of the interaction of the sample with the pulse.

- ViSible InfraRed spectroscopy (VISIR): also a vibrational spectroscopy technique, in this case it is based on the selective absorptions by the sample of parts of the electromagnetic spectrum. This technique has been used by orbiters due to its simplicity, since the only thing needed is to have sample illuminated by a continuous spectral source like the Sun. it provides structural information of the sample.

- Induced fluorescence: In this case the use of a high frequency laser allows to induce electronic transitions on the target. The relaxation of those excitations can provide additional information of the sample as the presence of rare earth elements.

- Sound: the sparks of the induced plasma by LIBS analysis produce a characteristic sound. By the analysis of this sound, even in the faint atmosphere of Mars, can provide information of the texture of the sample.

- Image: Images of the analyzed area are important to understand morphology of the sample, and also to have an idea of the possible individual components of a complex sample.

This analytical suite of SCAM has global needs but also particular needs for each technique when it comes to calibration. Example of a global need for all techniques is to have a calibration to calculate the assignment of a wavelength to each pixel in the detectors of the spectrometers. An example of a particular need of a technique is to calibrate the spectrum of the incident light on the sample for VISIR. All these needs, in addition to others, should be addressed by the calibration target. The complexity of this element has been increased for this reason when compared to ChemCam's.

All these needs, science requirements, need to be addressed with technical constrains in mind. The design of the SuperCam Calibration Target, SCCT, needs to meet technical requirements from different origins, from the space and mass available for the hardware, to those depending on the environmental conditions that the system will face. As a general description, the SCCT needs to be under 270 grams of mass, and the size, although is not critical given that there is no other hardware around that could be interfered by the SCCT, needs to be as contained as possible.

The SCCT is completed with a final element that is not intended to fly and serves as protection device during the integration and testing operations. This Remove Before Fly or Red Tag Cover, needs to cover the SCCT completely, protecting it from impacts of tools or fasteners during integration, also allowing a safe handling of the unit, but does not need to be hermetic and serve as contamination control measure. Since it is not an

operational element it does not impact in the mass limit, but some elements during ATLO could be close to it, so this element needs to be taken into account when talking about maximum dimensions.

All these requirements are explained and discussed in the following section.

2.3.2 Requirements that define the SCCT

2.3.2.1 Technical Requirements

Starting with the technical requirements, the first topic to be addressed is the technical resources that the hardware to be developed will consume. Typically, in this group are included the mass, power consumption, volume, and heat. The SCCT is a passive element from the point of view of power and heat, there is no need or prevision of including any power consuming element in the SCCT or measures to conduct heat from one point of the rover to the SCCT. But the mass and volume are technical resources that need to be addressed.

Mass and envelope: Starting with the mass, the maximum mass with margins that was assigned at the beginning of the project was 240 grams. At different stages of the project the mass has changed, as have done the margins applicable, from 20% at the initial stages of design to 10% at the final stage. Anyhow, the mass allocation is not be exceeded, or an increase needs to be justified and requested to the responsible of the upper system, in this case the Mars2020 rover.

This was the case for the SCCT, as those 240 grams were found not sufficient due to changes introduced by JPL in the possible location in the rover. In 2016 at PDR level, this is Preliminary Design Review, JPL had implemented an antenna to control the heliscout that was proposed for Mars2020 mission, and that antenna interfered with the SCCT by shadowing the samples intended to be used to characterize the ambient light, what is not acceptable. As a result, a trade was opened at instrument level to valuate possible solutions to this issue, solutions that included the relocation of the whole calibration target, or a redesign, that allowed the reflectance standards to be in a shadow-free location on the rover deck. This relocation changed the dynamics environment of the SCCT, basically increasing the shock level to be face by the hardware. To solve this issue two solutions were considered, or ruggedize the design, or split the SCCT into two separated targets, so the sensitive samples could be separated in a ruggedized separated holder, while the other could stay in the initial location, anyhow, both solutions required more mass to be implemented. As a result the maximum mass was increased from 240 to 270 grams.

Regarding the volume, or size, as was already commented, in the possible locations of the SCCT in the rover deck its difficult to find elements that could be mechanically interfered, so the size was just agreed with JPL without a Not To Exceed envelope requirement per se. Again, and as an example of how alive a project of this kind is, once the design was validated a new requirement was identified at instrument level. To prevent damages on the optics of the Mast Unit, a certain minimum distance was set, and the SCCT was closer than that distance at that moment. This time the impact fell on JPLs mechanical team that needed to redesign the bracket to accommodate the SCCT, but doing this the calibration target got closer to some ground support equipment that could harm the hardware during ATLO activities. This introduced special requirements in the envelope, that was defined with the remove before fly cover on place.

2.3.2.2 Environmental requirements overview

The SCCT will need to face very different environments during its assembly, cleaning, launch, cruise, landing and operation time, and the hardware needs to be proven to survive in those environments. These requirements can be verified by analysis or test, and will cover there the ones directly related to demonstrate that the hardware will be able to survive (Qualification), as other tests are just done to verify workmanship (Flight Acceptance) and are usually less severe.

Starting with the assembly, there are not specially harmful environments during this phase, but it is at the last stage, when the hardware is cleaned to accomplish with Planetary Protection requirements, that the SCCT faces the highest temperature of its whole operational time. The PP procedures will be explained later, but to summarize, during this process, the SCCT is introduced in a vacuum chamber at 115 ºC of temperature for at least 120 hours. This temperature could be a risk for any adhesive, that usually trend to behave plastically at high temperatures, or in worst cases, degrade completely.

Continuing with the launch, the main stress received by the hardware due to the experience of being launched into space by a rocket is mechanical, mainly in form of vibrations of different kind.

During its cruise stage the hardware is under low temperatures and vacuum, it is in this stage when lowest temperatures might be reached, and is also during this stage that any outgassing material could be a contamination risk for other parts of the Rover, but that will be covered in a different section.

During the descent and landing on Mars, the SCCT will suffer again vibrations, but the most demanding requirement appears in this stage, which is shocks. The SCCT is mounted near the pyrotechnic wheel restrain of the Mars2020 Rover, what introduces

a high g level, short duration, shock. Also possible contamination from rocket plumes from the SkyCrane needs to be addressed.

Finally, during its operation in Mars, the main risks to the SCCT are the extreme temperature changes between night and day, the omnipresent dust, and the radiation.

Taking all of these into account, the project sets some values for the different stress sources that represent the maximum aggression that could be faced with some safety margins. The requirements are then evaluated by means of analyses, or tested during what is called a qualification campaign. During this campaign a replica of the SCCT is built with the only purpose of being subjected to these tests and check its survival. This model is then considered stressed and is not available for flight, but if everything goes fine, it demonstrates that the design is solid and the final Flying Model can be built. For the SCCt the following tests were found necessary for the qualification of the hardware:

- Vibration test including random vibration and quasi-static loads.
- Shock test
- Vaccuum Thermal cycling
- Mars pressure thermal cycling

Quasi-static loads test:

The Quasi-static testing of the hardware its necessary to simulate the loads applied during the launch. It shall be performed for the SCCT with an acceleration of 72 g's (60g with a 20% margin). The acceleration shall be applied in directions which develop the worst case element loads. For SCCT, the article will be tested in the three axis.

Random vibration test:

The random inputs shall be incrementally and applied to the assembly under test in each of three orthogonal axes. The vibration amplitude distribution should be Gaussian. Both the power spectral density levels and wide-band levels are test parameters and they shall be controlled. And finally, it is important, if possible, to reach the local modes of the assembly during this test if they are within the limits stablished in the requirements.

The Design/Qual exposure time is 2 minutes per axis, as well as for Proto Flight (PF) and Flight Acceptance (FA).

Pyroshock test:

This tests is introduced to verify the survival of the SCCT after the pyrotechnic release of the wheels of Mars 2020 Rover. The shock response spectrum (SRS) level of 3500g shall be applied to the test article in the X-, Y-, and Z-axis. Two pulses shall be applied in each axis. The synthesized shock waveform shall meet the following criteria: the time history

shall be oscillatory in nature, and the pulse shall decay to less than 10% of its peak value within 20 milliseconds. In addition, at least 50% of the maximum spectrum values shall exceed the nominal spectrum values (not the number of points of the curve, but the curve itself).

Thermal test:

To reproduce the possible mechanical stress suffered by the SCCT during the thermal cycles, it was agreed to do no less than 30 cycles between the worst temperature cases, and of those 30 cycles at least one will be done under martian pressure of N2, while the rest will be done in vacuum.

During the first 29 cycles, the conditions are:

- Temperature range: from +80ºC +5/-0 to - 130ºC -5/+0.
- Temperature ramp should be <= 5ºC/min.
- Dwell time at the limits: 120 minutes for the first three cycles, 15 minutes for the other 26 cycles.

For the last cycle, nitrogen is pumped into the chamber up to Mars pressure, continuing then with the following requirements for the test:

- Temperature range: from +80ºC +5/-0 to - 130ºC -5/+0.
- Temperature ramp should be <= 5ºC/min.
- Dwell time at the limits: 15 minutes

Other environmental requirements:

In general the main concern for the SCCT is the optical properties of the geometric target and the reflectance standards after the UV irradiation and several sols of dust deposition. The general requirement is to keep at least one area of 1 mrad diameter clean, this clean zone can be seen by the Mast Unit and used for calibration purposes of the VISIR or imaging capabilities.

The dust in Mars is a great concern for every hardware to be working on its surface. Adverse effects of its deposition on equipment can limit the operational life of instruments or even the Rover, so every system directly exposed to Mars environment needs to be designed to minimize the dust deposition and be ruggedized against possible damages caused by this element. Despite of the light martian atmosphere, dust is present everywhere in Mars, even forming planet scale storms that can cover the whole surface of the planet. The dust is also interesting from a scientific point of view, since it presents the average composition of the surface of the planet, being the same from one landing site to another (mainly thanks to the mentioned global dust storms). Thanks to experiments incorporated since Viking missions, or like the ones included in pathfinder mission, or the Mars Exploring rover, MER (JPL, 2013) , the composition of

the martian dust is well known to some extent, and it has been observed that it is indeed quite homogeneous among the whole planet. Composition % can be shown in the following table:

TABLE 2-4 ELEMENTAL COMPOSITION OF MARTIAN DUST IN DIFFERENT LANDING SITES (JPL)

Oxide	Gale Crater measurements (MSL)	Gusev Crater mesurements (MER)	Meridiani Planum measurements (MER)	Average Martian Soil
SiO_2	39.3 ± 1.7	45.0 ± 0.5	45.0 ± 0.3	45.41
TiO_2	1.06 ± 0.09	0.89 ± 0.08	1.01 ± 0.07	0.90
Al_2O_3	8.91 ± 0.39	9.56 ± 0.16	9.14 ± 0.09	9.71
FeO	21.0 ± 2.2	16.5 ± 0.15	17.5 ± 0.04	16.73
MnO	0.42 ± 0.10	0.31 ± 0.02	0.34 ± 0.01	0.33
MgO	8.31 ± 0.38	8.25 ± 0.15	7.57 ± 0.08	8.35
CaO	7.04 ± 0.60	6.17 ± 0.07	6.54 ± 0.04	6.37
Na_2O	2.75 ± 0.22	2.9 ± 0.3	2.22 ± 0.19	2.73
K_2O	0.47 ± 0.09	0.49 ± 0.07	0.48 ± 0.06	0.44
P_2O_5	n.d.	0.91 ± 0.09	0.93 ± 0.09	0.83
SO_3	8.34 ± 0.42	7.61 ± 0.13	7.28 ± 0.07	6.16
Cl	1.08 ± 0.12	0.88 ± 0.03	0.78 ± 0.01	0.68

In the case of the SCCT, among the 28 samples that will be part of the target, different kinds are directly identified: the 22 mineral samples, most of them sintered, that will be shot with the infrared pulsed laser to obtain LIBS spectra, two Raman targets, that will be only shot using the green laser, and the reflectance standards, that will be not shot by laser, and need to provide a clear 4mm diameter area clean in the center of the sample for calibration purposes. In the case of the mineral samples, the laser itself will clean the surface of the samples of dust, making it not concerning. For the Raman targets, one of them is intentionally exposed to the martian environment, as it will be described in the science requirements section, to monitor the evolution of organics in the surface of Mars, and the other sample present enough Raman cross section not to be concerning. The last samples, the reflectance standards, are capital for the operation

of the instrument and the data acquisition using VISIR technique or the capture of images by the RMI, these samples need then to be designed to be protected by the dust.

Regarding the UV radiation on the surface of Mars, the absence of an atmosphere that can act as al filter to the radiation means that the surface of the planet is continuously irradiated by UV and other ionizing radiations. This radiation can induce chemical changes in the materials used to build space hardware degrading them. In the case of the SCCT all structural parts are not sensitive to this effect, or are protected from

FIGURE 2.30 CURIOSITY'S ROVER DECK COVERED WITH DUST AFTER 1197 SOLS

radiation (as adhesives for example), but some elements can change their optical properties due to the UV radiation. Thermo photo oxidation is a well known degradation process on Earth, it is something to be taken into account when designing materials to be used in the exterior, as agricultural polymers, and its results are also part of our daily experience, as it can be observed changes in the colors of paints due to the exposure to sunlight, and this happening in reflectance standards (turning a white surface into a yellowish one for example) means a great threat to the long life operation of the instrument. This changes come from the oxidation of the material induced by the energy of the UV radiation. Of course, in Mars, the UV will be present but the oxygen will not be, as the atmosphere is too faint, other oxidants as perchlorates can be present but their impact on hardware on the surface has not been described yet. So the presence of external oxidants that can interact with the hardware helped by the UV radiation can be almost neglected, but other changes as internal reorganizations of long chains in organics can definitely happen, introducing that feared changes and degrading the optical performance of certain materials. In the SCCT all the elements used to calibrate the RMI and the VISIR must be designed to take this effects into account, as for the organic sample, as explained before, it is intentionally exposed to the environment, and this effect doesn't need to me mitigated.

A final environmental requirement to be taken into account is the thermal behavior of the wholes assembly once exposed to the Sun. The SCCT is a passive element, that means that no heaters or coolers are implemented, and its thermal regulation if fully dependent on the absorptivity and emissivity of the different parts of the calibration target. Requirements on the albedo of the whole system are introduced to limit its heating during daytime. This also needs to be taken into account when designing the interface with the Rover.

Contamination and Planetary Protection requirements

Mars should be considered one of the best laboratories available to understand the origins of life. Its past conditions that could make Mars a habitable place make the Red Planet a high priority target for life origins studies.

This great laboratory is to be kept clean from foreign contamination or microorganisms that could jeopardize the data, measurements and scientific conclusions on this topic. Because of that, strict policies apply that have been included under a relatively new concept(This concept has its start in the treaty on the peaceful uses of outer space from 1967), the so called Planetary Protection (Rummel, 1989).

Regarding planetary protection, the main concern is the population of spores, more than bacteria or other microorganisms. Spores have been identified as a dormant form of bacteria that could survive to very hostile environments, as space, and been able to live and reproduce in harsh conditions, as Mars, making them the greatest concern in terms of Planetary Protection.

Not only Mars needs to be protected from this foreign contamination sources, also the instrumentation on board any spaceship needs special care to prevent it from malfunctioning, or mistaken measurements. The main concern on this is the possible volatiles that in the vacuum of space can outgas from some material and be deposited on sensitive surfaces, as the optics.

The main effect of a molecular film on the calibration samples of the SCCT is a variation of signal, either for Raman, LIBS or other spectroscopic instruments, giving as a result interference. Particles on a surface affect the signal intensity by a factor equal to the obscuration factor, expresses in PPM [mm2/m2] or in %.

SCCT elements that could result to be possible sources of contamination are all those composed by materials which could outgas. Therefore, all materials in SCCT will be carefully selected and evaluated, to make sure that they not constitute a problem regarding molecular contamination.

With respect to particulate contamination, non-flacky, non-shatterable and non-dusty materials will be selected as much as possible. However, most of the samples are sintered materials….

In addition, clean areas will be used for integration and testing, and all measures and controls to keep these areas under the cleanliness level specified will be taken through specific procedures. Also, all transport steps from one area to another, or for delivery, will be designed so that the hardware does not degrade its cleanliness level.

Humans are the major source of contamination in clean-rooms, and therefore the control of people, their clothing and behavior constitutes the most important task to the maintenance of reduced bioburden levels. The major sources of contamination considered to be associated with humans are the following:

- Particles mainly derived from dead skin are dispersed into the atmosphere. It is also recognized that people's behavior patterns significantly affect the number of particles generated by an individual.
- Bacteria, fungi, viruses and other kinds of microorganisms.
- Static charge
- Chemical residues

The requirements in numbers are as follows:

- Planetary Protection: $3x10^5$ spores in total or an average of 300 spores per square meter of exposed surfaces. Whatever is more restrictive.
- Molecular contamination: At its delivery to JPL the SCCT should have a surface cleanliness of 0.1 micrograms per square centimeter.
- Particle contamination: The requirement for the SCCT is L300, understood to be better than the following distribution:

TABLE 2-5 DEFINITION OF L300 PARTICULATE CLEANLINESS REQUIREMENT

PARTICLE SIZE	MAXIMUM LIMITS FOR PARTICLES. PARTICLES PER 0.1 SQUARE METER
25	7450
50	1020
100	95
250	2,2
300	1

These requirements are to be taken into account at every moment of the integration, assembly and testing of the hardware, and are measured over witnesses, as the direct measurement on the hardware could be a contamination source itself.

2.3.2.3 Science requirements

I am going to cover here the different needs and requirements that the calibration target needs to fulfil, and that are directly related to the science outcome of the instrument.

Wavelength calibration:

During the overview of the instrument, and in the block diagram (Fig. 2.21), were shown the different spectrometers that need to be calibrated. All the spectrometers but the IR spectrometer (which is part of the SCMU) are located in the SCBU. Starting with these spectrometers, all of them work, in a simplistic description, by introducing a dispersive element, a grating, that disperse the light in different angles according to its wavelength. With the appropriate optical design a polychromatic light spot in the entrance of the monochromator will have different images in the output of the spectrometer, spatially separated according to the different wavelengths. By placing a CCD in this image plane, or output of the monochromator, what we have is an array of light detecting elements (pixels), each of one measuring the amount of light in a certain range of wavelengths (depending on the resolution of the instrument). So, the first thing needed to have a calibrated instrument is to obtain a unique relation between wavelength and pixel number in our array. Usually in the laboratory this is done using spectral lamps that provide a set of known and fixed spectral lines that can be used to obtain de calibration polynom, ideally of 3rd grade or higher, providing an expression that assigns a wavelength to each pixel. That's the first need in terms of calibration, to provide a known, stable source of spectral lines that covers the whole range of SCAM.

Raman Rayleigh calibration:

During the theoretical introduction, when the Raman effect was introduced, it was shown that this effect is an effect relative to the excitation source. This means that the same Raman scattering happening for a certain molecular vibration will have the same value when talking about Raman shift, not depending on the wavelength of the excitation source, but this of course means that using different excitation sources, that same Raman band will have different wavelengths. When calibrating a Raman instrument using only Raman bands of well-known compounds, any effect depending on the laser is automatically taken into account, but in the case of SCAM, the calibration of the spectrometers needs to cover a wide range of wavelengths, and LIBS needs a calibration in wavelength, so, our calibration polynom will give the pixel/nm relation,

but not directly the pixel/Ramanshift relation. The Raman shift can be calculated then using the known expression:

$$RamanShift[cm^{-1}] = \frac{10^7}{\lambda_{ex}[nm]} - \frac{10^7}{\lambda[nm]}$$

The wavelength of the Raman band will be known, but there is a dependence on the wavelength of the excitation source, λ_{ex}, to provide the Raman shift, that even in the case of laser, supposed to be stable and fixed, can vary in time. One initial approach could be to measure the position of the laser directly, but this operation cannot be performed by SCAM due to the different interferometric filters that are part of the instrument. So the approach taken in this case is to include a sample with a Raman band with a high Raman cross section, that provides a high intensity when shot with the green laser, and also needs to be a band related to a vibration that is not sensitive to pressure or temperature and does not change with environmental conditions, this Raman band could be used to calculate the wavelength of the laser then and correct, if needed, the calibration in Raman spectra. This gives, In my point of view, a second need for calibration, a sample that is a good Raman scatterer, allowing short integration times and high intensity signals, and provides a Raman band that can be considered fixed and will not degrade when exposed to UV radiation.

VISIR calibration:

Visible and Infrared reflectance spectroscopy is a technique with a long history in space exploration due to its capability of providing mineralogical characterization (to some extent) of the surface of planets from orbit. In the case of SuperCam this technique is, along with the imaging, the technique with the farthest range, being able to obtain spectra from a few meters to “infinity”.

The way this technique works is by analyzing the reflectance spectra of the samples irradiated by a continuous light source, considering that some gaps in the spectra of the reflected light correspond to absorptions by some molecular groups. In the case of SuperCam this kind of analysis will be done using three spectrometers: the violet and visible spectrometer in the SCBU and the IR spectrometer that is part of the SCMU. This last spectrometer consists on an acousto-optic tunable filter that sweeps the IR region from 1300 to 2600 nm. focalizing the collected light into a single photodetector. In Mars the continuous light source will be the sunlight, so it is important to characterize the spectrum of the light irradiating the sample before any absorption is produced, and also it is important to understand what is measuring each element in the absence of light, the dark current. It could be also useful to have samples with a well-known reflectance to evaluate better the differences induced by the illumination light source.

So, these are, to summarize, the requirements to calibrate the VISIR technique: to have a white sample that reflects almost all the spectra of the received light (in the measuring range), a dark sample that absorbs the received light, and then some samples with a known reflectance along the spectrum of interest. Since it is interesting the way the calibration samples absorb or not the incident light, the samples should be designed in a way that avoid any specular reflection, and of course, given the importance of performing calibration activities before measurements for this technique, the samples need to be clean of dust and other contaminants during the mission time.

Image calibration:

RMI, as described before, will provide high magnification images of the areas were SuperCam will perform the measurements. This support of images gives context and morphology information from the targets to be analyzed and thus, a good calibration of the focusing and the color balance is important to get the best possible images.

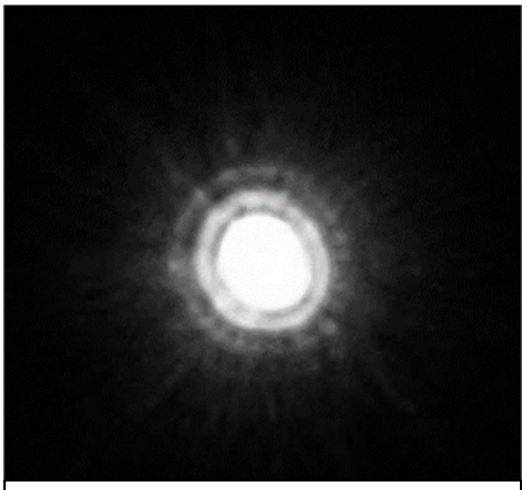

FIGURE 2.31: A STAR IMAGED BY A TELESCOPE (WIKIPEDIA)

For every optical system different effects make that the input from the object plane does not match with the output at the image plane. This happens when we stop considering the light and the telescope from a pure geometrical optics point of view, and we start treating the light as a wave. The system's aperture cut the extent of the wavefronts of the light inducing diffraction, and making that even in a perfect system with no optical aberrations the object doesn't match its image, and that change is described in the Optical Transfer Function, OTF. This directly seen in telescopes where a star is observed differently in the image plane depending on the pupil of the system and its symmetry and aberrations, for an ideal refractive telescope this typically turns the star (a point) into a diffraction pattern called airy discs. To understand this transfer function can give us information of how well we are focusing our system and the limit resolution that can be achieved. In the figure 2.32 obtained from the main article on Wikipedia it is shown how this function depends on the focusing of the system:

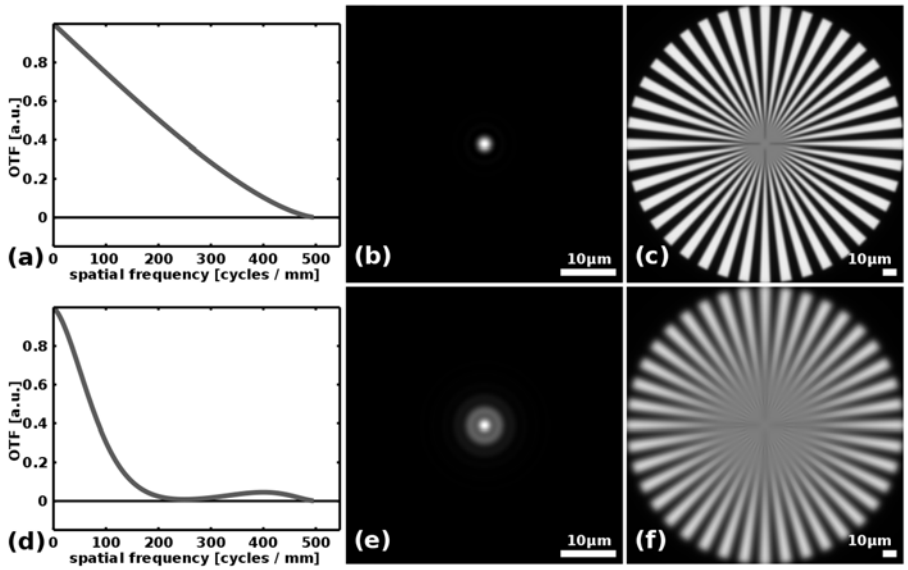

FIGURE 2.32: OTF VARIATION WITH IMAGE QUALITY (WIKIPEDIA)

To have perfectly characterized our imaging system, along with the OTF, we need to take into account the ccd that will collect the image, and that implies to correctly balance the whites, that depend on the fact that the illumination might not have a perfectly distributed intensity along the spectrum, and to adjust the contrast.

For the SCCT this means to provide a typical set of RGB targets to calibrate the three color channels, white and black targets to serve as reference, and then intermediate gray scales to adjust the contrast. For the OTF it is needed a geometric pattern similar the one shown before, where different spatial frequencies are provided and used to optimize the focusing of the system and obtain the transfer function, although in this case it could be better to talk of a Modulation Transfer Function, which is a particular case of the OTF that neglects the phase effects.

Organics:

It is one of the main scientific objectives of the mission, to evaluate the habitability of Mars, past and present, and look for possible traces of markers that could mean the presence of organics or past life on Mars. During the introduction of the environmental requirements it was commented that the surface of Mars is continuously irradiated with the UV from the Sun, and its effect on the organics. This means that it is not expected to find complex organic molecules in the surface of Mars, possible organics that appeared at some moment in the geological past of Mars may have been degraded into simpler molecules due to the environment. It is then interesting to know as much as possible of this degradation process, see if the degradation occurs just by the break of long organics chains into smaller groups, or the appearance of new groups due to the introduction of oxidants, for example. Since LIBS is not sensitive to the structure of the sample, only Raman spectroscopy will have the ability to see these variations in Mars. So,

summarizing into a science requirement, as part of the calibration target there should be a organic sample providing different molecular groups and Raman bands that can be measured while degrading when exposed to martian environment, it also needs, of course, to be a good Raman scatterer in order to have a good signal to be analyzed.

Chemometrics calibration:

Finally, the objective of SCAM is not only to provide identification of the targets, but to provide measurements of the abundance of certain elements or molecular groups. In the case of LIBS, while the position of the different emission lines that conform a spectrum can be considered fixed, the relation between intensities can be affected by matrix effects, environment, etc. To take everything into account and improve the calculations based on the different spectral data that provided chemometric information of the sample. Not only it is useful to calibrate each technique individually, but to have a cross calibration among the different techniques. In the final section of this work we will present an example of the power of data fusion techniques for chemometric calculations, it is important then to be able to calibrate properly how the different chemical abundances of different elements, as seen by LIBS, correspond to molecular abundances as seen by Raman, or relate luminescence from certain element with its intensity in LIBS spectra.

To have this kind of calibration it is necessary to carry with the instrument a set of samples of different mineral species with very well known chemical composition that can be used as reference for calculations.

Of course, for these samples to be useful in terms of calibration it is important that they are homogeneous and the same measurement is obtained no matter where in the samples we shoot. Given the spot size of the analysis and the pointing accuracy, we can set this limit to be around 100 microns for SuperCam. This means that at a scale of 100 microns the different samples need to be homogeneous in terms of elements distribution, and also homogeneous from Raman point of view. This homogeneity needs to be characterized, as needs to be the final chemical composition of the samples that will fly to Mars.

2.3.2.4 Summary table

As a summary, a more complete list of requirements to be met by the SCCT is included in the following tables, according to the level or kind of requirements considered. Please note that part of the requirements are under Non Disclosure Agreements with NASA, some information is part of their know how and it is not for public release, that's the reason for some gaps or undefinitions:

REQ. TEXT	Evaluation
The not-to-exceed envelope for SuperCam components shall be as shown on the appropriate SuperCam interface definitions agreed with JPL	Demonstration Inspection
The not-to-exceed value for SuperCam Calibration Target mass is 0.27 Kg	Test
The accommodation of SuperCam laser calibration targets (LIBS & Raman), should make them viewable by SuperCam Mast-Unit, at a distance between 1.5 and 1.7 m (goal is 1.56 m to compare with ChemCam). The passive samples used for VISIR and imaging should be placed in a way that ensures that no shadowing of other hardware on the Rover's deck can shadow them during operation time. Note: for the laser targets only, there is no requirement on shadows. Rationale: This distance is important to keep MSL heritage and to avoid exclusion zones/distances, where the laser cannot be fired.	Demonstration Inspection
All enclosed spaces shall have vent paths for releasing entrapped air during launch and for repressurizing during Mars entry.	Demonstration Inspection
SCCT functional performance shall be verified before and after environmental testing.	Demonstration
M2020 instruments which are sensitive to plume heating and/or contamination shall be designed or protected against such heating and contamination. This is due to the Sky Crane rockets, that could impact or contaminate the SCCT during landing.	Analysis
Due to the wide range of latitudes covered in the initial definition of the mission (before setting a landing site) and the large diurnal swings of Mars surface temperatures, the SCCT will need to face temperatures going from -130 ºC to 80 ºC during its operation on Mars	Test
During the Mars surface mission phase, the SCCT shall be designed to maintain temperatures as required when exposed to the Surface Solar Fluxes and this should be done passively.	DESIGN
SCCT shall be designed to maintain temperatures, as required when exposed to the Mars diurnal near-surface and ground temperature profiles, and again, this should be done passively.	Analysis Test
The SCCT shall be designed to maintain temperatures as required when exposed to the sky temperatures of Mars. This should be done passively.	Analysis Test
The SCCT shall be tested in the appropriate thermal environment for design verification according to the parameters, levels, and margins agreed with JPL	Inspection

REQ. TEXT	Evaluation
The Project specifies the type of test to be run (ie. Qual, PF or FA). The test medium and pressure shall be as required by JPL.	Inspection
Assemblies subjected to thermal testing shall demonstrate performance within specification over all mission operational modes during the cold and hot temperature extremes and during transitions between thermal states.	Test Hierarchy
The SCCT shall be designed for the following Mars atmospheric composition. Based upon Viking Lander measurements, the mole fractions of gases in the Mars atmosphere are approximately: 0.955 ± 0.0065 CO2 0.027 ± 0.003 N2 0.016 ± 0.003 Ar 0.0015 ± 0.005 O2 0.0007 CO 2.5 ppm Ne 0.3 ppm Kr 0.08 ppm Xe	Inspection
The SCCT shall be designed to operate and/or survive, as required per applicable Functional Requirements, over possible atmospheric pressure values it could face.	Hierarchy
The SCCT shall be designed to withstand a the atmospheric pressure decay rate associated with the launch and also designed to withstand the Mars descent repressurization rate.	Analysis
The SCCT shall be designed to operate as required per applicable Functional Requirements during and after exposure to sustained winds required by JPL	Analysis
The SCCT shall be designed to survive after exposure to sustained winds as required by JPL	Analysis
The SCCT shall be designed to survive after exposure to wind gusts as required by JPL	Analysis
The SCCT shall be designed to mitigate the effects of dust contamination during Mars descent and surface operations.	Analysis
It shall be shown by analysis (or test) that the performance of the assembly will not be impaired by this deposition of dust over the required M2020 mission lifetime.	Analysis

REQ. TEXT	Evaluation
The SCCT shall be designed for or mitigate for the survivability for a Mars dust storm condition.	Hierarchy
The random vibration design and test requirements for assemblies are specified by JPL. These spectra shall be applied in each of three orthogonal axes at the mounting interface of the assembly. The Design/Qual exposure time is 2 minutes per axis, PF and FA exposure is 1 minute per axis.	Test
The assemblies shall be tested to the random vibration zone requirements of JPL, and may be force limited to reduce over-test at hard mounted resonance frequencies.	Test
Assemblies to be mounted onto/within the M2020 spacecraft shall be designed to withstand the pyrotechnic shock environment.	Test
As a minimum, all materials used in the construction of instruments shall be non-shedding and low outgassing with a Total Mass Loss (TML) of <1.0% and a Collected Volatile Condensable Material (CVCM) of <0.1% as tested in accordance with ASTM E595 â€œStandard Test Method for Total Mass Loss and Collected Volatile Condensable Materials from Outgassing in a Vacuum Environment	Inspection
The Outgassing Rate Measurement should meet ECSS requirements: 1.) Assume temperature causes no damage to hardware. 2.) The time period for the bakeout phase does not begin until the specified temperature and chamber pressure of 5.0E-5 Torr are reached. Certification at the specified certification temperature may be attempted after 50 hours of thermal-vacuum conditioning at the bakeout temperature.	Analysis Inspection
SCCT Exterior Cleanliness Requirements at Last Access: Calibration Target: Molecular = 100 ng/cm^2; Particulate = L300	Analysis Inspection
The bakeout operations and outgassing measurements should be done at the specified pressure. Outgassing rates shall be demonstrated to be less than the maximum rates listed prior to hardware delivery. JPL with measure the global outgassing rate after delivery.	Analysis Inspection

REQ. TEXT	Evaluation
SCCT Exterior Cleanliness Requirements at Delivery: Calibration Target: Molecular = 100 ng/cm^2; Particulate = L300	Analysis Inspection
SCCT's external surface average bioburden density shall not exceed 300 spores/m2.	Demonstration
The SCCT shall be compatible with PP microbial reduction processing (e.g. alcohol wiping, HMR, etc) and bioassay verification (water dampened swab or wipe).	Inspection
The SCCT hardware shall be cleaned with isopropyl alcohol (or ethanol) prior to assembly.	Inspection
The SCCT shall incorporate multiple microbiological samplings at different stages of the assembly process.	Inspection
The SCCT Ground Support Equipment (GSE) shall also be cleaned with isopropyl alcohol prior to entering a clean room facility/bench. The cleaning level of the GSE shall be performed to the same stringent levels that the flight hardware.	Inspection
The SCCT team shall apply planetary protection requirements to any potential flight hardware (e.g. qualification, proto-flight, flight spare) or hardware that may be processed along with flight hardware.	Inspection
The SCCT team shall conduct PP cleaning and microbial reduction on ground support equipment and hardware used for integration and environmental testing.	Inspection
The SCCT team shall use a Class 100K/ISO Class 8 or better clean room facility or clean bench to assemble major piece parts and sub-assemblies, perform functional testing, final integration, and continued testing. Various parameter specifications permitted for burden estimates where bioassays are not feasible can also eliminate the need for a bioassay.	Inspection
All microbiological sampling and assays for the SCCT shall be carried out by certified personnel.	Inspection
The SCCT team shall package and transport flight hardware to minimize biological and organic contamination.	Inspection
The SCCT team shall identify any PP handling constraints as part of the PDR, CDR, and HRCR/IDR packages.	Inspection

REQ. TEXT	Evaluation
The SCCT team shall provide an organic materials inventory of bulk constituents with the associated mass for all launched hardware.	Inspection

A minimum of 20 calibration targets shall be implemented for LIBS. They should be representative of major rock units, following recommendations of the SuperCam calibration group.	Design
One 10X10 mrad FOV Ti target shall be used for spectral calibration with LIBS.	Design
A minimum of 2 calibration targets shall be implemented for Raman. They should be representative of 2 mineralogies, following recommendations of the SuperCam calibration group.	Design
There shall be a geometric target to measure resolution and modulation transfert function (MTF) of the imaging capability.	Design
There shall be 3 RGB targets for white balance of the imaging capability. Magnets will be used to minimize dust over >= 1 mrad.	Design
Two targets (white > 95% (TBC) and dark < 5% (TBC)) shall be used to monitor the radiometric and spectral calibrations of the VisIR capability. Magnets will be used to minimize dust over ≥ 1 mrad.	Design

Each individual LIBS calibration target shall be able to accommodate > 100 analyses of 50 laser shots each.	Inspection Test
Each individual LIBS calibration target shall have an angular extent of ? 5 mrad as viewed from the MU	Inspection
Two targets (white > 95% (TBC) and dark < 5% (TBC)) shall be used to monitor the radiometric and spectral calibrations of the VisIR capability. Magnets will be used to minimize dust over ? 1 mrad.	Inspection
One target shall be used for the Raman investigation wavelength and intensity calibration. Its angular extent shall be larger than 2 mrad.	Inspection
At least one target shall use a magnet to collect dust for LIBS analysis.	Inspection
Several targets shall be used for the RMI investigation, to check for resolution, the RGB scale, and Grey scale.	Inspection
At least one target shall be used for the calibration of the IR capability. Its angular extent shall be larger than 2 mrad. It will use a magnet to minimize dust.	Inspection
Several targets shall be used for the Raman investigation Their angular extent shall be larger than 2 mrad.	Inspection
Three targets shall consist of samples of the plagioclase-feldspar family, being close to the end-members albite, anorthite, and orthoclase.	Inspection

REQ. TEXT	Evaluation
At least two targets shall consist of samples of the pyroxene family, with at least one low-calcium pyroxene and one high-calicium pyroxene	Inspection
Two targets shall consist of olivines, one being Mg-rich and one being Fe-rich	Inspection
At least one target shall consist of fluorine-bearing apatite. The F, Cl, and H abundances shall be documented.	Inspection
At least one target shall consist of a carbonate (calcite, aragonite, dolomite, and/or siderite)	Inspection
At least one target shall consist of a calcium sulfate. The H and Sr abundances shall be documented.	Inspection
At least three targets shall contain significant amounts of phyllosilicates (e.g., smectites or saponites) of known composition.	Inspection
At least three targets shall consist of fine-grained material near the average composition of Mars soil.	Inspection
At least three targets shall be doped with significantly different levels of the following elements: Li, B, Mn, Cr, Ni, Cu, Zn, As, Rb, Sr, Ba, Pb	Inspection
All LIBS targets shall be assayed for major, minor, and trace elements at uncertainties typical of XRF (where applicable) or of typical laboratory measurements	Inspection
All LIBS targets shall be characterized for heterogeneity.	Test
All LIBS targets shall produce a consistent LIBS spark.	Inspection

2.3.3 Samples

The SCCT's main components are the samples themselves. These samples need to calibrate the instrumentation and provide the support that science team needs for calculation on the acquired data from samples on Mars.

The scope of this section is more focused on the mineral samples that have been included in the SCCT. Other calibration targets were briefly described in section 2.3.2.3.

2.3.3.1 Description

Every spectroscopist that has at some point worked with LIBS technique knows that the first thing you need to have a good analysis is a solid target. If trying to do LIBS on a powder, the shockwave of the laser shot displaces the surrounding material changing the sample for next shot, and making more difficult to obtain a good ablation.

In the laboratory what we do is a previous processing of the sample aggregating it into a pellet with a hydraulic press. However, this processing can be not enough in some samples that doesn't aggregate well. This was the example of the amorphous zinc borate (Sanz-Arranz, 2018), making impossible to get a good pellet of this substance.

Also, SuperCam instrument will measure the samples at a fine scale, the LIBS spark at the distance of the calibration targets will be of 300 microns diameter. This means that the homogeneity of the samples needs to be warrantied at a lower scale, and this requirement introduces two needs into de manufacturing of the samples:

- To ensure the homogeneity it was considered that the best partice was to crush the original materials (that would have been more inhomogeneous than the requirement) and then obtain pellets from an homogenized powder.
- The samples need to be characterized not only to know the average composition of the samples, but to asses the homogeneity of their elemental composition (for LIBS), and their structure (for Raman)

In the case of ChemCam, the samples were also manufactured from powder and were of ceramic nature. These ceramics were obtained at low temperature, 800 ºC, with the addition of lithium tetraborate flux (Vaniman, 2012). The mentioned processing allowed to manufacture ceramic discs of materials typically soft and instable, but now in a matrix more durable and reliable from the Mission Assurance point of view.

For SuperCam, the processing changed trying to get samples with enhanced mechanical properties, when compared to those from ChemCam, while keeping the science value of the selected samples. In this case the technique used to prepare pellets was flash sintering.

Sintering is a processing that makes objects from powder materials by heating them to a limit, bellow their melting point, in which, by diffusion of atoms, bonding between grains starts to happen. This is also the basis of the manufacturing of ceramics. In Spark Plasma Sintering, SPS, or also known as flash sintering, the process is much quicker than conventional sintering, minutes versus several hours. The heating rate in a conventional furnace can reach ramps of 10 ºC maximum, meaning that to reach 1200 ºC it would take two hours, and this is just to reach the temperature of the processing.

In flash sintering simultaneous application of pressure and temperature occurs, what can speed up the heating of the sample and achieve the working temperatures in a matter of minutes, with ramps that can be over 300 ºC easily. Another advantage come from the increase speed of the process. The grain growth is almost stopped, meaning that individual grains at nanoscale will coagulate with surrounding grains instead of having bigger grains, what helped in the final homogeneity for the analysis. This leads to an enhance in the mechanical properties of the final product, making pellets harder than the regular ceramic processing.

The samples for SuperCam Calibration target were manufactured reaching temperatures exceeding the 1000 ºC, what also introduced another advantage form the

contamination control point of view, the processing itself reduced the amount of volatiles in the samples to the minimum.

By this manufacturing process more samples than the required 22 were prepared. This extended list of candidates allowed to have backups for materials that could be problematic during qualification (a critical activity given that the samples are not standard materials), and also providing more materials that the science team could consider of interest after the final selection of the landing site.

2.3.3.2 The samples

The samples to be onboard the SCCT need to cover a wide variety of composition to get good calibration curves, having different mixtures of different elements, bur they also need to be of different rock types. Having different rock types helps also with the impact of different matrix effects from the different structures of the samples, and that might affect the LIBS spectrum. Because of this several samples covering different mineral families have been selected.

Some ratios of main elements are of great interest when analyzing rocks on Mars, and for that reason samples providing different ratios of this mixtures need to be provided. Examples of this are Al/Si, (Fe+Mg)/Si, Na+K/Si, Ca+Na/Si, Na/K ratios, of great interest in geochemistry (Cousin, 2018). Six slots of the SCCT were reserved for targets that could help with this calibration, covering feldspars, olivine and pyroxenes. These samples were directly sintered to a pellet of the final diameter (1 cm) that was later remanufactured to achieve the tolerances and shape required by the SCCT mechanical team.

In addition to this mayor elements compositions, come trace elements are also of interest for SuperCam. For this reason five slots of the SCCT were reserved for samples with different amounts of minor elements of interest: Sr, Rb, Ba, Cr, Cu, Li, Ni, Zn and Mn.

Apart from the mayor and minor elements calibration samples, addition materials were included to have a good database of different rocks and materials. In this group of samples covering carbonates, basalts, sulfur rich target and a martian soil analogue were included.

Finally two specific targets close the composition of the LIBS samples selection on the SCCT. The first one is an apatite containing fluor, chlorine and hydrogen, that could be taken as reference when compared with the phosphor from the sample. The other special samples has more to do with a cross calibration with ChemCam, and consists on a synthetic shergottite from a ChemCam's Calibration Target spare.

2.3.3.3 Characterization

The described samples, candidates to be included in the SCCT FM, had to be analyzed to check their homogeneity and that their final chemical compositions fitted with the requirements from the science team.

The whole characterization process included several techniques and institutions, and the results were evaluated by the science team so the final selection of candidates covered all the science requirements.

Homogeneity assessment: The homogeneity of the samples was checked, as was found necessary, at two levels: elemental distribution and compounds distribution on the samples. Two different measurements were done at the University of Basque Country that were used in a methodology developed in the analysis of meteorites (Aramendia, 2018): XRF imaging to check the elemental distribution in the samples, and Raman imaging also to check the distribution of different compounds or phases in the surface of the samples.

Functional assessment: As the objective of the samples is to provide calibration to a Raman-LIBS instrument, a functional tests were done on each sample at relevant martian conditions of pressure. This test was used to check the measurements on different points of the samples, so also assessed the homogeneity, and that the spark was produces and could be measured. The analyses were done mainly in Toulouse using a bread board of ChemCam, but some of them were done at the facilities of the University of Malaga.

Composition measurement: In order to relate measurements from the different techniques with a certain composition of material, it is needed to characterize the target to obtain a measurement of their compositions as exact as possible. This was done by two different methods: microprobe analysis and Laser Ablation Mass Spectroscopy. The first one introduced a problem in the assessment given the huge difference in the size of the analysis spot. Given the micro scale that is evaluated by the microprobe, different grains (bellow 60 microns diameter) are evaluated at each measurements, what introduced great uncertainties in the final measurement from this technique. Finally, the LA-ICPMS provided an area of analysis similar to the one that is going to be used, providing also a greatly accurate measurement on the chemical composition of the samples. This technique, in comparison with the dilution method, allowed to have measurements directly obtained on the samples to be mounted on the FM.

The results from the different analyses will be included in a collection of papers related to Mars 2020 mission. But as an example the characterization of the homogeneity of a ferrosilite sample is included:

XRF results:

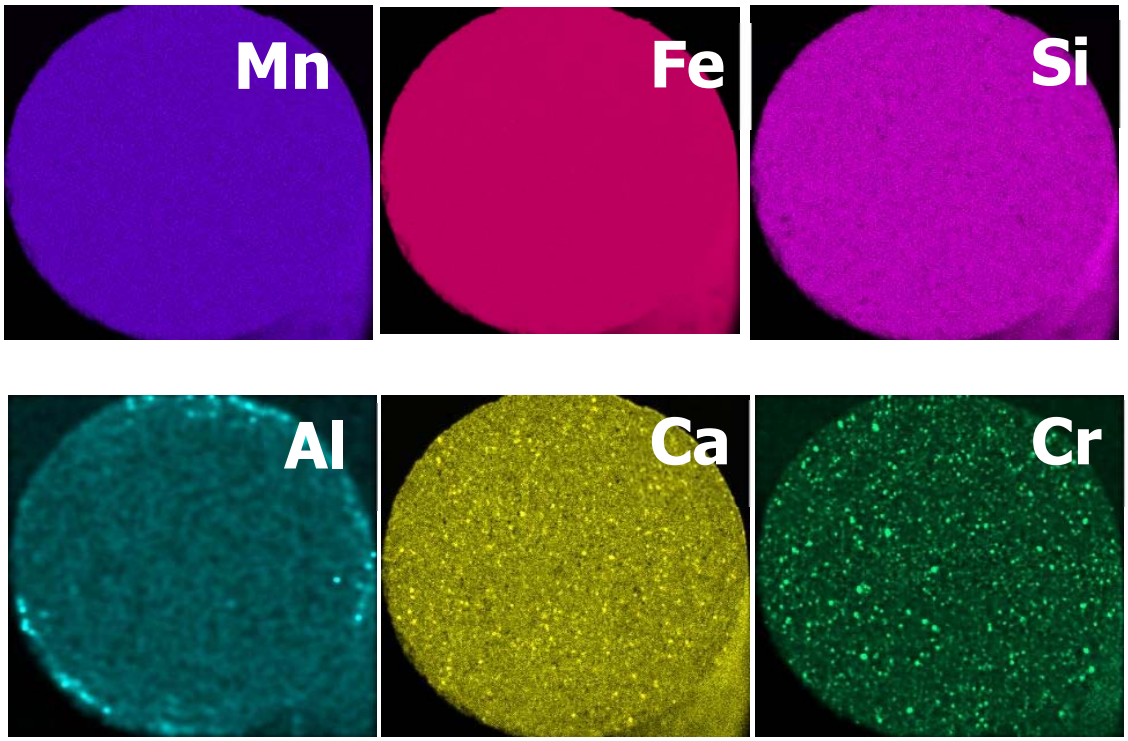

FIGURE 2-33 XRF IMAGING OF FERROSILITE SAMPLE (EHU)

The previous figure, Fig. 2.33 , shows the distribution of the different elements as provided by the XRF imaging instrument Bruker M4 Tornado. The imaging capability of this instruments allows a first assessment based on imaging, getting a quick conclusion, the elements in the top row are well distributed, and the sample can be considered homogeneous for those elements, while the elements in the bottom row are not well distributed and present hot spots. Also % composition can be calculated, and obtain a measurement in a selected number of points so relative standard deviation of the concentration can be evaluated. Whit this data it can be measured what samples are homogeneous for what elements:

TABLE 2-6 ELEMENTAL CONCENTRATION OF DIFFERENT ELEMENTS AND ITS RSD (EHU)

%	Mg	Al	Si	P	K	Ca
Mean	3.21	0.79	25.2	0.084	0.072	2.33
Dev	0.24	0.21	1.1	0.061	0.027	0.52
RSD	7.37	26.9	4.41	72.7	38.4	22.2
%	Ti	Cr	Mn	Fe	Zn	Sr
Mean	0.0315	0.082	2.539	65.6	0.0089	0.0117
Dev	0.0082	0.047	0.080	1.5	0.0085	0.0018
RSD	26.0	58.0	3.16	2.41	95.1	15.6

This analysis provides enough data to select what elements can be considered homogeneous in this sample, and therefore can be used in a calibration based on LIBS spectra of this target.

Raman imaging:

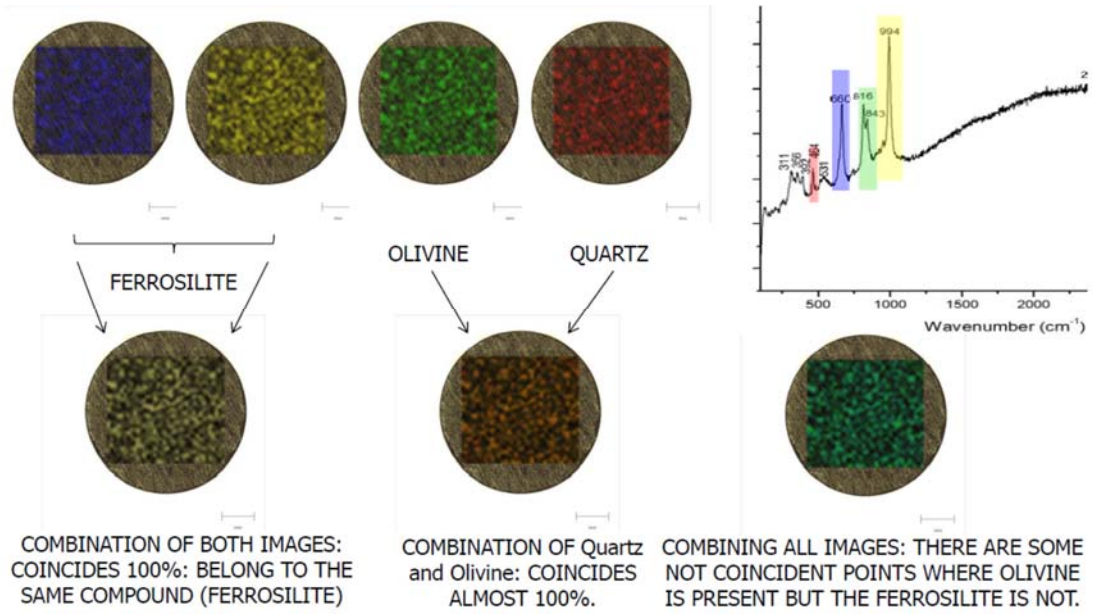

FIGURE 2-34 RAMAN IMAGING ANALYSIS AND MAJOR FINDINGS

The images obtained by a Renisaw inVia instrument are based on individual Raman spectra obtained with this confocal instrument, with a excitation source of 532 nm. The figure 3.34 shows how this sample of ferrosilite has points were olivine is present and ferrosilite cannot be found. This result was expected, as the flash sintering process can induce, given the high temperatures and pressures, changes in the samples. The samples can keep the oxides distribution but the phases have changed, with ferrosilite turning into olivine, or dehydrations occurring in other kind of samples (Gomez-Nubla, 2018).

Finally, the results from the LIBS and fine characterization will also be published in a paper form A. Cousin, but preliminary results have been published in (Cousin, 2018). As for today they are not available for disclosure.

The final selection of the samples is described in the section of the FM.

2.3.4 SCCT development: the path to Mars

2.3.4.1 Development plan and model philosophy

The main risk on the development of the SCCT was the great variety of nonstandard materials involved in its design. The samples themselves were one of the main potential issues to be addressed during the design and development of the unit, specially having into account the shock leves that needed to be faced.

The SCAM instrument is a high heritage instrument inheriting come components or design solutions from Chemcam. In the case of ChemCam CT, the materials used for the target were ceramics, and some of them showed cracks after landing. As an improvement and lesson learned, the baseline is to use flash sintering to manufacture the samples to be included in the SCCT, what should provide a better mechanical performance, this in addition to a smaller size of the targets should provide a higher reliability than ChemCam's targets. Anyway, the fact of having at least 20 different samples from 20 different materials, passing through sintering presented some challenges:

- From the mechanical point of view: The behavior of the samples is unknown, and the amount that was available made it not feasible to perform a full characterization of their properties. This limited the accuracy of simulations and analysis.

- From the thermal point of view: Different materials presented also different thermal behaviors, this needed to be taken into account when designing the SCCT, the thermomechanical design needed to adapt to a great variety of materials.

- The final samples included in the SCCT were not totally defined until a stage of the project far passed Critical Design Review, when a final design was already closed. This implied that several candidates needed to be taken into account, more than really needed, and the design needed to be reliable for any possible combination of these candidates.

- Glued materials. Gluing is always a risk, especially when happening in hardware going through high temperatures, as in DHMR. The SCCT has gluing procedures in the magnet-sample stack of the passive samples, and in the geometric targets and the diamond.

- High g shock zone. The SCCT is included in 3.5 g zone, this means that needed to be qualified for 3500 g pyroshock test. This kind of test can be hardly simulated, having an impact on the development, and is difficult to be tested. Also, the presence of nonstandard materials that could be damaged for high g shocks was the main risk.

Model Philosophy:

As for SCAM project, four main models were identified as required:

- SCCT CU (Calibration Unit): this model consists on a set of calibration targets, not limited to the number that can fit into the SCCT holder, and not mounted in any supporting structure. The purpose of this model is to serve as targets for calibration and functional tests for SCAM's development.

- SCCT EM (Engineering Model): this is an engineering model. The model itself needs to be representative of the shape, envelope, weight and interface of the FM. This model is not intended to serve as STM. The Rover's EM model functionality will be limited, since it will have no laser on, what makes not necessary to include real

samples. However, it should serve for pointing and accuracy testing. As this is not a STM, there is not need to be flight-like in terms of coatings or paints, which are the only thermal-control measures of the target. This model is deliverable to JPL.

- SCCT EQM (Engineering and Qualification Model): the qualification model needs to be absolutely representative of the flight model. No differences in envelope or size (farther than manufacturing tolerances) will be allowed. Also, the coating, surface finishing and paint need to be as close as possible. The set of samples to be included in this model needs to be also flight-like. Any changes and differences between this model and FM should be addressed through change notes and be taken into account if they could invalidate qualification campaign. This model is not a deliverable.

- SCCT FM (Flight Model): this model includes the final set of samples provided by the science team. Needs to fulfil all the requirements applicable to the SCCT, with the exception of those related to the qualification tests campaign. This model is deliverable to JPL and is the one that will fly to Mars.

- SCCT FS (Flight Spare): a twin model of the FM. The idea, given the kind of hardware, is to manufacture FM and FS together, so same processes, materials or workmanship are assured to remain the same between FM and FS. This model is to be kept under project's custody clean and ready to deliver upon JPL request.

Given the mentioned constrains and risks, it was also found advisable by SCCT development team the manufacturing of an Engineering Testing Unit (ETU). To perform the most concerning environmental test, which is the shock test, on a flight-like model. For this model the mass, the mechanical design and the interface need to remain the same as SCCT FM. It should be able to accommodate the same samples as the SCCT FM and be able to go under pyroshock testing. This model is not a deliverable.

Development path and model details:

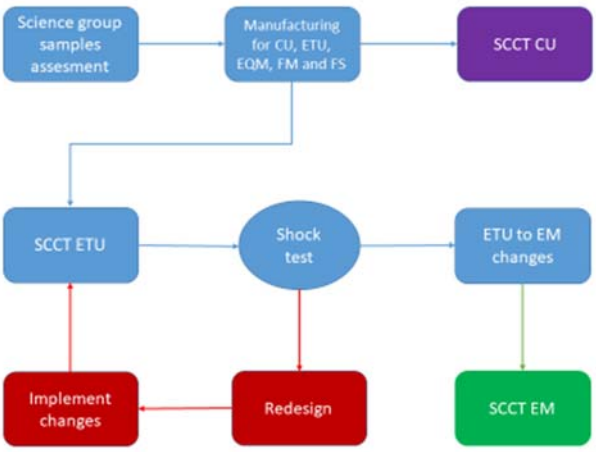

FIGURE 2.33 SCCT DEVELOPMENT PATH

First milestone to be accomplished was the definition of a good set of candidates for the samples to be implemented in the FM. The number of candidates needed to be higher than the needed samples for the FM, in order to have backup options if a sample didn't survive the testing campaign, and also to provide a variety of candidates to the science team to decide the best fitting set to Jezero mineralogy. Due to requirements of homogeneity, the samples for all the models were manufactured together in sets of at least six replicates (CU, Development, qualification, FM, FS and science backup). One full set of these candidates is to be delivered to LANL as SCCT-CU.

Once the possible candidates were manufactured, a preliminary was integrated into the SCCT-ETU for shock testing. This test served to evaluate the performance of the mechanical design and the different samples against pyroshcok.

SCCT-ETU:

This model needed to implement the following features:

- Needs to accommodate five passive samples in their flight configuration.
- Needs to be able to accommodate at least 23 mineral samples in flight configuration.
- Elements such as the Geometric plate or Ti plate can be substituted by dummies.
- Nameplate can be also substituted by a dummy.
- General envelope of the model needs to representative of FM as should be the mass.
- Rover interface needs to be the same of FM.
- Materials of the holder structural parts need to be the same of FM.
- Fasteners will be similar to those intended for FM, as they have to provide similar fixation.
- Surface finishing, coatings, paints or cleanliness are not needed to be representative of the flight configuration.

SCCT-EM:

Taking advantage of the parts manufactured for the SCCT-ETU and ETU 2 integration, once this model is no longer needed, ETU can be refurbished into the SCCT-EM, as a cost-saving measure. The SCCT-EM is intended to be implemented in the Rover EM model, model with limited functionality, and therefore, representativity of the EM is also limited. Here are the features to be provided by SCCT-EM:

- Needs to accommodate five passive samples or dummies.
- Needs to accommodate 23 sample dummies.
- Ti plate can be substituted by a dummy.
- Flight-like geometric target is required.
- Nameplate to identify the model.
- General envelope of the model needs to representative of FM as should be the mass up to a 20% uncertainty in the mass.

- Rover interface needs to be the same of FM.
- Materials of the holder structural parts need to be the same of FM.
- Fasteners will be similar to those intended for FM, as they have to provide similar fixation.
- Surface finishing, coatings, paints or cleanliness are not needed to be flight-like.
- No remove before flight cover or other GSE needs to be provided.

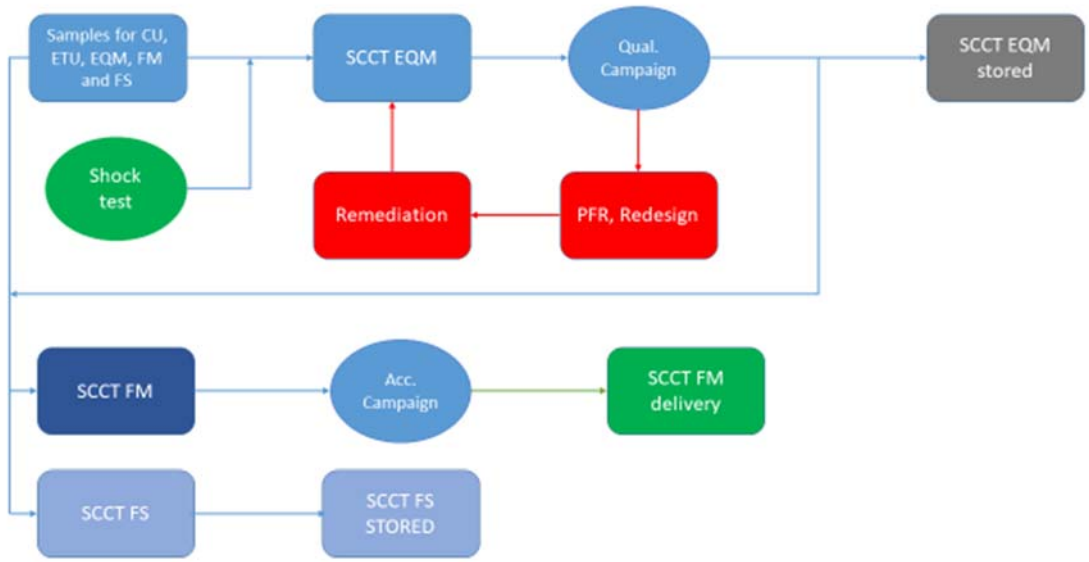

FIGURE 2.38 FLOWCHART FOR THE FINAL DESIGN.

SCCT-EQM

This model should be absolutely representative of the flying model and serves to validate the design and to verify the design capability to survive the qualification levels. For that purpose the design, envelope and mass need to be equal, within margins, to those of the FM. Should any change need to be implemented between EQM and FM, change note should be issued and the impact of this change in the qualification needs to be addressed.

All the processes and materials need to be flight-like, and the model is intended as rehearsal and testing of CC & PP plans. All the samples and plate elements needed to be like those of the FM. Exceptionally, small differences in not structural/science elements were allowed upon agreement with the project.

This model served to demonstrate that the design was solid enough to be sent to Mars, so it was after the qualification campaign that the manufacturing of SCCT FM and FS was authorized, following same manufacturing procedures, mechanical parts and providers used in the EQM. This model is not a deliverable. The details on the qualification campaign are showed in a later section.

SCCT-FM and FS

These models are the final design, after validation and in agreement with science team, that is manufactured to be sent to Mars. While the FM was delivered to JPL after the acceptance campaign to verify workmanship, the Flight Spare remains in clean environment waiting for final actions and acceptance campaign in case it is required by JPL. This is a common measure in space project not to risk the launch in case an unlucky event makes the FM not able to be flight.

2.3.5 The path to a final design

After the introduction of the model philosophy and the development plan followed to get to the final, flight, model, I wanted to introduce a narrative of the different events and advances made in accordance to this plan, now with dates.

After the announcement of the inclusion of SuperCam in the payload of Mars 2020 Rover, the team in Spain was set. Between the date on the announcement and the Delta PDR, held in Valladolid in Feb. 2016, where the preliminary design was evaluated by the project, all the work done until that moment was related to development of different models and concepts that could be worthy evaluating.

Pre PDR:

FIGURE 2.39 CHEMCAM'S CALIBRATION TARGET

Before the PDR was held, a concept design based on ChemCam's calibration target was the baseline. In this concept design just 20 mineral samples were included, along with a spectralon white target for the IR. The color calibration and grayscale was initially planned to be done using a plate. Regarding the fixation of the samples in place, it was done by means of a manufactured screwed lid and the load was applied by a spring washer. This model had several issues to meet all the requirements.

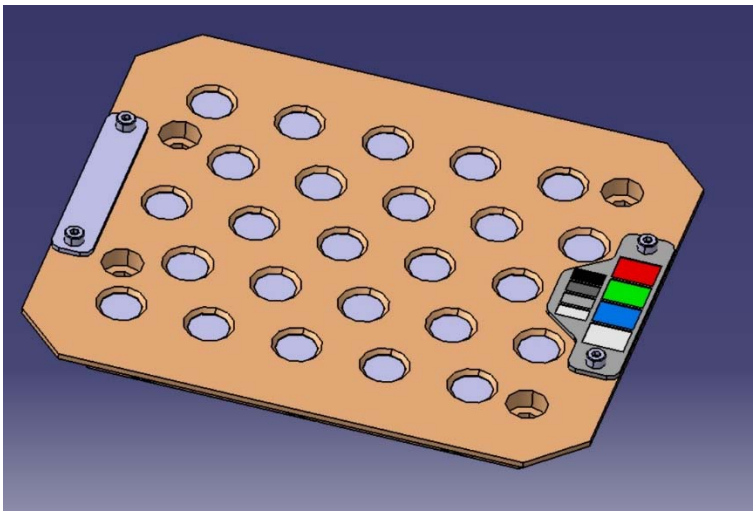

FIGURE 2.40 SCCT CONCEPT BEFORE PDR (AVS)

To start, nor the spectralon or the color plate had any measure to prevent the deposition of dust. Also, the fixation mechanism for the samples was considered a risky, although it was later kept during PDR.

In this concept the main concern was the thread of the sample screw. The lid was too thin, what required the thread of the screw to be extra thin. This couls have been a potential issue during integration if at any point the lid was damaged.

The different Belleville, or spring washer, were introduced to absorb vibrations, shocks, and manufacture tolerances of the samples.

PDR level:

The PDR, standing for Preliminary Design Review, served as the first opportunity for the whole SCCT development team to be together. This milestone meant a great boost to the project, with several details changing towards a more defined model that could me manufactured.

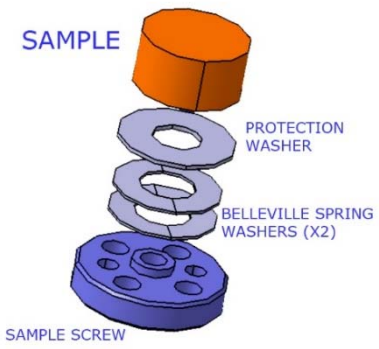

FIGURE 2.41 SCCT SAMPLE FIXATION INITIAL CONCEPT

The first change was the need to prevent dust deposition on selected samples. This was addressed using a development similar to the one used in MastCam's calibration target, that was also based on the magnetic experiments on board the MER. This consist on the inclusion of a magnetic ring around the samples that will make the ferromagnetic dust on Mars to follow the

field lines. This leaves a small area in the center of the sample where just non-magnetic dust could deposit.

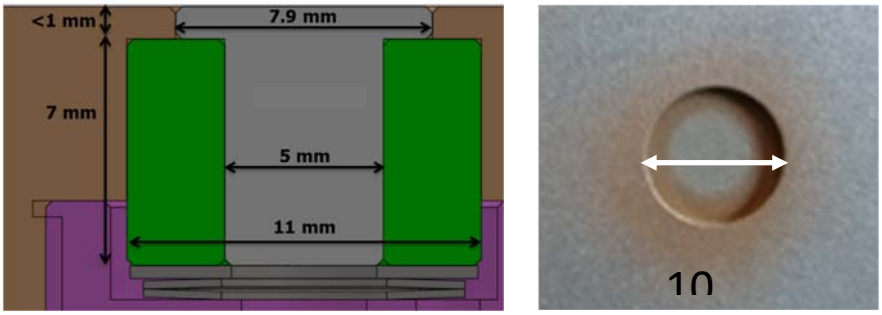

FIGURE 2.42 A) CROSS SECTION OF THE SAMPLE-MAGNET STACK. B) TEST SHOWING HOW FERROMAGNETIC DUST AVOIDS THE CENTER OF THE SAMPLE.

The sample-stack is assembled using adhesive. The magnets were selected to be the same MastCam used and MastCam Z was planning to use, so the heritage and experience with these elements minimized risks. These magnets are delicate SaCo magnets that are manufactured by sintering. By themselves they are a brittle component that requires of the sample and the bonding with it to have a certain level of structural resistance.

Another change introduced during the PDR was a change in the kind of samples to be used for the color balance, and the VISIR spectroscopy. The usual samples that are used in similar aplications on earth, the Spectralon™ for example, are usually based on PTFE, a polymer know to have a bad endurance against UV radiation. This material was selected to be changed, and the color samples also changed from a plate to adapt to the magnetic dust removal system.

Finally, something that back then was still on discussion, the heliscout, introduced a concern in the project. The antenna used to communicate with the helicopter was placed on a position of the rover deck that, under some orientation at certain times of the day, could cast a shadow over the reflectance standards. This was identified as an operational risk and discussions and iterations between SuperCam team and JPL started so this could be solved. The different options evaluated during these iterations had their impact in the development of the SCCT.

The project, ant the development team of the SCCT gained momentum thanks to this meeting, and because of that this meeting should be marked as a milestone in the history of SCCT. In the previous meetings before the formal PDR the definition of the samples and the holder evolved quickly, and in parallel analysis were provided on these latest evolutions of the design. As a result, a good design for the level of definition required at PDR level was achieved.

Pre CDR:

At this moment of the project one of the main drivers in the changes and different evolutions suffered by the SCCT was the possible change in the accommodation on the rover, and a major concern regarding the shock level to be applied to the SCCT.

Also, a new element that wasn't at a good definition level at PDR was the Remove Before Fly cover of the SCCT. This element is intended to protect the SCCT during transportation and handling, and also, one it is mounted on the rover, to prevent it from scratches or impacts during ATLO activities. This element is not intended then as a contamination control element. The SCCT is not expected lo leave controlled environments at any time. The design of this element and its fixation to the SCCT is also an element that changed at different moments of the project and introduced small changes in the SCCT design.

The samples used for VISIR calibration changed, from just white and black samples using the magnetic dust removal system, and a separated color plate, to dedicate 5 slots to have RGB and white and dark reflectance standards protected by the magnet, with a separated geometric target.

As mentioned before, the parts of the SCCT that suffered more changes and reevaluations were those related to the protection against shocks. The possible change in the accommodation of the SCCT to a higher shock zone gave a increase in the mass budget for the SCCT. At tis stage the fixation system changed several times, and also the design of the SCCT. One option considered was to split the SCCT into two holders, with the samples affected by shadowing in a separated, smaller, dedicated holder, and the resto of the samples in a model similar to the one designed at PDR. Other option was to prescind the individual lids and use just one back cover to fix the samples in place. Different options had different advantages and disadvantages. At the end, a few extra grams allowed a redesign of the holes and fixation lids, changing also the shock

absorbing measurements that now allowed the SCCT to deal better with different sizes of the samples. This is the final model presented at CDR.

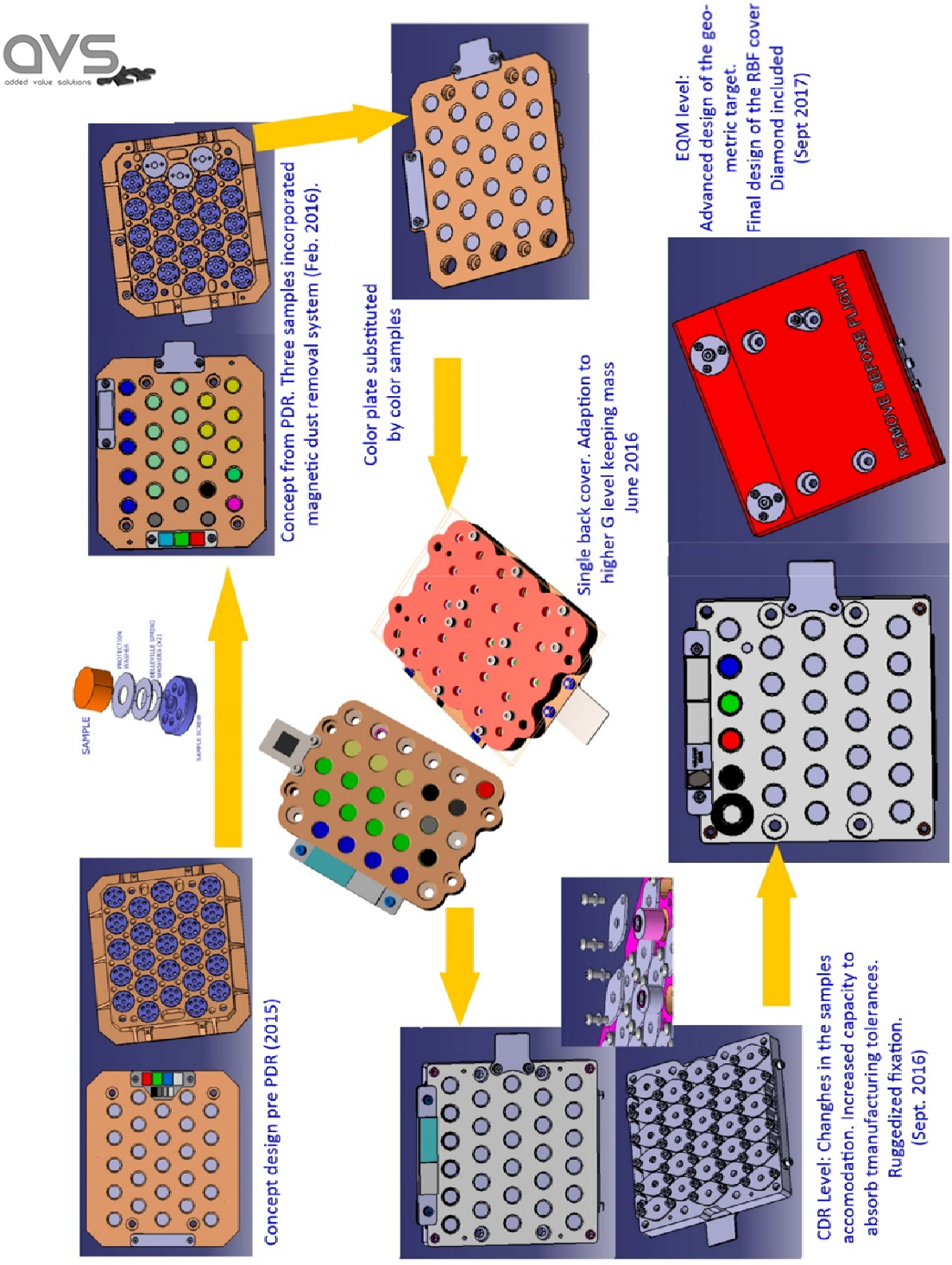

FIGURE 2.43 MAIN REDESIGNS OF THE SCCT BETWEEN INITIAL CONCEPT AND EQM (AVS/UVA)

CDR level:

At CDR, another typical important milestone I space engineering, the SCCT design had evolved significantly. The mode, at CDR had incorporated several changes and suggestions from the mechanical team. The most important was the change in the fixation system of the samples.

The initial concept that used individual screwed lids and Belleville washers needed to change. First reason was the inadaptability of the preloading springs to a wide margin in manufacturing tolerances. Again, the usage of several kinds of samples, manufactured with a new process (sintering), made difficult to estimate the manufacturing tolerances achievable in the final machining of the samples. Once the samples were manufactured the differences among them were in the same order of the length of the Belleville spring loaded, meaning that using the same design for all the samples one sample could receive excessive loads, increasing the probability of damages, while other sample could receive almost none, being loose into the slot. Also, this kind of fixation system was too stiff, meaning a better propagation of the shockwave during the pyroshock event. Both issues were solved by the introduction of different element, a wavespring, with a greater operative length that implies a better adaptability to different sizes while better absorbing shocks.

Another change implemented was the lids to fix the sample in place. The screwed lids in the initial concept, the same system ChemCam used, was identified as risk during assembly. The thread line of this individual screws was very thin, the material, although is hard, could be damaged during assembly, and in that case the damaged part could be the main holder body. The final solution implement was an individual lid that was fixed to the main body by means of two screws fastening against an insert that protected the holder, allowed several operations of fastening and unfastening without risk, and also provided the locking solution itself.

Minor change included was four threaded holes in each corner of the main body to allow the fixation of fiducial elements that will allow JPL to correctly align and position the SCCT according to the requirements.

A final element that was also better defined, although not showed, was the RBF cover. At that moment it was fixed to the structure using dedicated threaded holes in the main structure.

During CDR analysis were showed, along with a better definition of the samples that would be included in the final FM model. Again, one of the concerns at the project level was the performance against shocks. As a result a development test using JPL facilities was encouraged.

Shocks issue:

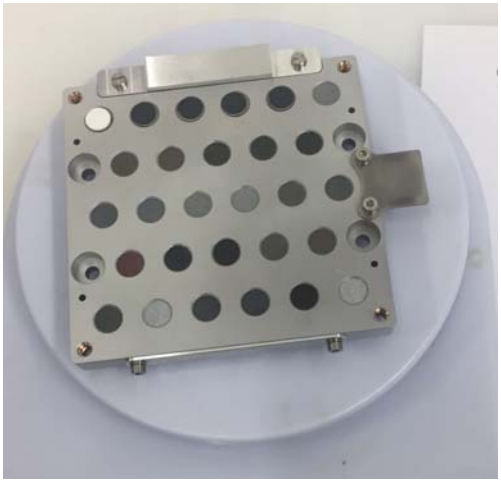

FIGURE 2-44 SCCT ETU MODEL

The SCCT team manufactured, based on CDR design, a new model to be used in the development shock tests. This model, described before, was the ETU.

In the ETU model a full set of samples was assembled, to evaluate their performance. This samples sent included several of the baseline samples at that time, as well as the reflectance standards:

TABLE 2-7 SAMPELS TESTED WITH ETU

SAMPLE	SAMPLE CODE	ETU (JPL SHOCKS)
Minor elements glass	NTE01	
Minor elements glass	NTE02	x
Minor elements glass	NTE03	x
Minor elements glass	NTE04	x
Minor elements glass	NTE05	
andesine	PMIAN	x
Orthose	PMIOR	x
clinopyroxene	PMIDN	x
enstatite	PMIEN	x
ferrosilite	PMIFS	x
olivine	PMIFA	x
chert	LCMB	x
Martian soil analogue	LJSC	x
Mn-Rich Nodule	LJMN	x
Fe rich target (no standard name)	LGIOP	x
Andesite	LAGV	x
Basalt	LBHVO	x
calcite	LCA53	x
Apatite	TAPAG	x
apatite	TAPAX	
epoxy resin	PORGA	x
Carbon rich sample (No FM)	Shungite	x

The test done during the fall of 2016 at JPL shock beam showed a good performance of all the samples, just the apatites tested at that moment broke down, and required further work. This test served to demonstrate that the sintered samples could survive to the dynamic loads of the launch, cruise and landing on Mars.

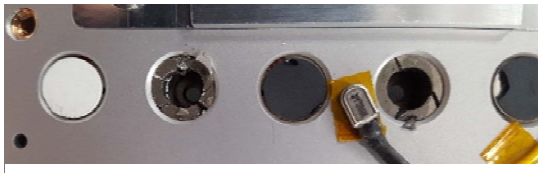

FIGURE 2.45 MAGNETS BROKEN AFTER SHOCK TEST (JPL)

Unfortunately the passive samples, the ceramic standards with the magnet, weren't that successful at that moment and all but one broke. This failure was considered a high risk in the development of the SCCT and was extensively analyzed.

It was agreed to do a second shock test in Spain to evaluate the solutions that the team would find. During the months between the shock test failure and the new shock test a risk mitigation team formed by UVA, AVS and Niels Bohr Institute personnel evaluated several options to improve the shock performance of the holder and the samples. Deep analysis done with Raman spectroscopy at UPV/EHU showed that while traces of the selected glue could be found in the magnet, no signals from the glue were obtained from the surface of the ceramic inserts. This meant that the problem was related with the bonding of the glue to the surface of the ceramic inserts, and the glue selection needed to be revisited.

The following counter measures were implemented to solve the shocks issue:

- Two adhesives were selected to be tested: EA9309 and 3M2226.
- Kapton shims and lateral wraps were included to limit displacements of the samples inside the holes.
- An ETU 2 model was assembled.

The ETU2 model used the structural parts of the ETU model but this time only two samples were included for testing, as the other samples passed the initial shock test successfully. The other sample slots were filled with mass dummies. This second ETU model and the shock test done on it also served to evaluate other two possible issues: the clocking of the samples, and dust that was seen coming out of two sintered samples in the first shock tests. In Fig 46 the final ETU2 model and the changes implemented are shown. This model was tested for shocks in an incremental tests, first testing at 2500 g,

to evaluate how far from the nominal shock limits could be in case of failure, and the final sock test done at 4000 g that was successful.

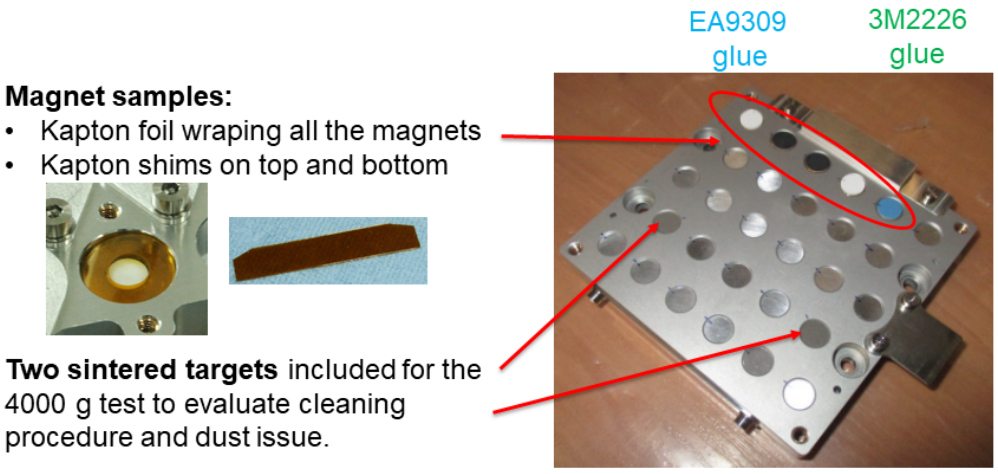

FIGURE 2.46 ETU2 MODEL IMPLEMENTING SHOCK IMPROVEMENTS

All the samples survived to this second shock test, the clocking of the samples was also evaluated and could be neglected as a risk, as it was done with the possible cross contamination by the dust coming out from one of the samples.

As a result of the two development tests, and the iteration of the risk mitigation team with JPL, the SCCT team could demonstrate that the design was solid enough to face a qualification campaign. An extraordinary effort by people from different institutions coordinated by UVA. The changes introduced were:

- Adhesive changed to EA9309 with improvements in the gluing procedure.
- Kapton shims were included on top and bottom of the samples. These pieces prevent the shockwave to propagate directly to the ceramic inserts.
- Kapton pieces were rolled around the magnets. This pieces once in the holes expanded to limit the lateral displacement of the samples and absorb shockwave.
- Additional ultrasonic bath was done on the samples to remove material not aggregated by the sintering process.

Final design, EQM:

Once the design demonstrated that a set of samples could survive to the dynamics qualification tests, and therefore to the launch, cruise and landing on Mars, the manufacturing of the EQM was authorized.

A few changes were introduced between the model evaluated at CDR and the final design to be manufactured, starting with the Remove Before Flight cover that changed for two main reasons:

- The assembly/disassembly could be tricky given the small size of the holes and fastener to fasten the cover to the main body.
- The changes in the position of the SCCT due to new distance to SCMU requirement. By moving up the position of the SCCT the whole assembly was getting closer to some GSE used to move the rover, violating a minimum safety distance.

The design was changed to be a thin as possible in the bottom part of the SCCT, and the fastening holes disappeared to be substituted by the threaded holes for the fiducials. This also allowed thicker, and safer, fasteners in the cover.

Another change introduced was to mill a small cavity between the first and second row of samples. This cavity was used to glue a 4 mm diameter diamond in it, for Raman Rayleigh calibration.

A final change was introduced in the design of the geometric target by the French colleagues from IRAP. In this bracket a small cavity was milled to glue a piece of a Martian meteorite in it. This inverse return mission counted with a meteorite from Mars found in the Sahara desert that could have arrived to Earth 180 millions of years ago. This meteorite travelled to the International Space Station with the astronaut Thomas Pesquet, and was returned to be mounted in the SCCT so it can be returned to its original planet.

Other minimum changes were related to the definition of paint. Previous model weren't painted, so the paint to be used and the design needed to be set on this unit. The final choice was to use S13 white paint, from JPL, the same paint used for the rover, this implied that the whole main body needed to be sent to JPL for painting before assembly. A small black ring around the white target was introduced to enhance contrast, aeroglaze Z306 was selected, as it is a paint widely used in aerospace applications, and it's known to be resistant.

Deeper details on the design of the SCCT are given in the next section 2.3.4.4, and a history of changes from concept design to EQM can be seen in Fig. 2.43.

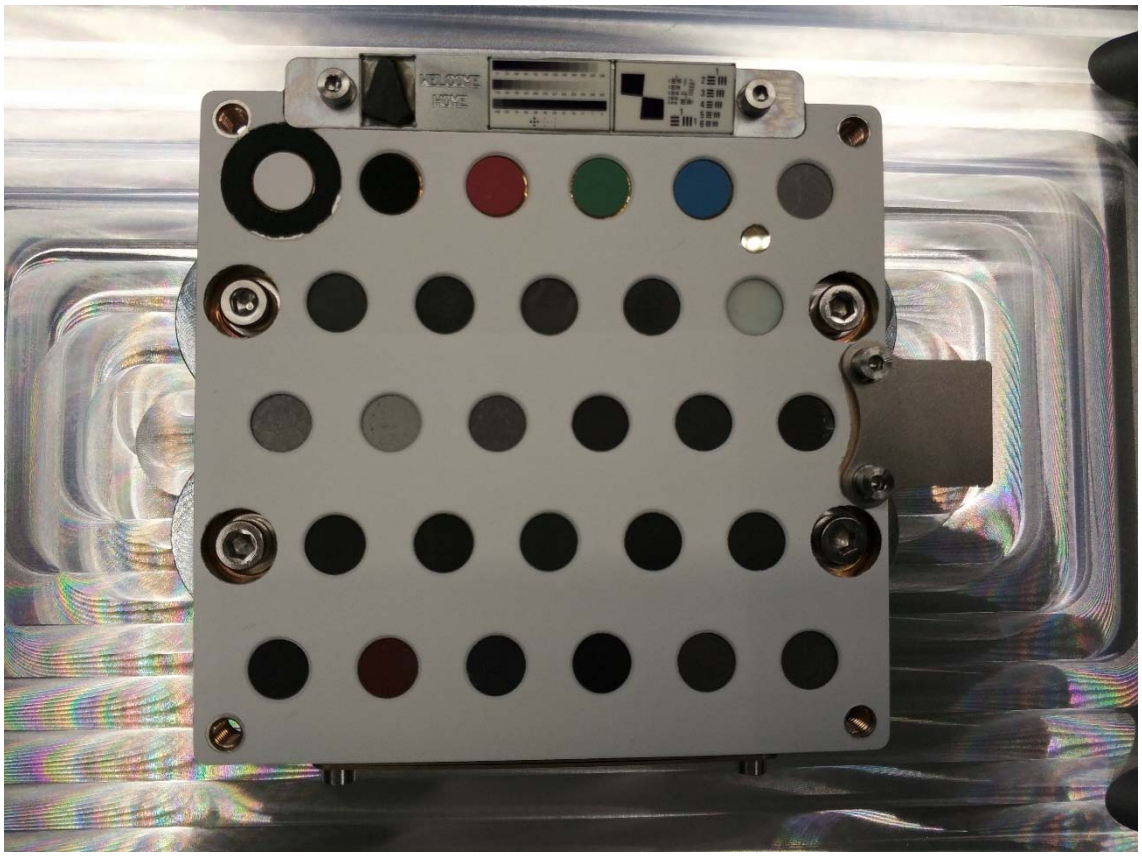

FIGURE 2.47 SCCT EQM MODEL MOUNTED ON ITS HANDLING FIXTURE

Considering the samples, during the definition of the samples to be included in the EQM, the final selection for the FM was not closed yet. Most of the samples were tested in the EQM and ETU, but some were introduced with the aim of having a set of samples as big as possible that could be mounted in the FM with warranties.

TABLE 2-8 DIFFERENT SAMPLES MOUNTED IN THE DIFFERENT MODELS

SAMPLE	SAMPLE CODE	ETU (JPL SHOCKS)	EQM
Minor elements glass	NTE01		x
Minor elements glass	NTE02	x	x
Minor elements glass	NTE03	x	x
Minor elements glass	NTE04	x	x
Minor elements glass	NTE05		x
andesine	PMIAN	x	x
Orthose	PMIOR	x	x
clinopyroxene	PMIDN	x	x
enstatite	PMIEN	x	x
ferrosilite	PMIFS	x	x
olivine	PMIFA	x	x
chert	LCMB	x	x
Martian soil analogue	LJSC	x	x
Mn-Rich Nodule	LJMN	x	
Fe rich target (no standard name)	LGIOP	x	
Andesite	LAGV	x	x
Basalt	LBHVO	x	x
calcite	LCA53	x	x
Apatite	TAPAG	x	
apatite	TAPAX		x
epoxy resin	PORGA	x	x
Carbon rich sample (No FM)	Shungite	x	
ankerite	LANKE		x
Serpentine	TSERP		x
BHVO basalt + K2SO4	TSRICH		x
BHVO basalt + Fe/Ti oxide	TILBA		x
siderite	LSIDE		x

2.3.5.1 Design and analysis

Deep details on the mechanical design of the SCCT cannot be disclosed, as it could intersect with knowhow and proprietary information of AVS, the technical partner. Anyhow, as a general description of the SCCT a sketch corresponding to the EQM model is shown:

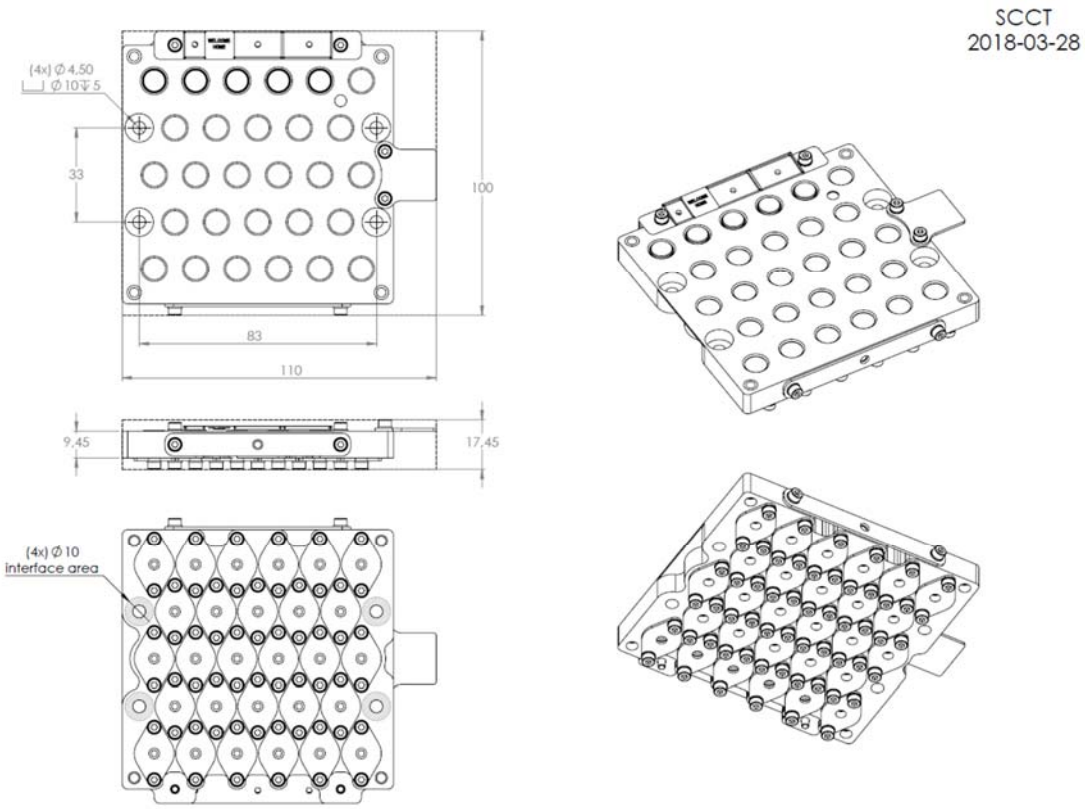

FIGURE 2.48 SKETCH OF SCCT EQM

The whole frame is made of aluminum 7075, an aluminum alloy with zinc of wide use in aeronautics for its strength and low density. Unfortunately this kind of alloy has a limited resistance to corrosion, reason why (in accordance with ECSS standard) all the 7075 parts were coated with a chromatic conversion treatment.

Each sample was mounted in the SCCT with the previously described wavespring and lid design. To dimension the holes in the SCCT a material with the farthest thermal behavior to the T7075 was selected, in this case PTFE, so the samples slots could still house the samples under the worst case of thermal expansion or contraction given the huge Thermal Expansion Coefficient mismatch. As for the temperatures, the worst case was selected, covering a range from -135 ºC to 115 ºC.

For general simulations an average sample was selected, with a mass of 1.61 grams in the case of mineral samples, and 4.22 for the passive samples including magnet. This estimation was kept for design purposes and also for the calculation the mass budget, and it is important to remark that the whole mass of the samples was considered (and in fact it was) to be less than 60 grams, what less than a 25% of the planned mass for the whole SCCT, number that pictures how the whole main body frame dominated the mechanical behavior of the SCCT.

Information regarding the FEM analysis of the SCCT can be found in the report from AVS: AVS-SCCT-ANA-0002 and requested upon approval by UVA and AVS. General conclusion of this report matches with the previous statement. The aluminum structure dominates the frequency response of the whole system, with a local mode in 1724.3 Hz with an associated mass fraction of 68.38%.

Different loads were evaluated in the previous FEM analysis report, showing that the final design of the SCCT could meet, with margin, the dynamics loads required by the project. Other loads were considered as:

- Winds loads: given the low density of the martian atmosphere, the calculations showed that for speeds up to 100 m/s the force applied by the winds could be neglected. The following expression was used:

$$F = \frac{\rho \cdot V^2 \cdot C \cdot A}{2}$$

  Where the density of the atmosphere is multiplied by the square of the wind speed, the drag coefficient and the area exposed in the direction of the wind. For the SCCT this force was 0.28 N

- Thermal loads: as was commented before, the greatest thermal expansion mismatch happens in the samples and that was solved by design. Other stresses for the mismatches between the alumina of the geometric target and the bracket, or the Titanium plate and the main body structure were analyzed and considered safe. Rocket plumes were also evaluated and their effect was found not a risk for the integrity of the SCCT.

Contamination considerations:

Another element that was evaluated in terms of analysis is the contamination. There were some concerns regarding the possible impact of contamination in the SCCT targets that could impact the calibration measurements. For the estimated contamination that could be received by the SCCT the following table shows some estimates per activity, with the global amount:

TABLE 2-9 CONTAMINATION PRE DELIVERY

Stage	Particle cont. (mm^2/m^2)	Molecular cont. (g/cm^2)
Integration ISO-4	0.4	5.48E-10
thermal test	20	5.00E-08
mechanical test	14	1.10E-10
storage 30 days ISO-5 (bagged)	1	3.29E-09
Final level	**35**	**5.39E-08**

Values far from the L300 requirement for particulate, and 0.1 micrograms pero square centimeter for molecular.

Another consideration should be taken into account when evaluating contamination sources that could appear after the assembly and delivery:

- All the activities previous to the launch will be done in an ISO 8 environment or better. Contamination rates per year in these environments are shown in the following table:

TABLE 2-10 CONTAMINATION PER YEAR IN CLEAN ROOMS

Environment	ISO5	ISO6	ISO7	ISO8
Molecular contamination per year (g/cm^2)	$1*10^{-7}$	$1*10^{-7}$	$2*10^{-7}$	$2*10^{-7}$
Particulate surface contamination per day ($mm^2/m^2/24h$)	2	10	52	275

- For any contamination source previous to the landing (rocket plumes, degassing of near parts in vacuum), where dust would be the main concern, the amount that could be absorbed by the samples should be minimum and superficial. In the case of LIBS, as a general procedure, the first 5 shots are discarded and clean the sample, so no contamination should affect the LIBS measurement. For Raman, given that is a standoff Raman system, the contamination level should be very high to be detected by this technique or VISIR.

As a result, possible contamination was evaluated and found not concerning if the cleaning procedures and contamination control plans are followed properly.

For the dust, however, the greatest concern is that some samples needed for imaging or the sample used for Raman could be covered by dust, resulting in an opacity of the samples. It was already described how the magnetic dust removal system is implemented in critical samples to cope with this risk.

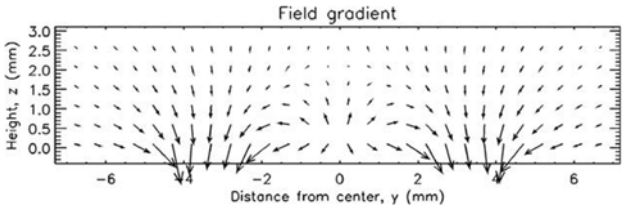

FIGURE 2.49 MAGNETIC FIELD LINES FROM THE MAGNETS AROUND THE PASSIVE SAMPLES (NBI)

Figure 2.49 shows how a ferromagnetic dust particle would follow the field lines and be deposited far from the center of the sample, leaving a 4mm diameter clear area in the center.

In addition to this dust counter measures, the whole SCCT will be tilted, limiting the amount of dust that will be deposited on it. In the following picture, Fig 2.49B from Curiosity's rover deck after 1197 Sols it can be seen how while the flat rover deck is covered by dust, ChemCam's calibration target remains clean.

FIGURE 2.49B CURIOSITY'S ROVER DECK AFTER 1197 SOLS (JPL).

This tilted position of the SCCT clearly contributes to keep it clean.

The following expression, more related to solar panels, relates the dust deposition rate on a general surface at a certain tilt angle, in the worst case scenario:

$$r = (0.0072)\ (\cos \text{Tilt.})\ /\text{sol} = 0.0046\ /\text{sol for } 50º \text{ tilt.}$$

So, according to the previous expression, and considering r=1 for a total coverage of the samples, it will take 217.39 sols to reach the total coverage of the samples, in the worst case scenario.

This worst case scenario is far from the reality that can be seen in the pictures from Curiosity, and accounts for an extraordinary dust activity on unprotected hardware. This calculations can be then evaluated with the effect of the magnetic dust removal system.

Considering the data from Phoenix's magnetic experiments in which the dust settling rate was 18 times higher in the dirty area of the magnets when compared to the clean area (Drube, 2009), and assuming that this is related to the amount of dust that is ferromagnetic and is effectively affected by the magnet ring, if considering the effectivity of the system to reduce the deposition rate in a factor 10 in the central area, this means that the total coverage of the protected area in the center of the samples would happen after 2173 sols, far from the 670 mission sols of nominal mission, and it gives an idea of how protected these samples are.

Other countermeasures were introduced to protect all samples, as the inclusion of a chamfer in the lip of the holder on top, that limits the thickness of dust that can be accumulated in this interface. Again, as a general approach, the LIBS targets will be cleaned by laser, and samples surrounding LIBS samples will be also cleaned by this lase shots.

Final conclusion:

As far as can be evaluated by analysis, the design is solid enough and meet all the requirements. Plans and simulations were done to make sure the SCCT will endure during its operation time. Other factors needed to be evaluated by test.

As was discussed before, the tests done on the model to be delivered for its assembly in the rover, the acceptance tests, are only done to verify workmanship, reason why they weren't included in the present work. Integration and testing of the different models

Different tests and inspections have been planned to verify that the SCCT complies with the endurance, interface and functional requirements for this element. Different inspection points were identified, some of them direct responsibility of UVA and others Mandatory Inspection Points (MIPS) that are done in accordance, and if desired with concurrence, of JPL.

In general, UVa led and chaired most of the inspections, with the exception of incoming inspections of material that were carried out by AVS. For several inspections and measurements UVa counted with the expertise and help of INTA. Depending of the model, the AIT flow is as follows:

CHART 2-1 ETU/EM AIT FLOW CHART

- I-1: Samples incoming inspection. Dimensional and physical properties (mass). Visual inspection with aid (microscope for microfracture identification).
- I-2: Holder parts dimensional verification
- I-3: Geometric Target incoming inspection
- I-4: Post-integration visual inspection with aid (camera)
- I-5: Post-shock visual inspection with aid (camera)
- I-6: Post-vibration visual inspection. with aid (camera)
- I-7: Final visual inspection with aid (microscope for microfracture identification).
- I-8: EM final visual inspection with aid (camera)

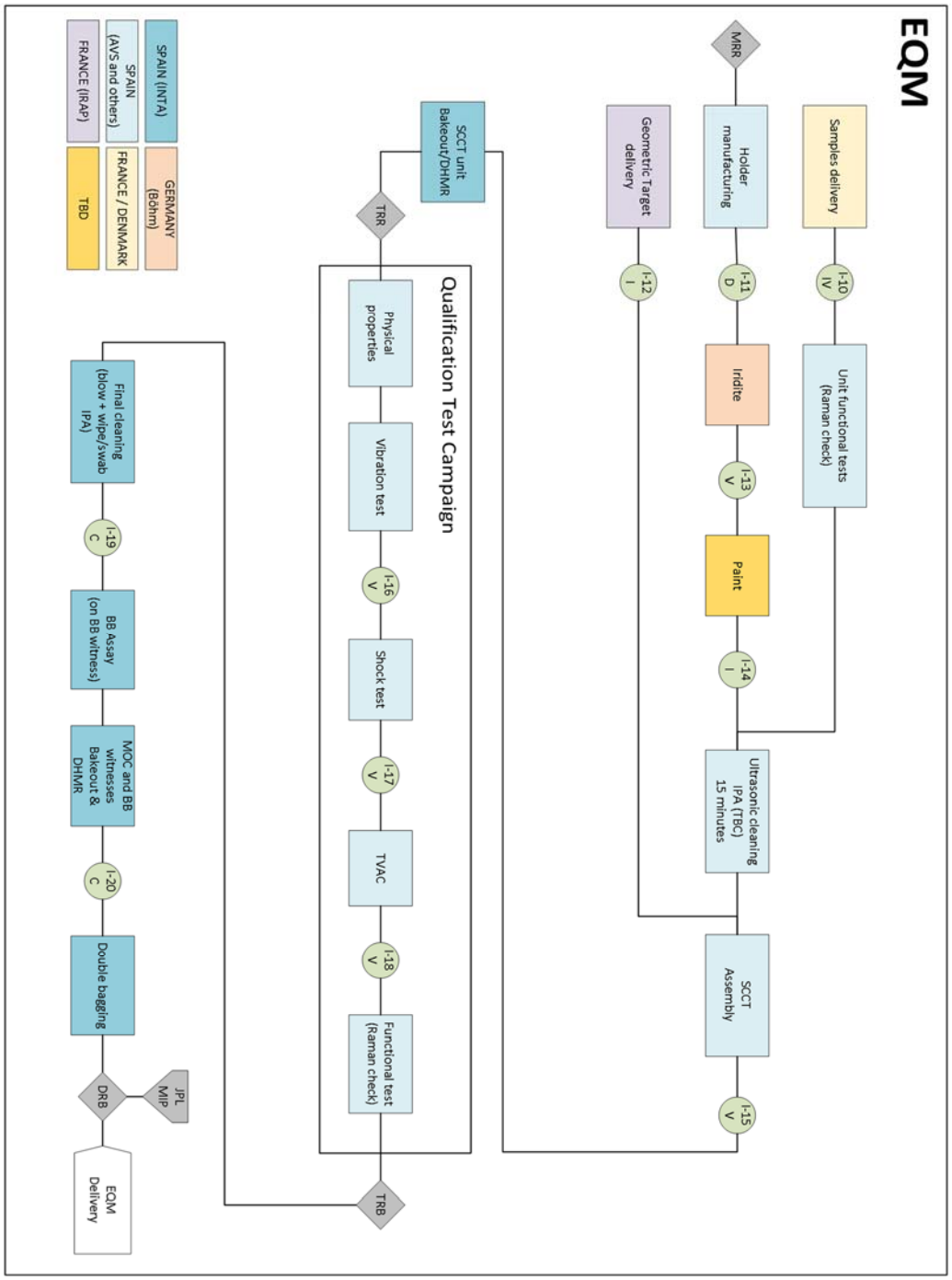

CHART 2-2 EQM AIT FLOW CHART

- I-10: Samples incoming inspection. Dimensional and physical properties (mass). Visual inspection with aid (microscope for microfracture identification).
- I-11: Holder parts dimensional verification
- I-12: Geometric Target incoming inspection
- I-13: Aluminum parts visual inspection with aid (iridite finish)
- I-14: Holder painted parts incoming inspection
- I-15: Post-integration visual inspection with aid (camera and microscope for microfracture identification)
- I-16: Post-vibration visual inspection (camera)
- I-17: Post-shock visual inspection (camera)
- I-18: Post-TVAC visual inspection (camera and microscope for microfracture identification)
- I-19: Cleanliness Inspection. Particulate: UV light, PFO witness
- I-20: Cleanlines Inspection. Molecular: MOC witness

- I-25: Samples incoming inspection. Dimensional and physical properties (mass). Visual inspection with aid (microscope for microfracture identification).
- I-26: Holder parts dimensional verification
- I-27: Geometric Target incoming inspection
- I-28: Aluminum parts visual inspection with aid (iridite finish)
- I-29: Holder painted parts incoming inspection
- I-30: Post-integration visual inspection with aid (camera and microscope for microfracture identification)
- I-31: Post-vibration visual inspection with aid (camera)
- I-32: Post-TVAC visual inspection with aid (camera and microscope for microfracture identification)
- I-33: Cleanliness Inspection. Particulate: UV light, PFO witness
- I-34: Cleanlines Inspection. Molecular: MOC witness

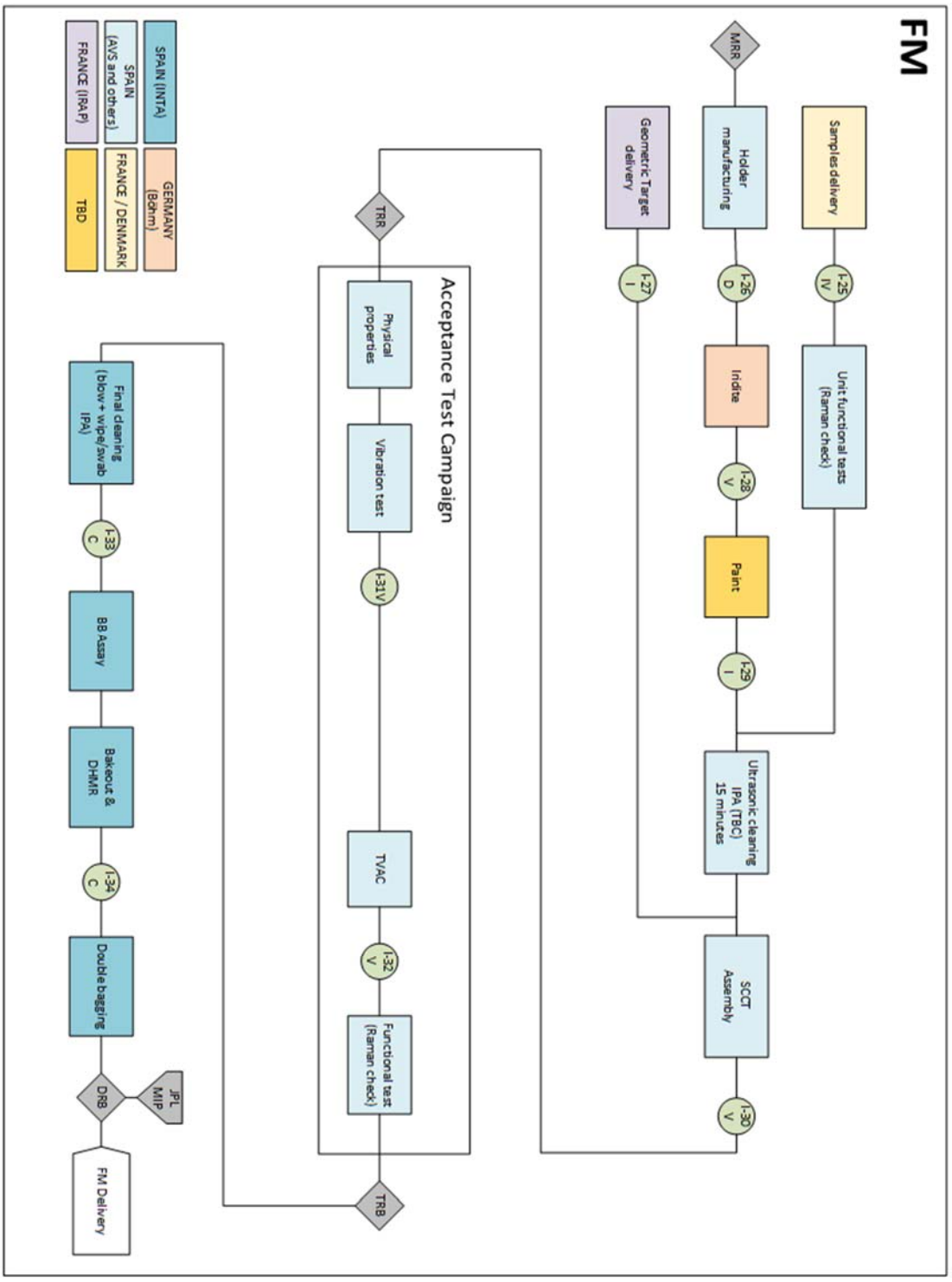

CHART 2-3 FM/SPARE AIT FLOW CHART

As a remark regarding the flow charts, the SCCT unit bakeout was decoupled from the contamination witnesses bakeout in order to subject the SCCT unit to the DHMR temperatures *before* the qualification tests. This wasn't the case for the FM.

Is author's understanding that the qualification campaign, the tests done on the EQM, served to demonstrate that the SCCT could face the environmental threats associated with the mission. For this reson details on the campaign and results are shown in the following section.

2.3.5.2 Qualification and tests

The qualification campaign of the SCCT was agreed with JPL, and included several tests that can be separated into two different groups: dynamics tests and thermal tests.

2.3.5.2.1 Dynamics tests

For the dynamic tests the SCCT was firstly mounted on a vibration table. In this table three tests were done, two as part of the qualification campaign, and one done repeatedly as verification.

For verification of the hardware, sine surveys are done at different moments of the tests looking for variation in the modes that could mean that something is broken, or loose.

Additionally, before the dynamics test, a thermal vacuum at 115ºC for 120 hours was done on the hardware. This induced the thermal stress in glues before dynamics testing and allowed to asses the endurance of the bonding line.

AS part of the qualification campaign then, two different tests were done, quasistatic loads, QSL, and Random Vibration.

After the vibration tests, the SCCT EQM was mounted on the shocks table to receive two 3500 g shocks (the levels were lowered by JPL between development tests and qualification) in each axis.

Test instrumentation

During RV and quasi-static tests on the shaker, accelerometers in the excitation axis were included to monitor the response on SCCT. These will be placed as close as possible to the unit center of gravity. Given the impossibility to mechanically attach the accelerometers, these were glued on acrylic Kapton tape. The figure below show an example of configuration for this test.

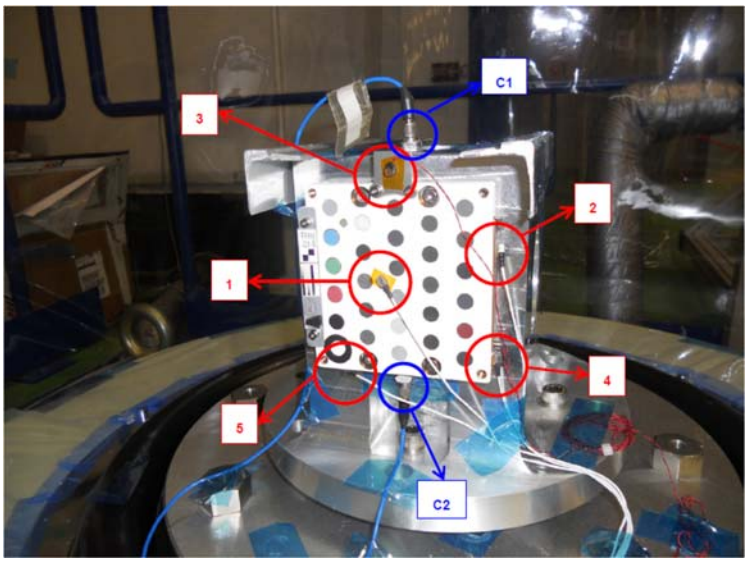

FIGURE 2.50 SCCT ON THE SHAKER WITH THE ACCELEROMETERS ON PLACE. C (BLUE ONES) ARE CONTROL ACCELEROMETERS, WHILE THE RED ONES WERE MONITOR ACCELEROMETERS.

During shock testing, at least one response accelerometer was mounted in each direction, the use of mechanical fixation instead of gluing for these accelerometer was enforced by JPL. The response accelerometers were placed in the fixture were the SCCT was mounted, and some additional monitor accelerometers were glued to the SCCT. As a general procedure, before mounting the EQM a mass dummy was use for several tuning shocks until the response was according to test parameters.

Tests parameters

The sine survey, used as status check of the SCCT, consisted on a low-level frequency survey test prior to and following each axis of vibration, and prior to and following the shock tests that were done. Given that the resonance frequency of SCCT is found around 2000Hz, the survey applied covered from 20 to 2500 Hz, to ensure that the mode is excited and can be evaluated.

For the Quasi-static test, it was done on the SCCT with an acceleration of 72 g's (60g with a 20% margin). The acceleration was applied in the three axis. No dynamic factor need be applied provided as the instrument fundamental frequency is above 20 Hz. The parameters used for this test were:

- Sine dwell
- Fundamental frequency: 32 Hz
- Duration: 5 to 10 pulses.
- Acceleration: 72 g

For the Random Vibration test, the vibrations applied covered from 20 to 2000 Hz, with a gaussian intensity distribution and levels according to JPL requirements (not disclosed), during 2 minutes per axis.

For the shock test, the 3500g shock was applied in the three axes simultaneously for two times, something that was possible thanks to the stiffness of the whole system. The shock was generated with a gunpowder nailgun shooting against a ringing table. The synthesized shock waveform met the following criteria: the time history shall be oscillatory in nature, and the pulse shall decay to less than 10% of its peak value within 20 milliseconds. In addition, at least 50% of the maximum spectrum values shall exceed the nominal spectrum values (not the number of points of the curve, but the curve itself).

Results:

The whole results can be checked upon request to the University of Valladolid and are too extent to the present work. As a summary, the SCCT passed through the QSL and RV tests without any damage observed and no variations in the sine surveys before and after the tests.

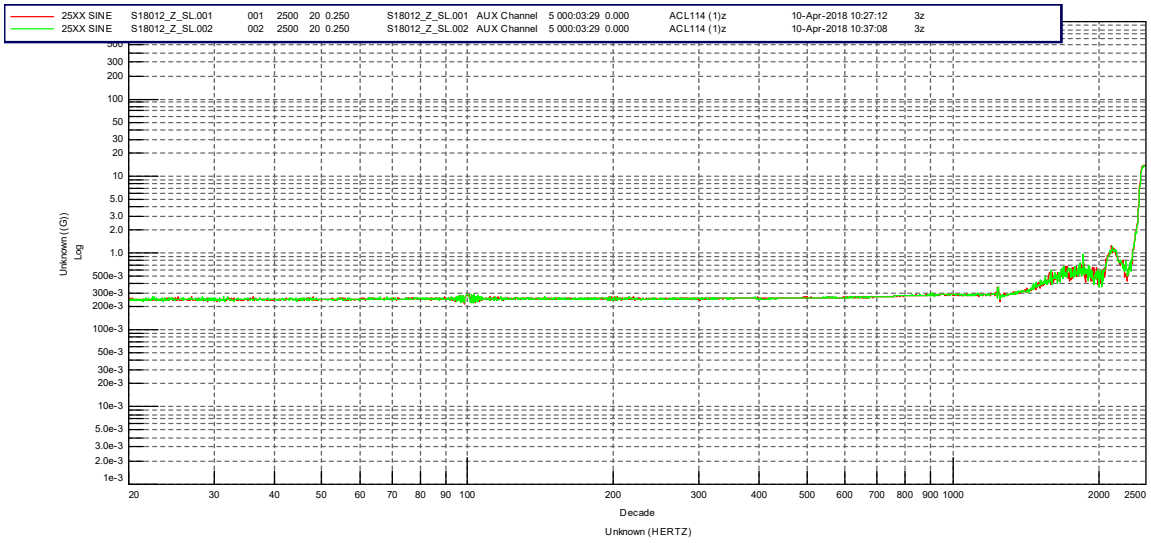

FIGURE 2.52-23 EXAMPLE OF SINE SURVEY BEFORE AND AFTER QSL TEST ON Z AXIS. RED LINE BEFORE TEST AND GREEN LINE AFTER TEST.

As an example, in Fig. 2.51 it is shown how after the QLS test on the Z axis on the SCCT (off plane) there is no variation measured by this accelerometer during the sine survey. Meaning that no deformations or damages were found.

For the shock test, the following figures show an example of the data gathered and analyzed during the first run of the test (it has to be done twice). Measurement s by each accelerometer in the three axis at the two positions in the were they were placed on the mounting plate:

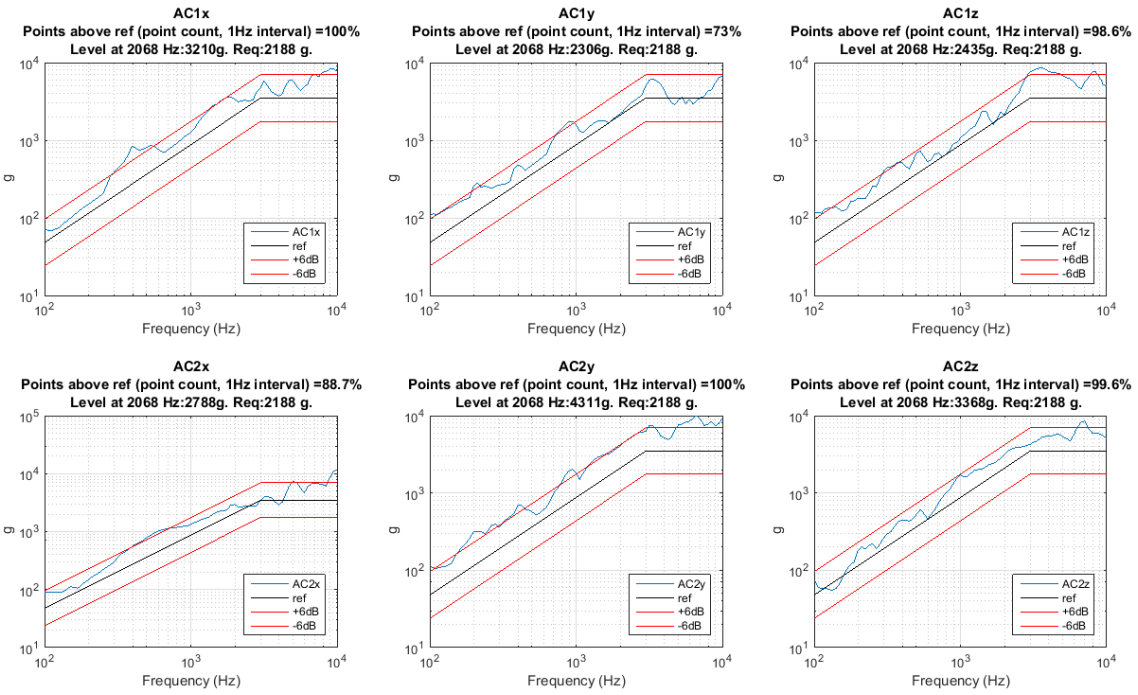

FIGURE 2.52 SHOCK RESPONSE OF THE SCCT AT MOUNTING PLATE

As a requirement for the test, the temporal responses were also recorded and evaluated:

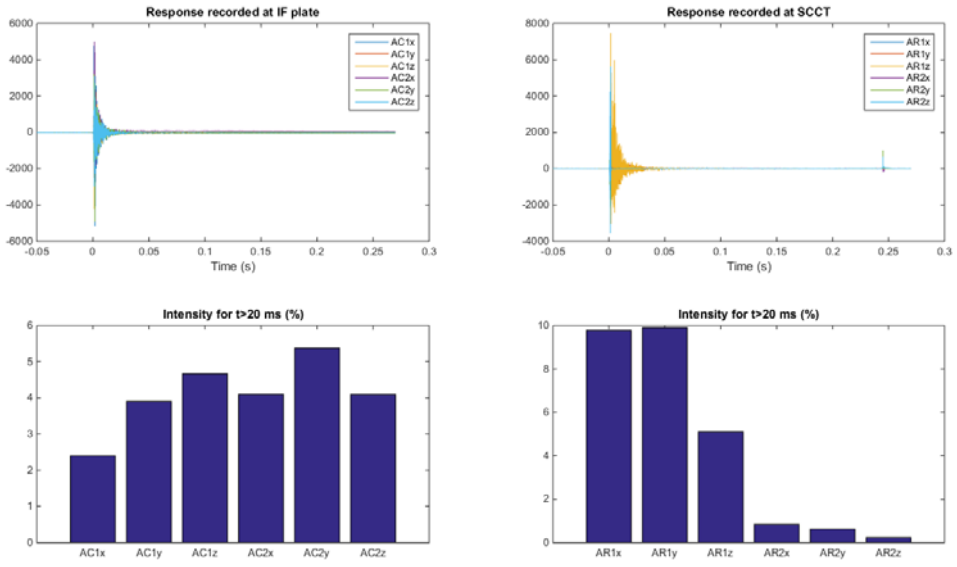

FIGURE 2.53 SHOCK TEMPORAL RESPONSES

For the SCCT during this test, all the parameters were within requirements and the different inspections, including the sine surveys done before and after, showed no damages.

In deeper observations with microscope, the SCCT EQM showed no cracks or any sign of deterioration. This part of the qualification campaign was later discussed with JPL and evaluated as a PASS.

2.3.5.2.2 Thermal test

During this extended test the SCCT is exposed to thermal cycles covering the worst upper and lower temperatures that it might face. The objective of the test is to evaluate the stress induced because of this thermal cycling in the different parts of the SCCT, particularly in the interfaces and in the bondlines of glued hardware.

Test parameters and setup:

The temperatures used in this test were designed by UVA team to substitute a longer test that used more cycles with less severe limits in temperature. Three different phases can be identified in the test done:

Thermal Test Phase 1

- Number of cycles: 3 cycles
- Maximum temperature level: +80ºC +5/-0
- Minimum temperature level: -130ºC -5/+0
- Temperature rate <= 5ºC/min
- Dwell time at the limits: 120 minutes
- Vacuum: The chamber pressure was maintained at 1.0 x 10-5 torr or lower for the complete duration of this phase.

Thermal Test Phase 2

- Number of cycles: 26 cycles
- Dwell time at the limits: 15 minutes
- Other parameters remained as in phase 1

Thermal Test Phase 3

- Number of cycles: 1 cycle
- Maximum temperature level: +80ºC +5/-0
- Minimum temperature level: -130ºC -5/+0
- Temperature rate <= 5ºC/min
- Dwell time at the limits: 15 minutes

- Mars pressure: Using GN2 as media for the test, and a pressure between 2 and 12 torr.

After the first phase the SCCT was inspected before continuing with the long phase 2.

The SCCT was placed inside a vacuum chamber with several thermal sensors attached. The temperature at the interface with the mounting plate was the control temperature for the test. All the other sensors were monitors.

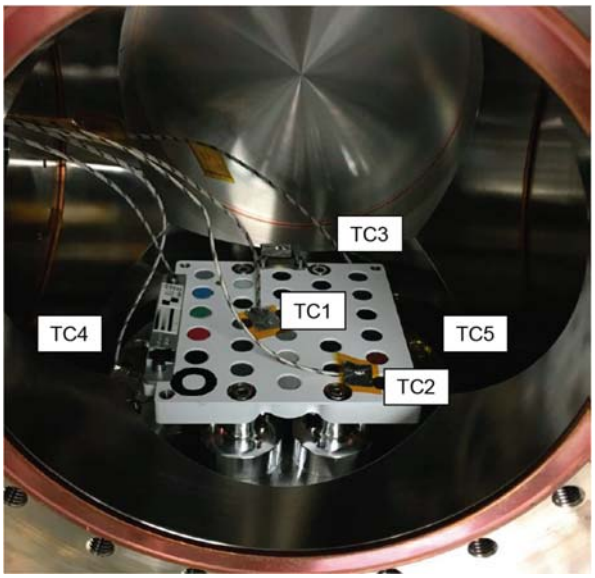

FIGURE 2.54 SCCT EQM INSIDE THERMAL CHAMBER WITH THE THERMOCOUPLES ON PLACE

Results from this test:

For the First 3 cycles, the three cycles curves are as follows:

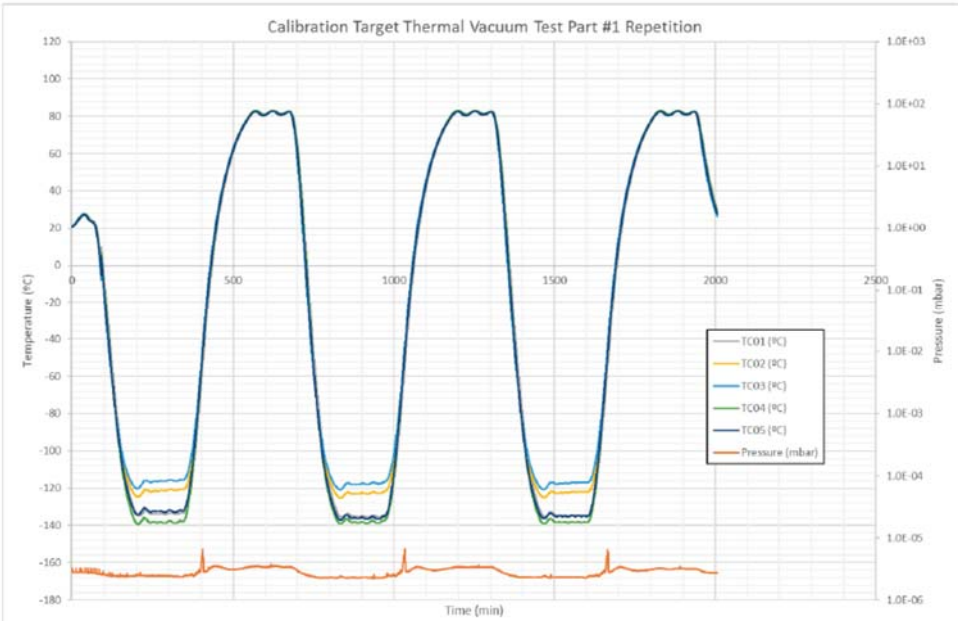

FIGURE 2.55 FIRST 3 CYCLES OF THERMAL TEST. 120 MINUTES DWELL TIME

After the completion of the first three cycles, a visual inspection was performed on the specimen. This inspection showed how one of the thermocouples was detached, TC2, but kept in contact with the walls of the chamber.

The TC2 thermocouple was replaced. The visual inspection showed no damages in the samples or in the paint that could mean a stopper to the test. Therefore, the test was authorized to continue with the remaining cycles.

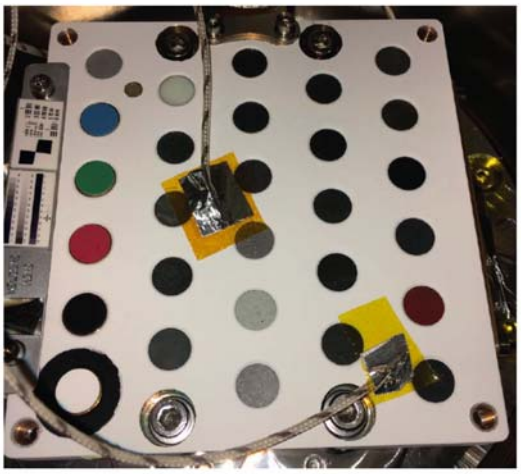

FIGURE 2.56 SCCT EQM DURING INTERMEDIATE INSPECTION AFTER PHASE 1.

After the initial phase 1, the 26 remaining cycles continued as follows:

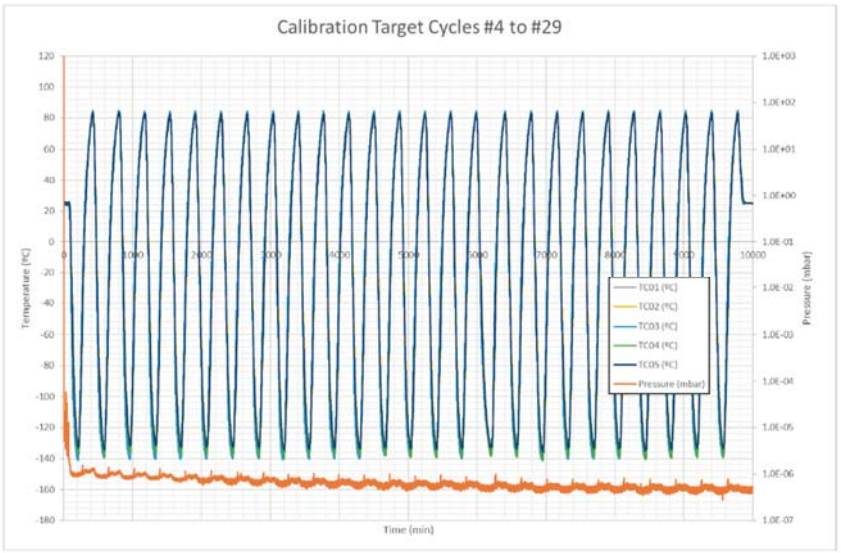

FIGURE 2.57 THE 26 CYCLES OF PHASE 2

With detailed view of the initial cycle:

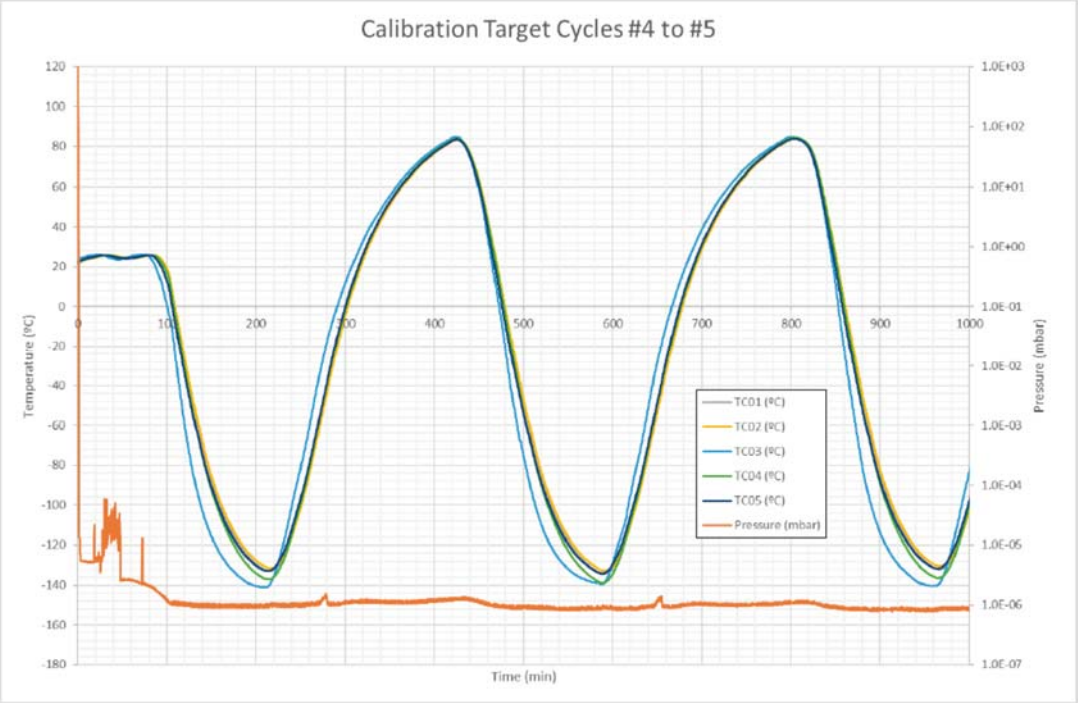

FIGURE 2.58 INITIAL CYCLES IN PHASE 2

The test stopped after the completion of this phase 2 to introduce GN2 gas up to 6 mbars of pressure, and then performed the last cycle at Mars pressure.

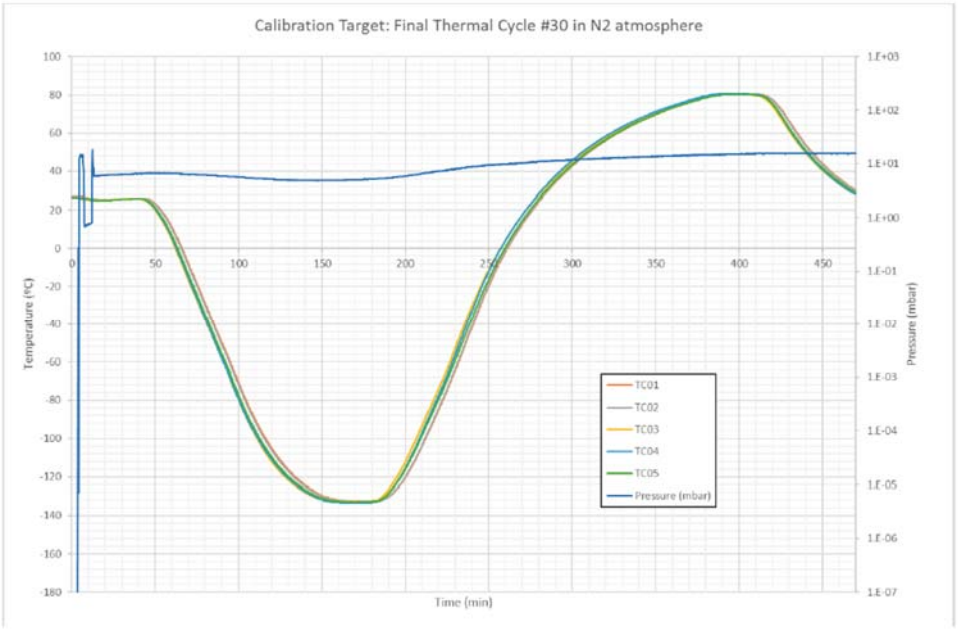

FIGURE 2.59 DETAIL OF THE LAST CYCLE AT MARS PRESSURE

Showing that the temperatures required by the test procedures agreed with JPL were reached during the whole test.
After this test the SCCT was deeply inspected showing no signals of fatigue, or damages of any kind, with special attention to the reflectance standards and the geometric plate.

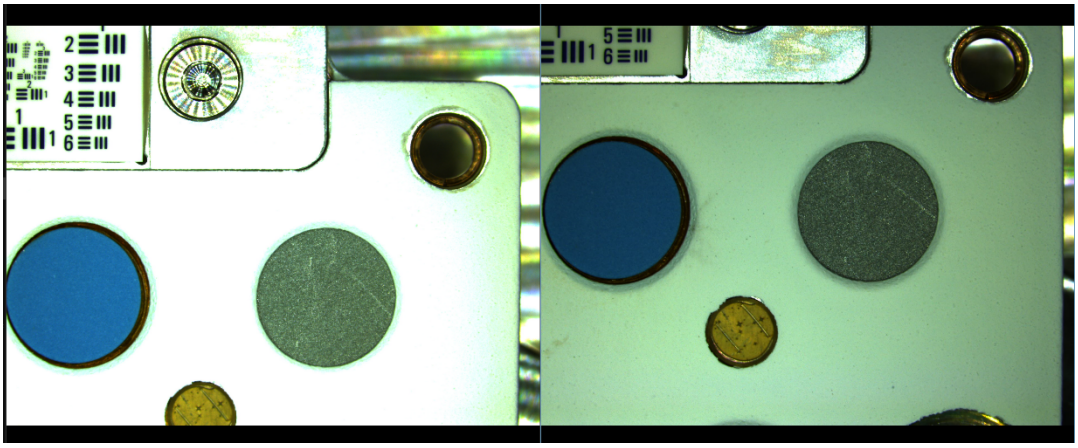

FIGURE 2.60 EXAMPLE OF INSPECTION BEFORE (LEFT) AND AFTER (RIGHT) WITH A MAGNIFYING GLASS. NO DAMAGES WERE FOUND.

The final step to consider in the qualification campaign is that during this rehearsal the hardware is also compliant with the Contamination and Planetary Protection requirements.

Contamination witnesses for PAC and MOC were in place during the whole qualification process. Whenever the unit is uncovered, the witnesses were uncovered first. For bioburden verification, swab assays were done on the SCCT unit.

PAC: The particulate contamination was measured using PFOs and witnesses during integration, mechanical tests and TVAC tests. The measured values are the following:

- Integration: 26 ppm
- Mechanical tests: 11 ppm
- TVAC tests: 7 ppm
- Total: 44 ppm

Given that the allowed PAC obscuration corresponding to the L300 requirement imposed for the SCCT is 329 ppm, the PAC levels are found inside the requirement.

MOC: The MOC witness was unique during the whole qualification campaign, including integration and the qualification tests. The measurement performed (IR) after the whole qualification was 4 ng/cm2 of molecular contamination, which is much lower than the allowed 100 ng/cm2.

Note: during the TVAC test, the MOC witness could not be placed inside the chamber. This point is covered in section 7.5, lessons learned.

BB: Several BB assays are performed along the process, all of them providing zero spores. This means that the total contamination is the minimum possible (by process, 500 spores/m2). Given the total surface of the SCCT, the total number of spores is 160 spores/m2, which also complies with the allowed 300 spores/m2. Nevertheless, a DHMR is foreseen to be carried out on the FM before delivery (for the EQM it was performed before the qual. testing in order to test the unit after the DHMR).

2.3.5.2.3 Final Inspections

Visual inspections were done before, during and after the qualification test campaign on the SCCT unit to verify the physical integrity of the unit, as well as its cleanliness status. In addition, during the dynamic tests, low-level frequency surveys were executed to verify the modal response of the unit. After the qualification campaign, a thorough inspection including the dismounting of several samples was performed to verify the internal status of the samples and mechanical parts (e.g. wavesprings). The following pictures show some details of the inspections. These were carried out with a magnifier for detail.

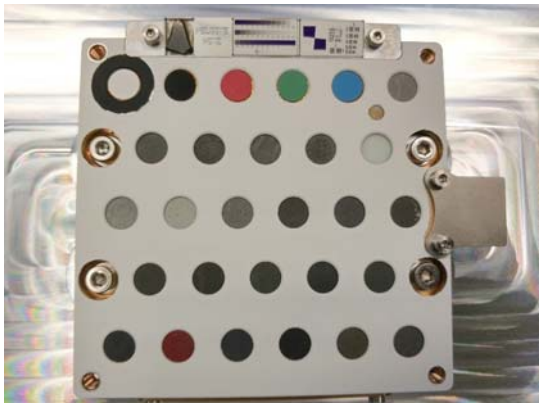
After integration

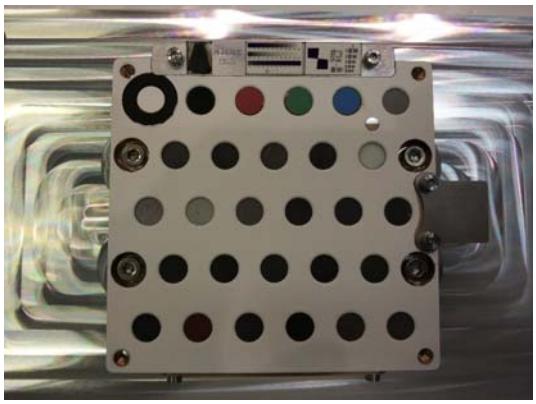
After DHMR and dynamics tests


After TVAC tests

The most critical tests are the dynamic tests. The detailed pictures of the samples, before and after the test are shown below:

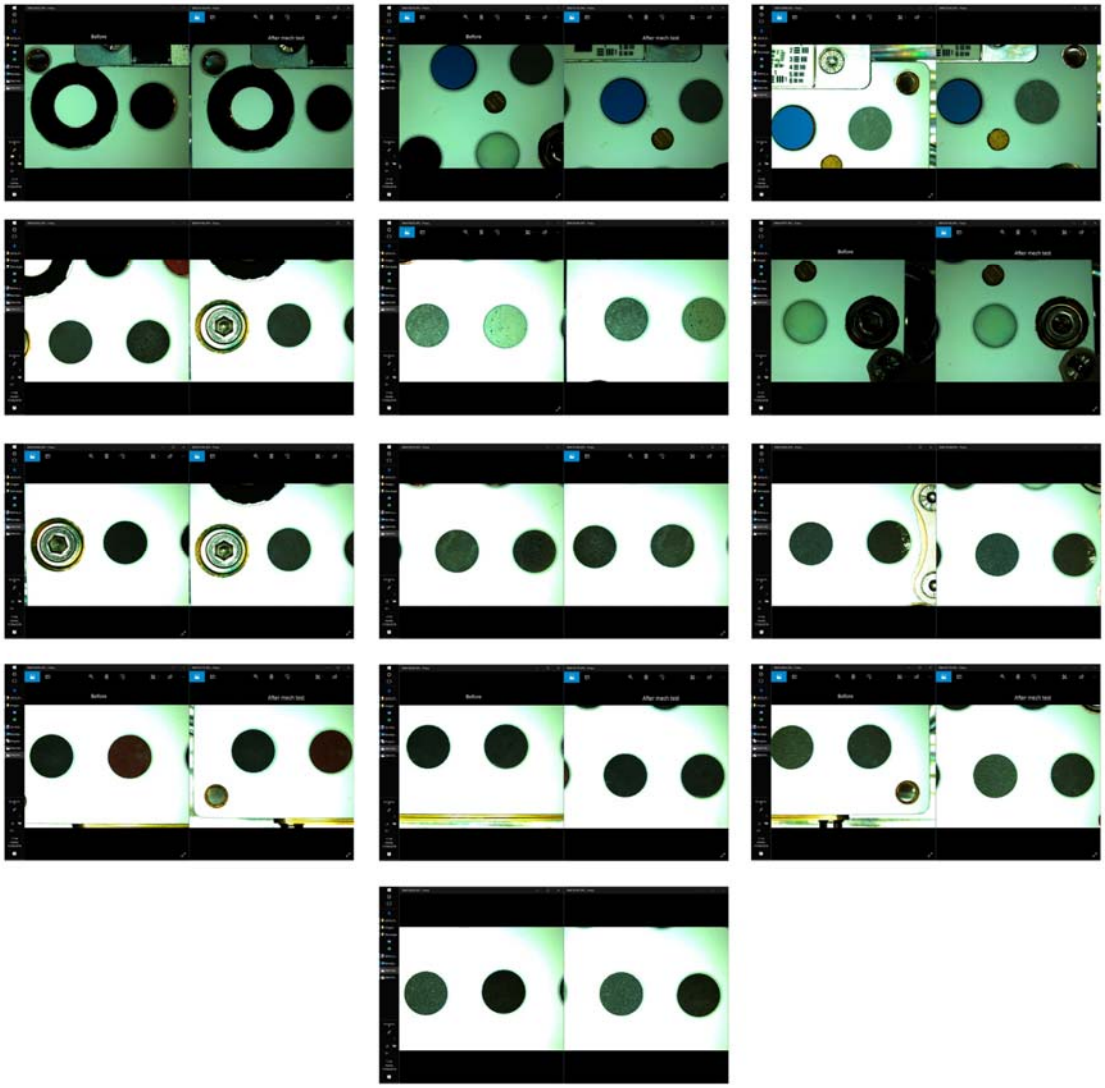

The final inspection included dismounting of several of the samples. No damages were found in any of them, nor in the wavesprings or any other mechanical part (not even on the samples with pre-existing damages as for example sample 5.1).

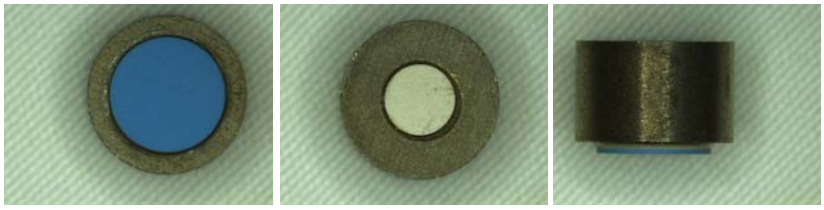
Cyan magnet (after)

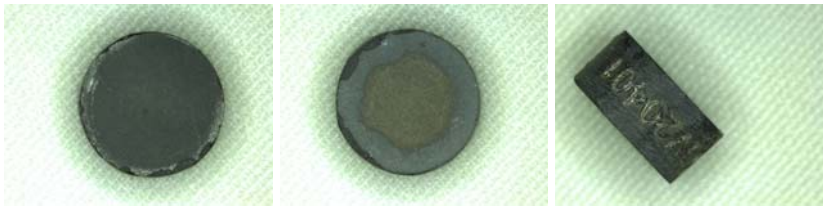
Sample 5.1(after)

2.3.5.2.4 Incidences and lessons learned

As an example of the value of the qualification campaign a list of lessons learned is included. These lessons allowed to improve the design, integration and testing of the FM, what is the real critical model of the SCCT.

CC and PAINT INCIDENCES FOUND DURING THE VIBRATION AND SHOCK TESTS AT CTA. 9-13/4/2018:

Acrylic kapton left adhesive residues in the gloves and was therefore changed for silicon based Kapton. In the end this demonstrated to be a bad idea, as it bonded too well to the paint and removed part of the paint on one side of the SCCT

LESSON LEARNED 1: Do not use silicon based Kapton tape, even if the latter leaves residues on the gloves.

After vibration test, particles were trapped in the magnetic samples. SCCT was bagged, but the IF screws were not covered, and this is the probable source of contamination.

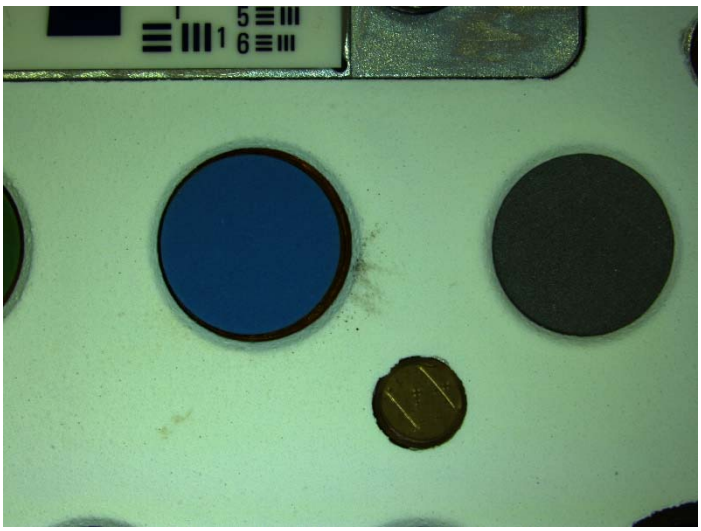

LESSON LEARNED 2: Use Kapton to cover the IF screws, or prepare a better setup for bagging the FM.

LESSON LEARNED 3: to remove particles, first blow, second use Kapton, then dry wipe, then IPA wet wipe.

After the tests, this dirt is swabbed/wiped to try to remove it, with the following results.

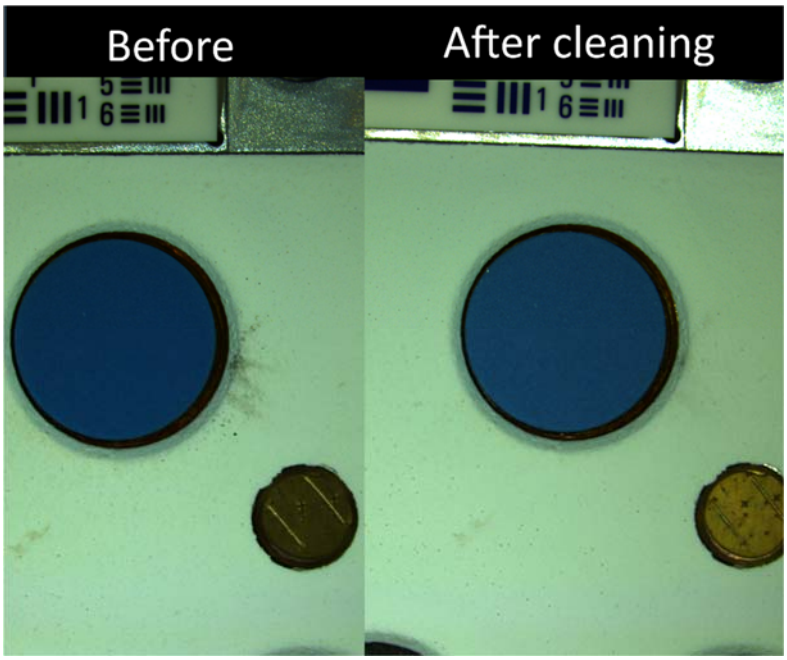

It could be seen that it was partially removed. No further swabbing were done, as the paint seemed to be affected by the swabbing. Actually, using Kapton tape some powdered paint was removed.

When removing the vibration accelerometers to go to the shock configuration, it was observed that some adhesive contamination is found on the paint. It is not possible to remove it with wiping or tape lift with Kapton.

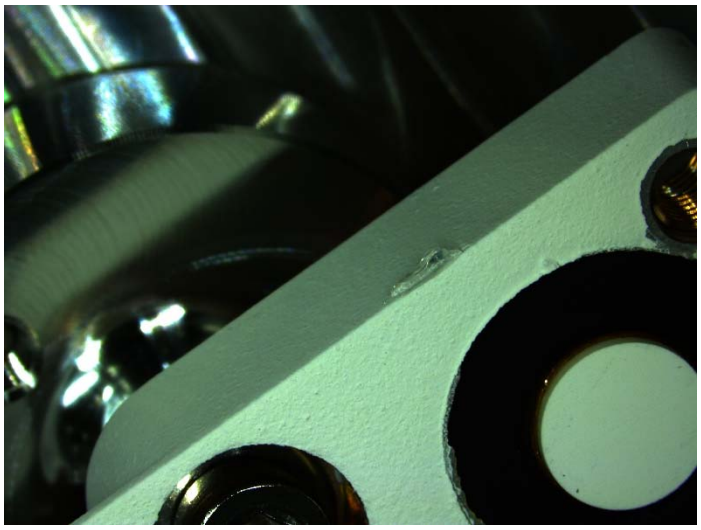

Also in the central part, some adhesive is found. It is possible to clean it with swab.

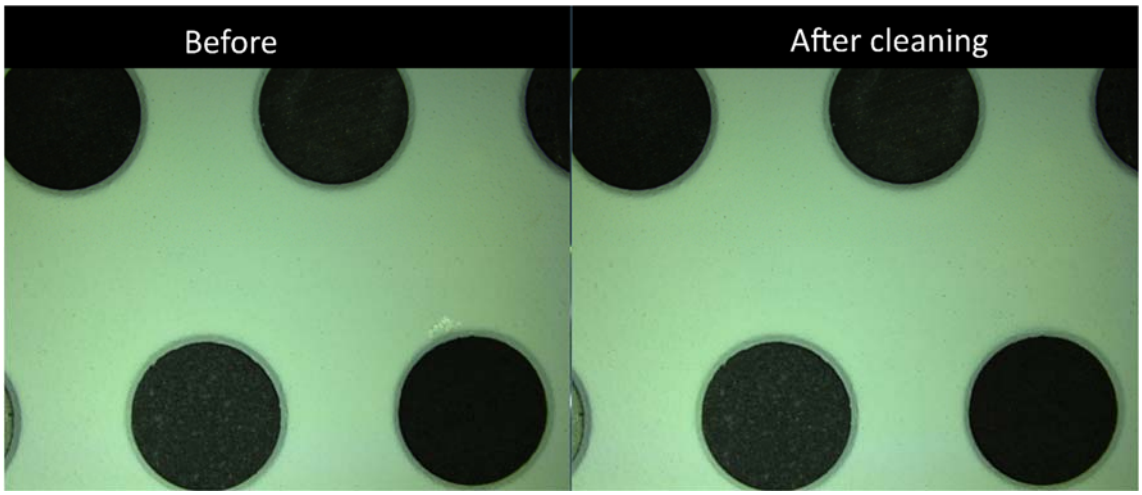

LESSON LEARNED 5: use larger pads of Kapton to place the accelerometers on the FM model.

However, it was noted that, after cleaning, some black spots that were not there appeared on the surface, and a general decrease of the paint was observed -> this means that swabbing with IPA removes the paint surface, as commented before.

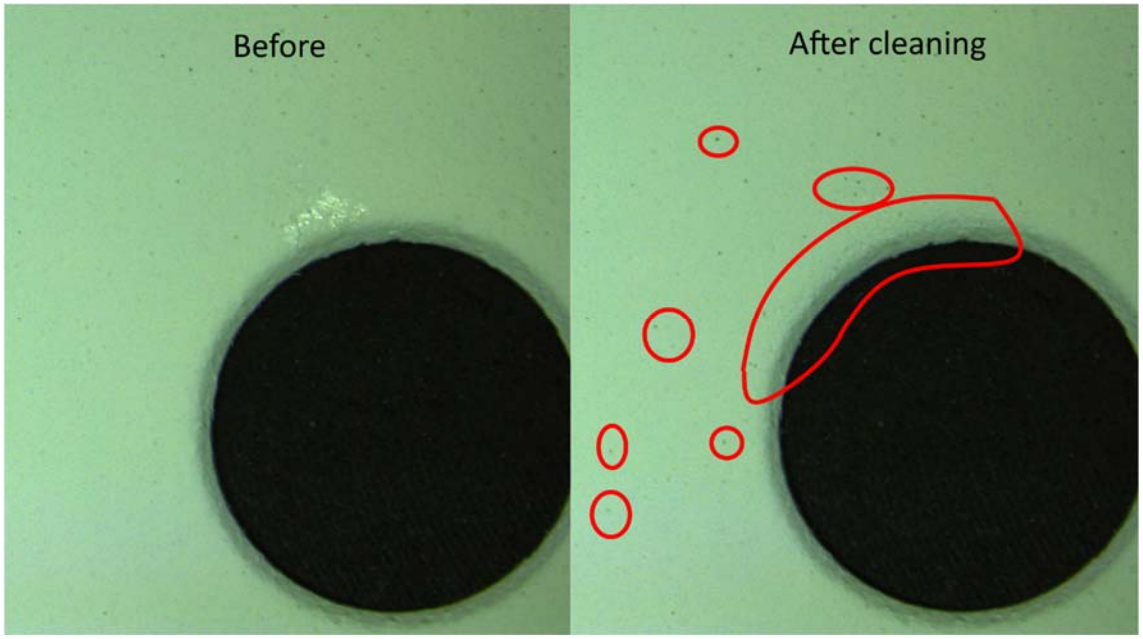

A general dirty aspect of the SCCT was found after the tests. After cleaning it was possible to recover the cleanliness of the surface, but taking into account the previous issues with the paint.

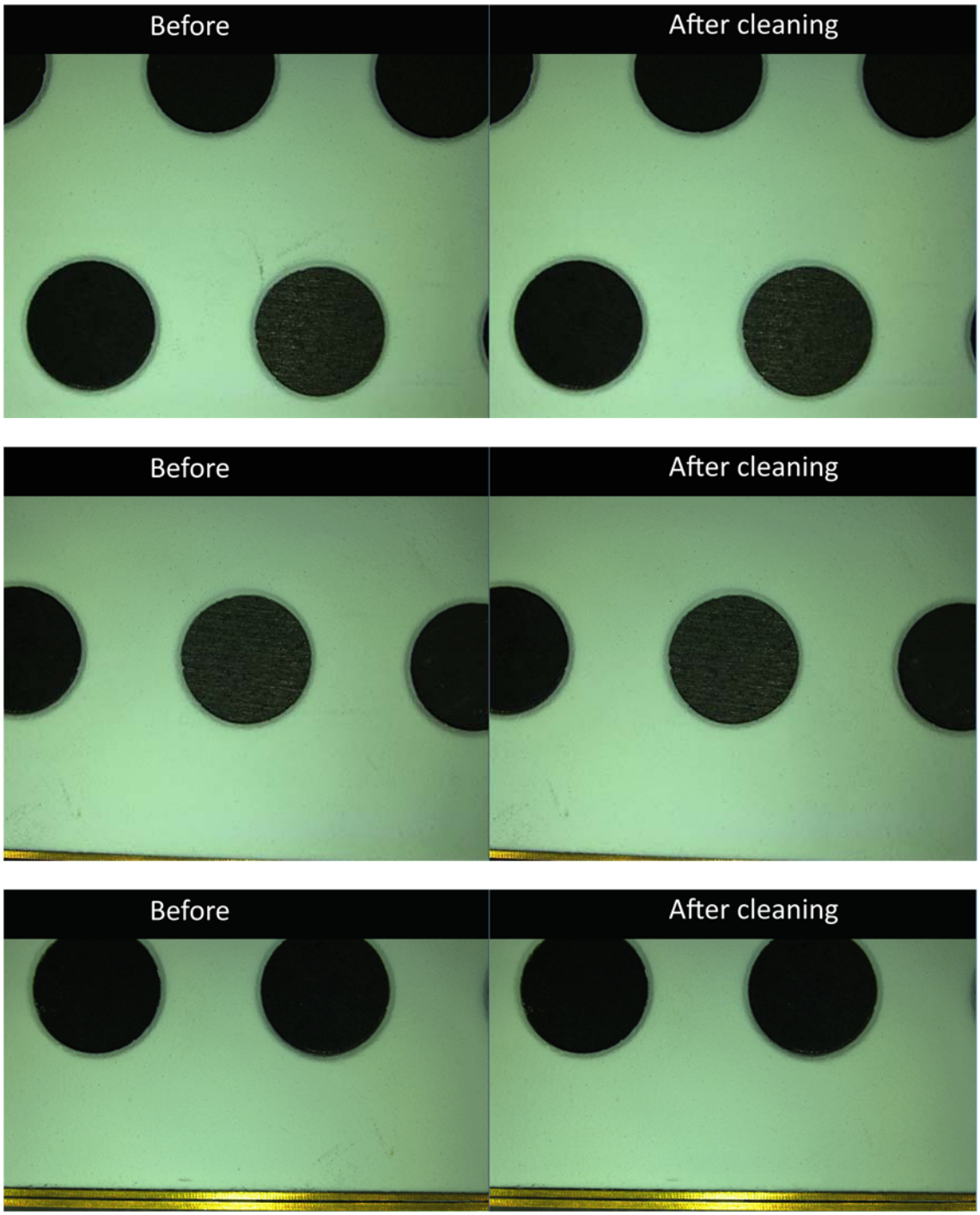
Before
After cleaning
Before
After cleaning
Before
After cleaning

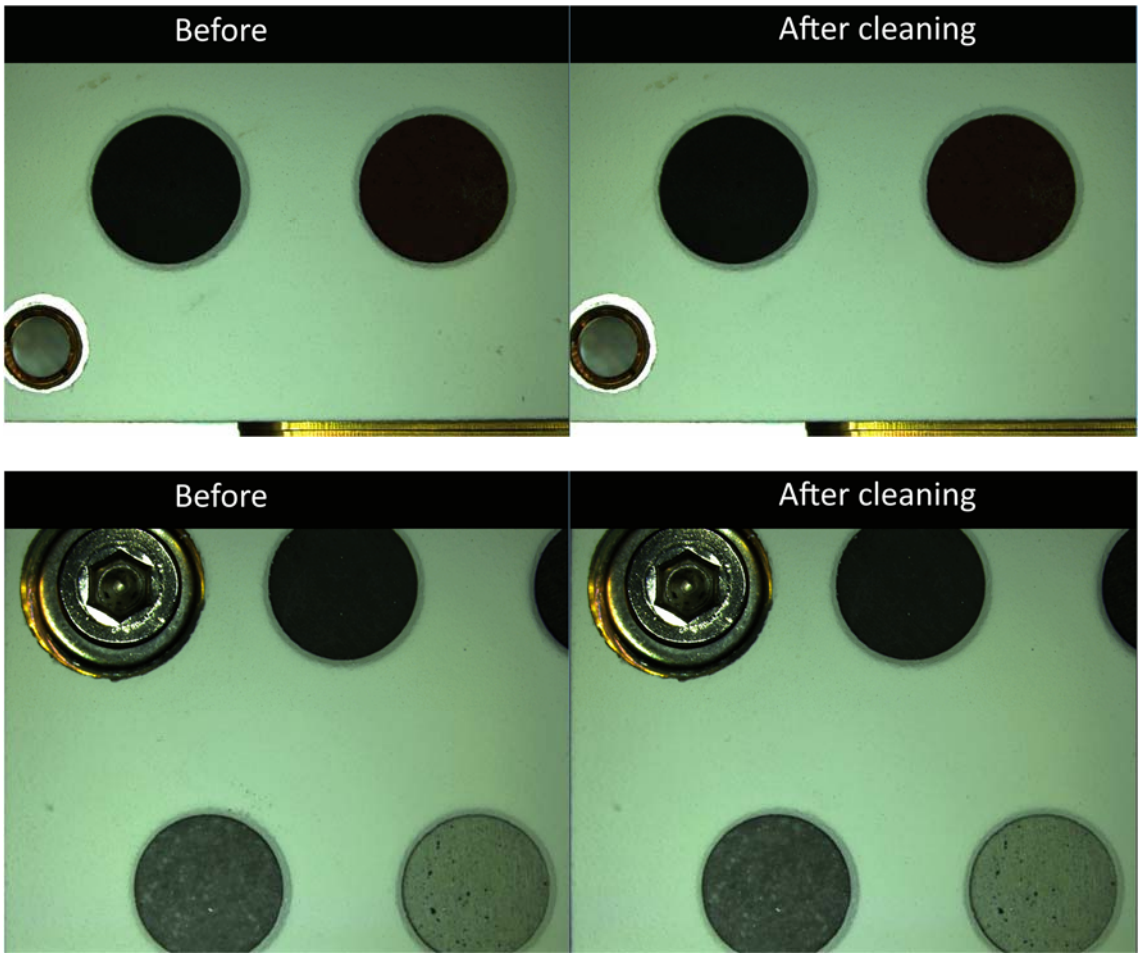

2.3.6 MOC witness placement during TVAC test

During TVAC, the MOC witness could not be placed inside the chamber together with the unit. This was corrected for the FM, although the impact of the TVAC test on the MOC was very limited.

2.3.6.1.1 Final conclusions from the qualification campaign

The Qualification of a system is one of the most demanding phases in a space project. Although the manufacturing and assembly of the FM is the final goal and it's the most important and precious piece of hardware, EQM demonstrates that all the previous work done during the design and analysis stage was correct.

The SCCT EQM passed successfully the qualification campaign in the summer of 2018. What allowed the manufactuturing of the FM that was finally delivered in spring of the next year, 2019.

2.3.6.2 The Flight Model and final schedule of the milestones accomplished during this work

As a result of the lessons learned during the manufacturing and the qualification campaign of the SCCT, some small changes were introduced in this model. These

changes were agreed with JPL and meant no invalidation of the qualification campaign since the SCCT-FM has no mechanical differences with the SCCT-EQM model.

During the qualification campaign and the manufacturing of the EQM the team found some issues that were solved changing the surface finishing of some areas of the FM.

- Black ring: this black ring around the white target is necessary to provide a high contrast between the calibration target and the holder. The EQM design was difficult to mask during the painting, and left small details where the paint was easy to detach from the holder during the cleaning activities.

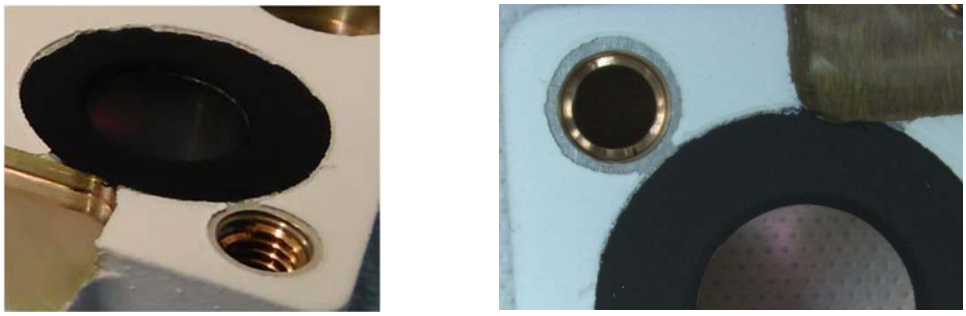

FIGURE 2.61 IMPERFECTIONS IN THE AEROGLAZE Z306 CIRCLE AROUND THE WHITE PASSIVE SAMPLE (EQM)

To solve this issue the design of this ring changed to provide a greater area painted with Aeroglaze Z306 paint, more reliable than the S13 paint, and an area easier to mask.

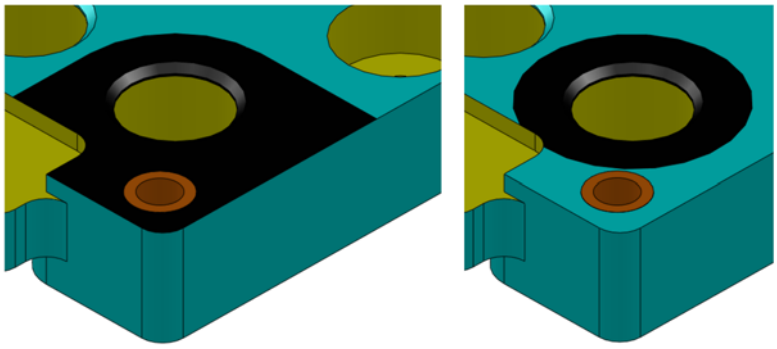

FIGURE 2.62 CHANGE IN THE SHAPE OF THE BLACK AREA AROUND THE WHITE PASSIVE SAMPLE. FM ON THE LEFT, EQM ON THE RIGHT

- Name plate used to mark the model: the case was similar to the black ring, but in this case the problem was the masking during the application of the Alodine coating. The areas were changed to make easier the manufacturing and painting process. This change is almost not visible once the plate is on place.:

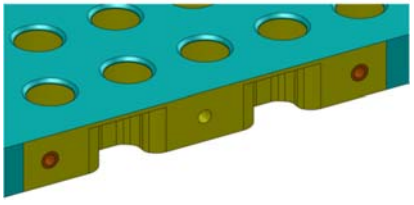

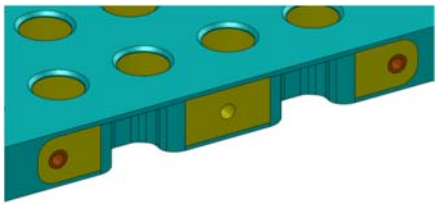

FIGURE 2.63 CHANGE FROM EQM (LEFT) TO FM (RIGHT)

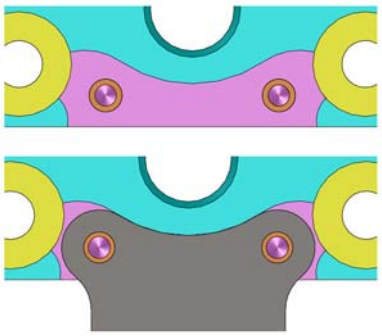

FIGURE 2.64 CHANGE IN THE PAINT AROUND TI PLATE

- Titanium plate: The problem with the masking during the coating was harder to solve in this case due to the geometry of the Ti plate. An also, again, small borders and areas painted with S13 paint were avoided. The result for the FM is an area easier to mask during painting that will be un coated.

- Samples: the development tests and the EQM samples were planned to provide a wide set of samples that were at least tested during a shock test. Providing a wide set of potential candidates to be implemented in the FM. Two exceptions escaped from this tests campaigns due to different reasons:

· the Shergotite samples that will be mounted on SCCT FM and Spare come from a bigger piece that was the Spare model of Chemcam's Calibration Target. The low amount of sample available (just two pieces) and the importance of this sample to do a cross calibration between SCAM and ChemCam, made advisable not to include any of the two samples available in the EQM, and keep them directly for the FM and Spare models. Also, It needs to be remarked, that a bigger piece of shergotite was qualified for chemcam, passing the ERD qualification tests for this mission.

· Organic sample: Some tests done after the end of the qul campaign showed that the raman performance of the sample included in the EQM (epoxy resin) was poor when compared with other candidates as the PET. Later tests by Exomars science team showed that UV radiation in combination with no or low oxygen atmosphere, was not enough to induce changes in the Raman signature of this sample, making the PET compatible with the environment. Given the plastic nature of the PET, and the experience of this group with the material during the qualification of Exomars RLS's CT, it was found a minor change that shouldn't be a concern and can be considered a great improvement.

TABLE 2-11 SAMPLES MOUNTED IN THE FM

SAMPLE	SAMPLE CODE	ETU (JPL SHOCKS)	EQM	FM
Minor elements glass	NTE01		x	X
Minor elements glass	NTE02	x	x	X
Minor elements glass	NTE03	x	x	X
Minor elements glass	NTE04	x	x	X
Minor elements glass	NTE05		x	X
andesine	PMIAN	x	x	X
Orthose	PMIOR	x	x	X
clinopyroxene	PMIDN	x	x	X
enstatite	PMIEN	x	x	X
ferrosilite	PMIFS	x	x	X
olivine	PMIFA	x	x	X
chert	LCMB	x	x	X
Martian soil analogue	LJSC	x	x	X
Mn-Rich Nodule	LJMN	x		X
Basalt	LBHVO	x	x	X
calcite	LCA53	x	x	X
apatite	TAPAX		x	X
ankerite	LANKE		x	X
Serpentine	TSERP		x	X
BHVO basalt + K2SO4	TSRICH		x	X
siderite	LSIDE		x	X
Shergottite				X
PET				X

Different elements and position in the SCCT can be seen in the following figure:

1.1	White passive sample (Aluwhite98)	3.6	Serpentine (Silicate)
1.2	Black passive sample (AeroglazeZ307)	4.1	Basalt standard BHVO-2
1.3	Red passive target (LUCIDEON)	4.2	Martian soil analogue JSC-1
1.4	Green passive target (LUCIDEON)	4.3	Ankerite (Ca, Fe, Mg, Mn carbonate)
1.5	Cyan passive target (LUCIDEON)	4.4	Siderite (Fe carbonate)
1.6	Ertalyte organic sample (PET)	4.5	Manganese nodule Standard (silicate)
1.6b	Diamond	5.1	
2.1	Sulfur rich target	5.2	Minor elements samples: trachybasalts doped in Cu, Cr, Mn, Zn, Ba, Rb, Li, Sr, Ni
2.2	Chert (Quartz mostly)	5.3	
2.3	Calcite (Ca Carbonate)	5.4	
2.4	Ferrosilite (orthopyroxene)	5.5	
2.5	Apatite (phosphate)	5.6	Chemcam Shergottite
3.1	Orthose (feldspar)	MM	Martian meteorite (NWA10170)
3.2	Diopside (Clinopyroxene)	G1	Geometric target 1 (grey scale)
3.3	Olivine (silicate)	G2	Geometric target 2 (USAF)
3.4	Andesine (plagioclase)	Ti	Titanium plate
3.5	Enstatite (pyroxene)		

FIGURE 2-24 POSITION OF THE DIFFERENT SAMPLES IN THE SCCT.

The final FM integration and the assembled model can be seen in the following pictures:

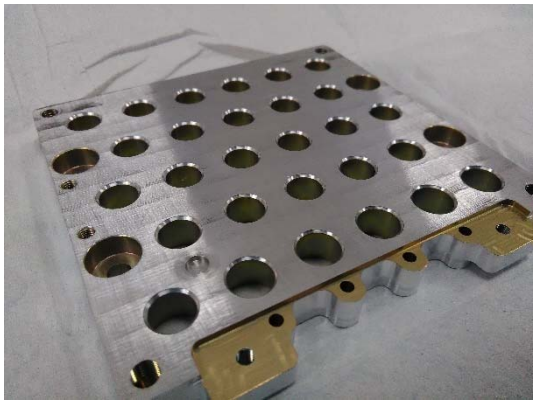

FIGURE 2-27 MAIN BODY OF THE SCCT AFTER MANUFACTURING AND COATING (AVS).

FIGURE 2-25 SAMPLE LIDS AFTER MANUFACTURING (AVS)

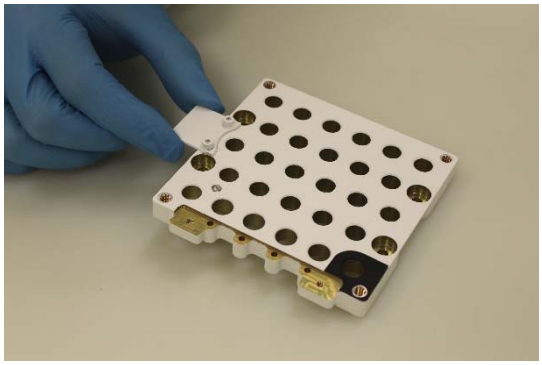

FIGURE 2-26 MAIN BODY AFTER PAINTING AT JPL (AVS)

FIGURE 2-28 SCCT PARTS CLEANING IN ISO4 ENVIRONMENT

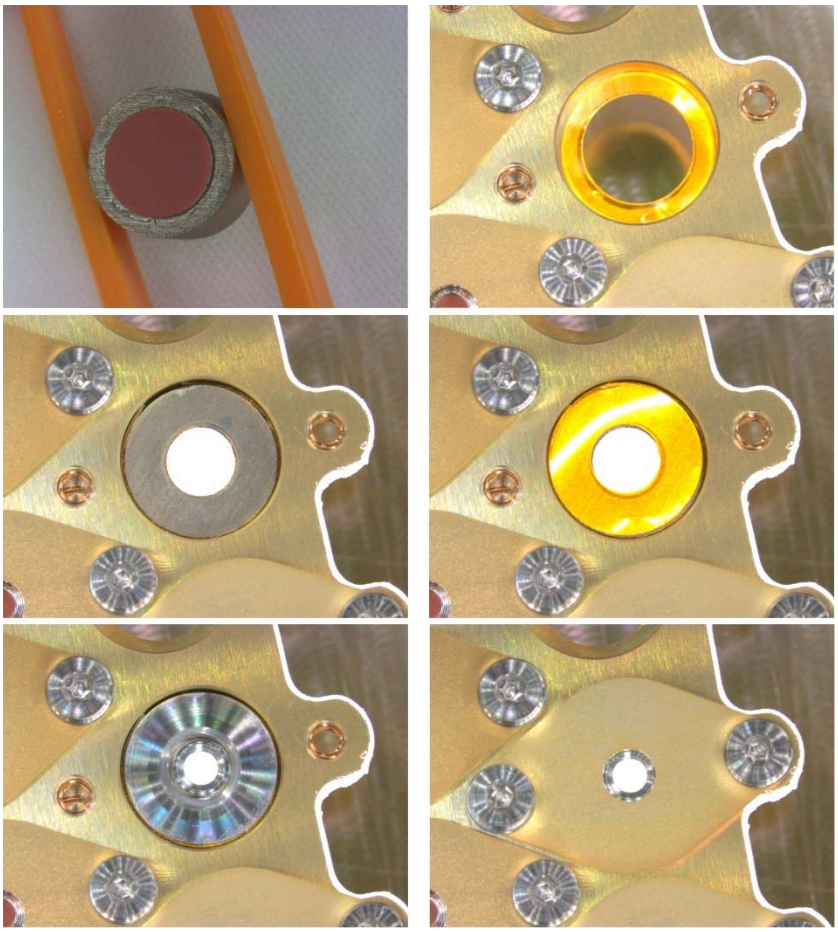

FIGURE 2-31 ASSEMBLY PROCESS OF RED PASSIVE SAMPLE

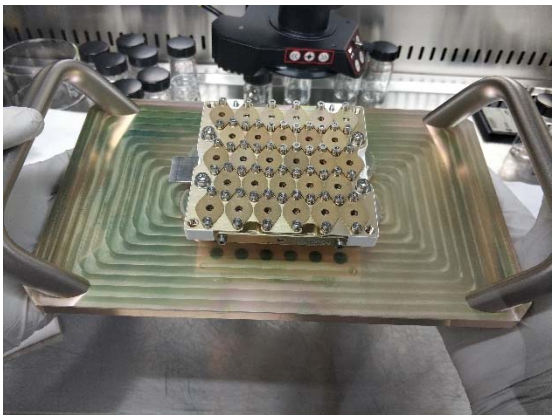

FIGURE 2-30 ALL SAMPLES ASSEMBLED. BACK END OF THE SCCT IS FINISHED

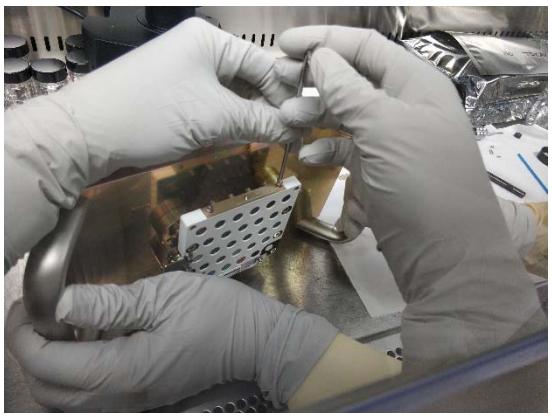

FIGURE 2-29 ASSEMBLY OF THE MODEL NAME PLATE

FIGURE 2-33 SCCT FM MODEL ASSEMBLED. THE MARTIAN METEORITE AND GEOMETRIC TARGET CAN BE SEEN. ALL THE SAMPLES ARE IN PLACE, AND THE PASSIVE SAMPLES ARE RECOGNIZABLE IN THE FIRST SAMPLES ROW.

FIGURE 2-34 SCCT AFTER DRY HEAT MICROBIAL REDUCTION, AT LAST ACCESS BEFORE ASSEMBLY

FIGURE 2-32 THE SCCT WITH THE REMOVE BEFORE FLIGHT COVER ON PLACE

2.3.7 Conclusions

Since the final selection of SuperCam to be part of Mars2020's payload in 2014 to the final delivery of the SuperCam Calibration Target to JPL in April 2019, almost 5 years were required to develop and deliver a relatively not complicated piece of space hardware.

As was stated by the quality responsibles from JPL during the PDR held in Valladolid, the opportunity to send any component to Mars should be considered unique. So special attention to all minimum details applies and make every step of the development and final manufacturing a long process.

In this time, we have developed a new technological component under the constrains of the space exploration and operation on Mars. A Flight Model has been delivered to NASA by our group, making this University, and the others that helped in this process, part of the history of the Solar system exploration

The effort and amount of time of a small group of two researchers as technical responsible, myself and G. Lopez as MA responsible, it's difficult to measure and of course hard to reflect in the present manuscript. After this effort and time, I wanted to make several considerations.

The first one is that it is a honor to be part of a space mission, and be directly involved in a project that will carry the name of the University of Valladolid to Mars. And besides the honor, the experience of being involved in every single task of the project, not only as a documentarian or schedule keeper, but participating in the design, cleaning, assembly, testing, etc. was unique experience.

It also served to identify systemic problems for every space project in Spain, from the most complex and expensive, as RLS or MEDA, to others simpler and cheaper as the SCCT. The lack of a Spanish Space Agency, and the associated tools for funding, long term planning or assistance, was a serious inconvenient during the project execution, especially when compared with our colleagues from other countries were this body exists. This agency should be top priority in the Spanish space agenda.

Th lack of a Space agency was solved in part by the good coordination and collaboration among independent institutions as INTA, EHU, UMA and UCM, and subcontractors as AVS. It would be a mistake to let this team and working collaboration framework perish after the achievement of the objectives of this project. The presence of a space agency could help with the continuity of this network, but besides of the agency, a lack of tools and mechanisms to give continuity to these teams have also been identified.

In this line of problems, a general problem of the whole research environment in Spain is evident: it is depauperated. Most of the work in this thesis has been done by personnel hired to volatile funding, or *soft money*, the current situation in the Spanish Universities and research centers make almost impossible to apply to a permanent position by these personnel. Without proper mechanisms to give stability to key researchers projects like this one might have serious problems in the long terms planning, as the positions of the researchers are volatile, but at the same time project depends on the skills and formation received by them in a long and complex process.

As final result, I have to thank for the opportunity to acquire a unique profile thanks to this thesis, as it lies in an interface between a pure science profile and an engineer profile.

3 Combined and standoff Raman-LIBS spectroscopy: some experiments

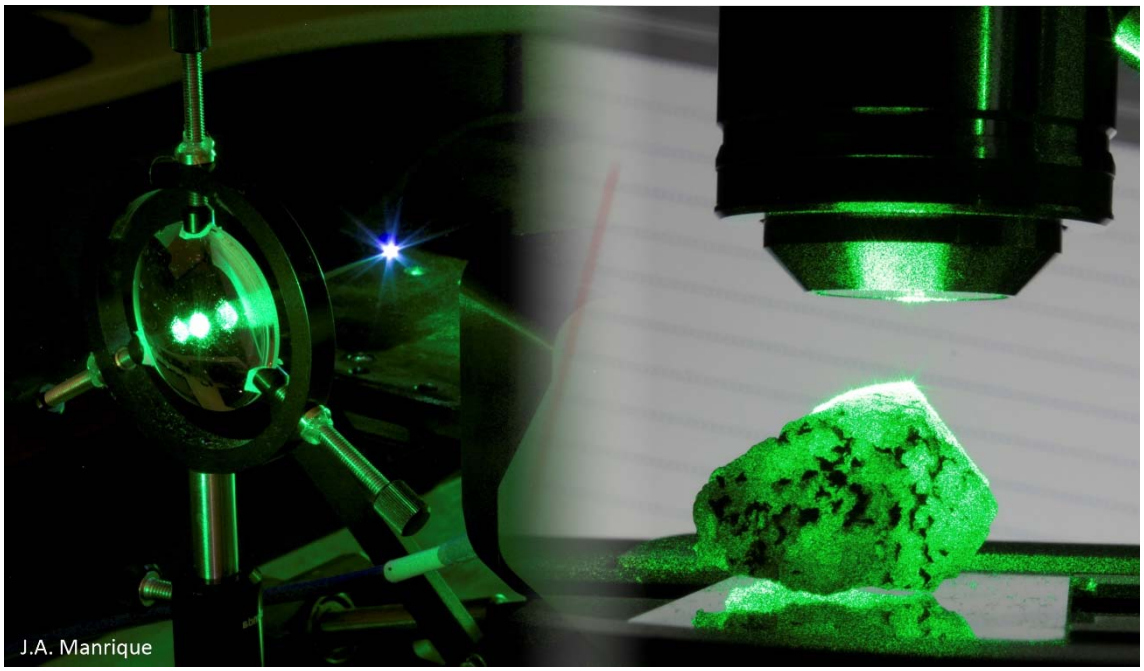

3.1 Introduction

LIBS spectroscopy has already demonstrated its capability to contribute to the exploration of the Solar System thanks to ChemCam (Wiens, 2012), which has been providing information of the elemental composition of the surface of Mars since 2012. With its standoff capabilities, Chemcam, has demonstrated how this kind of standoff instruments could play a capital role in the operations of an exploration mission. This kind of instruments facilitate the analysis of areas of interest with simpler operations, getting valuable spectroscopic data from an active technique, and then use that data to decide where to go with a rover to perform more complicated analysis. Not only it is useful in operations, but in science outcome, as several discoveries made in Mars thanks to ChemCam can demonstrate (Schroder, 2017).

LIBS has demonstrated its capabilities and will continue doing it in future missions. In addition, in the following years several rover missions will also include Raman spectroscopy in their payloads. Examples of these instruments are: Sherloc (Beegle, 2015) in Mars2020 rover's payload, the Raman Laser Spectrometer (RLS) (Rull, 2017), part of ESA's Rosalind Franklin rover's payload, and SuperCam (Wiens, 2017), part of NASA's M2020 mission. RLS has been developed under the science lead of the University of Valladolid, and it is a 532 nm continuous Raman instrument, while SCAM is a remote multi-technical instrument including Raman spectroscopy, as described in the previous chapter, counting also with participation from our research group both, with technical responsibilities and as part of the science team.

Both Raman and LIBS spectroscopic techniques have been successfully adapted to standoff developments, not only for space exploration such as SuperCam or ChemCam, but also as laboratory systems in research centres worldwide. Both techniques have typically been used separately, but a new area of study is emerging in the last few years related to the combination of both techniques.

This section covers different experiments and their associated results obtained with our laboratory setups, which help define the potential science that can be obtained with a standoff combined Raman-LIBS system in different scenarios.

Starting in section **¡Error! No se encuentra el origen de la referencia.** I cover one i nteresting result, already published in the Journal Of Raman Spectroscopy (Sanz-Arranz, 2018), that explains the use of a material as baseline reference for Raman acquisition. This result could have more implications as the possibility of getting the instrumental function in a wide variety of spectroscopy instruments. It's so effective and simple that has been implemented in the spectra acquisition procedures in our lab. Because its widespread use in the works included in this manuscript, and its potential usages, I

found it interesting enough to be proposed as one of the samples for calibration of SuperCam and included in this thesis.

Section 3.3 presents a brief experiment on how biomarkers can be detected using a compact standoff system will be shown. This experiment was done to evaluate the performance of an asynchronous standoff Raman system with certain biomarkers. For these experiments, pure substances were analysed to evaluate the identification capabilities of the endmembers; and then deposited in limited amounts over a mineral substrate to evaluate real detection capabilities.

In the same line of work, based on biomarkers, an assessment of the detection capabilities using different excitation wavelengths (Rayleighs) with contact instruments is done. The objective of this experiment is to evaluate if the relation of the Raman cross section with the fourth power of the frequency can be limited by other effects in real samples.

These two experiments are directly related to the possible detection of biomarkers by space-oriented developments.

Section 3.4 describe another set of experiments directly related to the geochemical characterization, and geological process assessment in an astrobiological context.

In a first experiment will use methods developed for a contact instrument as RLS for evaluation of the weathering of olivine. These methods will be applied to standoff Raman data sets to evaluate performance of the methods against the constrains related to these instruments.

Finally, section 3.5 includes a study of the application of multivariate analytical techniques for the analysis of Raman and LIBS data. In addition, profiting from the multianalytical capabilities of SuperCam or the different instruments in a payload, a study on the application of data fusion techniques. Either in the case of SuperCam, where the same instrument will gather data using different analytical techniques, or in the case of RLS or Sherloc, that will have the possibility to collaborate with other instruments, the combined science using different techniques, and the data fusion analysis will be an interesting way to enhance the scientific outcome that can be derived from two independent measurements. In this framework, the main objective of the work presented in this section is to explore the advantages provided by the combination of complementary Raman and LIBS data, being both techniques part of the SuperCam's analytical suite, with a brief look to the combination of two Raman measurements from different instruments.

3.2 Luminescent materials as intensity reference

This section covers a work that has been already published and has been referenced in several points along the text (Sanz-Arranz, 2018). In this paper we propose the use of a compound to be used for baseline correction, which could be of use in space instruments.

Due to the apparatus function of every instrument, the relative intensity between two bands in different regions of the spectrum can be different between different instruments. Furthermore, the apparatus function of the instrument also modifies the spectral emission as detected in the instrument sensor. These differences make the baseline to have different shapes depending on the instrumentation. Depending on the intensity of this baseline modification the resulting observation might present different relative intensities along the spectrum when compared with other instrument; or it can it might even impair the ability to detect signals in more extreme cases. These responses are not only different for every instrument, but it can also vary with changes in the experimental setup (Ouillon, 1982).

There are several approaches to solve this issue, but the most widespread is the absolute intensity correction of the instrument (Rodriguez, 2011). For this correction the use of a calibrated light source with a perfectly defined distribution of the spectral intensity is needed. Since we know the emission function of the signal we introduced in our setup, we should be able to evaluate the detected spectra with our instrument to calculate its apparatus function, where the footprint of the instrument is included and can be identified and removed. There are two main options to use as standard for this correction:

- A calibrated tungsten halogen lamp, which is a lamp certified to emit light with a very specific emission curve, characterized by a provided polynomial.

- A luminescent intensity standard, which is a material that presents a very intense luminescence response to the excitation laser. This material can be solid, like a rare-earth doped optical glass, or a solution of a fluorescent molecule (McCreery, 2000). The best examples of this option are the NIST Standard Reference Materials (SRM) belonging to 224X series (Choquette, 2007).

In our case, focusing on space applications, the option of placing a lamp into any spaceship that requires power, additional electronics, controls, qualification, etc. implies a too high complexity. Passive elements are safer and easy to send to space, and given the complexity of sending hardware to space, the safest option that complies with its requirements.

However, the use of passive samples is not perfect either. For example, we had to face some difficulties when tried to use one of these standards for calibration of the RLS instrument, given the potential temperature dependence of the NIST standards.

In many situations this kind of approaches to obtain an apparatus function calibration, but to have a picture of the shape of the baseline of an instrument. We have faced situations with high etaloning, or weird shapes on the reading of an instrument, interferences in filters or all kinds of effects that were problematic for the spectrum analysis. For us, any material valid for several excitation lasers, presenting a broad emission which is also resistant enough to be shot by a pulsed laser would be a great help in our daily basis.

Based on our group's experience in Raman spectroscopy and the great variety of samples we have analysed in almost 30 years of existence, we started this search by the materials with a similar composition to NIST standards, and more specifically to SRM 2241 (intended for 785 nm excitation) and SRM 2242 (intended for 532 nm excitation). These standards are, respectively, a chromium doped (mole fraction of 0.202% Cr2O3) sodium borosilicate matrix glass, and a manganese-doped (0.15 wt % MnO2) borate matrix glass (Sanz-Arranz, 2018). We started evaluating different borates and borosilicates, and finally selected the zinc borate, a white substance, that presented a high luminescence after being thermally processed to induce an amorphous phase (Schubert, 2003).

The resulting substance presents a high intensity luminescence, making easy to obtain a good spectrum using the whole dynamic range of the detector. Having this into account, we obtained several spectra of the Amorphous Zinc Borate (A-ZB), averaging a great number of accumulations to reduce shot noise in the baseline. It is important to remark that the noise has a high impact on the quality of the correction, as the noise from the reference will add to the noise in the spectrum to correct using this procedure. The use of further digital processing, as Savitzky–Golay filter, is discouraged for the A-ZB spectra since this could eliminate some kind of noise (high

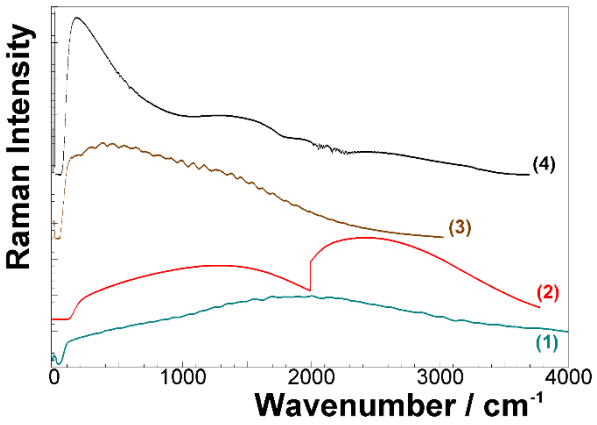

FIGURE 3-1 EXAMPLE OF SPECTRA FROM THE A-ZB TAKEN BY 532 NM MOVING GRATING INSTRUMENT (1), 633 NM TWO TRACK INSTRUMENT (2), 785 NM INSTRUMENT WITH ETALONING PROBLEM (3) AND 1064 FT RAMAN INSTRUMENT WITH CO2 DISTORTIONS (4)

frequency fixed-pattern noise) and spectral artifacts (transmission filter ripple), which is needed in the reference spectrum to be removed from the spectrum to correct.

3.2.1 Description of the method

The correction procedure proposed in tis work is, in some aspects, similar to the procedure described for the standard correction using a NIST SRM. It consists in dividing, for the same wavenumbers, the intensity of the problem spectrum by the intensity of the A-ZB spectrum reference. The procedure is so simple, that a non-expert can handle the initial Raman information and easily get the corrected spectra without special software for spectra edition.

The correction procedure proposed is summarized below:

1- A Raman spectrum of a sample is recorded.
2- The Raman spectrum of A-ZB is recorded, with the same optical configuration of the Raman device. A high number of scans is recommended to reduce the noise.
3- The Raman spectrum of A-ZB, and the one from the sample, are normalized in intensity to one, making the intensity of the lower point of spectrum equal to zero, and the intensity of the higher point of spectrum equal to one.
4- The intensity of the Raman spectrum of the sample is divided by the intensity of the Raman spectrum of A-ZB.

Using this method we have been able to work with a 785 nm instrument that presents a very high etaloning problem, making it almost impossible to find signals when there is a luminescence background.

Figure 3-2 shows an example of the effectiveness of the method for baseline correction, when compared to the other two standard methods for the correction: the calibration lamp and the SRM materials.

I have selected the case of the 785 nm Raman because of the severe etaloning problem, but similar results were obtained with other instruments using different excitation lasers from 1064 nm to 532 nm.

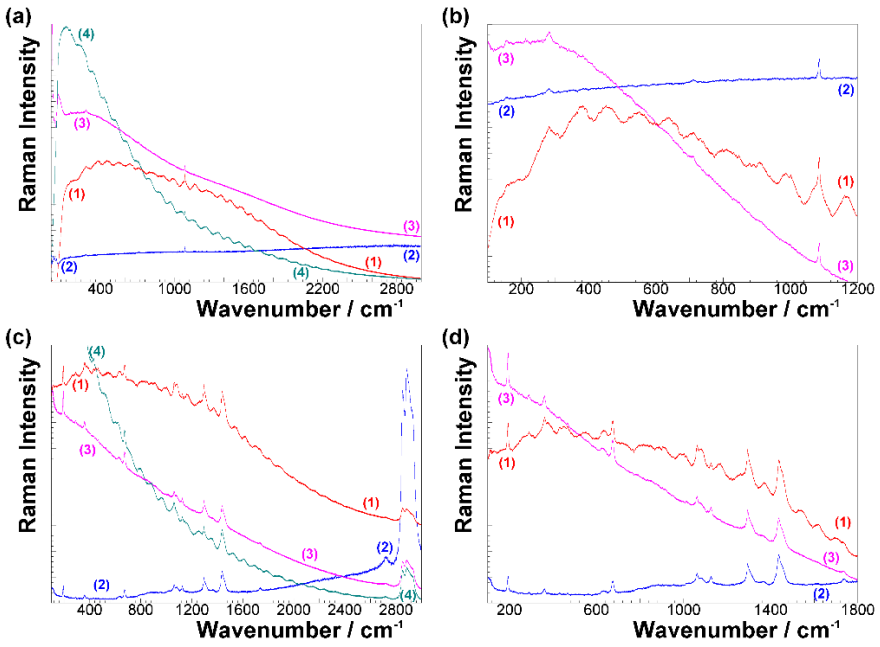

FIGURE 3-2 (A) 785 NM SPECTRA OF A LIMESTONE SAMPLE, (1) ORIGINAL, (2) A-ZB CORRECTED, (3) LAMP CORRECTED, (4) NIST CORRECTED. (B) DETAIL OF A REGION OF INTEREST (WITHOUT THE NIST CORRECTED SPECTRUM). (C) SPECTRA OF PE+TALC, (1) ORIGINAL, (2) A-ZB CORRECTED, (3) LAMP CORRECTED, (4) NIST CORRECTED. (D) DETAIL FROM (C) (WITHOUT THE SRM 2241 SPECTRUM)

In order to quantify the goodness of the method we did measurements of the Signal To Noise Ratio for certain bands from the spectra shown in Figure 3-2. Taking the band at 194 cm^{-1} and 2881 cm^{-1} from the PE+Talc, and the band at 1086 cm^{-1} from the limestone.

	PE+talc 194 cm^{-1}		limestone 1086 cm^{-1}		PE+talc 2881 cm^{-1}	
	Orig.	A-ZB	Orig.	A-ZB	Orig	A-ZB
$\bar{I}$ (a.u.)	1369	792	1476	932	886	12565
$\bar{\sigma}$ (a.u.)	151.1	86.0	123.8	97.9	36.8	800.3
RSD (% $\bar{I}$)	11.0	10.9	8.4	10.5	4.2	6.4
SNR	9.1	9.2	11.9	9.5	24.1	15.7

TABLE 3-1 AVERAGE PEAK INTENSITY ( ), STANDARD DEVIATION OF THE PEAK INTENSITY ( ), RELATIVE STANDARD DEVIATION RSD (%), AND SIGNAL-NOISE RATIO (SNR) CALCULATED FROM TWO RAMAN BANDS OF PE+TALC AND ONE OF LIMESTONE (9-POPULATION-SPECTRUM), ORIGINAL AND CORRECTED WITH A-ZB.

The results from this SNR measurements are included in Table 3-1 average peak intensity ( ), standard deviation of the peak intensity ( ), relative standard deviation RSD (%), and signal-noise ratio (SNR) calculated from two Raman bands of PE+talc and one of limestone (9-population-spectrum), original and corrected with A-ZB.

3.2.2 Results and conclusions

As we can see in the published work and in the brief description in the present thesis, amorphous Zinc-Borate presents a broad luminescence emission that covers the reading range from 1300 nm to shorter wavelengths than 532 nm. This means that it can be used in several instruments in a wide spectral window, as for example with LIBS.

More specifically, in the case of our 785 nm instrument, most of the spectra taken show a succession of undulations (etaloning) present for almost all the useful range of the instrument, from 200 to 2400 cm-1. This interference artifact has a dramatic effect on the baseline, especially in spectra coming from samples presenting weak Raman signals, with an intensity comparable to this effect in the acquired spectra.

As was shown in Figure 3-2 (a) 785 nm spectra of a limestone sample, (1) original, (2) A-ZB corrected, (3) lamp corrected, (4) NIST corrected. (b) Detail of a region of interest (without the NIST corrected spectrum). (c) Spectra of PE+talc, (1) original, (2) A-ZB corrected, (3) lamp corrected, (4) NIST corrected. (d) Detail from (C) (without the SRM 2241 spectrum), in the untreated spectrum only the 1086 cm-1 signal emerged clearly over the etaloning, while the 280 cm-1 signal hardly emerges over the crest of a big baseline undulation and the other signals are completely masked. In the corrected spectrum with the A-ZB the wavy baseline is almost corrected and the weaker signals, between 155 and 711 cm-1 are now clearly present. On the spectrum corrected with the lamp all these signals are also visible, although the etaloning correction is not as good and a slight residue coming from the undulations can be observed. Also, the NIST SRM 2241 doesn't really help with the etaloning of the baseline.

The same comparison for the PE+Talc can be done: On the original spectrum, almost all the Raman signals are influenced by etaloning. The wider signals (with maximums at 1061, 1294 and 1437 cm-1) get their band profiles altered. In the spectrum corrected with A-ZB the etaloning has almost disappeared and the wider signals recover their usual profile. The amplification suffered around the 2881 cm-1 region on the spectrum corrected with A-ZB is noticeable; this amplification is due to the low intensity of the A-ZB spectrum in that region and the division by a value near to zero. In the spectrum corrected with the lamp, the effect is practically the same. Once again, the NIST SRM 2241 wasn’t really helpful with the etaloning.

In the SNR analysis the 194 cm-1 PE+talc signal decreases its intensity to roughly a half and the SNR remains almost the same. The 1086 cm-1 limestone signal decreases its intensity on one third and the SNR also decreases but not as much. The 2881 cm-1 PE+talc signal increases its intensity drastically, more than 14 times; nevertheless the SNR decreases on almost one third. The decrease is due to an increase, of almost 22 times, produced by the standard deviation of the signals intensity. This means that the

main bands suffer almost no variation, or small decrease, in their SNR while we are recovering the weaker signals of the spectrum.

The A-ZB showed how it can be useful for treatment of spectra in our labs, helping us to cope with artifacts and baseline problems in our Raman spectra. It also demonstrated that instead of having a selection for every spectral window of use, one sample can do the job for the whole ranges of measurement, meaning it could also be used in combined instrumentation with LIBS. The fluorescent emission can be acquired by all the spectrometers and been used for post treatment and instrument health check.

One feature has not been achieved so far with this material and it is the ability to be used for absolute intensity correction. This kind of correction might need a much more extensive work on the characterization of the emission and assessment of its stability. For its use in laboratories or in space missions, once this characterization is done it can be used to correct the instrumental function on every place. In fact, we have implemented the acquisition of A-ZB sample in every field trip and measuring session, as it gives a picture of the status of the instrumentation at the moment of use.

A final factor to be commented is that the amorphous zinc borate is a very resistant substance, that can be used with pulsed lasers, at least with our standoff systems, without any appreciable damage or change in the spectrum.

For all the features, and with the option of calibrating the emission, this sample was proposed by our group to the project, to be implemented in the SCCT. However, the slots available in the SCCT are just a few and this sample wasn't considered, as samples for a correct calibration of LIBS were more necessary. Nevertheless, it could be considered for future missions, as it is a material that is space friendly:

- Low degassing due to thermal treatment
- Works at a wide range of temperatures
- Allows several ways of conforming and processing.

3.3 Standoff Raman and detection of biomarkers

In section 2.1.2 when the objectives of the Mars2020 mission were defined, the direct detection of biomarkers was one of them (objective B). Although it may be unlikely, due to the degradation of organics on Mars (Stoker, 1997), this section is an example of the use of a standoff system for characterization and detection of biomarkers. Covering one of the objectives.

As it was discussed in the introduction (1.2.3), in the case of Raman spectroscopy, the main problem is that this weak intensity of the effect can be competing with other light sources that could be more intense, covering the Raman spectrum.

One mechanism competing with Raman to be detected is the fluorescence. This radiation comes from electronic states that are excited by the incoming light, relaxation of these states is produced by the emission of a photon of certain energy. The intensity ratio between fluorescence and Raman is variable with the material and can vary from a small background in the spectrum to a mechanism that competes (even covering) with the intensity of Raman bands. This is an issue with more difficult approaches, as was discussed in the first chapter, 1.2.1.3, like Time Resolved Raman Spectroscopy, although it is important to remark, anyway, that in a Mars exploring framework fluorescence has been evaluated as not concerning by some authors (Wang, 2019).

A typical standoff instrument includes a detector that is intensified and time gated, introducing the ability of Time Resolving the measurement (Sec. 1.2.3). However, the intensifier is an expensive and complex add-on to a detector, that is desirable, but is not mandatory as was introduced. As example, I am going to use the not synchronized standoff system described in 1.3.2.

3.3.1 Experiment description

This work is focused on the detection of biomarkers using our experimental standoff instrument previously described in 1.3.2. The objective is triple: 1- verify the identification capabilities on pure aminoacids for their characterization, 2- the detection capabilities when deposited on mineral samples, and 3- Evaluation of the detection capabilities of an *in vivo* sample.

Amino acids are interesting from the astrobiological point of view for several reasons. Amino acids are the building blocks of the structural and functional elements of life, proteins. The origin of this compound can be as a product of metabolic activity of living systems, but also can have an abiotic origin, as was demonstrated by the famous Miller-Urey experiment (Miller, 1959). It is obvious that for life to appear in a place, these abiotic processes to generate organic compound are needed, and their detection could mean that in a certain place, at least, the conditions for life were given.

On the other hand, this kind of compounds have been already detected in our solar system. Same products from Miller-Urey experiment were detected by Giotto mission in a comet (Balm, 1991), or in the returned samples from Stardust (Elsila, 2010). Titan can also be a place where these processes could lead to the formation of amino acids or nucleotide bases (Horst, 2012). Summarizing, there is some evidence of the appearance of amino acids in different places of the Solar System, and their presence is a condition for living systems to appear. Reason of the interest on these compounds in the present work.

Asa first step of the work, we selected several amino acids and tried to detect and identify these compounds from a distance of five meters, which is an average operation distance for a hypothetical rover. The objective of these measurements was to evaluate the identification capabilities of the technique, assuming a relatively easy detection, given that aminoacids are good Raman scatterers. These were directly analyzed inside glass vials.

In a second step we tried to detect three of the selected substances at the same distance but now deposited on a mineralogical substrate.

Finally we tried to detect a bio marker in vivo, and for that purpose we used a green alga that produces a carotenoid called astaxanthin, and what we found growing on a substrate of dolomite. As this is a closest case to the detection of a real biomarker in real conditions.

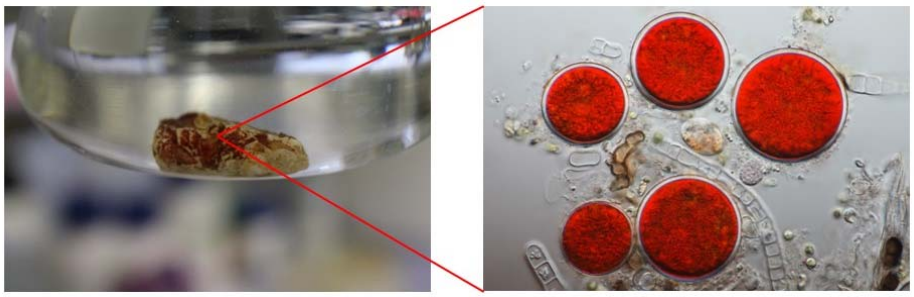

FIGURE 3-3 HEMATOCOCCUS PLUVIALIS COLONY USED IN THIS EXPERIMENT

The carotenoids are interesting for living systems as they play an important role in the protection against Sun radiation, and also absorbing energy to be used in photosynthesis, making them an important biomarker to be found in highly irradiated environments as Mars.

3.3.2 Experimental setup

Regarding the instrumentation, as excitation source we used the second harmonic of a Litron Nano S Nd:YAG pulsed laser (60mJ, 30Hz, 6-8 ns pulse length). The laser beam was collimated and the irradiance used was varied using a beam expander attached to the

laser, this of course adjusted the spot size on the sample. As light collector we used a Canon SLR photographic objective (F 300 mm f: 4). The collected light was filtered on a Raman Probe for 532 nm (Inphotonics) and analyzed with a two-track spectrometer developed by our team attached to an Andor Newton CCD camera. For pointing and to adjust the spot size of the excitation to the spot size of collection, we used a continuous Elforlight 532 nm laser system focused on the excitation fiber of the Raman probe. With this setup and at a distance to the sample of 5 meters we estimated that the area we were able to analyze was a 5mm spot, adjusting laser spot diameter to that size, for picture of the system see Figure 1-14.

Regarding the Samples. We selected a variety of compounds from our database: Arginine, Cysteine, Histidine, Lysine, Phenylalanine, Valine, Glutamic acid, Pyrene, Tryptophan, Glycine and Apocarotenal. We also used a Hematococcus Pluvialis colony grown over a dolomite substrate that we collected from the field.

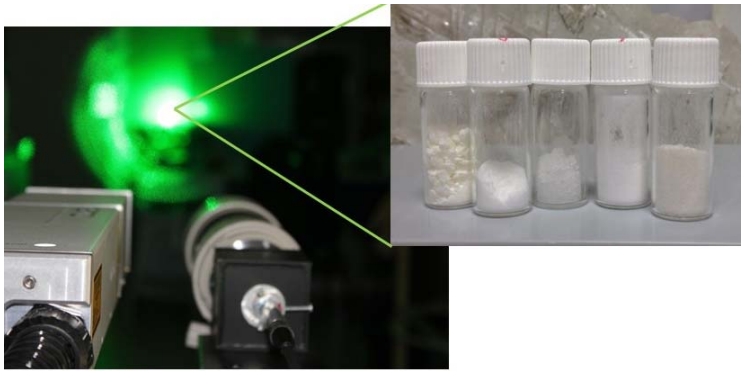

FIGURE 3-4 VIALS OF AMINO ACIDS AT 5 METERS OF THE INSTRUMENT

FIGURE 3-5 AMINOACIDS DEPOSITION ON THE BASALT

Regarding the acquisition parameters. The camera used is not gated and does not provide an internal delay generator for camera-Raman emission synchronization purposes. However, the camera is externally triggered by the laser. We varied the number of scans to accumulate but the integration time was the same for all the samples (0.001 seconds). With the exception of the spectra of Hemat. Pluvialis and Apocarotenal, both easy to damage with the laser, we used the laser energy set up to its maximum level of 60 mJ per pulse.

Regarding the sample preparation. For the spectra of pure substances no preparation was needed, except for the use of glass vials, neither was needed for the spectrum of Hematococcus Pluvialis. For the spectra of biomarkers over mineral substrates we dried two solutions of L-Cysteine and L-Glycine over basalt at a temperature of 50 ºC. In the case of Apocarotenal we used a mixture of propanol and water, and dried the solution over a dolomite at room temperature.

3.3.3 Results:

For the pure substances, as was mentioned before, they are highly efficient

Raman scatterers and their spectra are well known (Gelder, 2007), each spectrum was obtained after 300 scans. The resulting spectrum was then smoothed using a Savitzcky-Golay filter, and baseline correction was applied to eliminate the transition between the two tracks of the spectrometer. The resulting spectra are shown bellow:

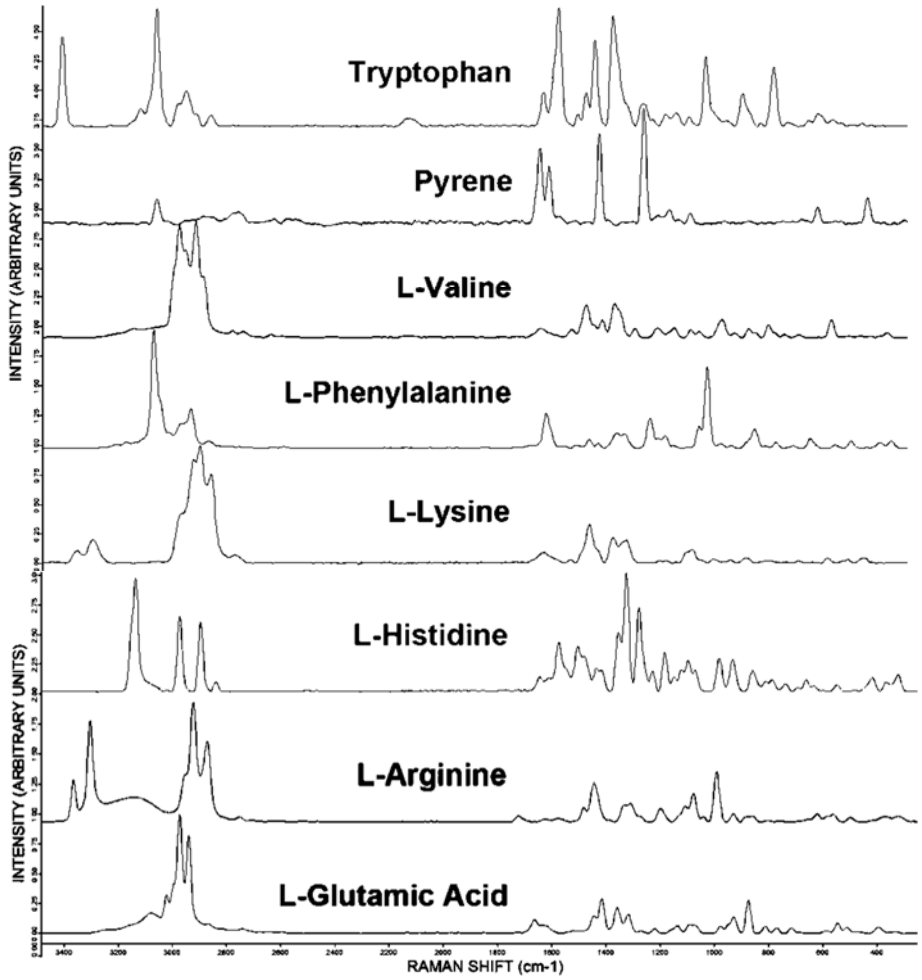

FIGURE 3-6 RAMAN SPECTRA FROM THE PURE SUBSTANCES IN VIALS AT 5 METERS

In the case of the spectra of Glycine, Cysteine and Carotenal over the mineralogical substrate, and given the low amount of substance deposited, we found a high presence of noise in the spectra. This noise is coming from the reduced integration time of the CCD, but also as the intensity of the light decays, the artifacts from the optics and the spectrometer became more evident. The artifacts were removed by the process previously described using amorphous zinc borate (Sanz-Arranz, 2018). The spectra required a total of 1000 scans per spectrum and the averaging of three different spectra

per sample. Below are shown the comparisons between the pure substance and the substance on the basalt substrate, this is glycine and cysteine.

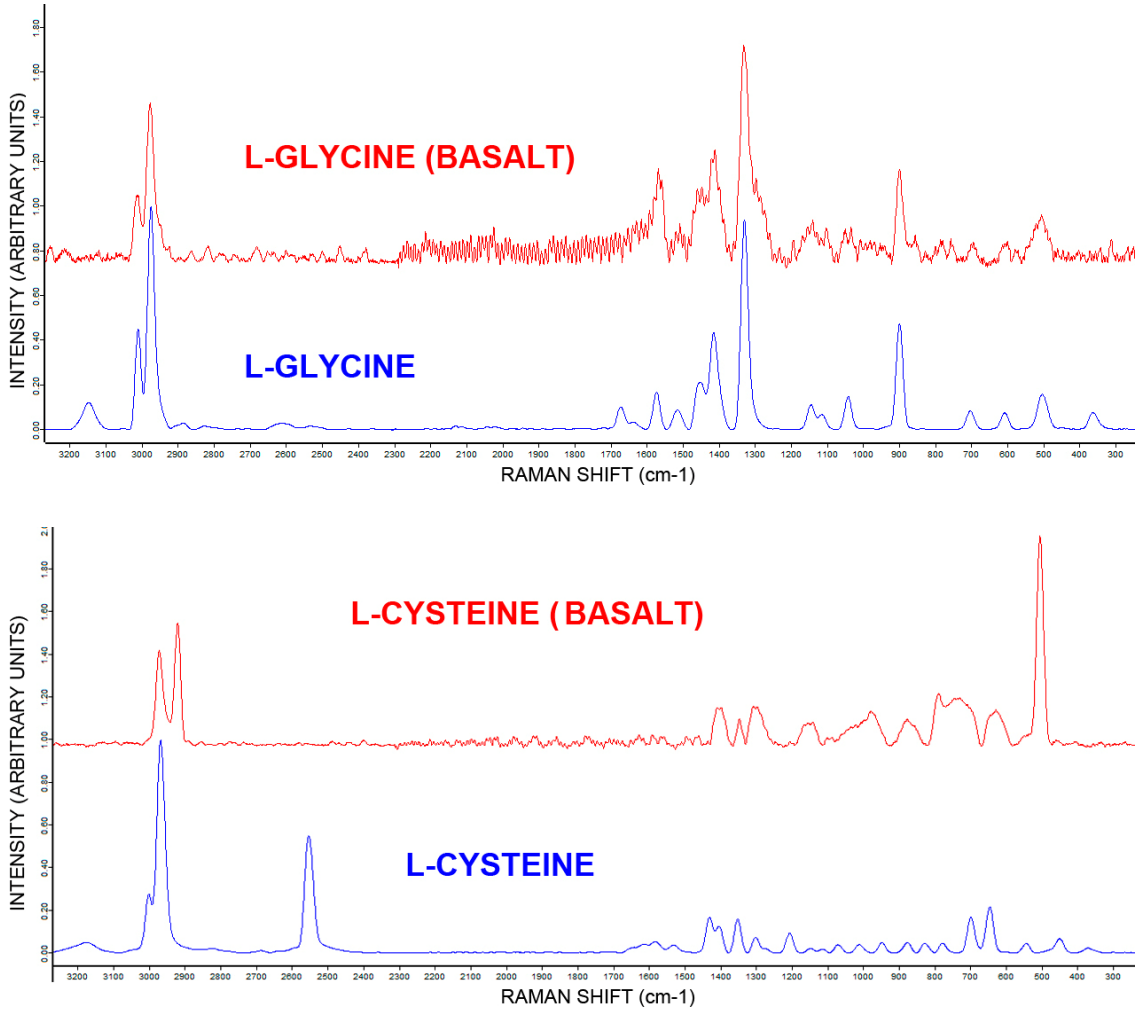

FIGURE 3-7 SPECTRA FROM PURE SUBSTANCES AND THE DEPOSITION ON MINERAL SUBSTRATE.

In the case of the glycine, we observe just a difference in the Signal to Noise Ratio, that in the case of the bands around 3000 cm^{-1} has changed from 898 to 42, in arbitrary units. This is due to the aforementioned decrease in the quantity of material that is producing Raman scattering. The spot size has been kept the same in both cases (vials and over mineral substrates) so this change comes from the fact that the thickness is really low. In fact, in Fig. 3-6 the area where the deposition of glycine was done is almost not visible, as the layer is semitransparent. In the first experiment, a pure white sample in a vial, the Raman scattering is actually happening in a volume. This volume is given by the shape of the beam and the penetration of the laser in the sample. The sample in this case is a poweder made from translucent grains of aminoacids, and the laser is collimated, so we can presume that the Raman scattering is happening in a cylinder of a couple of mm diameter and a few hundreds of microns height (the penetration depth of the laser). On the other hand when considering a biomarker deposited on a substrate, this situation

changes, the volume changes, as the thickness of the layer can be thinner than the penetration depth of the laser, and then we will have also light coming from the substrate, this is reflections, fluorescence or Raman bands from the substrate. As a result, the strength of then signal will be lower, mainly because the amount of material illuminated by the laser is also lower.

More interesting is what happened in the case of cysteine, where surprisingly a change in spectrum happened with the appearance of new bands, and disappearance of others. At first glance, the band that was present in the pure substance but is no longer present in the mineral is the band around 2550 cm^{-1} that corresponds to Sulfur-Hydrogen bonds. On the other hand, the spectrum from the mineral presented a band around 500 cm^{-1} that corresponds to disulfide bridges.

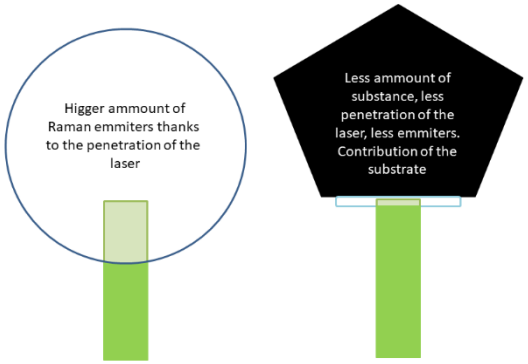

FIGURE 3-8 LASER PENETRATING IN A VIAL AND IN A THIN LAYER.

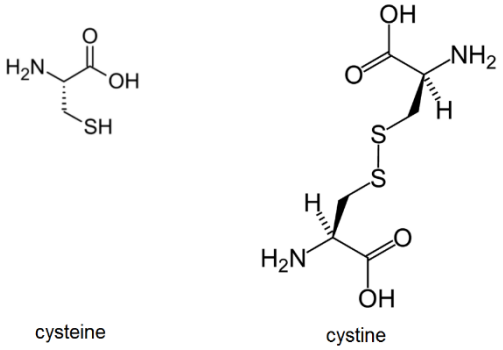

FIGURE 3-9 DIMERIZATION OF THE CYSTEINE TO FORM CYSTINE

Conclusion to be obtained is that certain S-H bonds have been destroyed to form new S-S bonds. Cysteine is one of the few amino acids that have sulfur, and is one of the two, along with methionine, that are incorporated in proteins (Brosnan, 2006). In proteins, the presence of sulfur, is important due to this ability of forming disulfide bridges that stabilize the folded configuration of these macromolecules. In its neutral form, when not in a protein, cysteine is known to form a dimer known as Cystine, shown in Fig. 3-9, that is, apparently, the compound the is detected on the mineral substrate. This change was not observed when spectra were taken from a similar deposition on a glass slide. Suggesting a role played by the basalt.

As mentioned in the introduction of this experiment, carotenoids are compounds that are used in plants and algae as a protection against the UV radiation from the Sun. In an environment as the last days of habitable Mars, possible extremophiles surviving under the extreme UV radiation of the Sun may have metabolized these compounds. For a Raman spectroscopist they are quite interesting because of the resonance that carotenoids present in their main band when excited with a green laser, like it is the

case. This increase in the intensity of the band, that can be of several orders of magnitude, lowers the detection limit of this possible biomarker.

The first spectra from carotenoids in this experiment were obtained from a dissolution of apocarotenal, and a deposition of this solution over a dolomite:

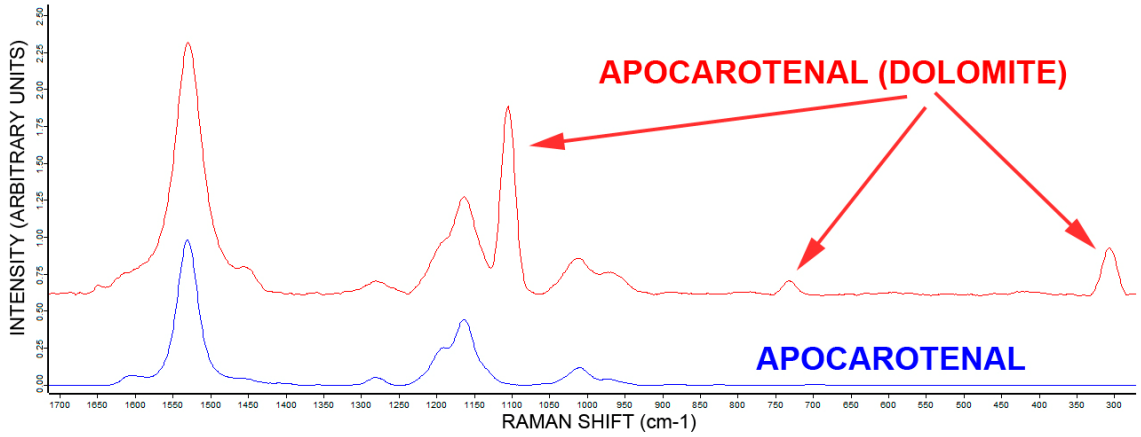

FIGURE 3-10 SPECTRA FROM APOCAROTENAL OVER A DOLOMITE SUBSTRATE

In this case the thin layer was still detected and could be identified, but in addition to the biomarker we got signals from the underlying substrate of dolomite. The laser power was set to 80%, as it was observed that at full power the layer of carotenal was damaged.

In the case of the *in vivo* detection of another carotenoid, astaxanthin, from the colony of hematococcus pluvialis, the spectra needed to be acquired also with a lower power of the laser not to damage the algae:

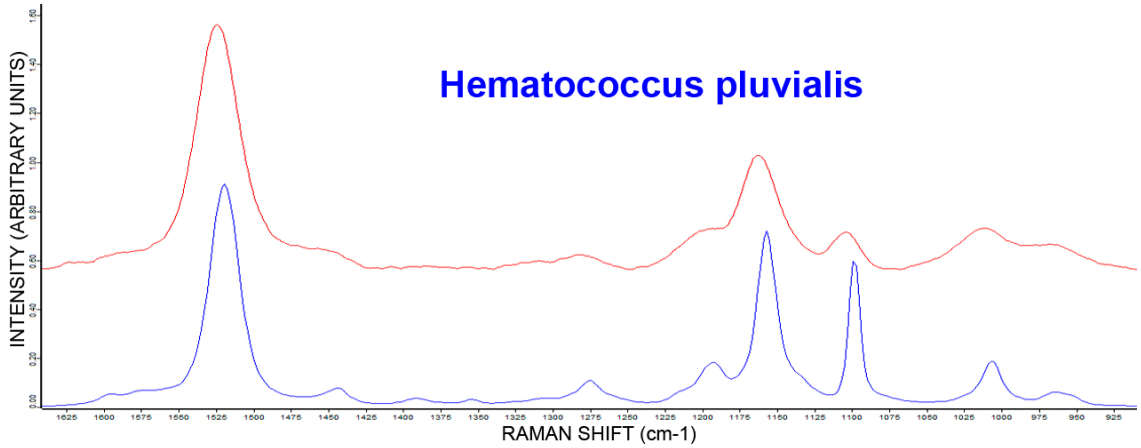

FIGURE 3-11 SPECTRA FROM THE COLONY OF HEMATOCOCCUS PLUVIALIS. THE BLUE SPECTRUM WAS ACQUIRED WITH A 1064 NM RAMAN INSTRUMENT. IN RED IS SHOWN THE SPECTRUM FROM THE STANDOFF INSTRUMENT.

In addition to the spectra acquired with the standoff system, a different spectrum was acquired using a 1064 nm Raman instrument to avoid fluorescence, and shown compared with the standoff spectrum in Fig. 3-11.

3.3.4 Conclusions

Although the desirable configuration of a standoff Raman instrument includes an intensified detector to enhance the detection, in this work we have demonstrated that a simpler configuration also works.

The instrument developed was able to detect the pure substances with a quality good enough to do identification of the amino acids. All the selected substances provided a good spectrum at five meters. Also, when moving to a more realistic case, when the substance is not pure and in great amounts, it was also possible to detect these lower amounts despite of the possible interference of the mineral substrate.

Not only the instrument detected these biomarkers, the measurements provided served to identify an alteration suffered by the cysteine. This alteration was not reproduced when spectra were acquired from a deposition of the same solution over a glass slide, making clear that the basalt had role in the change. Cysteine dimerization, and in general the formation of disulfide bridges is known to happen in oxidative environments, the higher surface of contact of the porous basalt, in combination with the energy of the laser pulses and the atmosphere could induce this change.

Finally, the detection of a relevant biomarker was achieved, also in lower quantities over a mineral substrate, and more specifically, on a real colony of algae, *in vivo.*

The system used is working at a shooting frequency of 30 Hz, with a great energy, but the selection of this laser was done on base of availability. Since this operating way of the standoff instrument is based on the ability to acquire short spectra gathering a few laser pulses, the detection limit and performance of the whole system could be significantly improved by using a higher repetition rate. DPSS pulsed laser can work at repetition rates of several kHz, which is two orders of magnitude greater than the one used in this experiment. This high repetition rate still allows the sample to relax from one shot to the next, so an improved system could still use pulses with an energy in the order of the mJs.

Finally, this kind of system could prescind of all the complicated hardware associated to the intensifier, as well as simplifying the spectrometer avoiding the reduction of resolution due to the ghosting on the intensifier's phosphorus screen. Our setup could be used with a RLS-like ultraluminous spectrometer, a high repetition rate laser and small optics to deploy a competent standoff Raman instrument on the surface of a planetary body.

3.4 Olivine weathering assessment

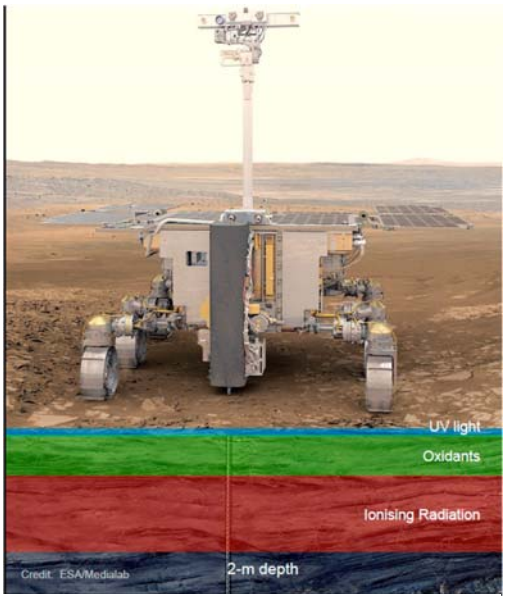

FIGURE 3-12 ROSALIND FRANKLIN ROVER DRILLING DOWN TO THE ORGANICS PRESERVATION ZONE.

The work on section 3.2 is focused on the detection of biomarkers using Raman and standoff Raman. It was pointed out how the detection of biomarkers is possible with standoff systems, but generally needing very high concentrations. On Mars the expected extant biomarkers accessible to SuperCam might be in very low concentrations, and in degraded status. For these reasons Mars 2020 is oriented to the selection of good candidates for caching for Mars sample return, where they could be optimally analysed.

On Mars's surface a hypothetical biomarker faces several harmful factors that impair its integrity. The possible factors that play against organics preservation are:

- UV radiation: with no atmospheric protection against UV, the surface of Mars is continuously sterilized by this radiation. UV radiation can penetrate a depth of a few millimetres down the surface of Mars.
- Oxidants: Mars Surface is highly oxidized, as can be assessed from the presence of iron oxides over the surface and regolith. Also, recent detections of perchlorates on Mars suggest that this kind of oxidants are more present than expected. This constitutes a riskfor human exploration (Davila, 2013), but also a great harm for possible life, or for the preservation of organics or biomarkers, in combination with UV (Wadsworth, 2017). These oxidants can penetrate down to one meter or more.
- Ionizing radiation: the conditions of present Mars, without a strong magnetic field (that could have been present in the past), present no shielding against ionizing radiation. These high energy radiations can also damage the organic molecules, and can penetrate down to the 1.5 meters in Mars.

This is the main reason why the Rosalind Franklin Rover on the ExoMars mission features a drill to look for the biomarkers in possible reservoirs at 2-meters depth, where they might be better protected from these aggressions (Vago, 2017). Rosalind Franklin Rover will use its drill to gather and analyze samples in situ on the rover's analytical laboratory, which includes a Raman spectrometer (RLS).

Other organics reservoirs have been proposed that could be at surface level, or in the first centimetres bellow the surface. Mainly it has been proposed that some minerals could have the ability to preserve organics, or even past life intertwined between the mineral layers, as for example, in phyllosilicates (Fornaro, 2018). The detection of these minerals is related to objective C of this thesis (see section 2.1.2) and the assessment of the best possible candidates for samples caching.

Taking all this into consideration, the processes related to the formation of phyllosilicates and their related geochemistry needs to be studied on Mars in order to assess the habitability of Mars, as covered by objective A (see section 2.1.2).

3.4.1 Importance of serpentinization.

Serpentinization is the process that turns ultramafic minerals into the phyllosilicate serpentine. The process has great relevance for astrobiology for several reasons, including the previously described ability to protect and preserve biomarkers.

Ultramafic rocks are greatly present in the oceanic crust. These minerals are generated as cumulates in basic magma and then transported to the surface. These kinds of minerals, belonging to the phase triangle in fig. 3-13, start alteration as soon as they are over the crust when interacting with liquid water.

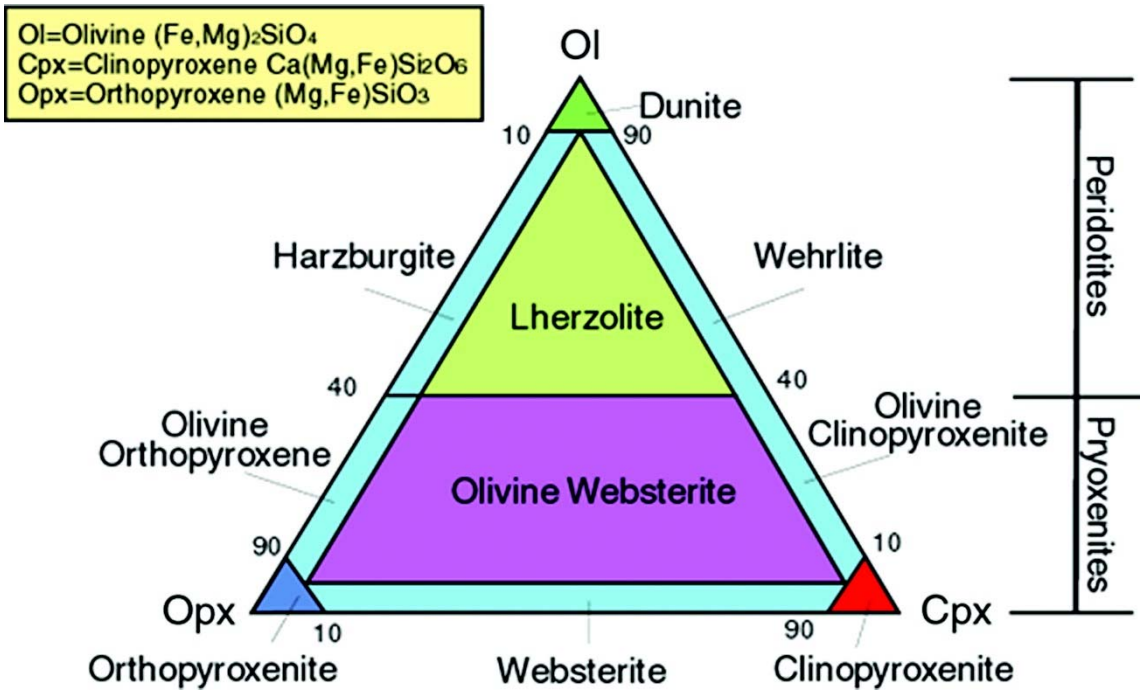

FIGURE 3-13 CLASSIFICATION OF ULTRAMAFIC ROCKS (LEMAITRE, 2002).

This kind of interaction represents an state of chemical disequilibrium from which an organism could obtain energy for metabolism (Schulte, 2006), one of the conditions needed for life (Fig. 2-3).

This energy can be also used for abiotic processes that can produce organic molecules. These environments are of great relevance from an astrobiological perspective, as this are potential candidate environments where life might have appeared. Thus, the serpentinization process could have played its role in life emergence and preservation in Mars, as it indicates the presence of the ingredients for these organic compounds (Holm, 2015).

The serpentinization process is described by the reaction below:

(a) $\mathbf{Fe_2SiO_4 + 5Mg_2SiO_4 + 9H_2O \rightarrow 3Mg_3Si_2O_5(OH)_4 + Mg(OH)_2 + 2Fe(OH)_2}$

(b) $\mathbf{Mg_2SiO_4 + MgSiO_3 + 2H2O \rightarrow Mg_3Si_2O_5(OH)_4}$

In the reaction (a), both constituents of the olivine, fayalite (Fe) and forsterite (Mg), react with water to produce serpentine and hydroxides (Schulte, 2006). Also pyroxene and olivine can react with water (b) to produce serpentine.

The iron hydroxide from reaction (a) can later suffer oxidation providing a source of hydrogen:

(c) $\mathbf{3Fe(OH)_2 \rightarrow Fe_3O_4 + 2H_2O + H_2}$

As suggested by some works, this reaction could be the reaction that provides the hydrogen and energy for the abiotic synthesis of organics, or biochemical reactions for emerging life. Also, this reaction could have played a role in the formation of the methane on Mars, as this hydrogen can react with the atmospheric CO_2, compounds of interest as they serve as nutrients for some bacteria (Stamenkovic, 2014).

Places where serpentinization occurred could be then places where conditions were given for life to appear and persist, and the minerals previously described have been found on Mars already. An assessment of the maturity of this process can give an idea of the geological past and dynamics of sites that were habitable.

Not only the products of these reactions can produce interesting products for astrobiology, which in Mars is important, they also can help preserving them as was already described. Several authors have proposed and demonstrated how the structure of phyllosilicates, composed of several sheets of silicate, can work as reservoirs for organics and water. Organics would be trapped in the interplanar space and protected from outer aggressions as oxydants and UV radiation. Other works (Röling, 2015) also suggest that some minerals might have antimicrobial properties, like those where solubility of iron is produced, or others with high presence of aluminium, potentially toxic to some bacteria.

Taking all of the previous factors into account, serpentinization and its products are of high interest for life origins studies and the search of biomarkers on Mars.

Giving a context for this process, looking to a primitive Earth, before life appeared, these compounds emerged from the volcanic activity on the bottom of the oceans at the ridges, where crust is formed. These minerals can be present in regions of oceanic crust that have drifted to the continental crust, ophiolites, and started suffering the weathering of the conditions on land. As soon as these minerals started interacting with water, serpentinization started to occur. Serpentinization gave the products useful in the prebiotic synthesis of organics, and nutrients and energy for early microorganisms. Not only serpentinization provided necessary elements for life, it also provided a reservoir where biomarkers and microorganism could be preserved.

May the same process occur in Mars, where CRISM has detected Serpentine in several sites, and more specifically in Mars 2020 landing site, Jezero (Dobrea, 2019). Not only serpentine was found, but also the precursor mineral species as olivines or pyroxenes. Having a good assessment of the serpentinization process, knowing the ratio of serpentine and olivine, could be of interest as it can provide an idea of interesting factors for biomarkers search: for how long have been the olivines exposed to liquid water, amount of interesting compounds for organics formation, energy sources for metabolic reactions, and finally, if there has been a good chance of having a life-friendly environment for a time enough for life to appear.

3.4.2 Spectroscopic assessment of serpentinization

Among the Mars 2020 payload, just a few tools will be able to provide some valuable data in the assessment of the serpentinization on the analysed environments. PIXL will provide elemental composition, as will do the LIBS from SCAM. However, it is evident from the serpentinization reactions that this process is a change in the arrangement of some elements, without a variation in the elements in play. Concentration of some elements could be an indicator this reorganization, but this is quite difficult to correlate to the actual process. Figure 3-15 Spectrum of olivine (green), serpentine (red) and a mixture with a 25% content of olivine (blue) as obtained by RLS simulator (UVA)shows LIBS data from olivine and serpentine. Differences are too subtle for a model to be done that could work in intermediate mixtures. Thus, detecting the changes in structure is the best way to calculate the portion of serpentine and olivine in a mixture, i.e. the serpentinization level of a sample. Raman spectroscopy is sensitive to structure and therefore can directly detect serpentine, olivine and pyroxene, meaning that data sets from Raman can be used for the calculation of concentration.

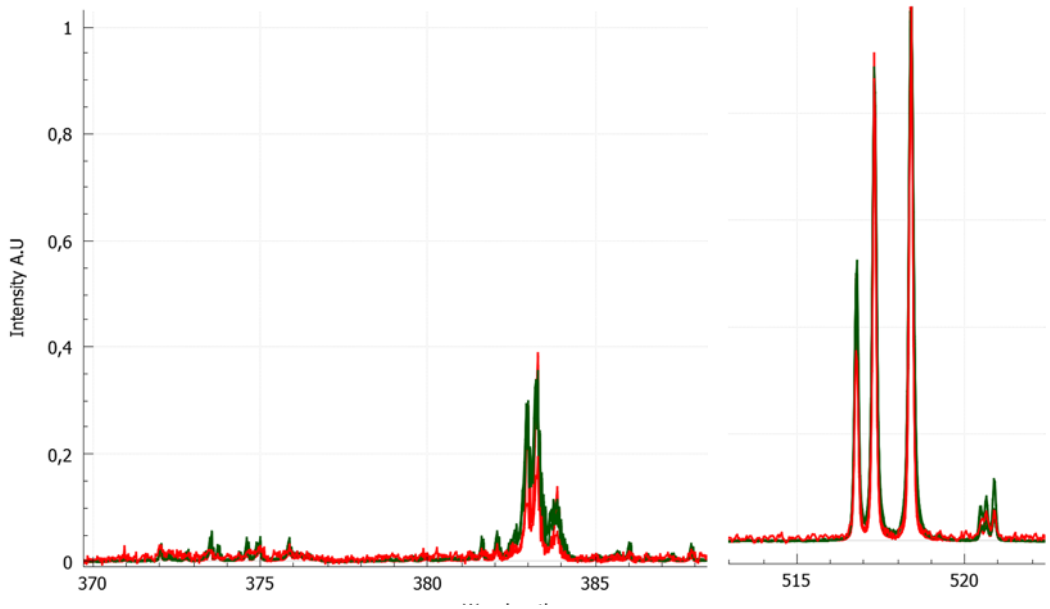

FIGURE 3-14 SELECTED ROIS OF LIBS SPECTRA OF OLIVINE (GREEN) AND SERPENTINE (RED). (UVA)

Two Raman instruments, Sherloc and SuperCam, will be available on the Mars 2020 rover. On the ExoMars 2020 mission, the RLS instrument will also provide Raman measurements of selected samples on the Rosalind Franklin rover. The definition of methods to calculate the olivine/serpentine proportion based on Raman spectra is thus of great interest, and something not typically possible with Raman spectroscopy data. At this moment we are leaving behind the possibility of using LIBS or XRF, something that could be interesting to evaluate also the Fo/Fa ratio in the olivine, and the amount of iron, which also is an astrobiological factor of interest.

We have developed models to obtain the relative concentration of one of the compounds based on spectral features of the Raman spectrum. These methods were prepared for a continuous instrument as part of the scientific support of RLS; In this work, however, we have used the calibration curves obtained from the continuous instrument to the data obtained from a standoff instrument. The main constraints on this application are the signal strength in the case of data coming from a SuperCam like instrument as a consequence of distance on one hand, and the influence of the apparatus function on the other.

In this case, the standoff system data used against the RLS calibration target is obtained in two different configurations: 1- using the best possible acquisition parameters of the instrument; and 2- acquiring data based on SuperCam's parameters and constraints. Slight variations or deviations could be expected as we didn't compensate the different instrumental responses, but the exercise will provide useful information regarding the capabilities of doing these calculations based on SuperCam measurements.

FIGURE 3-15 SPECTRUM OF OLIVINE (GREEN), SERPENTINE (RED) AND A MIXTURE WITH A 25% CONTENT OF OLIVINE (BLUE) AS OBTAINED BY RLS SIMULATOR (UVA)

A previous consideration that needs to be made before moving from a model based on contact Raman to another based on standoff Raman is that phyllosilicates, as a general, are poor Raman scatterers, and therefore they should be a hard sample for a standoff system.

First step is to understand the change that is happening in the sample and how that translates into its Raman spectrum. In the case of olivine, $(Fe,Mg)_2SiO_4$ the cell of this mineral presents orthorhombic symmetry, containing 4 blocks of silicate+cation per unit cell (Chopelas, 1991). The four internal SiO_4 modes from the silicate are present in the spectrum but modified by the crystalline context where the tetrahedron is included. Considering the two main bands from olivine, both coming from the silicate, they correspond to two modes that contain both, symmetric and asymmetric stretching character. Depending on the cation present around these modes, the position of the band can shift, from 822 and 854 cm^{-1} for the magnesium, to 814 and 840 for the iron. The shifting occurs because of the change in the mass, and volume, around the silicate. These bands corresponding to inner modes of the silicate are dominating in the Raman spectra of the olivine, and their intensity is much higher than the intensity of bands corresponding to lattice modes.

In the case of phyllosilicates as the serpentine, the cation around the silicates is now substituted by a heavier unit. In the case of serpentine, the changes is from having the Mg cation coordinating the SiO_4, now in serpentine it is Mg(OH). As a result, the bans coming from inner modes of the silicate no longer dominate the spectrum and other features arise. Also this change is the basis of the laminar structure of the serpentine, as layers of silicate and Mg(OH) are formed.

The Raman spectrum from serpentine changed deeply when compared to olivine's. The first main change is the appearance of OH bands in the higher Raman shifts region. The other main bands from serpentine correspond to antisymmetric modes from OH-Mg-OH at 630 cm^{-1}, symmetric stretching of the silicate at 380 cm^{-1} and vibrations of O-H-O groups at 230 cm^{-1}. So it is clear that the silicate is no longer dominating the spectrum, and more bands appear from the Mg-OH.

Said this, it is clear that from the Raman spectroscopy point of view both components present features that don't overlap one with the other, making it promising to use this technique as reference.

As for the LIBS, the test done in the laboratory made clear that, at first glance, the spectroscopic features from both compounds are quite the same, reason why at this stage LIBS was discarded from the study. However, in Mars conditions, where OH can mean difference observable in LIBS, situation can change. Unfortunately at this moment we don't have the facilities to obtain LIBS under martian conditions.

3.4.3 Building a Raman based model

To build the model used in this section, we used mixtures of well characterized serpentine and olivine. The mixtures were grinded and mixed in a mortar in controlled proportions.

The certified serpentine used in the mixture is mainly composed of antigonite (serpentine family) and traces of other minerals as magnetite or epidote. The olivine selected is a Mg rich olivine standard, mainly forsterite). The proportions used in the mixture are as follows:

TABLE 3-2 OLIVINE-SERPENTINE PROPORTIONS USED

OLIVINE	SERPENTINE	OLIVINE	SERPENTINE
0	100	63,34	36,66
1,1	98,9	75,1	24,9
5,09	94,91	89,94	10,06
9,99	90,01	94,89	5,11
24,98	75,02	98,9	1,1
37,45	62,55	100	0
50,1	49,9		

The mixtures were then measured using RLS operation simulator (Lopez-Reyes, 2013), consisting on a 532 nm Raman instrument that mimics the operation of RLS. This instrument is fully automated in acquisition, being able to autoadjust parameters as integration time or number of accumulations. Spot size is 50 microns and the analysis are done in the samples in powder form, like the configuration of RLS, by getting up to 39 spectra from a line across the sample as RLS will do on Mars.

The total number of spectra available allowed to cope with possible statistical deviations, or minimum inhomogeneities from the sample. The method for the calibration curves is based in a univariate method described by (Lopez-Reyes, 2013). The univariate method is based on intensity ratios, and for this model the band at 230 from serpentine, and the one at 855 for olivine, were used. The band at 230 was selected because in the different polytypes of serpentine it was shown that this band doesn't change, making the model wider in application and not restricted to antigonite only. The method automatically eliminated the baseline by straight lines between 200 and 242 cm^{-1} for serpentine and between 800 and 866 cm^{-1} for the olivine. The value of the intensity for both bands was then used in the following expression to calculate an indicator:

$$R_x = \frac{I_x}{I_{oli}+I_{serp}} \quad \textbf{(eq.3.3.1)}$$

Where x could be the olivine or serpentine, and Rx represents the estimated ratio of that component. This indicator was calculated for all the points on a line to obtain a calibration curve, then averaged among several lines in order to get the quantification uncertainty. The uncertainty estimation was calculated using the standard deviation (σ) between different lines with a confidence interval of 95% (i.e. representing the uncertainty with a value of ±2σ). The resulting calibration curves were used for validation with real samples from Leka ophiolites. The results showed different degrees of serpentinization that were correlated with data from X ray diffraction, with pretty good results. All the details from the method development, as well as its validation using mars analogues is in process of being published in a paper from this group.

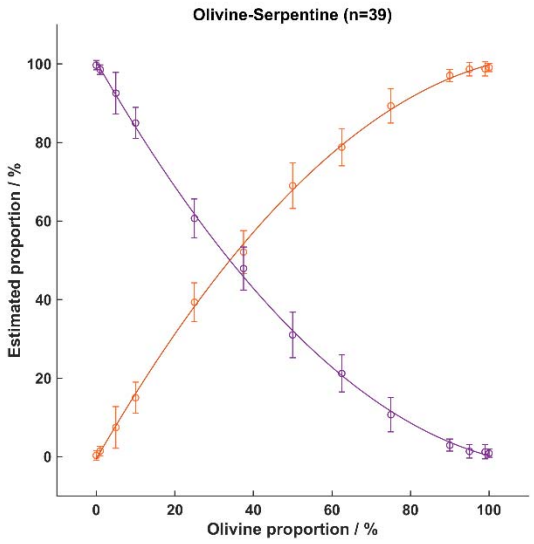

FIGURE 3-16 CALIBRATION CURVE: ESTIMATED PROPORTION OF OLIVINE VS REAL PROPORTION (BLUE). IN RED THE SAME CALCULATION IS DONE FOR SERPENTINE ESTIMATION.

The expressions for the obtained curves are obtained from the solution of:

$$\boldsymbol{R_{oli} = -7.328 \cdot 10^{-3} \cdot \%_{oli}^{\,2} + 1.736 \cdot \%_{oli} - 0.5731} \quad \textbf{(eq.3.3.2)}$$

$$\boldsymbol{r^2 = 0.9994}$$

$$\boldsymbol{R_{serp} = 7.328 \cdot 10^{-3} \cdot \%_{serp}^{2} - 1.736 \cdot \%_{serp} + 100.6} \quad \textbf{(eq. 3.3.3)}$$

$$\boldsymbol{r^2 = 0.9994}$$

Detailed paper on this work, developing the method, as well as its validation using mars analogues will be published in a paper from this group. Nevertheless, these expressions were used on data collected with the same instrument from samples collected from a real ophiolite, showing different degrees of serpentinization. The results obtained in this real sample were correlated with data from X ray diffraction, considered a gold standard for crystalline identification and quantification. Results showed an excellent correlation, giving an experimental validation of the model on natural samples.

The concentration calculations demonstrated to were very reliable using this method. However, the data collected from the RLS simulator have not been corrected in absolute intensity. This means that possible differences in the intensity rations among the spectrum may appear when using this method with data from another instruments. For continuous Raman instrumentation this can be achieved using reference materials (Sanz-Arranz, 2018), in a more general case it can be done with intensity correction lamps, but unfortunately non of them were available for the correction on the standoff system.

3.4.4 Data from time resolved Raman and standoff time resolved Raman

In this section we present the results from running the calibration curves for data from a SCAM-like instrument. The instrument used in this section belongs to the laboratory of O. Beyssac, from the French CNRS, and is a standoff/closeup Raman remote system that can be setup to mimic SuperCam acquisition(Beyssac, 2017).

The instrument has a 532 nm pulsed laser, with a pulse of 1.5 ns width, 10 to 2000 Hz repetition rate and an energy per pulse of 1 mJ. The data can be collected from two different configurations: a contact configuration using microscope lenses, and a standoff configuration, using a 8” Schmidt-Cassegrain telescope as collection optics, with the sample set at a fixed distance of 8 meters. On the spectrometer side, this instrument uses an isoplane spectrometer from Princeton Instruments, and an intensified CCD from the same manufacturer.

The samples were analysed using different acquisition setups, as the instrument counts with a neutral density filter that allowed to vary the irradiance on the sample. The different setups done were:

- Micro mode:
    - SCAM like: The irradiance and gating parameters are set to SuperCam values.
    - Optimized for low irradiance: with irradiance levels like SuperCam, the number of shots is increased to optimize the signal in these conditions.
    - High irradiance, optimal parameters: In this setup, the irradiance is set to the safe maximum value, and the acquisition parameters are optimized for this irradiance.
- Standoff mode:
    - SCAM like: similar to the previous description but in standoff configuration
    - Optimized: similar irradiance as SCAM, but with optimized parameters, and increased number of shots.

In the case of SCAM like acquisitions the total spectrum was acquired in two separated windows, as the spectrometer uses a moving grating design. For the other acquisition setups the configuration was changed to another grating and the total range needed three windows.

The acquisition parameters were:

- SCAM like: 1000 shots, 100 ns delay, 100 ns gate width. The number of shots is much greater than the number of shots that have been approved for the operation of SCAM, but the irradiance is the same.
- Optimized and high irradiance: 200.000 shots, 117 ns delay and 5 ns width.
- The delay values were changed in the standoff mode to adapt to the longest optical path.

3.4.4.1 Results

The results obtained showed how the number of shots has a great impact in the quality of the final spectra. Considering a mixture of 50% of olivine and serpentine (w%), the bands from the olivine were barely visible over the noise in the SCAM configuration:

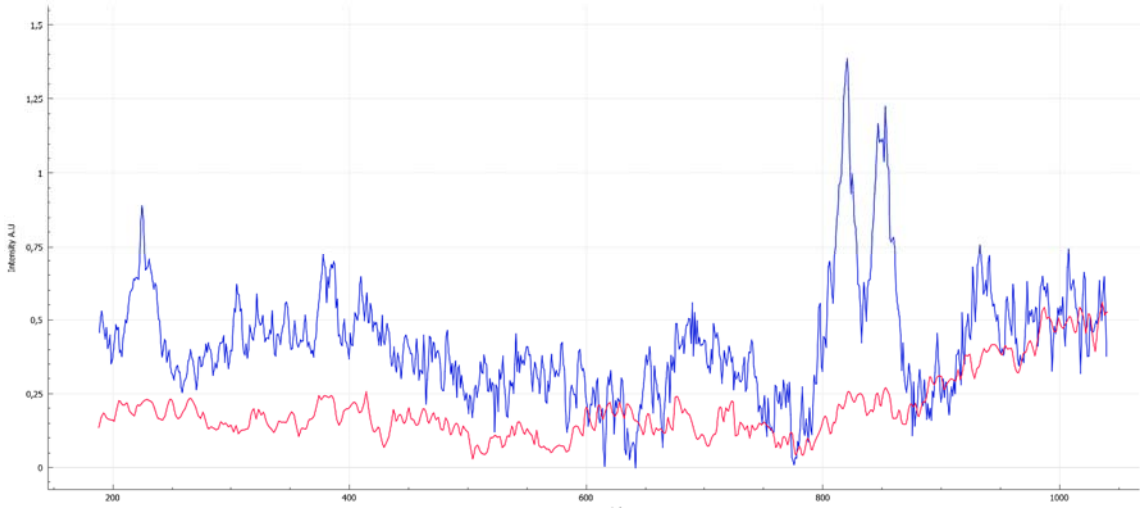

FIGURE 3-17 RAMAN SPECTRUM FROM A 50 / 50 % MIXTURE OF OLIVINE AND SERPENTINE. 1000 SHOTS (RED) AND 200.000 SHOTS (BLUE)

In the case of the spectra taken in micro configuration (Figure 3-18) It can be observed in the spectra from the contact configuration how the instrument provides spectra with a quality similar to other benchtop Raman instruments.

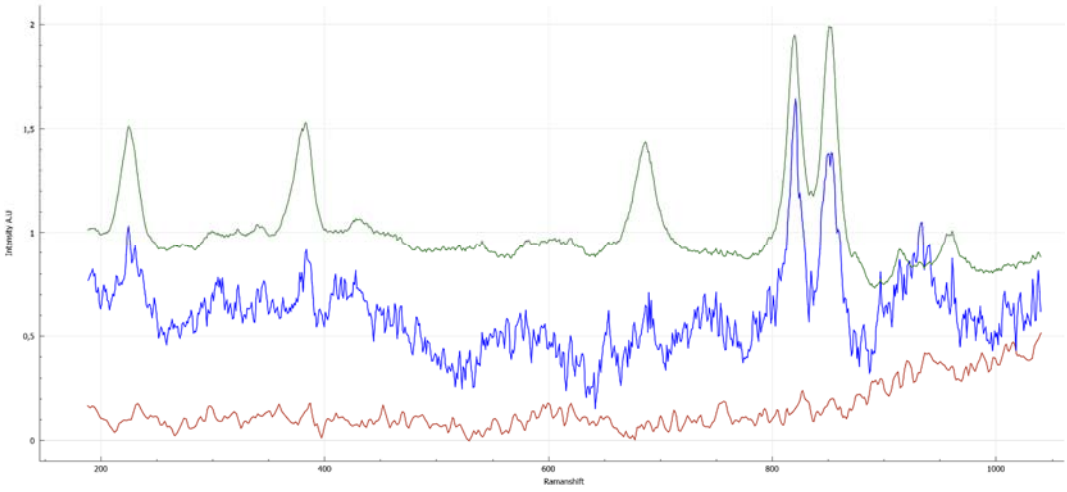

FIGURE 3-18 RAMAN SPECTRUM FROM A 50750 % MIXTURE OF OLIVINE AND SERPENTINE. SCAM LIKE (RED), LOW IRRADIANCE OPTIMIZED (BLUE) AND HIGH IRRADIANCE (GREEN)

The spectra acquired were then used to calculate the indicator given by equation 3.3.1 and introduced in the equation 3.3.2 and 3.3.3 to obtain the calculated concentration of olivine or serpentine. The results obtained by each setup are tabulated bellow, also including a graph comparing the nominal concentration with the calculated concentration in each case:

TABLE 3-3 VALUES CALCULATED FOR THE MIXTURES USING STANDOFF SCAM LIKE SETUP

Oli %	Serp %	Roli	Rserp	Calc. Oliv. %	Calc. Serp. %
100	0	70	30	52	48
95	5	55	45	38	62
90	10	51	49	35	65
75	25	71	29	53	47
50	50	53	47	36	64
25	75	60	40	43	57
10	90	47	53	31	69
5	95	48	52	33	67
0	100	6	94	4	96

TABLE 3-4 VALUES CALCULATED FOR THE MIXTURES USING STANDOFF OPTIMIZED SETUP

Oli %	Serp %	Roli	Rserp	Calc. Oliv. %	Calc. Serp. %
100	0	90	10	78	22
95	5	85	15	70	30
90	10	85	15	70	30
75	25	83	17	67	33
50	50	63	37	45	55
25	75	46	54	31	69
10	90	25	75	16	84
5	95	17	83	10	90
0	100	11	89	7	93

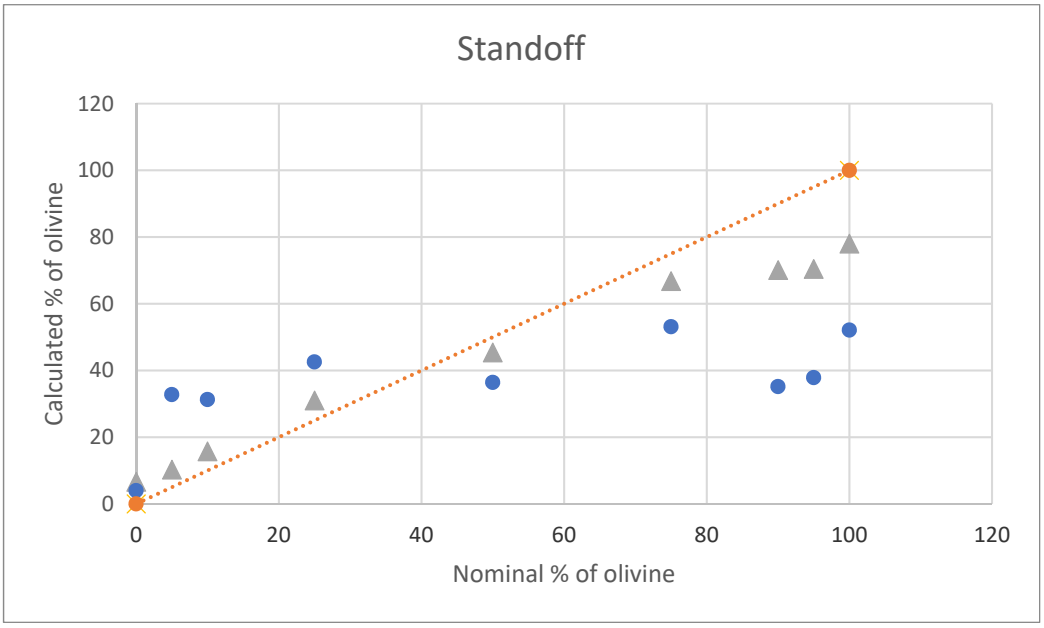

FIGURE 3-19 REAL CONCENTRATION VS CALCULATED CONCENTRATION. ORANGE LINE SETS THE IDEAL CASE, BLUE DOTS THE CALCULATED POINTS FOR SCAM LIKE, AND GRAY TRIANGLES OPTIMIZED SETUP

TABLE 3-5 VALUES CALCULATED FOR THE MIXTURES USING CONTACT SCAM-LIKE SETUP

Oli %	Serp %	Roli	Rserp	Calc. Oliv. %	Calc. Serp. %
100	0	87	13	73	27
95	5	56	44	39	61
90	10	60	40	43	57
75	25	61	39	43	57
50	50	55	45	38	62
25	75	67	33	49	51
10	90	54	46	37	63
5	95	21	79	13	87
0	100	9	91	6	94

TABLE 3-6 VALUES CALCULATED FOR THE MIXTURES USING CONTACT LOW IRRADIANCE SETUP

Oli %	Serp %	Roli	Rserp	Calc. Oliv. %	Calc. Serp. %
100	0	95	5	86	14
95	5	92	8	82	18
90	10	87	13	73	27
75	25	83	17	68	32
50	50	67	33	49	51
25	75	39	61	25	75
10	90	34	66	22	78
5	95	20	80	13	87
0	100	0	100	0	100

TABLE 3-7 VALUES CALCULATED FOR THE MIXTURES USING CONTACT HIGH IRRADIANCE SETUP

Oli	Serp	Roli	Rserp	Calc. Oliv. %	Calc. Serp. %
100	0	95	5	88	12
95	5	94	6	85	15
90	10	91	9	80	20
75	25	69	31	51	49
50	50	66	34	48	52
25	75	27	73	17	83
10	90	28	72	18	82
5	95	7	93	5	95
0	100	1	99	1	99

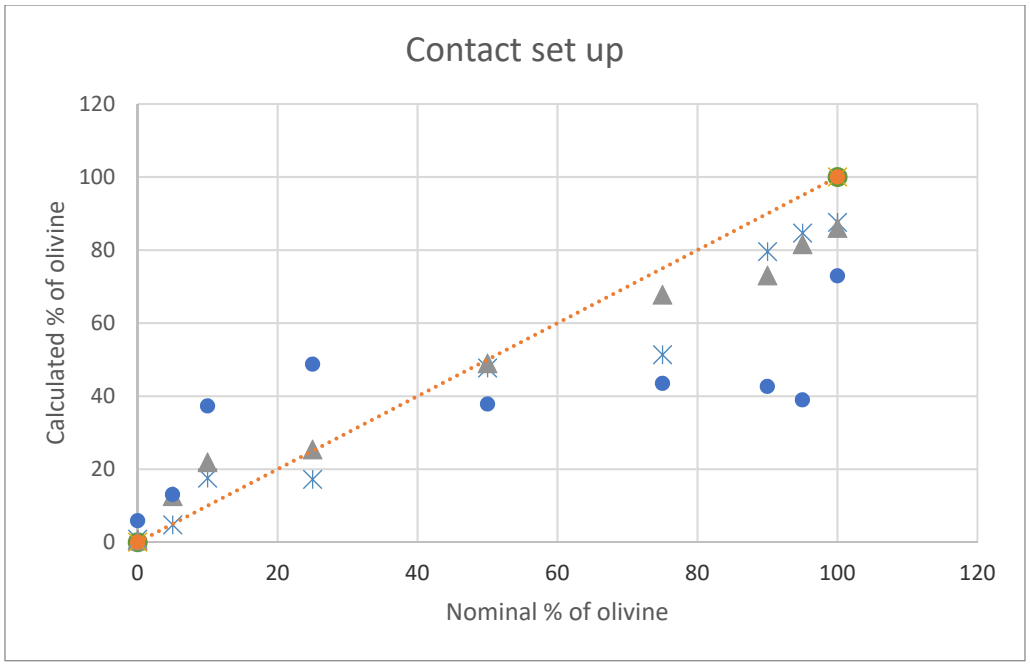

FIGURE 3-20 REAL CONCENTRATION VS CALCULATED CONCENTRATION. ORANGE LINE SETS THE IDEAL CASE, BLUE DOTS THE CALCULATED POINTS FOR SCAM LIKE, GRAY TRIANGLES LOW IRRADIANCE SETUP AND BLUE ASTERISKS FOR THE HIGH IRRADIANCE.

3.4.5 Conclusions

The model developed using micro Raman works well and have been checked in real samples, confirming that it is able to obtain a performance comparable to XRD for the analysed mixtures. This calibration and verification work on Martian analogues is currently in quite advanced publication status. The results obtained during the development of the method were obtained in the same instrument, so the effect of instrument response could be neglected in the validation of the method with the natural samples.

The results obtained from the data collected with the standoff instrument are remarkable, especially in the contact setup. In this configuration the instrument is capable of producing quality data comparable to the spectra from other regular top bench Raman spectrometers. When correlating this data through the model designed for RLS, the results show coherent correlation for the different olivine-serpentine mixtures.

However, a common trend is observable at the extremes of the range, for the low and high concentrations of olivine. This trend, consistently observed in the data from all configurations, is probably due to the apparatus function. These deviations would then be explained by the differences in the instrument response of the time-resolved

instrument, which is different to the RLS laboratory setup, the one used to build the model.

The results are anyway encouraging, as the correction to remove the instrumental function in both the data used to develop the method (to obtain an instrument independent method) and the data collected with the Time Resolved instrument used in this experiment would most probably improve the correlation of the results among different instruments. A future work that might be useful might be to repeat the calculations of the model using intensity corrected spectra, correction described in **¡Error! No se encuentra el origen de la referencia.** (Sanz-Arranz, 2018).

This kind of calculations and methods that can be done using ground-based equipment and applied to data from space instruments rely on a good characterization of the instrumental function on both ends.

One final conclusion based on the time-resolved data quality is that the operation in contact mode of time-resolved raman spectrometers is interesting. Small changes, sharing most of the hardware, may allow to obtain better results once the constraints associated with distance are removed. This kind of developments with a double feature (micro / standoff), may allow to get the best of both worlds: the operational advantages of a standoff Raman, combined to the analytical capabilities of a contact instrument.

As a final remark, and studying the results obtained with the standoff measurements, it is clear that the impact of the number of shots collected per spectra has a great impact in their quality. Results with irradiance values similar to SCAM might be capable of making an assessment in the degree of serpentinization of altered olivine samples by using the presented method, as long as the number of shots was importantly increased to optimize the spectral quality. This could also be improved by performing absolute intensity corrections.

Considering future analysis on these data, the application of multivariate analysis techniques might provide improved results from SCAM-like data. The following section presents the power of classification using Raman and LIBS data in a set of mixtures of different compounds, where the improvement in classification using multivariate analyses compared to univariate calculations similar to the ones used in this work is shown. Thus, the development of a multivariate model for the olivine-serpentine samples (work in progress) could hopefully improve the SuperCam capabilities to assess the serpentinization degree of olivine-altered samples.

3.5 Data fusion and multivariate analysis applied to relevant mixtures for planetary exploration

This section covers the science outcome that can be obtained from the use of different datasets coming from different techniques, either, obtained with the same instrument or with different instruments, from samples of interest in planetary exploration. The objectives of this work could be summarized as follows:

- Evaluation of univariate analysis in the classification of binary mixtures, as a base for comparison with more advanced methods. Evaluate possible options to obtain a classification using datasets from different techniques.
- Evaluate the accuracy of calculations using multivariate methods with individual data sets from each sample in binary and ternary mixtures.
- Evaluate the accuracy of calculations using multivariate analysis on fused datasets for binary mixtures, addressing different origins for the data to be fused. Evaluate the accuracy of calculations on fused datasets from ternary mixtures.
- Evaluate the use of models based on multivariate analysis from binary mixtures to describe more complex mixtures, ternary, without running a specific calibration.

3.5.1 Univariate and multivariate analyses

When doing chemometric calculations based on spectroscopic data the most direct and comprehensive calculation is the univariate. Having two compounds with two different features in their spectra (e.g. Raman or LIBS), could be directly used by relating the ratio between the intensities or areas of such spectral features to a concentration ratio. This kind of calculations are widely used as they are the most intuitive. An example of this calculation was used in 3.4.3. For univariate analysis a feature from the spectrum is used and introduced in calculations as one variable proportional to a certain characteristic. Depending on the data, we will use peak intensities in some spectra, or areas in others. Area is directly related to the population of oscillators and gives better results in superposed bands where find a maximum for lower concentrations could be hard, while provides worse results when the spectra have overlapping bands, for example.

Multivariate analysis on the other hand is based on building models that consider every (or many) points of the spectra, which are introduced as input variables in the model calculation. In some techniques such as Principal Component Analysis (PCA), those variables might or might not be related one to another, and the process tries to explain the variance of the model with a reduced number of variables in the coordinate space of the principal components (PCs), which is an orthogonal base in which the model can also be represented, but that is not necessarily related to any physical property of the

underlying observation. When the variance of the system can be explained with only two or three principal components, it is possible to represent them graphically in the PC space. With these representations, it can be seen how, representing each measurement in an orthogonal coordinate system based of the PCs, the spectra are spatially grouped in this new space.

When more than 2 or 3 PCs are needed for the explanation of the model, it will not be possible to do a graphical representation for classification, so some other classficiation method needs to be used. Artificial neural networks have been proposed to perform the classification on a PCA+ANN joint model. ANN can thus be used to classify the PCs into concentration values. To do so, this kind of model is trained by assigning coordinate areas in the PC space to determined concentrations.

3.5.2 Introduction to data fusion

The sensor data fusion in its general definition can be understood as the combined use of different sensors, each one providing a different measurement, to achieve a common goal or do certain task required by the system. Examples of this sensor fusion can be found around us, for example the different sensors in a car that collaborate to make the stability system work; or the data that several wearables can extract from our pulse ratio and movements to assess the quality of our sleep, or the intensity of our trainings.

Data fusion is not something new, but somehow unused on science applications to explore the Solar System. Scientists tend to be experts on one technique, and concentrate on the measurements and data coming from their instrument of expertise. Multianalytical instruments and coaligned studies using different instruments are here to change this paradigm, as they are able to multiply the data from the analysed sample potentially improving its understanding.

Considering one instrument performing a measurement on the surface of Mars such as RLS (Rull, 2017), in principle there is only one data source, and the limit in the quality of the data is reduced to the individual quality of the instrument. In this scenario, if RLS was unable to detect, for example, certain chlorates, those compounds would be unacknowledged. Also, considering those compounds that can be detected, the detection limits of this instrument are the limit of the science we will be able to do. This can change by the introduction of other data sources, which is in fact what the ExoMars mission intends by introducing other instruments (NIR spectrometer and mass spectrometer) in the analytical laboratory drawer of the rover that will be able to analyse the same sample, in the very same spot, with the three analytical instruments.

In this case, and attending to the type of data sources in play we can distinguish between two main cases:

- **Redundant data sources:** in this case the sensors are measuring the same observable, giving the same kind of measurement. The fusion of these data sources in this case is helpful to reduce uncertainties and increase the precision of the measurement. Also, this kind of systems are more robust to failures of one of the sources, or when one of the sources cannot provide the information of the whole system by itself.
- **Complementary data sources:** the data sources in play provide information of different observables, giving datasets that are independent but together provide two different -complementary- observations.

An example of redundant data sources is the fusion between Raman measurements using two different instruments. In this example, we can identify certain molecular bands, probably not with the same performance in both instruments, and the mixture of both measurements would provide more complete information for use in chemometric calculations, for example.

An example of complementary data sources would be the Raman and LIBS spectroscopic techniques, given that Raman will provide information of the molecular composition of the sample and its structure while LIBS will give us the elemental composition. In this work, we present results of both of these types of data fusion.

3.5.2.1 Combination of Raman and LIBS

The complementarity between these two analytical techniques provides two different pictures of the same sample. These two pictures together are pretty convenient when trying to characterize the surface of a planetary body, or when trying to get exact chemometric calculations from the available information. This combination can be used to increase our understanding of the cation present in certain compounds, where Raman could be not as well separating as LIBS. Raman will tell us that we have a mixture of sulfates, and LIBS will be able to collaborate to assess the different cations in play in that mixture. On the contrary, Raman can distinguish between hydration levels of the same sample (which LIBS cannot), or can provide information of the crystalline structure of a compound while LIBS only will provides information of the constituents of the lattice. Summarizing, from the point of view of sensor combination for Raman and LIBS the complementarity is very fruitful given that Raman will provide molecular information while LIBS the constituent atomic lines.

In addition to the complementary collaboration between techniques, there is another factor that makes Raman-LIBS combination of great interest: they both use common hardware.

In the case of Raman spectroscopy, a typical Raman setup includes a laser light source, focalization/collection optics and a spectrometer. In the case of Time Resolved Raman, the laser source is pulsed and the detector in the spectrometer is usually

intensified/gated. For the LIBS setup, a pulsed laser is also used, focalizing/collecting optics are also needed, and the spectrometer can as well use an intensified/gated detector. Of course there are differences, as the physics of the effects behind both techniques are different, but mainly can be reduced to:

1- The photon budget: while atomic emission lines are highly intense, the Raman effect is faint and the difference on the number of photons in play is high. Considering this, if a detector is good for collection of Raman spectra, it should be superb for LIBS.
2- The spectral windows: if a 532 nm Raman spectrometer is considered, the spectral region of interest for this instrument is located between 532 and 700 nm. This spectral window is much wider in the case of LIBS, with valuable information found from the UV to the IR, typically from 200 to 850 nm. This leads to the use of wide range spectrometers, or the separation among ranges in different spectrometers. This is the case of the SuperCam instrument, which has three separate spectrometers: two reflection spectrometers designed for LIBS spectroscopy, and one transmission spectrometer with intensifier that will cover the Raman range, while also used for the corresponding LIBS spectral window.

These arguments make the development of combined instrumentation attractive, but they make even more sense when thinking about space exploration and its associated constrains. These developments imply hardware sharing and low mass and power consumption, which are technical advantages compatible with the ability to perform elemental and molecular characterization of a sample, among other advantages. These are strong arguments in favour of the introduction of this kind of developments in future missions, and the reason why this combination was initially considered for missions such as RLS in ExoMars, which before budget cuts was intended to be a combined Raman-LIBS instrument (Rull, 2017) (Bazalgette, 2008).

When analysing different scenarios for the quantification of samples with Raman and LIBS, and having in mind the capabilities of both techniques, it is interesting to evaluate in what cases Raman will have a better performance than LIBS in the characterization of a sample, and when the opposite occurs. It is evident that in case of polymorphs, LIBS will be unable to distinguish between them while Raman could (e.g. calcite or aragonite will look the same for a LIBS instrument). Alternatively, certain materials are invisible for Raman, or in cases of cationic substitution, the differences in the Raman spectra could be subtle, while those differences are evident in LIBS spectra.

Another factor to evaluate is the impact of the different Rayleigh wavelengths for Raman acquisition. The best option for planetary exploration has been deeply discussed among the Raman community without a definitive agreement. Possible differences in the performances of two Raman instruments might be a consequence of other factors, as both instruments present more differences besides the wavelength of the laser.

However, the 532 nm excitation source provides a good trade-off when looking for good resolution, low detection limits, biomarkers detection and mineralogy capabilities (Rull, 2017). Furthermore, in the context of a combined instrument, the 1064 nm Nd-YAG laser emission used for LIBS plasma induction can be frequency doubled using, for example, a KTP crystal, to obtain a 532 nm laser source for Raman analysis. This is another example of hardware sharing between techniques, which is also the approach used in SuperCam (Perez, 2017).

The capabilities of Raman-LIBS data fusion techniques were evaluated in previous works (Sobron, 2014) (Rammelkamp, 2018). As shown in the literature, by concatenating the Raman and LIBS spectra for a certain set of mixtures of two sulfates, the multivariate analyses improved extensively the classification power when compared to the individual spectra sets. This can be explained by the fact that more information is introduced for the multivariate analyses, having more independent variables to analyse and relate.

Recognizing the critical importance of data fusion in the fulfilment of the forthcoming space exploration missions (Wiens, 2017), this work extends the use of spectral concatenation strategies to a broad range of materials relevant to upcoming Mars and other planetary bodies exploration missions. As a result, some mixtures of relevant compounds were prepared to obtain calibration curves based on measurements of individual techniques and fused data. These calibration curves per technique provide the classification power of this methods, as well as their limit of detection, by using univariate and multivariate analytical methods. In total, given the separation in time for the experiments corresponding to binary and ternary mixtures, two sets of mixtures were prepared, each set dedicated to build a model of binary or ternary mixtures.

3.5.3 Experiment setup

3.5.3.1 Samples selection

The selection of materials for this study were chosen according to literature (NASA/JPL, 2016) (Wang, 2006) for being interesting from the point of view of the Martian environment as well as of Europa, Jupiter's satellite. These consist in epsomite (labelled A), anhydrous sodium sulfate (labelled B) and hexahydrate magnesium chloride (labelled C), which have been identified in both planetary bodies. This is justified by the fact that Raman instruments are going to fly to Mars in different missions in 2020, and that a potential Europa lander mission will likely include a Raman in its scientific payload (NASA/JPL, 2016). The selected samples were mixed in three sets of binary mixtures to obtain the range of proportion shown in table 3-8.

TABLE 3-8 PROPORTIONS OF EACH COMPOUND IN THE ANALYZED MIXTURES

COMPOUND CONCENTRATION (weight %)					
AB mixtures		AC mixtures		BC mixtures	
A	B	A	C	B	C
100	0	100	0	100	0
99	1	99	1	99	1
90	10	90	10	90	10
75	25	75	25	75	25
50	50	50	50	50	50
25	75	25	75	25	75
10	90	10	90	10	90
1	99	1	99	1	99
0	100	0	100	0	100

In addition to this three sets of binary mixtures, for a later analysis, a set of ternary mixtures was prepared with the following proportions:

TABLE 3-9 PROPORTIONS OF A, B AND C IN THE 18 PREPARED TERNARY MIXTURES

A %	B %	C %	A %	B %	C %
0	0	100	25	50	25
0	100	0	33	33	33
100	0	0	50	0	50
0	50	50	50	25	25
1	98	1	50	50	0
10	10	80	70	10	20
10	70	20	70	20	10
10	80	10	80	10	10
20	70	10	98	1	1

The samples were prepared in a similar way to the previous sampes: crushing the powder of all the components in a mortar. The 532 nm data was gathered from powder in this case, although pellets were prepared for LIBS data acquisition.

TABLE 3-10 FEATURES FROM THE SAMPLES PER INSTRUMENT AND CAPABILITIES

COMPOUND	RAMAN 785		RAMAN 532		LIBS	
Epsomite (A)	Features from the sulfate	Y	Features from the sulfate	Y	Magnesium lines	Y
	Features from the water OH bending (very weak compared to sulfate band)	Y	Features from the water OH bending (very weak compared to sulfate band)	Y	Sulphur lines	N
	Features from water OH stretching (weak compared to sulfate band)	N	Features from water OH stretching (weak compared to sulfate band)	Y		
Na Sulfate (B)	Features from the sulfate	Y	Features from the sulfate	Y	Sodium lines	Y
					Sulphur lines	N
Mg Chloride hydrated (C)	Features from the chloride	N	Features from the chloride	N	Magnesium lines	Y
	Features from the water OH bending (very weak compared to sulfate band)	Y	Features from the water OH bending (very weak compared to sulfate band)	Y	Chlorine lines	N
	Features from water OH stretching (weak compared to sulfate band)	N	Features from water OH stretching (weak compared to sulfate band)	N		

Anyhow, it must be said that the mixtures are not intended to mimic any geological process in any of the aforementioned planetary bodies. They were selected only for their different features for both techniques, pursuing different scenarios for a proper testing of the analytical and data analysis techniques. For example, scenarios where Raman and LIBS have a great capability for classification (presenting features with a clear separation between the contributions of both components); scenarios where one of the techniques presents worse features for one of the components compared to the other; or scenarios where one or both techniques may have a hard time in differentiating among the different mixtures.

As a last comment regarding the selected compounds, the anhydrous sodium sulfate (thenardite), present in very dry environments as an evaporitic mineral, is unlikely to coexist with a hydrated sulfate as epsomite. However, the presence of these kinds of sulfates in different bodies of the Solar System, whatever their hydration state, as well as their spectroscopic features, made them interesting for this work.

Intermediate hydration states of both sulfates were expected to be found during the analysis, although it was limited by doing the measurements right after the preparation

of the samples. Also, the preparation of the samples was done to limit as much as possible the possible changes. Furthermore, in points where the epsomite turned into hexahydrite, or the thenardite turned into a more hydrated sodium sulfate, the spectra were discarded in a preliminary analysis in order to have just two phases for the analysis.

From the perspective of Raman, sulfates with different cations provide a scenario where intermediate mixtures are hard to distinguish, especially when the resolution of the spectrometer is low. The third compound was selected to have different Raman features to the two compounds previously selected, also with very different Raman cross sections. In this case the selected material is a hydrated chloride that, even being invisible for Raman, provides the features of the water molecules, and serves to the testing purpose, as long as the mixture is not dehydrated or in a brine.

Considering LIBS spectroscopy of these compounds, chlorine or sulphur cannot be detected in earth conditions (atmospheric pressure) with our experimental setup (Gaft, 2009). Sulphur lines in the UV region are the most intense, and are only visible under vacuum conditions. The chlorine line around 837 nm is too weak and close to the range limit of our spectrometer, preventing the use of the atomic emissions from chlorine. As a result, the sulfate-chloride mixture, with both samples having the same cation, provides a scenario where LIBS will not find any other element to compare with, potentially obtaining bad results for chemometric calculations.

Finally, the mixtures were made by mixing both components in a crusher that also lowered the grain size and homogenised the mixture. The resulting powder was later compressed into a pellet with a 10 tons press. The analysis was done right after the preparation of the samples. For Raman spectra acquisition the samples were encapsulated in glass petri capsules, and the measurements were done through the glass, as shown in Figure 3-21. The baseline artifacts introduced by the glass were corrected using a fluorescent material as reference (Sanz-Arranz, 2018). In the case of 532 nm Raman from ternary mixtures this analysis was done on powder presentation.

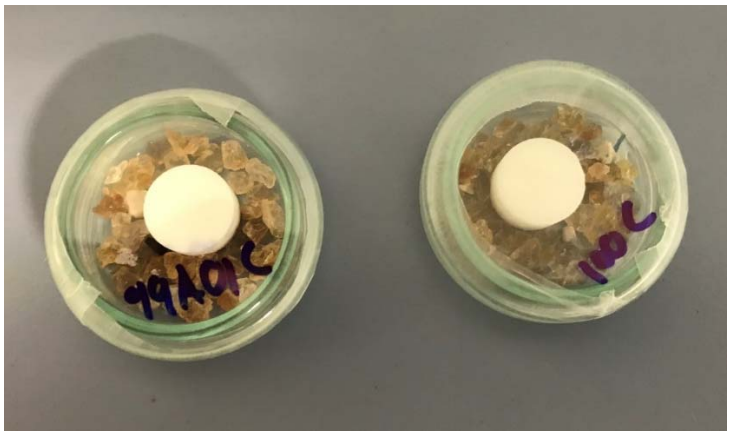

FIGURE 3-21 PELLETS ENCAPSULATED FOR ANALYSIS.

3.5.3.2 Instrumental setup

The analyses were performed with the following equipment:

- 785 nm Raman: BWTEK BRM-OEM-785 laser. BWTEK BAC100-785E Raman probe, focusing with an approximately 20x lens. BWTEK Prime T BTC661E-785CUST spectrometer. Hamamatsu S10141-1107S CCD. Spot size is 80 microns.

- 532 nm Raman: RLS ExoMars Simulator (Lopez-Reyes, 2013), which mimics the operation of Exomars RLS instrument by automating and optimizing the acquisition parameters considering RLS instrument constrains. Spot size is 50 microns.

- LIBS: The plasma is induced by means of a pulsed Nd:YAG laser, Litron Nano S, using its second harmonic, with a pulse length of 6 ns and 60 mJ energy. The laser is focalized with a 50 mm lens, and the spectra is acquired by an Andor Mechelle500 with iStar Andor iCCD camera with integrated DDG. Area of analysis is in the order of a few hundreds of microns.

For the 785 nm Raman and LIBS instruments, 20 points per sample were acquired by manually adjusting the acquisition parameters. For the 532 nm RLS simulator, between 40 and 100 points per sample were acquired in automated mode, resulting in variable total analysis times depending on the sample. To guarantee the stability of the samples during long periods of time, the pellets were encapsulated in sealed petri glasses, as explained before.

In terms of acquisition parameters, and starting with LIBS, it is well known that one of the main problems for the quantification using this technique is the high variability of the results from one shot to another. Differences in the pulse energy, matrix effects, fluctuations of the conditions of the plasma, etc. lead to a complicated approach when trying to do chemometrics based on LIBS spectra. The results here shown were taken after averaging a minimum of 100 shots, trying to overcome this issue. Regarding the other parameters relevant for LIBS acquisitions, the delay was set between one and two microseconds, and the width of the gating was set to eight microseconds. In certain samples only the delay needed to get adjusted due to the high bremsstrahlung radiation. A total of 20 spectra were acquired per sample. For the 785 nm Raman, also a total of 20 spectra per sample were acquired, in this case with a total of 30 accumulations per spectrum, with an integration time adjusted for each sample in order to use at least a 75 % of the total dynamic range of the sensor. In the case of the 532 nm Raman instrument, the acquisition parameters are selected automatically following the same operation of RLS instrument (Lopez-Reyes, 2013), with at least 60 spectra collected per sample. Finally, and regarding the area of analysis, it was quite different for the three instruments. Spot size is 50 microns for the 532 nm Raman, 80 microns for the 785 nm Raman and several hundreds of microns for the LIBS instrument.

3.5.4 *Analysis on binary mixtures*

3.5.4.1 Data analyses on binary mixtures

After a preliminary analysis for trimming the spectra, univariate analysis was done for each mixture of this binary set, looking for spectral features that could provide an estimation of the mixing ratio. Then, data were fused and analysed using multivariate techniques either on the fused data and the original data for each source. The data processing and analysis was done mainly using MATLAB.

Preliminary analysis:

For each mixture a preliminary evaluation was performed using SpectPro, a spectroscopy software developed by the RLS team to handle the Raman data that will be gathered on Mars by the RLS system.

- AB mixtures, both sulfates: The stability of the end members was evaluated by checking all the spectra, looking for signs of dehydration of the epsomite during the analysis. As already commented, exceptional spots with spectral changes were discarded.

For mixtures, a transition point between the main bands of both sulfates can be observed and used for the calculations of indicators used in univariate analyses.

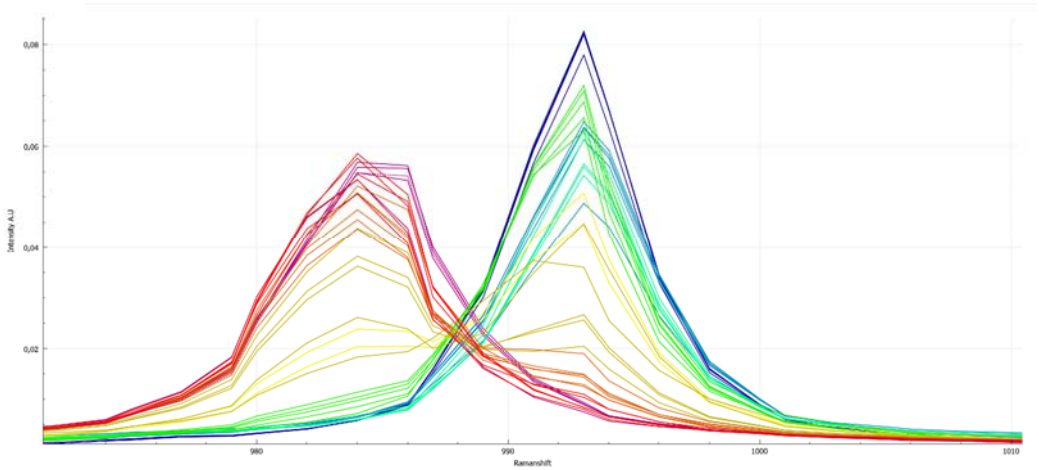

FIGURE 3-22 CHANGES IN RAMAN SPECTRA AS THE PROPORTIONS OF BOTH SULFATES CHANGE. BLUEISH ARE 100% B AND REDISH 100% A

When looking for useful spectral features in LIBS spectra to be used in the analyses, it can be observed that the main doublet of the sodium at 589 nm, suffers self-absorptions of the Na in the plasma, making it unusable for the analysis. Instead of this doublet, the lines at 819 nm were used. As a summary, the different spectroscopic features that can or cannot be seen by each technique were shown before in Table 3-10.

- AC and BC mixtures: in these mixtures for the univariate Raman analyses the main band of the sulfate and features from the water of the hydrated chloride were used. For the LIBS, the only option in the case of the AC mixtures was to use the differences induced by the matrix effects when moving from a high concentration of A to greater concentrations of C. In this case it consisted on a reduction of the SNR of the magnesium lines for the chloride rich mixtures.

Univariate analyses:

For this analysis a spectral indicator was evaluated that is proportional to the concentration of one of the components for each technique.

For the **Raman analysis of AB mixtures**, the indicator was calculated using the area under the spectrum in each compound's region. The calculation of this indicator was done with Matlab, in an automated process that:

- Takes the region of interest (ROI), in this case the region where the main bands of both sulfates are located.
- Corrects baseline using a straight segment from the initial point to the ending point of the ROI between 960 and 1020 cm^{-1}.
- Normalizes the resulting spectrum by area, making the total area under the spectrum equal to one.
- The indicator is then the integrated area of the magnesium peak, limited between the ROI end and the transition point, around 987 cm^{-1}, as defined in the preliminary analysis. This area is a good indicator from a physical point of view, as it has a direct relation with the population of oscillators coming from the Mg sulfate.

For the **LIBS analyses of AB and BC mixtures**, an indicator was also defined and calculated using the following automated process:

- Baseline correction using straight lines

- Normalization equaling to one the most intense line between the sodium lines near to 820 nm and the magnesium lines near to 515 nm.

- Select the maximum intensity of the magnesium and sodium lines in both ROI, [515-520] for magnesium, and [815, 822] for sodium.

- The indicator is then calculated using: $\frac{Max(Mg)}{Max(Mg)+Max(Na)}$ as in 3.4.3.

In the case of the **Raman analysis of AC and BC mixtures,** features coming from the main sulfate band and the water bands from the hydrated salt are used. After baseline removal, the indicator was calculated in a similar way to the indicator of the magnesium sulfate in LIBS. This time we used the intensity of the main sulfate band in both mixtures and divided it by the sum of this intensity and the intensity of the water bending band for the 785 nm Raman instrument, and the stretching band in the case of the 532 nm Raman instrument. This difference is needed to overcome the shorter spectral range of the 785 nm instrument compared to the 532 nm one.

The **LIBS analysis of AC mixtures** was challenging due to the lack of well differentiated spectral features between the pure compounds. The indicator was calculated using the maximum values of the triplet between 516 nm and 519 nm, adding the maximum values of the intensities of the three lines and dividing it by the sum of the intensity in the two local minimums between them.

Once all the indicators were calculated for all the spectra, the results were normalized by dividing all values by the maximum value calculated for each indicator. This way, we obtain three different sets of indicators ranging from zero to one, proportional to the concentration of magnesium sulfate for AB and AC mixtures, and to the concentration of sodium sulfate for BC mixtures.

A combined indicator of the three techniques is also calculated by adding the three indicators. This indicator ranges between 0 and 3 and is proportional to the sulfate concentration present in the mixture (magnesium sulfate in the case of AB mixtures). The number of points for each mixture in these series are limited to 20 for 785 nm Raman and LIBS, and to 60 for the 532 nm Raman, which is a relatively low number of spectra. In order to visualize the improvement of the introduction of more inputs coming from different measurements, we obtained the combined indicator taking into account all the possible combinations of the measurements with LIBS, 785nm Raman and 532nm Raman, generating 24000 combinations.

Multivariate analysis:

Multivariate analysis has proved useful for the analysis of spectroscopic data (Lopez-Reyes, 2014) (Clegg, 2009), as it provides a useful tool for reducing the number of variables of the system for better classification. From another perspective, data fusion between different techniques has also been used (Sobron, 2014) (Lopez-Reyes, 2018) as a means of improving the detection accuracy of samples when data from different techniques is available.

Concretely, we have developed a classification method based on a combination of Principal Component Analysis (PCA), which reduces the number of variables of the input spectra, with Artificial Neural Networks (ANN) in order to obtain an estimation of the mineral abundance in the different mixtures. This analysis was executed using the datasets of the individual techniques, as well as the fused data. In the end, the process was repeated five times per mixture for the following data: 532 nm Raman, 785 nm Raman, LIBS, 532 nm+LIBS and 532 nm+785 nm. This way we test the chemometric capabilities of the combination of PCA and ANN for each technique, as well as the improvement obtained from performing the data fusion of the individual sets of data.

The data treatment previous to the PCA analysis consisted on removing dead and hot pixels found on the spectra. Also, ignoring areas of the spectra which might affect the analysis as, for example, the area between 585 and 600 nm in LIBS spectra, where the Na self-absorption features handicap the classification of the scores.

The difference in the number of points between a Raman spectrum and a LIBS spectrum can induce LIBS to participate with a weight higher than Raman in multivariate calculations. Thus, the data was interpolated in order to reduce the computational load while balancing the influence among the three analytical techniques. This also introduces a way to assign different weights in calculations to each technique if it is desired, though for this work this has not been done.

The fusion of data was performed by a simple method based on the concatenation of data. In order to address the different number of spectra on the different techniques, a

subset of the data was used in which data from the three techniques were properly represented and balanced (generally 20 spectra per technique).

The five datasets were then scaled and centered (necessary to avoid bias in the PCA calculation) and analyzed with PCA. The graphical representation of the scores in the principal components (PC) space provides a good qualitative measure of the classification potential of the data, based on the separation of the different proportions on the plane (2 PCs) or space (3 PCs). However, graphical representation is only valid when using one to three PCs. So, in order to get a quantitative interpretation which takes into account the explained variance of more than 3 PCs, it is necessary to have a different type of classification method. In this case, the selected method for classification is a perceptron neural network with 15 neurons in the input layer, corresponding to the 15 principal components with highest explained variance of the system. The two network outputs indicate the calculated concentration of the mixture materials.

The training of the network followed an iterative process of training in which we used variable number of neurons in the hidden layer (from 5 to 100), and run the training 5 times for each network configuration. Then, the best-performing network (in terms of RMSE) among all of them was selected. The optimization was performed using a Levenberg-Marquardt algorithm for training. The input dataset was divided in three sets, one for training (70% of the data), another for validation (15% of the data) and a last one for testing (15%). During training, the neuron parameters are recursively adjusted to fit the expected responses (concentrations), and the validation and test sets are used to avoid the overtraining the network, by monitoring the error trend produced by the validation and test sets. I.e., the recursive process continues as long as the error on all the sets is being reduced. After training, the network is used with the whole dataset to calculate the estimated concentrations of the samples.

3.5.4.2 Results on binary mixtures

Univariate analyses:

For the AB mixtures the results obtained for the calculated indicators were tabulated and represented using boxplots.

According to the results displayed in previous figure 3-23, by using this indicator, the 532 nm spectrometer is capable of separating one mixture from the other when the concentration of magnesium sulfate is higher than the 25 %w. In the case of the 785 nm system, this separation could be effective from 10 %w. This can be related to differences in the resolution of both instruments, and to the fact that the kind of indicator selected is more sensitive, during the area calculation, to effects from this difference

.

As previously discussed, another factor considered is the different sensitivity of the two instruments towards the detection of inhomogeneities, being the 532 nm system more sensitive than the 785 nm one. For LIBS it can be seen that the detection limit is lower for this technique, being able to separate the 0 %w from the 1 %w effectively, but in this case the overlapping of the boxes in the intermediate mixtures is higher than the results obtained with Raman.

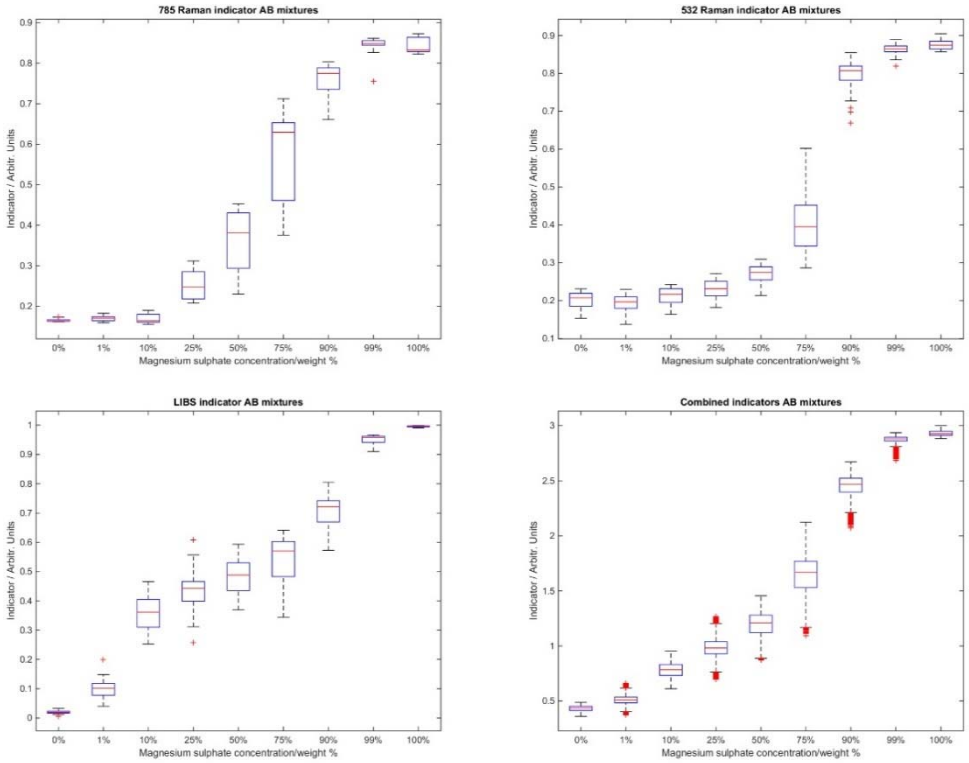

FIGURE 3-23 UNIVARIATE ANALYSIS OF AB MIXTURES

At first glance this looks like a good example of a case where the data fusion should improve the analytical capabilities, having a technique (Raman spectroscopy) with a better performance in the intermedium range of concentrations but with higher detection limit, and another technique that has an opposite behavior. Finally, the lineal combination of the inputs from the three techniques, as expected, is also combining the most deviated results, resulting in an increase of the outliers, but other effect is the compression of the boxes, representing the 50% closer to the median. This compression also encourages the aim for data fusion techniques, as it shows that considering inputs from different techniques can provide a better classification of the mixtures in this experiment. In this particular analysis it must be said that by combining all the possible triplets of values for the three indicators, we are increasing the population of points and, since the analyses are not done in the same spot, obtaining a better averaged result of the whole pellet.

For the other two sets of samples, when considering Raman, the difference in the cross section of the water bands compared to the sulfate bands led to a poorer capability of classification for lower concentrations of chloride in both datasets. This could be seen especially in the case of the results coming from the 785 nm Raman instrument. In this last instrument only the bending band of the water is visible, and the difference between the cross section of this band and sulfate's main bands is great, so, using the mentioned indicator, the mixtures can be classified up to a 25 % of sulfate (75 % chloride), presenting no classification power beyond the 50 %, result similar for the case of BC mixtures. However, the 532 nm indicator that used also the stretching band of water (more intense) showed a better performance than the 785 nm one, and when comparing both samples sets, it worked better in the range over 50 % in the case of BC mixtures than in the case of AC mixtures, what can be attributed to the presence of water from the hydrated sulfate.

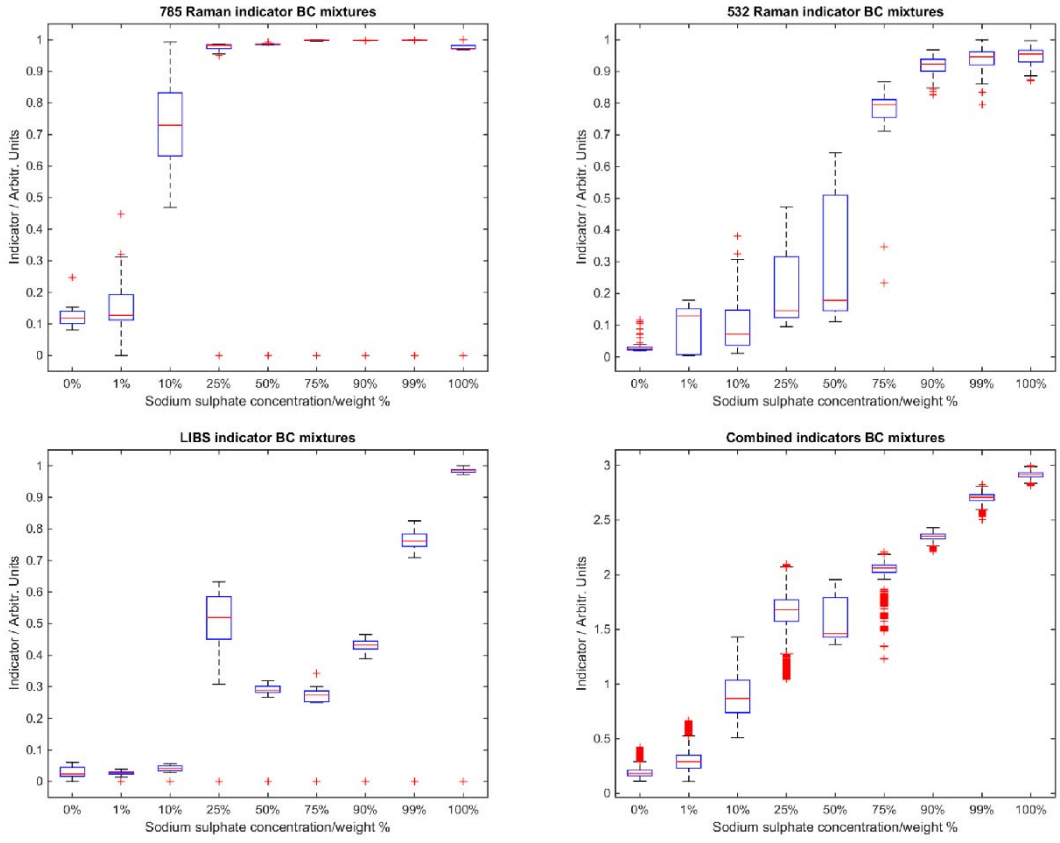

FIGURE 3-24 UNIVARIATE ANALYSIS OF BC MIXTURES

For the LIBS, in the case of BC mixtures the performance of the analysis is similar to the case of AB mixtures. Even though the 25% mixture was prepared and analyzed three times, it always provided atypical values. Thus, further studies need to be performed to better constrain the reason behind this unexpected Raman effect.

Regarding AC mixtures, it has been experimentally proved that the evaluation of the decay of the SNR of the magnesium lines worked to some extent for their classification. However, by using this indicator, the detection limit of chloride in these mixtures if quite high (over 50%). When comparing the boxplots for the combination of indicators, again, the general result improves, with special mention for the case of AC mixtures where, even with a poor result, the combination is a remarkable improvement. Results are shown in Figure 3-25 Univariate analysis of AC mixtures (AC) and 3-24 (BC).

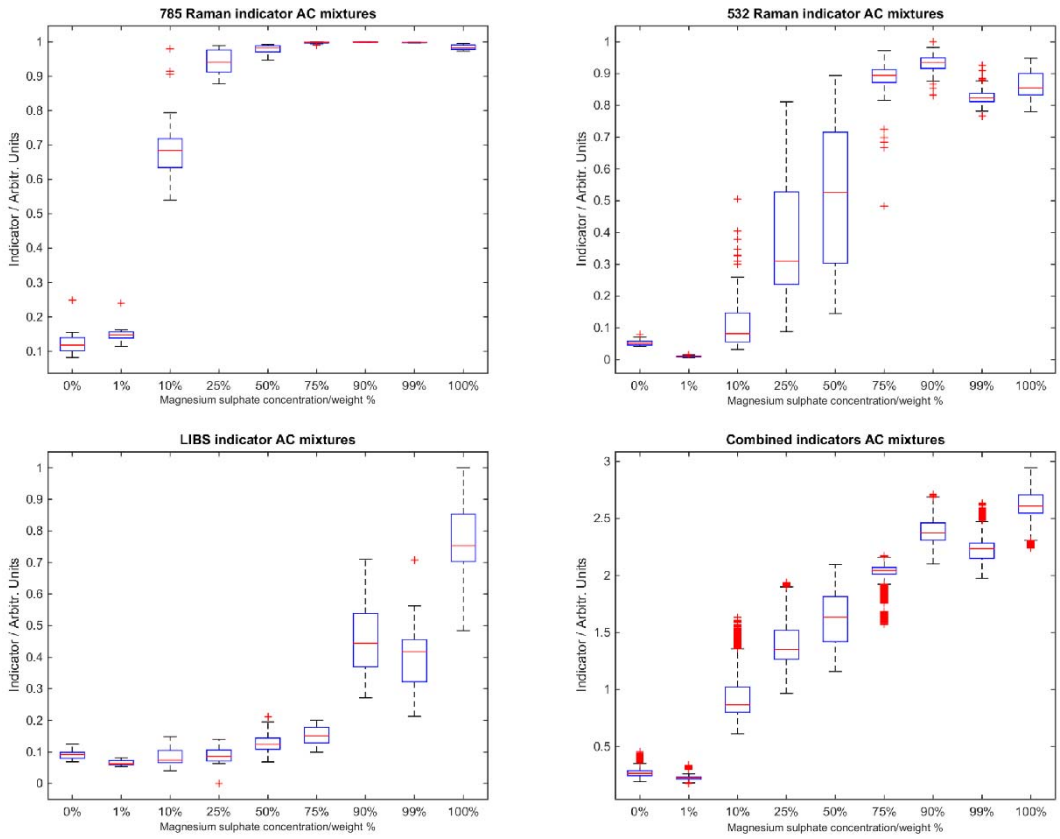

FIGURE 3-25 UNIVARIATE ANALYSIS OF AC MIXTURES

After the results obtained with combined univariate analysis, the increase of information available as a result of the fusion from different sources prior to the multivariate analysis, is promising when it comes to improve the classification power of this mixtures

Multivariate analysis:

The correlation between the expected and calculated concentrations for the different models trained in this work provides a good quantitative measure of their classification goodness. See following table.

TABLE 3-11 PERFORMANCE OF THE MULTIVARIATE ANALYSES FOR RAMAN 532 NM, RAMAN 785 NM, LIBS, 532 + 785 AND 532 NM + LIBS. CLASSIFICATION ERRORS ARE PROVIDED IN % WITH A CONFIDENCE INTERVAL OF 95%.

Technique	AB		AC		BC	
	R^2	mean 2σ (%)	R^2	mean 2σ (%)	R^2	mean 2σ (%)
532	0,99805	1,586	0,99109	3,5263	0,99955	0,82091
785	0,99812	1,5774	0,9932	2,7654	0,99934	0,70029
LIBS	0,99885	1,1268	0,9954	1,9981	0,99937	0,88347
532+LIBS	0,99894	1,1495	0,99106	3,366	0,99966	0,62355
785+532	0,99886	1,1675	0,99528	2,3683	0,99931	0,95572

- AB mixtures: The classification results after the training of the optimal ANN are shown in Fig. 3-26. The results obtained from the PCA analysis, represented using 2 and 3 PCs can be seen in Figure 3-33 and Figure 3-34 These graphs represent the mean values of the response of the network to the input data, with an error of ±2σ (confidence interval of 95%). As it can be seen, our multivariate analysis approach using PCA + ANN for the quantitative identification of the mixtures abundances results in quite a remarkable classification power on the individual Raman and LIBS data. However, after fusing the data and training again the models, the behavior of the model is further improved, with a slightly higher improvement in the case of the Raman + LIBS fusion. E. g., it can be observed how the classification between the 99% and the 100% concentration mixtures is improved after the fusion.

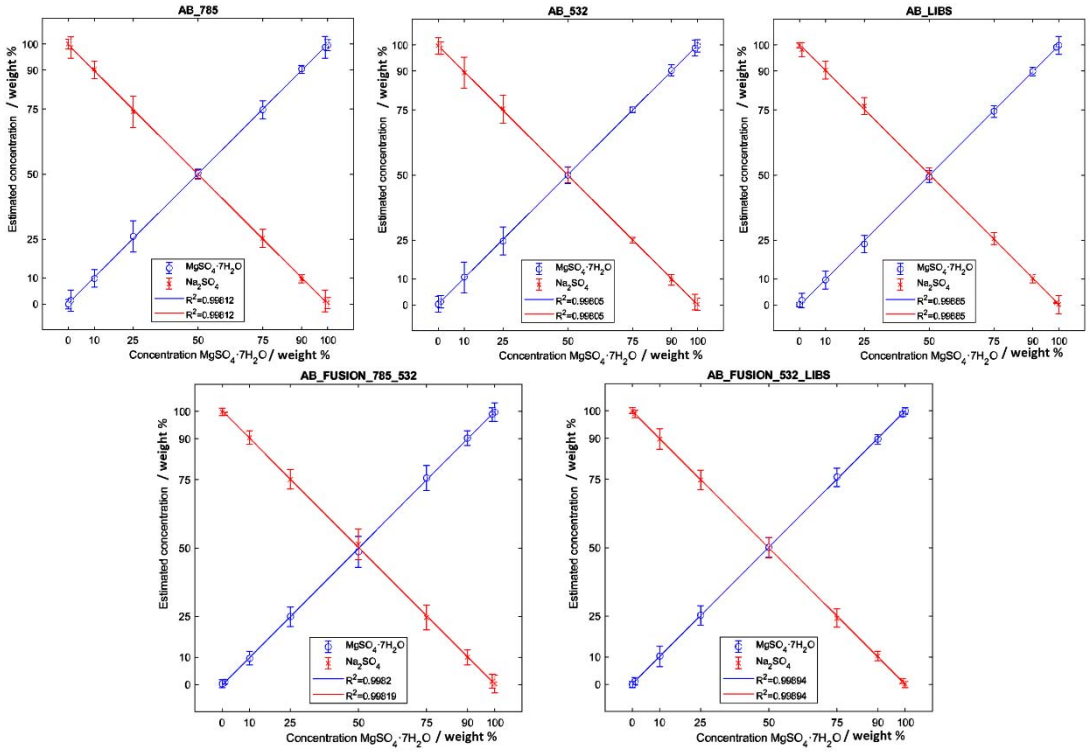

FIGURE 3-26 ***CLASSIFICATION RESULTS FROM ANN. RED LINE FOR SODIUM SULFATE AND BLUE LINE FOR MAGNESIUM SULFATE.***

- AC mixtures: Fig. 3-27**¡Error! No se encuentra el origen de la referencia.** shows the c lassification results from the ANN model for these mixtures, while Figure 3-35 and Figure 3-36 show the PCA analysis results. The models with Raman data for the AC mixture provide a less accurate classification than the other mixtures, probably due to the presence of water bands in the epsomite, that might interfere with the water band features of the chloride in the Raman spectrum, resulting in a worse classification accuracy. On the contrary, the LIBS-only model shows a -somehow unexpected- good behavior that might be explained by a common matrix effect response along all the LIBS spectra that might be identifiable by the multivariate model. The combination of Raman with LIBS improves the behavior of the models after data fusion.

- BC mixtures results are presented in Fig. 3-28,Figure 3-37 and Figure 3-38. These results show an improvement in the classification power using Raman + LIBS fused data.

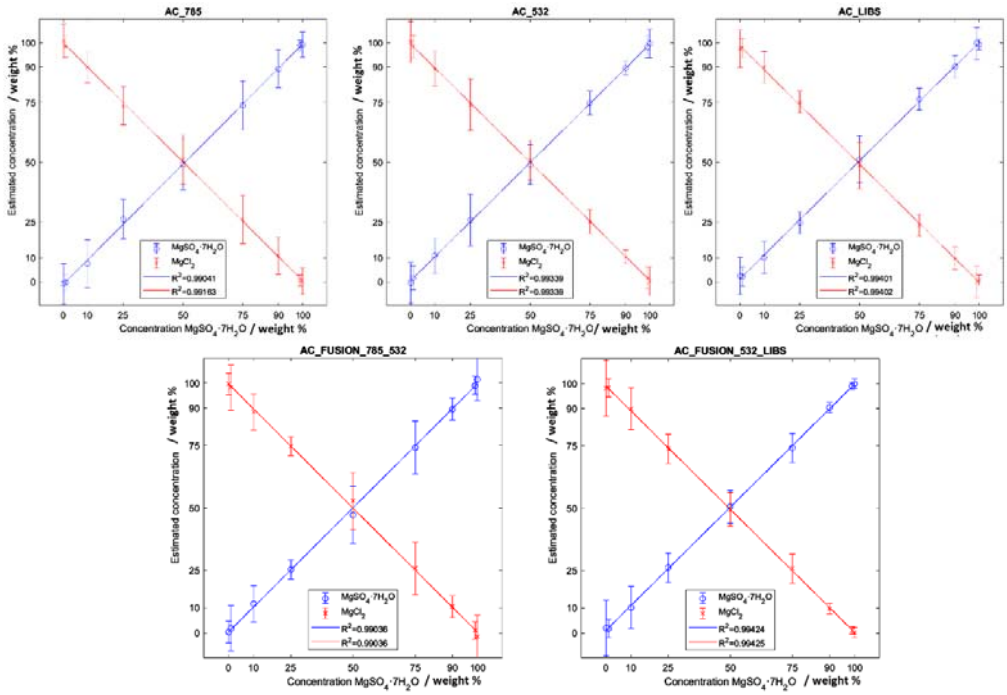

FIGURE 3-27 *CLASSIFICATION RESULTS FROM ANN. RED LINE FOR MAGNESIUM CHLORIDE AND BLUE LINE FOR MAGNESIUM SULFATE.*

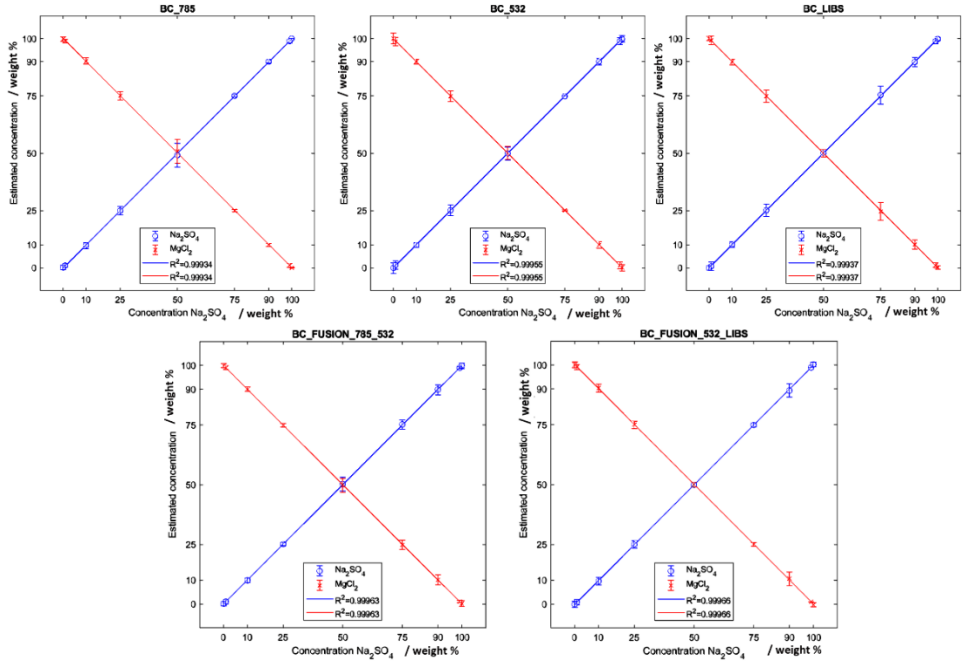

FIGURE 3-28 *CLASSIFICATION RESULTS FROM ANN. RED LINE FOR MAGNESIUM CHLORIDE AND BLUE LINE FOR SODIUM SULFATE.*

3.5.5 Analysis on ternary mixtures

Finding isolated materials, or mixtures of just two components in nature is unlikely. Therefore, the laboratory abstraction used in the previous analyses is very useful to build models or understand the physics behind the problem, but reality might be more

complicated. Natural samples will be more complex, including more than two components.

In order to address the classification of this kind of samples, the most immediate approach is to generate a model for ternary mixtures of ABC components. This would require the preparation of multiple mixtures of the three components to cover a great area in the spectrum of ternary mixtures and then run a model calibration. In order to avoid this intensive work, in this work we have proposed to perform the classification of these complex samples by extrapolating information from models trained with binary mixtures only. This greatly reduces the number and complexity of samples to prepare.

This idea is a sneak peek to a new line of research in our laboratory in order to study the feasibility of using models from simple mixtures to obtain chemometric calculations of more complex systems.

In order to complete this study, we run several models based on PCA+ANN on Raman 532 nm data to test several scenarios, comparing the classification results of the ternary mixtures:

- Model trained with binary mixtures only
- Model trained with ternary mixtures only

All these models were used to classify the ternary mixtures, representing the classification results on a ternary diagram.

From the data fusion perspective, we also studied the capability of classification based on the graphical representation of the PCA components for fused data, compared to individual techniques.

3.5.6 Discussion and conclusions

3.5.6.1 Classification of ternary mixtures

The model based on ternary mixtures was first used to show the classification potential of this kind of models. The PCA results for two and three PCs are shown in Figure 3-43 and Figure 3-42. After classification with the corresponding artificial neural network was used for classification. The representation of the classification results in a ternary diagram is shown in Fig. 3-29.

The representation shows the average value of the calculation for each one of the 30 spectra available per mixture. At first glance, the classification power is high, even in ternary mixtures where different features, and some coincident, could interfere, as the water bands from the hydrated chloride and the hydrated sulfate. Nevertheless, getting

this kind of very nice classification results is expected, given that the model was trained and verified with the same sample proportions.

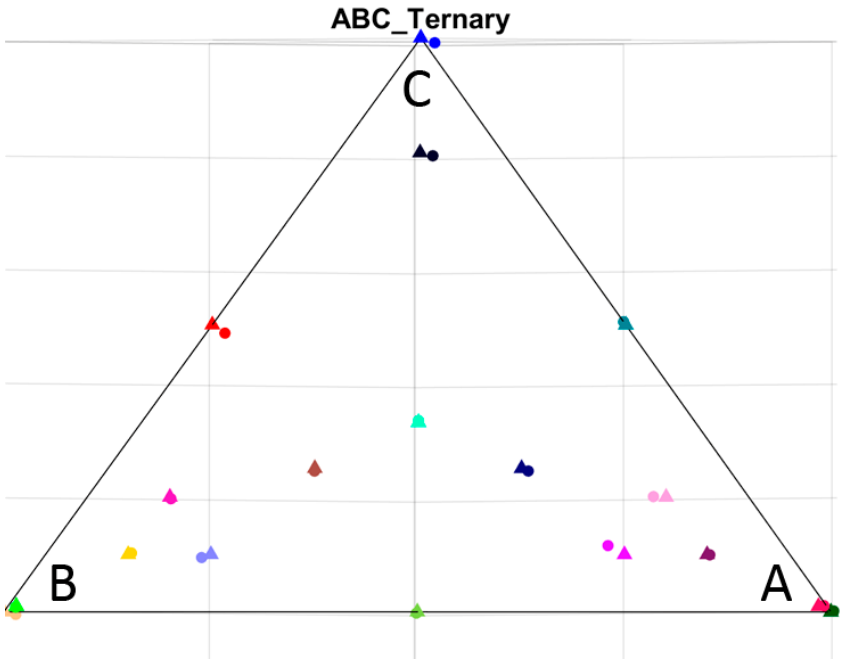

FIGURE 3-29 CLASSIFICATION OF THE TERNARY MIXTURES BASED MODEL. THE TRIANGLES REPRESENT THE NOMINAL COMPOSITION, AND THE CIRCLES OF THE SAME COLOR THE CALCULATED COMPOSITION.

The application of the model trained with binary mixtures only was trained with all the binary mixtures spectra, training the PCA+ANN combination as with all the others. The resulting model was used to classify the 532 nm data collected on the ternary samples set. The classification results are shown in **¡Error! No se encuentra el origen de la r eferencia.** Since the theoretical points are separated from the calculated points, we have included boxes and ellipses to enclose the related points.

At first glance it is quite obvious that the model is not performing especially well for some samples. However it works relatively fine with others. Especially remarkable are the deviations of the mixture containing 50% of B and 50% of C, as well as the one corresponding to 50% of A and 50% of C.

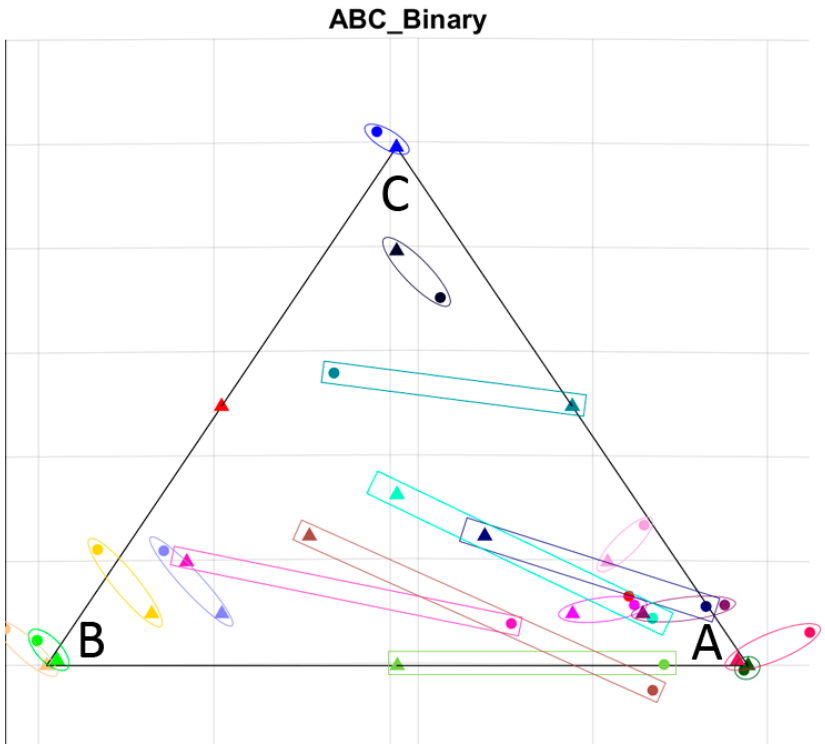

FIGURE 3-30 CLASSIFICATION OF THE TERNARY MIXTURES USING THE BINARY MIXTURES BASED MODEL. THE TRIANGLES REPRESENT THE NOMINAL COMPOSITION, AND THE CIRCLES OF THE SAME COLOR THE CALCULATED COMPOSITION.

It is important to remark that the mixtures for this set, the ternary mixtures were done in a previous step to the binary mixtures, and some lessons were not learnt yet, so the samples in ternary mixtures were not compressed into a pellet, and were analyzed in dust presentation. This could have led to differences in the samples. In fact, when checking the spectra shown in Fig. 3-31 and Fig. 3-32 there are some differences with respect to the expected bands. While in the samples processed for the binary the main band keeps its position, corresponding to thenardite, the pure compound in the ternary mixtures shows some shifting, being this shifting more intense in the mixture with the hydrated chloride. This shift is probably related to the hydration state of thenardite, whose main Raman band shifts towards lower wavenumbers with higher hydration levels.

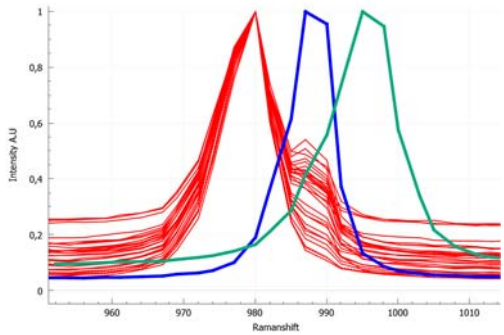

FIGURE 3-31 MAIN SULFATE BAND IN THE ORIGINAL 50/50 BC SAMPLE FROM BINARY MIXTURES (GREEN). PURE SAMPLE IN THE TERNARY MIXTURES SET (BLUE). 50/50 BC SAMPLES FROM TERNARY SET (RED)

Something similar is observed in the case of the 50% mixture of AC components. In this case the change occurs is the opposite direction, and it looks like the presence of the chloride somehow favors the dehydration of the sulfate, resulting in a shift towards higher wavenumbers of the sulfate band.

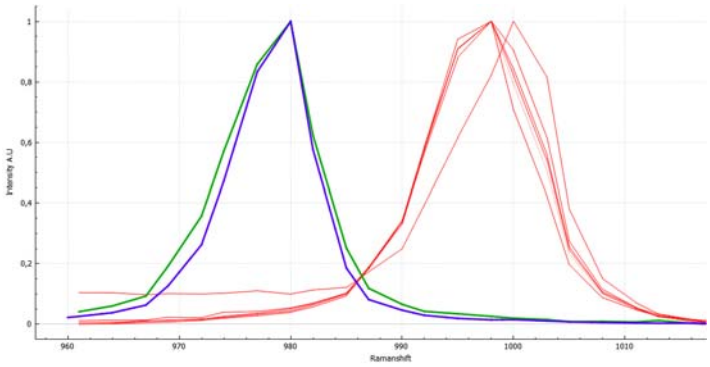

FIGURE 3-32 MAIN SULFATE BAND IN THE ORIGINAL 50/50 AC SAMPLE FROM BINARY MIXTURES (GREEN). PURE SAMPLE IN THE TERNARY MIXTURES SET (BLUE). 50/50 AC SAMPLES FROM TERNARY SET (RED)

All these effects are coherent with the samples that showed a bad classification in Fig 3-30. In conclusion, our results show that the errors in the classification of ternary mixtures based on the binary mixtures model might be explained by the spectral modifications occurred in the ternary samples used for the analysis. However, this approach is promising, and this line of work needs to be continued.

3.5.6.2 Data fusion study on ternary mixtures

This section covers the impact of data fusion in the case of ternary mixtures. As introduced in the previous section, the presence of certain mixtures with classification spectral features for one technique and no features for the other, might complicate a unique model based on fused data for ternary mixtures.

For this verification the fused data from 785 Raman and LIBS were used, as these techniques also address the complementary data fusion scenario. Also, the mixtures were pressed into pellets for the libs measurements and those pellets were used later for the 785 Raman analysis, so measurements of both techniques happened in the very same sample.

A total of 20 spectra per mixture were taken both with Raman and LIBS, and the fused dataset was prepared following the same procedure used for the binary mixtures experiment. In this case we haven't run the Artificial Neural Network to classify the results from PCA, but we are presenting the different results per technique of the PCA analysis, so the grouping ability of the analysis can be seen, as a qualitative analyses of the goodness of the model. The figures have been included in the supplementary figures section 3.4.9, at full page for better visualization: Figure 3-44, Figure 3-45 and Figure 3-46.

3.5.7 Discussion

3.5.7.1 Univariate analysis

The univariate analyses of the mixtures showed that the detection limit is different depending on the instrument, and changes depending on the compound under study. For lower concentrations of magnesium sulfate in AB mixtures, the 785 nm Raman couldn't distinguish effectively between the 0, 1 and 10 % mixtures, setting the detection limit over 10% while this limit is under the 10% for the sodium sulfate. This might be related to the relative intensity of the main band of the magnesium and sodium sulfates, making it easier to detect the latest. This was also observed in the mixtures of the sulfates with the chloride, small amounts of any of the sulfates were easy to identify, given the high difference in relative intensities between the water bending band and the sulfate band. With regards to the 532 nm Raman instrument, it presents a slightly better behavior around the 10% for the AB mixtures, presenting an abrupt change in this behavior when considering mixtures around 20% abundance,

With regards to AC and BC mixtures, the 532nm instrument showed a worse performance in the discrimination of low concentration-mixtures than the 785nm one. However, it allowed a better classification for intermediate and high concentrations, mainly thanks to its wider range that reached the water stretching band.

The LIBS technique, presented a better performance in the discrimination of low concentration-mixtures, ensuring a detection limit in the order of 1%. However, its performance decrease in the intermediate range. The calculations were easy when having compounds with sodium and magnesium, allowing a good classification. It the case of AC mixtures, even not having separate lines for both compounds, the matrix effects during the measurement allowed us the definition of an indicator. This effect

was present among the whole spectrum, so it could be expected that it will provide a good feature to be evaluated in the multivariate analysis.

Finally, the linear combination of these arbitrary indicators meant an increase in the population of points, passing from 20 or 60 measurements per instrument, to 24000 possible combined trios, which could help overcoming the influence of the possible heterogeneity of the samples. This combination was needed that way given that the analyses were not co-aligned. It is expected to have better results in the case of SuperCam, where Raman and LIBS measurements will be done on exactly the same spot. Having this combination made possible to reach a model, using the three indicators from the three techniques, that worked better in the whole range than the individual measurements, which is logical since the greater the amount of information, the better the classification. As remarks, this combination made it possible to separate all the mixtures evaluated for the AB set, it worked just fine from 1% to 90 % of sulfate in the AC mixtures, where LIBS couldn't help that much, but a great performance in the whole range for the BC mixtures. The great capabilities of LIBS in the lower concentrations played a main role in the final classification properties.

3.5.7.2 Multivariate analysis

The multivariate analysis results show that, in general, multivariate analysis on the individual datasets for each technique improved the classification of the mixtures when compared to the univariate analysis. It can be seen that in the case of multivariate analysis a classification of the mixtures of 10% concentration of Epsomite can be done using any of the Raman datasets, while it was more difficult in the univariate case. For the LIBS data, the classification of the middle range of concentrations of epsomite has been remarkably improved. These results can be observed better in the supplementary figures: Figure 3-39, Figure 3-40 and Figure 3-41, where the boxplots of the classification are shown, and, again, the 50% boxes get narrower showing that despite of outliers, the classification power has been improved. The case of LIBS in AC mixtures is especially remarkable when compared to the results of univariate analysis. The matrix effect in this case was modeled by the PCA+ANN model, resulting in an excellent classification of our samples. However, this result is difficult to translate into natural samples, were the matrix effect will be harder to be replicated in calibration runs.

The application of the multivariate analysis models to datasets conformed by fusion of data, improves the classification of the different mixtures compared with the standalone datasets, even with the low-level fusion technique used in this work. It can be observed that the classification uncertainty can be under 1% depending on the mixtures, resulting in a general average uncertainty lower than 3.5% with a confidence interval of 95%. In general terms, the more accurate classification happens with fused data as extracted from the values of R^2 shown in Figs. 3-26 to 3-28. The most complete fusion of data

seems to be the fusion between 532 Raman and LIBS, which is the complementary fusion. The data fusion of measurements of the same observable using different sensors (532 + 785nm Raman data fusion) wasn't found as useful as Raman-LIBS in this experiment. However, it showed improving capabilities, as this kind of fusion limits errors and increases the number of variables to analyze, i.e., the available information.

3.5.7.3 Classification of ternary mixtures

In the case of ternary mixtures it was demonstrated how the increased complexity wasn't a problem to obtain a good classification of the mixtures. However, the best results were obtained with a dedicated calibration experiment, though the model was tested against the same samples (though different spectra) used for model training.

The results obtained using a training based on binary data to be applied to a ternary system showed good or bad results depending on the samples. Based on the classification of the data from the ternary experiment it was observed a trend in some points to displace to the vertex of the epsomite. As shown in Figs. 3-31 and 3-32, the samples have changed their structure most probably changing their hydration degree. This change in the case of the thenardite, anhydrous sodium sulfate, displaced the main feature of the spectrum, the main sulfate band, to lower Raman shifts, where the main band of the epsomite is present. The model classifies the sample based on its Raman bands, and being these off their theoretical position, the classification cannot be good. This change happened most likely due to the use of powdered samples, that increased the area of contact with the atmosphere, and also the absence of an encapsulation as was used in the binary mixtures. This could be an opposite problem in the case of the AC mixtures, where a dehydration happened for the epsomite, displacing the main band of the sulfate in accordance. This change, epsomite turning into hexahydrite, happens naturally if time is given to the samples, but it has been accelerated in the presence of the magnesium chloride. The theoretical point of the 50/50 mixture of compounds A and C is displaced towards the region of ternary mixtures containing compound B, the dehydrated sulfate.

This result doesn't imply a failure in the use of simpler trainings to explain more complex systems. Furthermore, this approach seems promising, though further testing needs to be done. One conclusion though is that with a better choice of samples this effect might be avoided.

Regarding the data fusion of 785 nm Raman and LIBS, in this case only the PCA classification has been presented, so the goodness of the model is to be assessed in a qualitative way. Figure 3-45, corresponding to LIBS analysis, shows how the mixtures containing higher proportions of A or C, both with magnesium lines as only feature, are all grouped, potentially leading to a bad classification. Looking at the results from Raman

(Figure 3-44), we can see how the model groups well the end members, and the mixtures close to them. It is with intermediate mixtures like 25% A, 50% B and 25% C that we can find some overlapping of the different mixtures, also, the points are more spread. In this case the improvement observed in the 2 PC fused data is specially remarkable (Figure 3-46), where not only the endmembers have been individually grouped, but also the distribution of the different points confirm the better classification performance when using fused data from complementary techniques.

Conclusions

The different characteristics of both Raman instruments made it impossible to use this results in a discussion about the best excitation source to use. Indeed, the highest power of the laser in the 785 nm Raman played an important role in the final performance of this instrument. Also, its higher spot size and higher resolution play in favor of this instrument, making it less sensitive to possible heterogeneities that could be present on the samples despite of the small grain size and mixing. It is evident that the technique more sensitive to this inhomogeneity is the one with the lower spot size, 532 nm Raman in our case. The effects of this are expected to be more evident when analyzing mixtures with lower concentrations of one of the components, in that case the measurement will more sensitive to hot spots. This effect needs to be taken into account when comparing result from one technique to another, and in general when trying to fuse data from two instruments that see different areas of the sample. In the case of 532 nm Raman instrument, its higher range and making possible to see the stretching of the water is one of the factors playing in favor of this instrument. As a conclusion, we are not able to evaluate what excitation source works better, although the absence of fluorescence in this particular samples, the relation of the Raman effect cross section with the fourth power of the frequency of the incident light, and under equal instrumental characteristics could lead to a victory of the 532 nm. Also, these same considerations on both Raman instruments might affect also the multivariate analyses.

Just a quick linear combination of the indicators calculated in the univariate analysis showed that data fusion from different sources improved the classification power in these binary mixtures. This combination could not look as dramatic in the case of multivariate analysis, but in this case it is needed to have into account the great improvement introduced by the PCA+ANN analysis. Even after this improvement, the data fused data showed a better performance for the whole range of concentrations. This combination improved the classification limits based on the same datasets, with a limit between 0.5 and 3.5 % depending on the sample, with a confidence interval of 95 %.

SuperCam instrument will have a resolution in Raman spectra similar to the one used in this work, with better performance in the LIBS measurements, able to detect effectively elements like Sulphur or chloride. Also, both analyses will be done coaligned, at exactly the same spot, what makes the measurement less sensitive to local heterogeneities. Due to all of these factors, the results achievable buy SuperCam could be even better than the ones presented in this work.

In the case of ternary mixtures, it was demonstrated how, with correct training, results as good as the ones obtained for a two members mixture can be achieved in more complex mixtures. However, the preliminary results on the ternary calculations based on binary training showed, despite of the problems because of the change in the spectra, that the model had certain ability to classify some of the mixtures. Deeper work is to be done using samples more stable. It is important to remark that in the fused data we might introduce a technique not affected by this changes, and a model based in fusion could be expected to be more robust, and probably, more polyvalent.

Regarding this last topic, the data fusion on ternary mixtures datasets, the two techniques selected had their own limitations separately for different kinds of mixtures. These limitations could be observed in the PCA analysis from each dataset. Encouraging result is that the data fusion has improved the individual results, overcoming the possible difficulties of each technique individually.

General conclusion, in terms of implications for the exploration of the Solar System, is that the technical cost of implementing both techniques in one instrument is highly worthy. Not only taking into account the good results of data fusion analyses, also taking into account the different features of both techniques that individually could lead to a better identification of the samples.

3.5.8 Supplementary figures

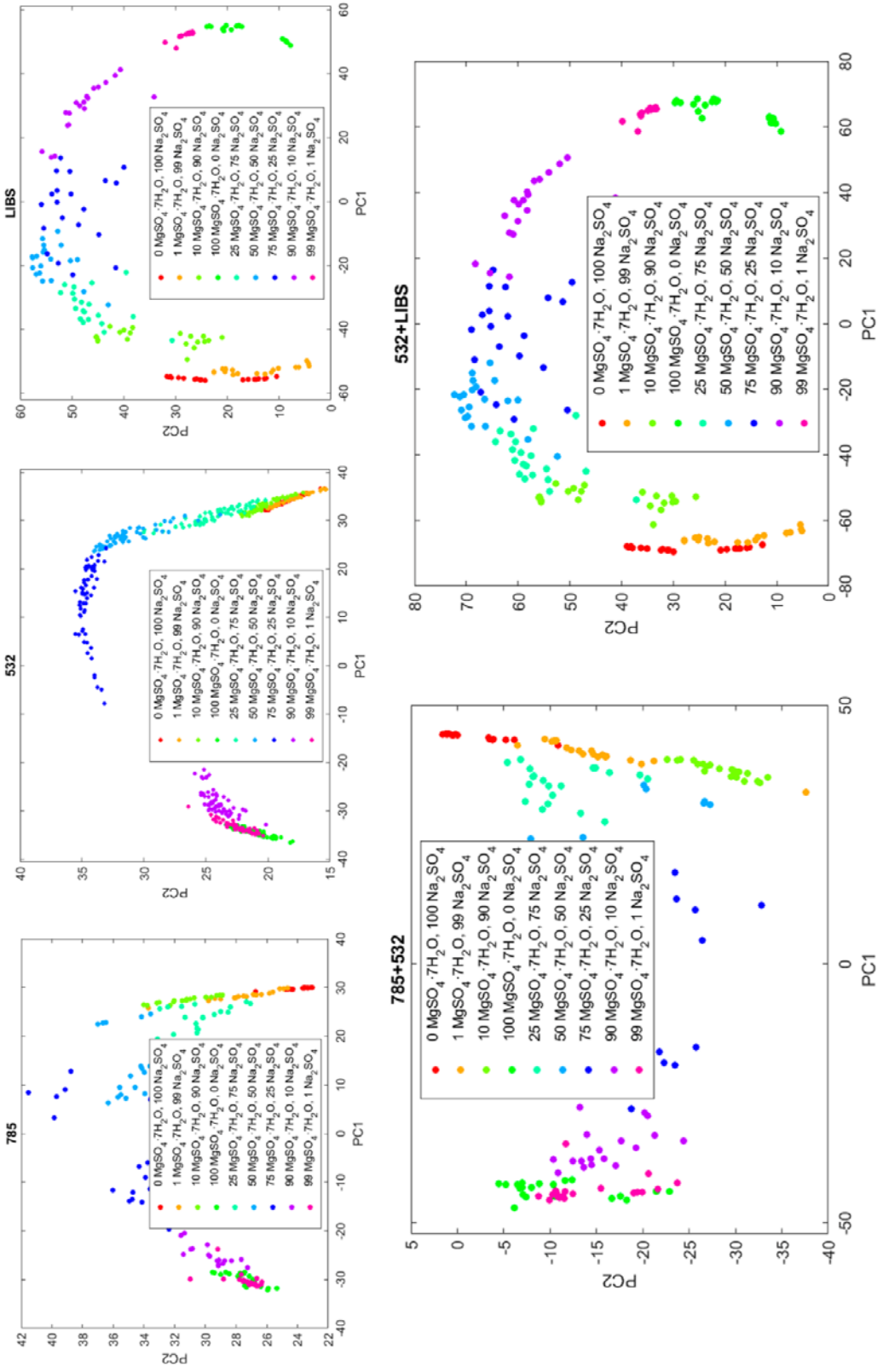

Figure 3-33 Two Principal Components analyses of AB mixtures (both sulfates) using individual datasets, and fused datasets

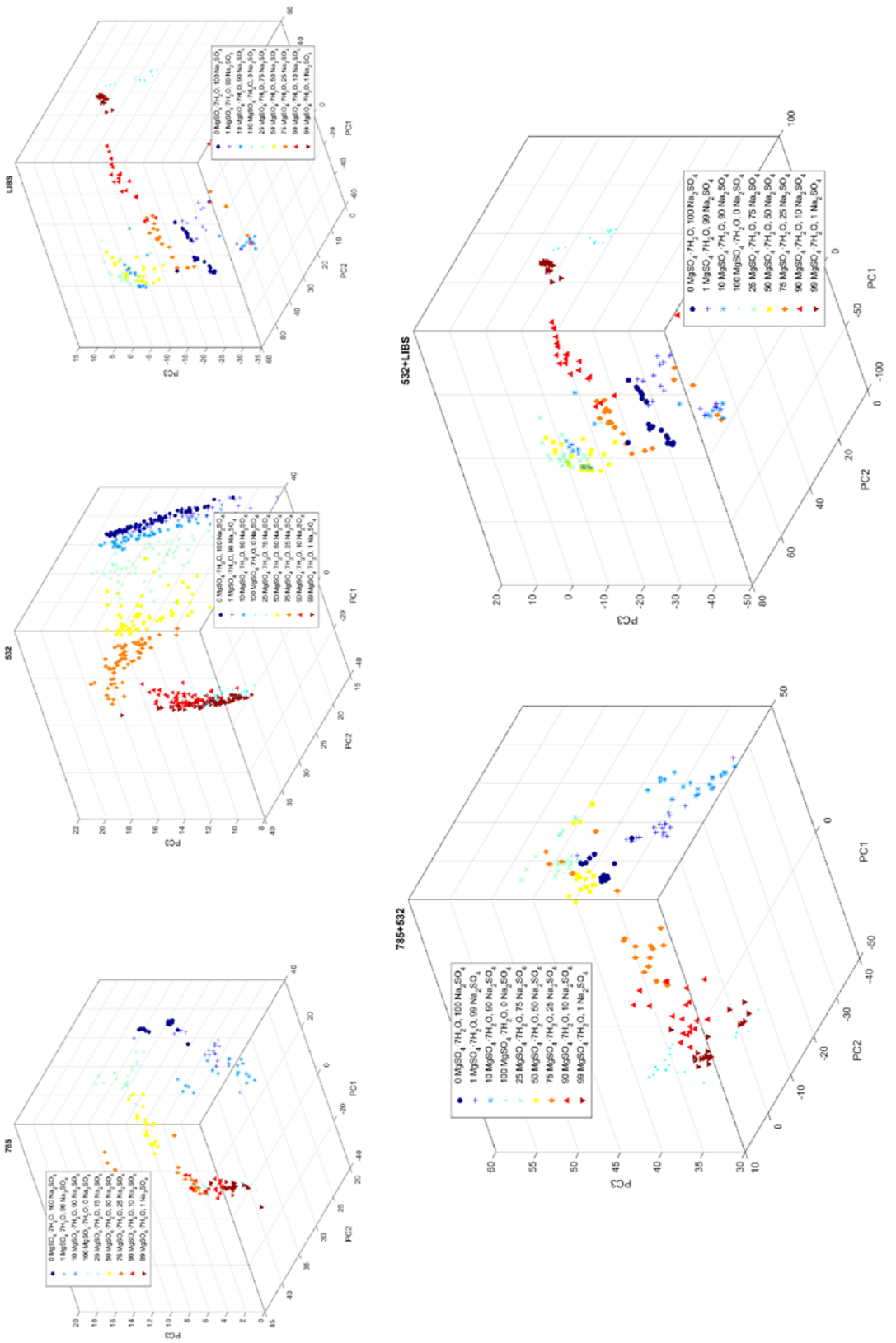

Figure 3-34 Three Principal Components analyses of AB mixtures (both sulfates) using individual datasets, and fused datasets.

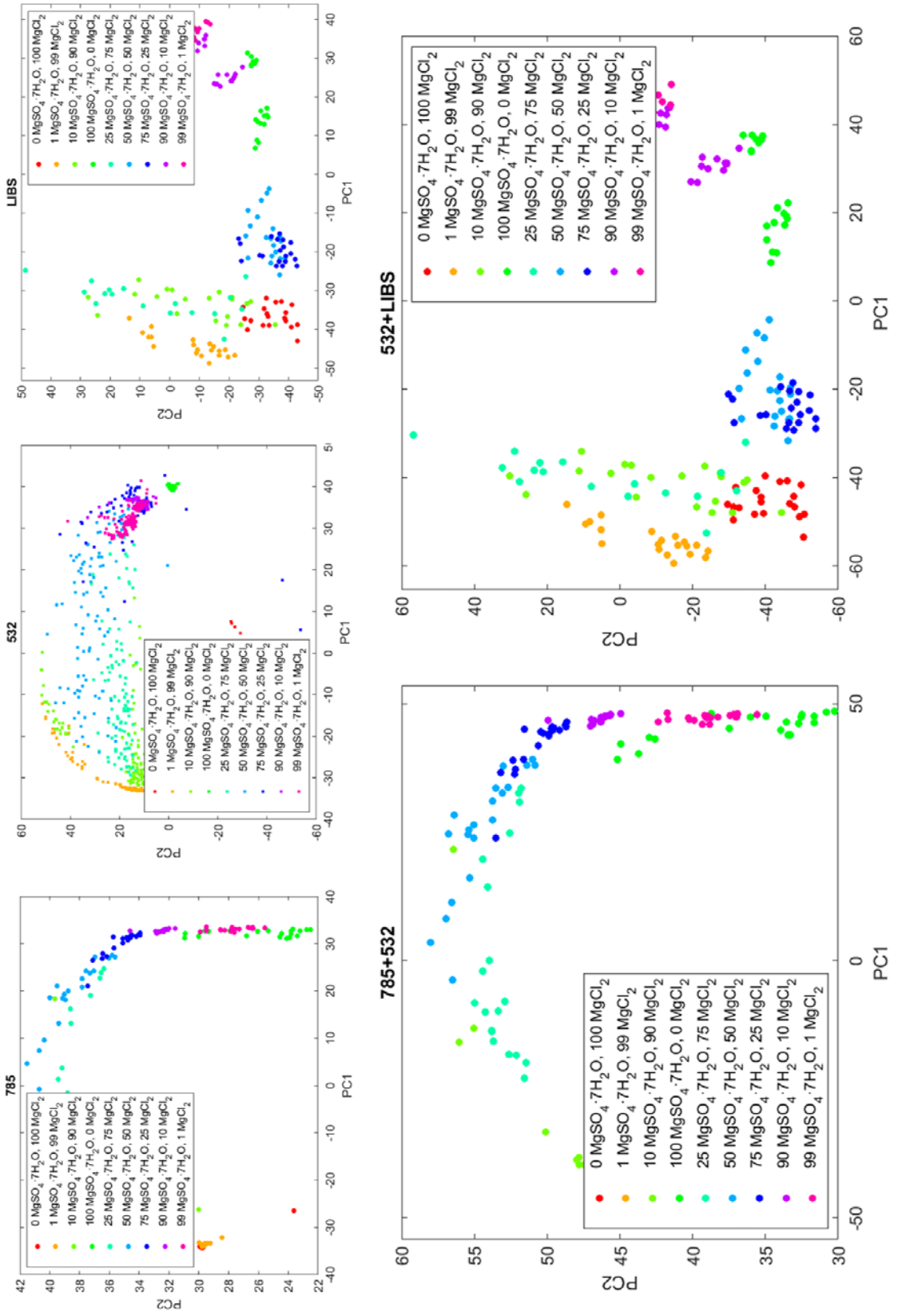

Figure 3-35 Two Principal Components analyses of AC mixtures (Mg sulfate and Mg Chloride) using individual datasets, and fused datasets

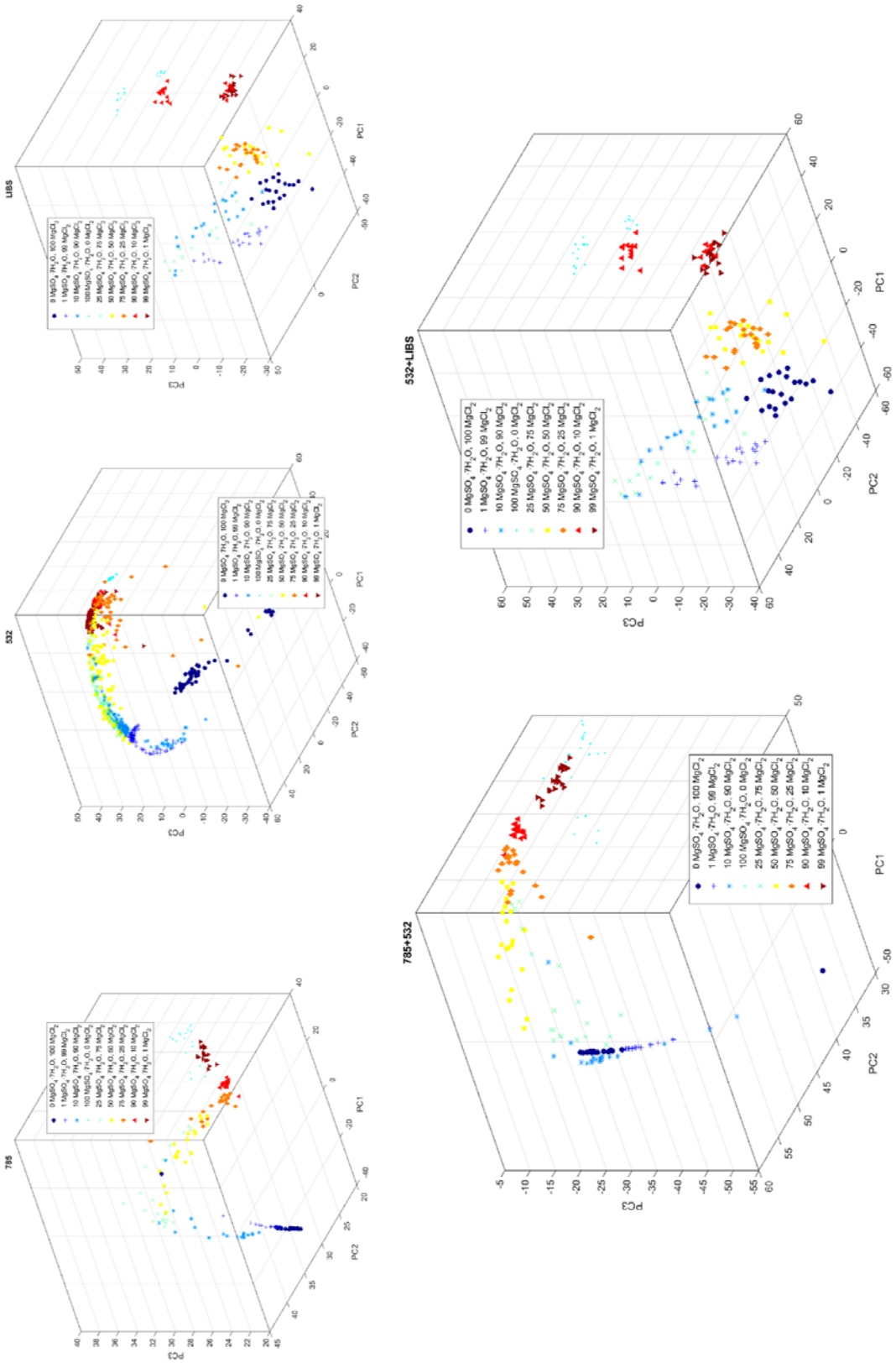

Figure 3-36 Three Principal Components analyses of AC mixtures (Mg sulfate and Mg Chloride) using individual datasets, and fused datasets

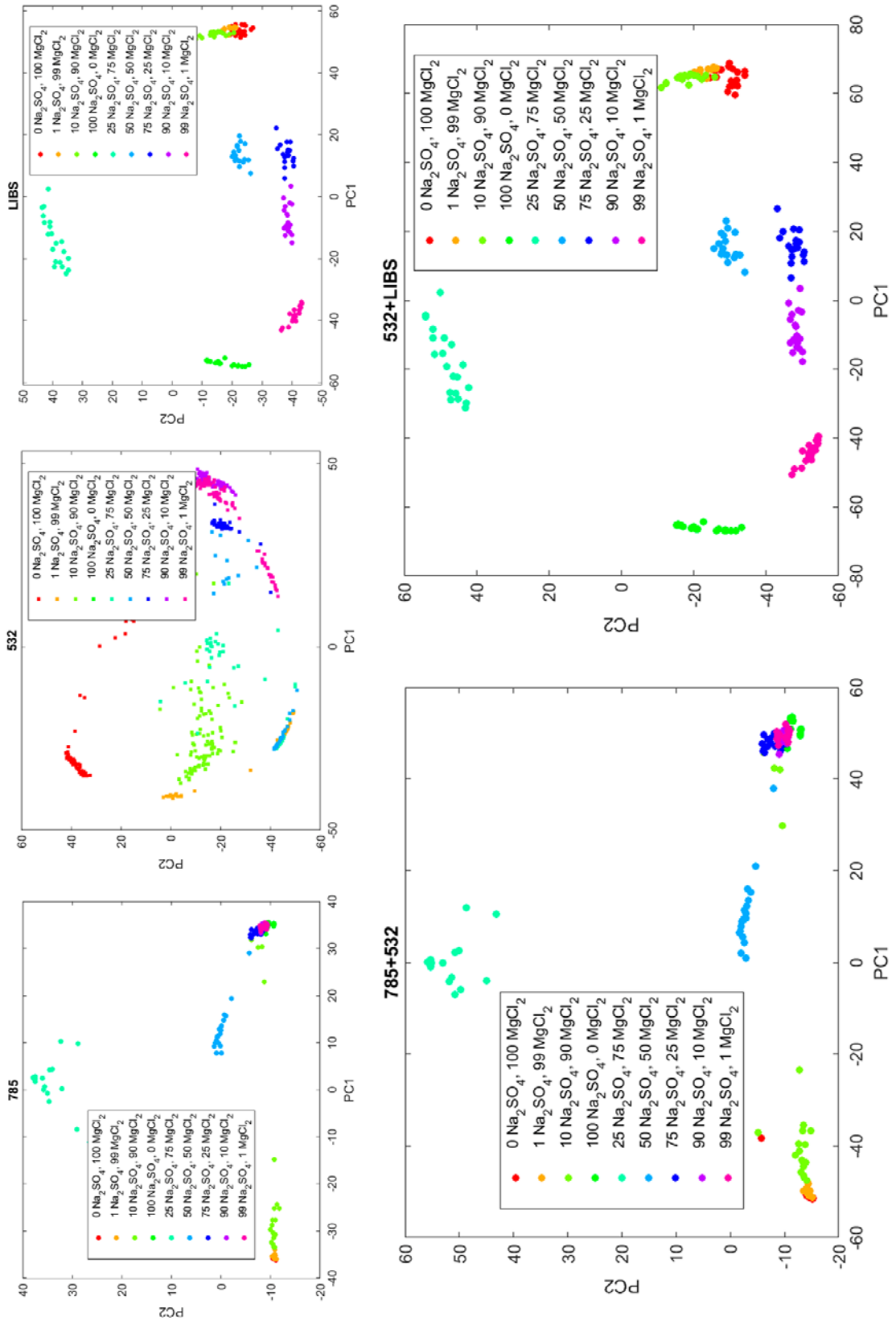

Figure 3-37 Two Principal Components analyses of BC mixtures (Na sulfate and Mg Chloride) using individual datasets, and fused datasets

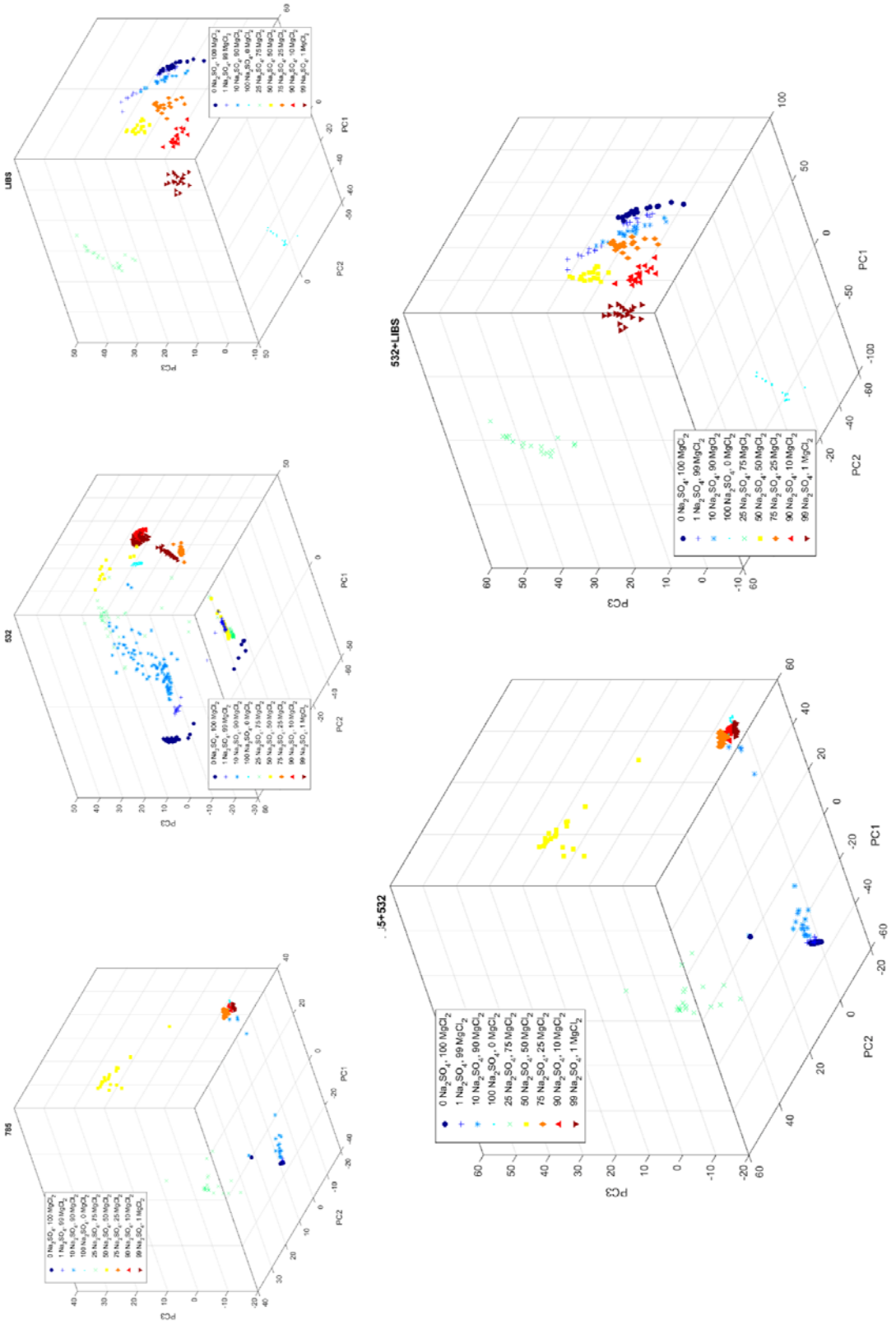

Figure 3-38 Three Principal Components analyses of BC mixtures (Na sulfate and Mg Chloride) using individual datasets, and fused datasets

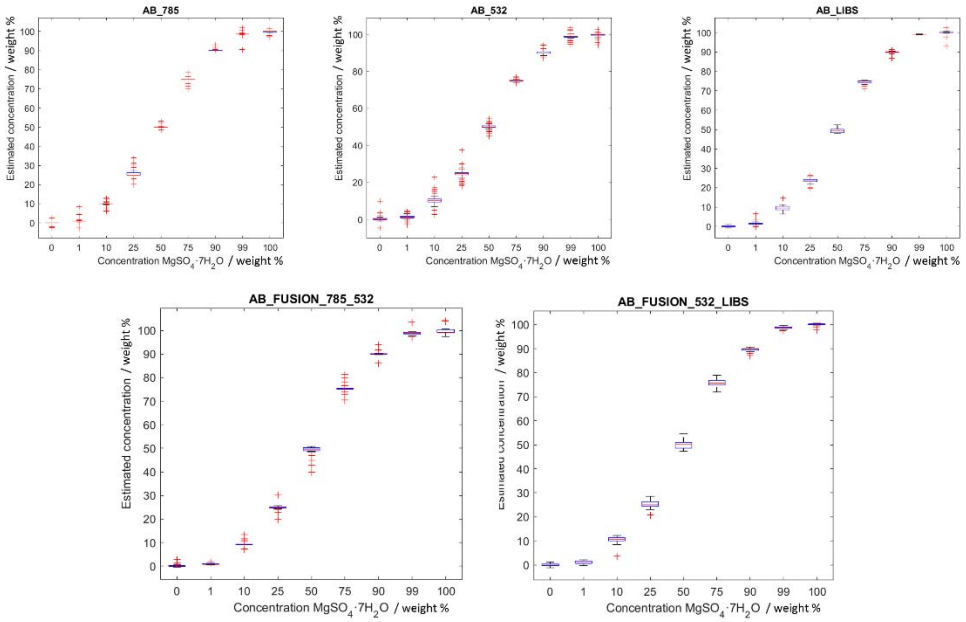

Figure 3-39 Boxplot diagram of the classification from the ANN for AB mixtures using different datasets

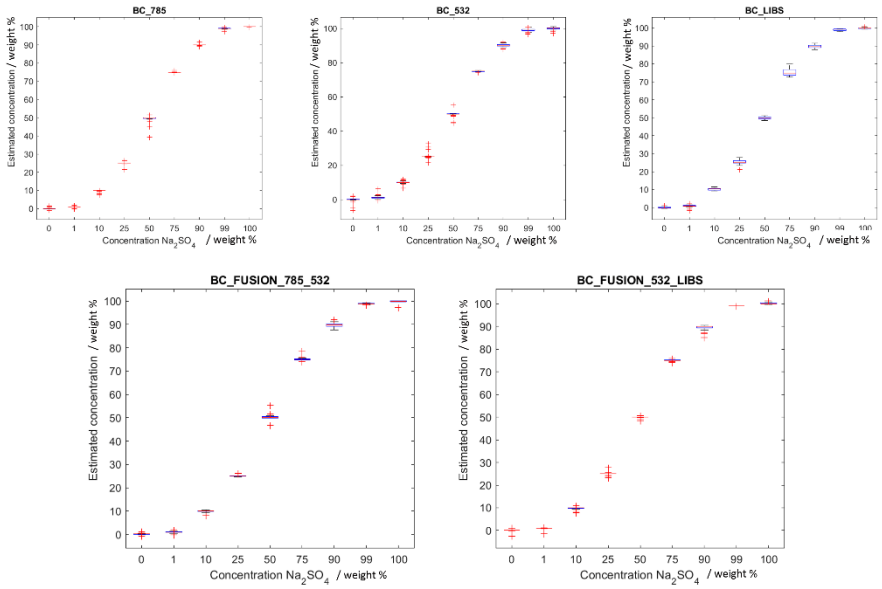

Figure 3-40 Boxplot diagram of the classification from the ANN for BC mixtures using different datasets

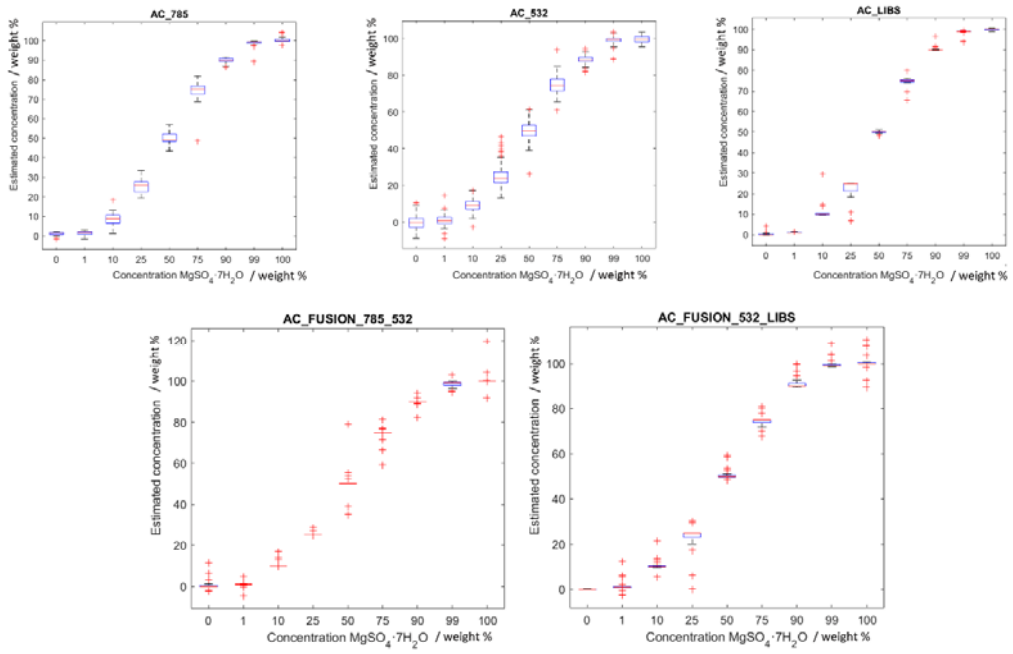

Figure 3-41 Boxplot diagram of the classification from the ANN for AC mixtures using different datasets

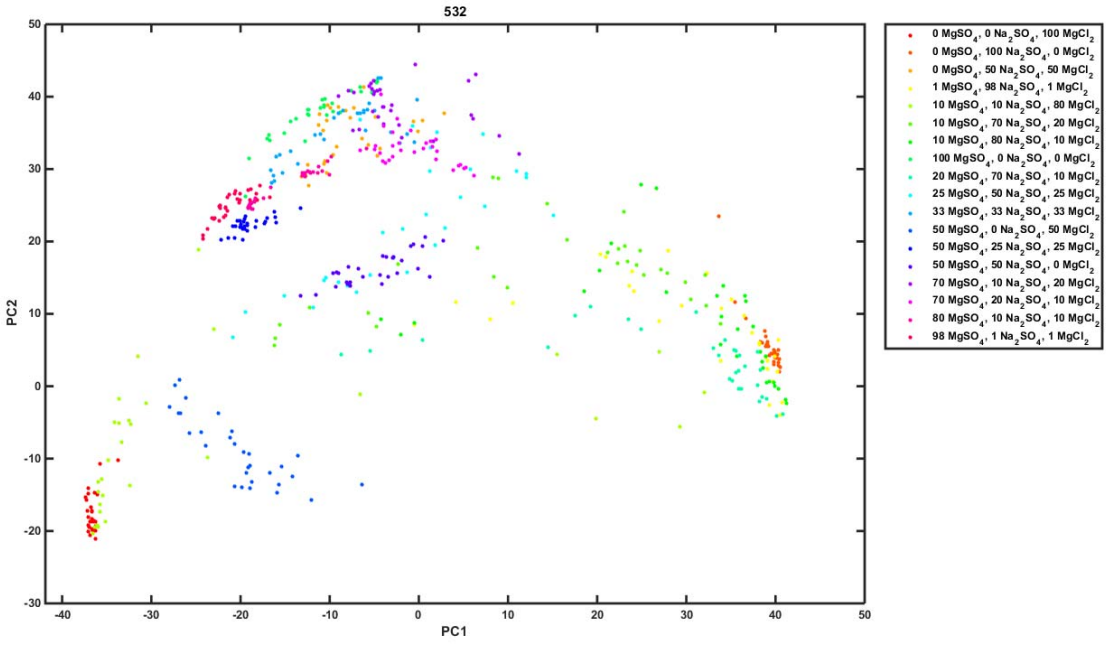

Figure 3-42 2 PCs classification of the ternary mixtures using 532 nm Raman, and training based on ternary mixtures

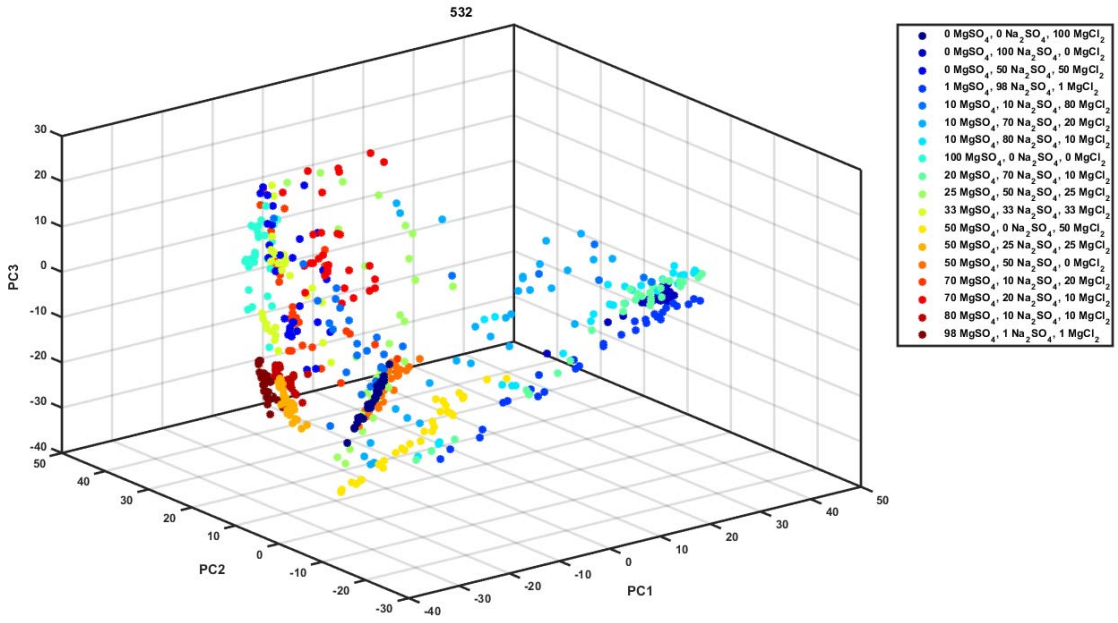

Figure 3-43 3 PCs classification of the ternary mixtures using 532 nm Raman and training based on ternary mixtures

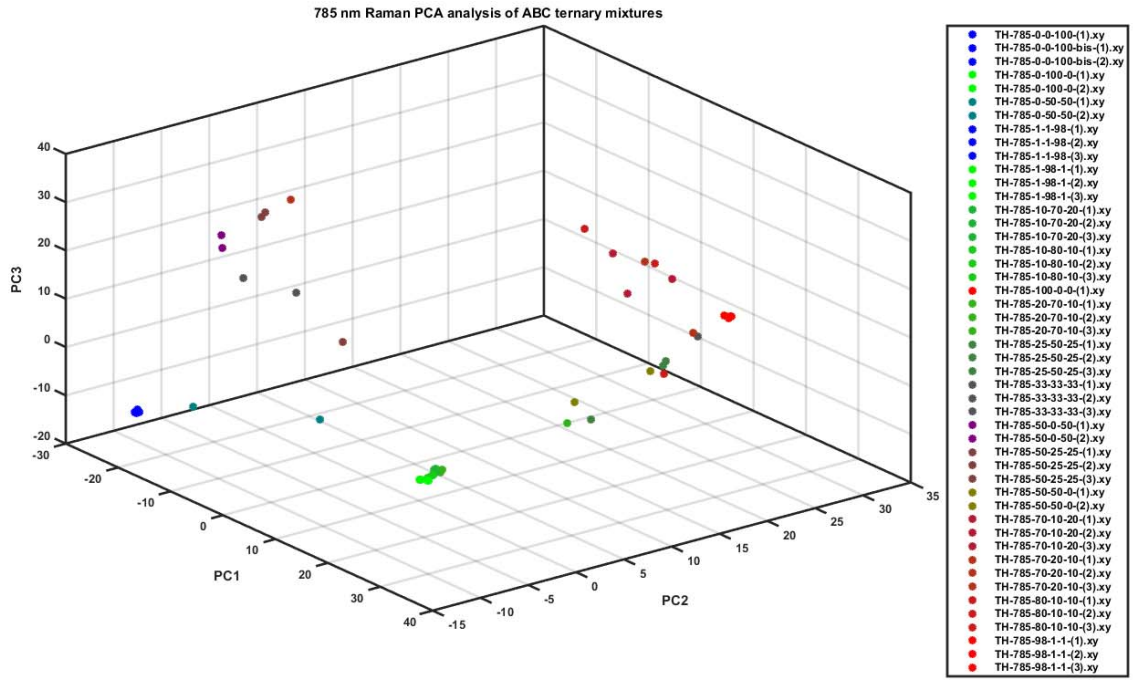

Figure 3-44 3 PCs analysis of the 785 Raman dataset from ABC ternary mixtures

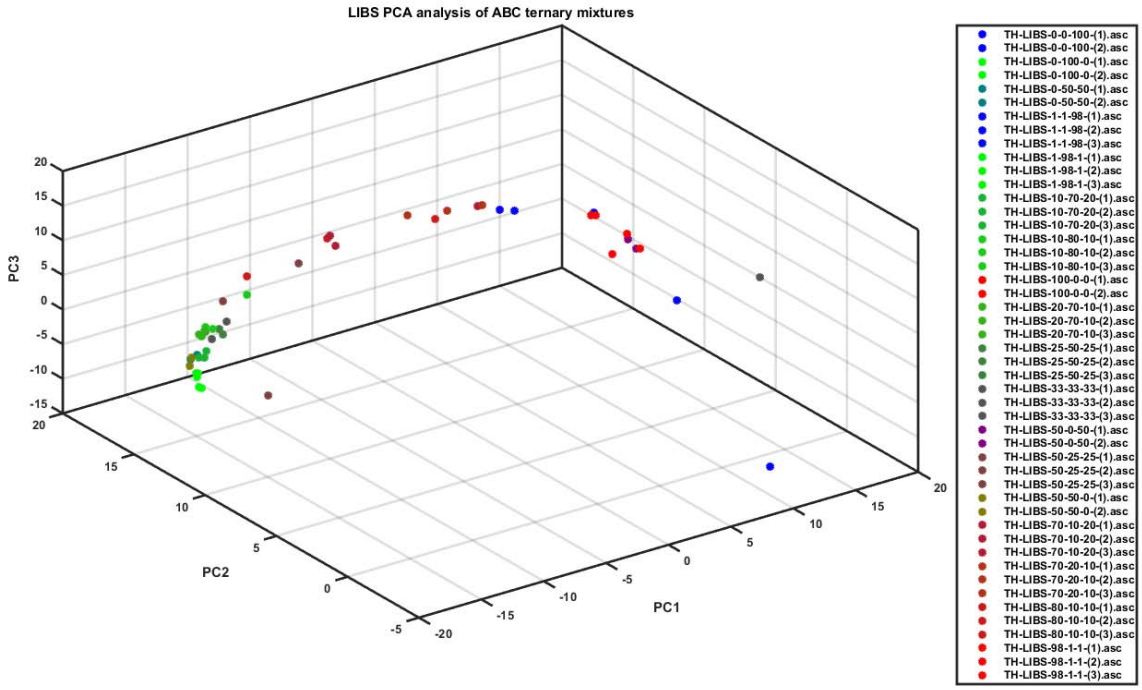

Figure 3-45 3 PCs analysis of the LIBS dataset from ABC ternary mixtures

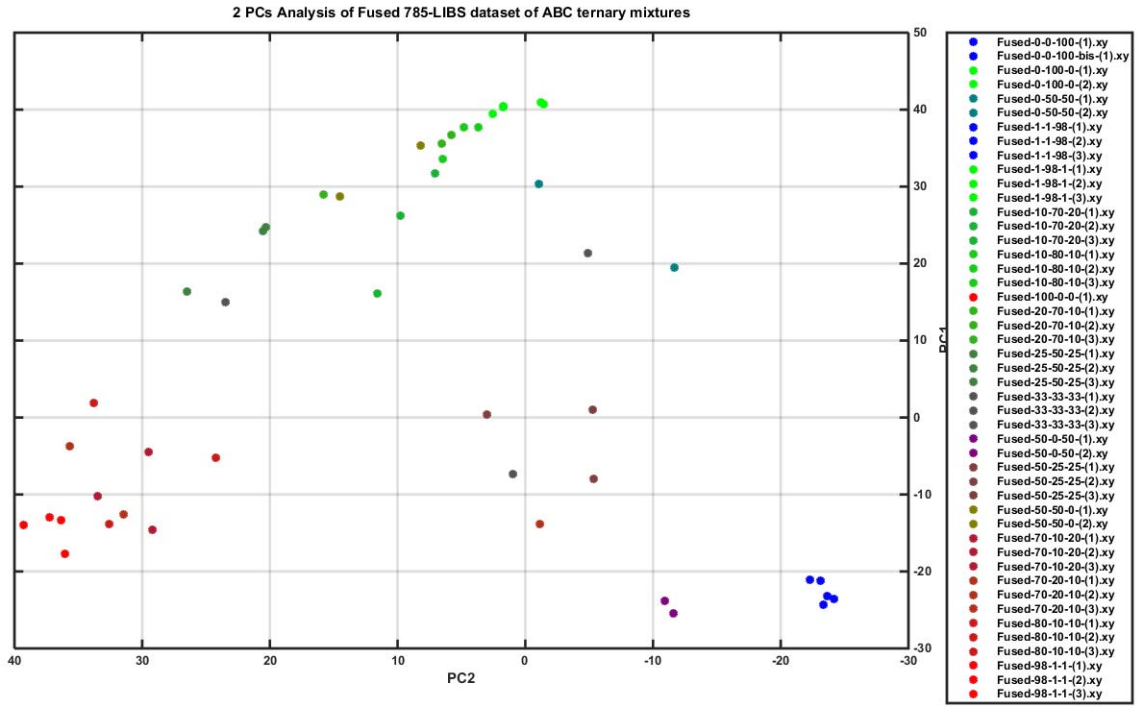

Figure 3-46 2 PCs analysis of the 785+LIBS fused dataset from ABC ternary mixtures

4 Conclusions

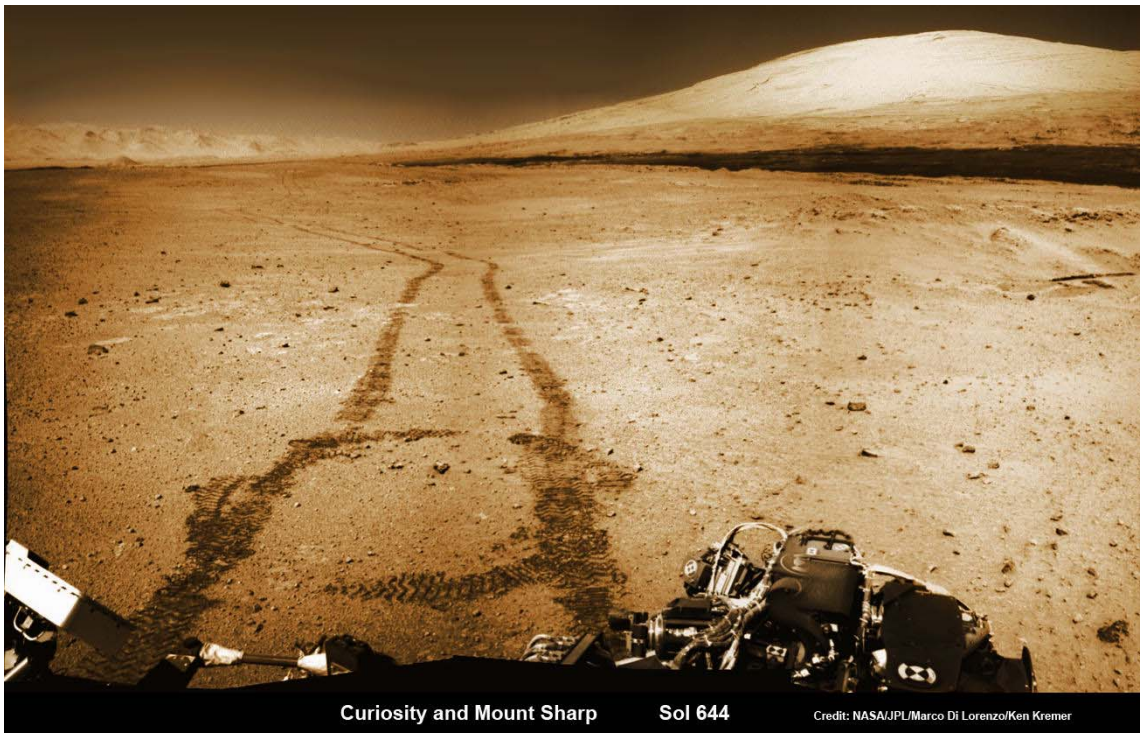

4.1 Standoff developments

Until the deployment of ChemCam with MSL's rover Curiosity, the spectroscopy techniques that could provide information of the surrounding environment of a rover were limited to passive techniques. VISIR spectroscopy and image analyses can provide good information from a sample but active techniques will always have a better performance. Raman or LIBS used in standoff instruments can provide complete information of the areas at some meters of a Rover, providing the structure and elemental composition with lower detection limits than achievable with passive techniques.

Not only for planetary exploration, but for earth applications, standoff developments are here to change the game in the characterization of samples when contact is not possible. SuperCam will start sending data from Mars in 2021; at the same time, a standoff LIBS from China will also start operating on Mars. The foresight is that more standoff instruments will come that will use standoff spectroscopy developments.

In this work I have provided the theoretical basis and information on how we have developed our standoff systems, and the scientific results that could be obtained from them.

In the context of Mars exploration missions these standoff systems will be able to provide assessment of habitability by getting a complete characterization of the geochemistry of a Region Of Interest. Furthermore, and as have been demonstrated in this work, Raman is a great addition to LIBS capabilities, being these two techniques complementary in nature.

It has to be noted, that there are physical limits that are difficult to cope with, and in the case of standoff Raman it is not easy to obtain a performance comparable to a contact instrument, differently from standoff LIBS.

The experiments performed for the assessment of the serpentinization degree of selected samples with a standoff Raman instrument showed that small changes or addons in the hardware configuration, a standoff instrument can share part of the hardware with a contact instrument, getting the best of both worlds. This one, one instrument would be a tool for remote characterization -helping in the decision making and sampling wider areas in less time-, while also having the option of performing contact measurements in selected samples, improving the characterization of the sample.

In this work we have presented a standoff system that has been integrated which is capable of getting time resolved Raman spectra from samples at distances from 1.5 to

5 meters (more if moved from the laboratory). Problems in the performance of this system have been identified and the solutions are in the process of being implemented.

4.2 SuperCam Calibration Target

Building any kind of hardware for its use in Mars is a challenge, as well as a unique opportunity, and the team lead by UVA has accomplished this task outstandingly.

SuperCam counts now with a calibration target that allows not only the calibration of each technique separately, but also the cross calibration between techniques, as some samples are visible by several techniques, and also do science with the calibration target.

The SCCT incorporates two experiments, one is the aggregation of dust to selected areas where it could be analyzed by the SuperCam suite. The other experiment will monitor the evolution of organics in the surface of Mars while being monitored by Raman.

As required by NASA we have delivered all the required documentation. We have also demonstrated, via tests or analyses that the design is reliable and will survive to the launch, cruise, landing and operation on Mars. The science team have all the necessary samples to correctly calibrate the instrument once in Jezero, and the team, included our group, can now focus in the training for operations.

In this aspect only a few actions remain open: the Engineering Model that is still to be delivered, and the Spare Unit that needs to go under acceptance campaign.

Both activities will be closed in the near future, irrespective that, and thanks to the work presented in this thesis, the objective has been accomplished and the SCCT has been delivered to JPL-NASA by the University of Valladolid.

4.3 Science with combined and standoff instruments

I have presented several examples of data obtained from standoff instruments that can be used for scientific goals of the Mars2020 mission. Our results show that the foresight of direct biomarkers detection by SuperCam is not very optimistic. As it could be seen by the results from our remote system, high concentrations and fresh organics are needed for detection, and none of them are expected to be on Mars.

We have also shown an example of how the past habitability of a region can be assessed by data coming from a standoff system very related to SuperCam. A problem might arise as the number of shots usually taken in a standoff measurement at the lab is much higher than the available shots that will be able to be done on Mars by SuperCam, although it is expected that more shots might be available for selected samples. The results of this work are promising for SuperCam and also for future developments.

One of the areas of interest in the last years that has also been covered in this thesis, is the application of data fusion and the chemometric calculations with this kind of instruments. We have shown results from a large set of experiments that showed how exact calculation can be based on each technique of interest, Raman and LIBS, and the bright future of combined developments given the potential of the fusion of data. Furthermore, we showed some promising results for the calibration of complex mixtures based on models built and trained with simple combinations of materials.

Data Fusion and the application of the multivariate analysis techinques, as shown by the results provided in this work, and the low amount of works published to the date, is a major path for future research and experiments. In fact, the results presented here are yet to be finished and published in a collection of papers.

4.4 Future Work

Apart from the current status of Mars 2020 and Exomars missions, both centered right now in the training for operations, this work presents interesting lines of research that will need to continue in the immediate future. Other lines of work are related to work that wasn't related to this thesis but that happened in parallel and will continue in the future, that could also have impact in the presence of Raman spectroscopy in planetary exploration missions.Multivariate analyses

In section 3.4, when analyzing the binary mixtures by univariate analysis first, and using multivariate analysis later, it could be observed how the accuracy of the classification of the samples increases dramatically when using multivariate methods. This result encourages the use of similar approaches in other mineralogical calculations. More concisely in the case of serpentinization, where the univariate analysis already competed with results from XRD, the use of multivariate techniques could give a new competitive and accurate model to determine the serpentinization degree of a sample.

More related to the analyses done in the section 3.4, it was found that the selection of samples could be improved to better evaluate the potential of the multivariate analytical methods. Nevertheless, the results shown in the models trained with binary mixtures, but used for classification of ternary mixtures are promising. In this sense, In this line of work the option to use simpler models to describe complex systems is also promising and will require further research.

Regarding the multivariate analyses using fused data, the fusion method used on this work is considered a low level data fusion: The spectra from different techniques are concatenated and changed the resolution to weight their participation. The use of more complex fusion techniques would be the next step following this line of work. Other fusion techniques based on some intermediate processing or the use of fuzzy logic could lead to a quicker, simpler and even more accurate models based on fused data.

4.4.1 Standoff / contact system

Results in section 3.3 were obtained using an instrument that could be configured as a stand-off Raman instrument, or as a contact Raman instrument. The possible impact of systems that could use both approaches in space is promising. The Standoff developments carried out by the author were always more related to high distances StandOff Raman-LIBS analyses. Future development should consider the development of a system that could combine Time Resolved Raman and LIBS in an instrument that is capable of acquiring data from a sample in micro mode, and also from a sample at some meters. This would provide the possibility of building an automated acquisition system using the heritage from the RLS algorithm development, resulting in an instrument capable of doing both analyses automatically. Such an instrument could analyze great volumes of samples and apply automatic chemometric models, multiplying the scientific outcome of the group.

4.4.2 Future missions

As for today, our group has been included in the science team of another mission, MMX, so future support science works related to mineralogy of the Martian moons, especially Phobos will be constitute by itself a new research line.

On the other hand, the author has been included as collaborator in the development of a new breed of spectrometer based on DMD. This technology, that uses chips with micromirrors, allows a new line of spectral treatment before the data acquisition by the sensor.

These developments can integrate in the detector the signals from different compounds, or signals corresponding to the same compound, what constitutes an equivalent to the definition of ROIs, but directly applied to the light collected and not to the reading of a pixel.

The instrument is called iSEE, and the project it's a joint venture from Impossible Sensing, SETI Institute, HoneyBee Robotics and NASA Ames center, in which the ERICA group is also involved. This project counts with funding by NASA and could be potentially applied to the exploration of the outer Solar System.

Also, and despite the bad news coming from NASA regarding a possible Europa Lander Mission, more work is to be done for the study of this kind of planetary bodies. The detection of organics in aqueous mediums is a priority for the study of icy worlds or Mars poles. These samples containing water, on solid or liquid state, clearly point to the need of using Raman developments in combination with SERS technology. SERS uses substrates that enhance the Raman signal and can boost the detection capabilities in several orders of magnitude, which is especially interesting for the detection of organics,

which, if found, would be potentially present in very low concentrations. In this line of work, the analysis of low-concentration dilutions of selected organics with SERS substrates with the RLS flight spare model would be of interest.

Bibliography

Allwood, A. (2015). Texture-specific elemental analysis of rocks and soils with PIXL: The Planetary Instrument for X-ray Lithochemistry on Mars 2020. *IEE Aerospace Conference*.

Aramendia, J. (2018). Overview of the techniques used for the study of non-terrestrial bodies: Proposition of novel non-destructive methodology. *Trends in analytical chemistry*, 36-46.

Ballou, E. (1978). Chemical interpretation of Viking Lander 1 life detection experiment. *Nature*, #271, 644-645.

Balm, S. (1991). The analysis of comet mass spectrometric data. *Space Science Reviews*, Vol. 56, Issue 1-2.

Bazalgette, G. (2008). Combined Raman spectrometer/laser-induced spectrometer for the next ESA mission to breakdown Mars. *Spectrochemica Acta A*, 68(4):1023-8.

Beegle, L. (2015). SHERLOC: Scanning Habitable Environments With Raman & Luminescence for Organics & Chemicals. *45th LSPC*.

Bell, J. (2016). MASTCAM-Z: Designing a geologic, stereoscopic, and multispectral pair of zoom cameras for the nasa Mars2020 rover. *3rd International Workshop on Instrumentation for Planetary Missions*.

Beyssac, O. (2017). Nanosecond time-resolved Raman and fluorescence Spectroscopy: insights for mineral and organics characterization. *48th LPSC*.

Brosnan, J. (2006). The sulfur-containing amino acids: an overview. *Journal of nutrition*.

Chopelas, A. (1991). Single crystal Raman spectra of forsterite, fayalite, and monticellite. *American Mineralogist*, Vol 76, 1101-1109.

Choquette, S. (2007). Relative intensity correction of Raman spectrometers: NIST SRMs 2241 through 2243 for 785 nm, 532 nm, and 488 nm/514.5 nm excitation. *Applied Spectroscopy*, 61(2):117-129.

Clegg, S. (2009). Multivariate analysis of remote laser-induced breakdown spectroscopy spectra using partial least squares, principal component analysis, and related techniques. *Spectrochemica Acta part B*.

Cousin, A. (2018). Characterization of the SuperCam LIBS Calibration Targets. *49th LPSC*, #2186.

Cremers, D. (1987). The Analysis of Metals at a Distance Using Laser-Induced Breakdown Spectroscopy. *Applied Spectroscopy*, Vol 41, Issue 4.

Davila, A. F. (2013). Perchlorate on Mars: A chemical hazard and a resource for humans. *International Journal of Astrobiology*, 12(4).

Dobrea, E. (2019). Detection of serpentine at Jezero Crater. *LPSC*, #1249.

Drube, L. (2009). Magnetic and optical properties of airborne dust and settling rates of dust at the Phoenix landing site-. *Journal of Geophysical Research*.

Eide, S. (2019). RIMFAX GROUND PENETRATING RADAR MODELLING: IMAGING THE SUBSURFACE OF THE JEZERO WESTERN DELTA. *Ninth Conference on Mars*.

Elsila, J. (2010). Cometary glycine detected in samples returned by Stardust. *Meteoritics & planetary science*.

Fornaro, T. (2018). UV irradiation of biomarkers adsorbed on minerals under Martian-like conditions: Hints for life detection on Mars. *Icarus*, 313, 38-60.

Foust, J. (July de 2019). *Mars sample return mission plans begin to take shape*. Obtenido de Space News: https://spacenews.com/mars-sample-return-mission-plans-begin-to-take-shape/

Gaft, M. (2009). Laser-induced breakdown spectroscopy for on-line sulfur analyses of minerals in ambient conditions. *Spectrochemica Acta B*, 64 1098-1104.

Gazquez, F. (2014). Caracterización mineralógica y geoquímica de minerales hidratados de ambientes subterráneos: implicaciones para la exploración planetaria. *Estudios Geológicos*, Vol 70, #2.

Gelder, J. D. (2007). Reference database of Raman spectra of biological molecules. *Journal of Raman Spectroscopy*.

Gomez-Nubla, L. (2018). EVALUATION OF THE ELEMENTAL AND MOLECULAR HOMOGENEITY OF THE SUPERCAM CALIBRATION TARGETS. *49th Lunar and Planetary Science Conference*, #2813.

Gregersen, E. (s.f.). *Lidar.* Obtenido de Encyclopaedia Britannica: https://www.britannica.com/technology/lidar

Hecht, M. (2015). The Mars Oxygen ISRU Experiment (MOXIE) on the Mars 2020 Rover. *46th LPSC*.

Hirschfeld, T. (1974). Range Independence of Signal in Variable Focus Remote Raman Spectrometry. *Applied Optics*, Volume 13, Issue 6, 1435.

Holm, N. (2015). Serpentinization and the Formation of H2 and CH4 on celestial bodies. *Astrobiology*, Vol. 15, #7.

Horst, S. (2012). Formation of Amino Acids and Nucleotide Bases in a Titan Atmosphere Simulation Experiment. *Astrobiology*.

JPL. (2013). *Report of the Mars 2020 Science Definition Team.*

JPL. (2016). *The Europa Lander Science Definition Team Report.*

Klein, H. (1978). The Viking biological experiments on Mars. *Icarus*, Vol.34, Iss 3, 666-674.

Krawczyk, C. (s.f.). *http://www.physics.drexel.edu*. Obtenido de http://www.physics.drexel.edu/~bob/Term_Reports/Krawczyk_hw3.pdf

LeMaitre, R. (2002). *Igneous rocks: a classification and glossary of terms.* Cambridge.

Lopez-Reyes, G. (2013). Analysis of the scientific capabilities of the ExoMars Raman Laser Spectrometer instrument . *European Journal of Mineralogy*.

Lopez-Reyes, G. (2014). Multivariate analysis of Raman spectra for the identification of sulfates: Implications for ExoMars. *American Mineralogist*, 99, 1570.

Lopez-Reyes, G. (2018). Raman-LIBS data fusion analysis on ternary mixtures. *13th Georaman Conference*.

Manfredi, J. (2013). MEDA: An environmental and meteorological package for Mars 2020. *45th LPSC*.

Maurice, S. (2012). The ChemCam Instrument Suite on the Mars Science Laboratory (MSL) Rover: Science Objectives and Mast Unit Description. *Space Science Reviews*.

McCreery, R. (2000). *Raman Spectroscopy for Chemical analysis.* Wiley.

Miller, S. (1959). Earth, Organic Compound Synthesis on the Primitive. *Science*, Vol.130 Number 3370.

Mills, I. (1964). Raman selection rules for vibrationrotation transitions in symmetric top molecules. *Molecular Physics*, 8:4, 363-373.

Misra, A. (2012). Single-Pulse Standoff Raman Detection of Chemicals from 120 m Distance During Daytime. *Applied spectroscopy*, Vol. 66, Issue 11, 1279-1285 .

NASA/JPL. (2016). *Europa Lander Scientific Technical Definition Report.*

Ouillon, R. (1982). Two accurate methods to obtain the spectral sensitivity of a Raman spectrometer device. *Journal of Raman Spectroscopy*, Vol. 12 Issue 3 281-286.

Perez, R. (2017). The supercam instrument on the NASA Mars 2020 mission: optical design and performance. *SPIE*.

Raman, C. (1928). A New Type of Secondary Radiation. *Nature*, 121, 501-502.

Raman, C. (1929). The Raman effect: Investigation of molecular structure by light scattering. *Trans. Faraday Society.*, 25, 781-792.

Rammelkamp, K. (2018). Advantages of Combined LIBS and Raman Data for the Identification and Quantification of Hydrated Salts for in-situ Planetary Exploration. *13th Georaman Conference*.

Reess, J. (2019). The SuperCam infrared instrument on the NASA MARS2020 mission: performance and qualification results. *SPIE*.

Rodriguez, J. (2011). Standardization of Raman spectra for transfer of spectral libraries across different instruments. *Analyst*, Issue 20.

Röling, F. (2015). The Significance of Microbe-Mineral-Biomarker Interactions in the Detection of Life on Mars and Beyond. *Astrobiology*, Vol 15, #6.

Rull, F. (2011). Analysis of Arctic ices by Remote Raman Spectroscopy. *Spectrochimica Acta Part A*, 80, 148– 155.

Rull, F. (2017). The Raman Laser Spectrometer for the ExoMars Rover Mission to Mars. *Astrobiology*, vol.17 No 6-7.

Rummel, J. (1989). Planetary protection policy overview and application to future missions. *advances in Space Research*, Vol. 9, Issue 6, 181-184.

Sanz-Arranz, J. (2017). Amorphous Zinc Borate as a simple baseline reference for Raman Spectroscopy. *Journal of Raman Spectroscopy*.

Sanz-Arranz, J. (2018). Amorphous Zinc Borate as a simple baseline reference for Raman Spectroscopy. *Journal of Raman Spectroscopy*.

Schroder, S. (2017). Overview of ChemCam Activities and Discoveries during 5 years at Gale Crater, Mars. *EPSC Abstracts*, Vol. 11 EPSC2017-726.

Schubert, D. (2003). Structural Characterization and Chemistry of the Industrially Important Zinc Borate. *Chem. Mater*, 15.4 866-871.

Schulte, M. (2006). Serpentinization and Its Implications for Life on the. *Astrobiology*, Vol. 6, #2.

Schurig, D. (2006). Metamaterial Electromagnetic Cloak at Microwave. *Science*, vol. 314, no. 5801.

Sharma, S. (2003). Portable standoff Raman and Mie-Rayleigh lidar for cloud, aerosol, and chemical monitoring. *SPIE Proceedings*, Vol 5154.

Singh, V. (2018). Laser-induced breakdown spectroscopy (LIBS): a novel technology for identifying microbes causing infectious diseases. *Biophysics Review*, 10(5): 1221-1239, doi: 10.1007/s12551-018-0465-9.

Skinner, H. (1996). Remote Raman microimaging using an AOTF and a spatially coherent microfiber optical probe. *Applied spectroscopy*, Volumen: 50 #8, 1007-1014.

Sobron, P. (2014). Data Fusion in Planetary LIBS+Raman Spectroscopy. *45th LPSC*, abstract #2875.

Stamenkovic, V. (2014). Serpentinization (Mars). *Encycl. Astrobiol.*, 1431-1433.

Stoker, C. (1997). Organic degradation under simulated Martian conditions. *J Geophys Res.*, 102(E5):10881-8.

Thompson, J. (2006). Remote laser-induced breakdown spectroscopy analyses of Dar al Gani 476 and Zagami Martian meteorites. *Journal of Geophysical Research Atmospheres*, May, 111.

Vago, J. (2017). Habitability on Early Mars and the Search for Biosignatures with the ExoMars Rover. *Astrobiology*, vol.17 #6-7.

Vaniman, D. (2012). Ceramic ChemCam Calibration Targets on Mars Science Laboratory. *space Science Reviews*, 170:229-255.

Venkateswaran, C. (1935). The fluorescence of ruby, sapphire and emerald. *Proceedings of the Indian Academy of Sciences - Section A*, Vol 2 Iss 5, 459-465.

Wadsworth, J. (2017). Perchlorates on Mars enhance the bacteriocidal effects of UV light. *Nature*.

Wang, A. (2006). Sulfates on Mars: A systematic Raman spectroscopic study of hydration states of magnesium sulfates. *Geochimica et Cosmochimica Acta*, 70-24.

Wang, A. (2019). Quantification of fluorescence emission from extraterrestrial materials and its significance for planetary Raman spectroscopy. *Journal of Raman Spectroscopy*.

Wiens, R. (2012). The ChemCam Instrument Suite on the Mars Science Laboratory (MSL) Rover: Body Unit and Combined System Tests. *Space Science Reviews*.

Wiens, R. (2017). THE SUPERCAM REMOTE RAMAN SPECTROMETER FOR MARS 2020. *48th LPSC*.

Wiens, R. (2017). The SuperCam Remote Sensing Instrument Suite for the Mars 2020 Rover: A Preview. *Spectroscpy Vol. 32 Issue 5.*

Wu, M. (2000). Stand-off detection of chemicals by UV Raman spectroscopy. *Applied Spectroscopy*, Volumen: 54 #6, 800-806.

Xiaona, L. (2014). Rapid Elemental Analysis and Provenance Study of Blumea balsamifera DC Using Laser-Induced Breakdown Spectroscopy. *Sensors*, Vol 15, 642-55, DOI: 10.3390/s150100642.